



Lehrstuhl Theoretische Physik IV

**Fixed Points
in Supersymmetric Extensions
of the Standard Model**

Dissertation
zur Erlangung des Doktorgrades
des Fachbereichs Physik
der TU Dortmund

Vorgelegt von
Kevin Moch
Geboren in Lünen

Dortmund
Juni 2020

Der Fakultät für Physik der Technischen Universität Dortmund zur Erlangung des akademischen Grades eines Doktors der Naturwissenschaften vorgelegte Dissertation.

Erstgutachter: Prof. Dr. Gudrun Hiller

Zweitgutachter: Prof. Dr. Daniel F. Litim

Datum der mündlichen Promotionsprüfung: 14. Juli 2020

Vorsitzender der Prüfungskommission: Prof. Dr. Götz Uhrig

Abstract

In this work, we are searching for supersymmetric extensions of the Standard Model (SM) of particle physics which are asymptotically safe. Such models are well-defined at all energy scales and provide hints for the scale at which supersymmetry gets broken. The combination of supersymmetry and asymptotic safety hereby turns out to strongly restrict the space of possible models. Within extensions of the minimal supersymmetric SM (MSSM), we perturbatively find candidates which all have a specific field content and low supersymmetry-breaking scales. For extensions of the MSSM with an extended gauge sector, we find models for which these scales appear at much larger energies. We then investigate whether the perturbatively found models are in agreement with non-perturbative results obtained from superconformal field theories. The exact supersymmetric Novikov-Shifman-Vainshtein-Zakharov beta functions suggest that these models are not asymptotically safe beyond perturbation theory. Finally, we present a model for which the non-perturbative results suggests that the SM can be UV-completed by this model. We also study perturbatively whether the fixed point needed for this UV-completion is physical.

Zusammenfassung

In dieser Arbeit wird nach supersymmetrischen Erweiterungen des Standardmodells (SM) der Teilchenphysik gesucht, welche asymptotisch sicher sind. Solche Modelle sind für alle Energieskalen wohldefiniert und liefern Hinweise für die Skala, an welcher Supersymmetrie gebrochen wird. Die Verbindung von Supersymmetrie mit asymptotischer Sicherheit stellt sich hierbei als starke Einschränkung für die Menge an möglichen Modellen heraus. Wir finden in Erweiterungen des minimal supersymmetrischen SM (MSSM) perturbativ Kandidaten, welche alle einen spezifischen Feldinhalt aufweisen und niedrige Supersymmetrie-Brechungsskalen vorhersagen. In Erweiterungen des MSSM mit erweitertem Eichsektor werden Modelle gefunden, für welche diese Skalen bei deutlich höheren Energien liegen. Die perturbativ gefundenen Modelle werden dann daraufhin untersucht, ob sie im Einklang mit nichtperturbativen Ergebnissen aus superkonformen Feldtheorien sind. Die exakten supersymmetrischen Novikov-Shifman-Vainshtein-Zakharov Betafunktionen suggerieren, dass diese Modelle über die Störungstheorie hinaus nicht asymptotisch sicher sind. Zum Schluss wird ein Modell präsentiert, für welches die nichtperturbativen Ergebnisse suggerieren, dass das SM durch dieses Modell UV-vervollständigt werden kann. Außerdem untersuchen wir störungstheoretisch, ob der für diese UV-Vervollständigung benötigte Fixpunkt physikalisch ist.

“You approximate the time curvature using a seventh order polynomial. But you made one small error. For the distance you require, it should be at least nine.”

- Walter Bishop (*Fringe* S2E18)

Contents

1	Introduction	1
2	Directions for BSM Physics	3
2.1	The Standard Model	3
2.2	Challenges within the Standard Model	8
2.3	Asymptotic Safety	9
2.4	Supersymmetry	13
3	Dark QCD With UV Fixed Points	15
3.1	Dark QCD	15
3.2	Benchmark	16
3.3	Phenomenology	19
4	Supersymmetry Basics	23
4.1	Constructing Supersymmetric Theories	23
4.2	The MSSM and its Features	27
4.2.1	Superfields and superpotential of the MSSM	27
4.2.2	Soft supersymmetry-breaking	29
4.2.3	Gauge-mediated supersymmetry-breaking	29
4.2.4	Mass spectrum of the MSSM	30
5	Supersymmetric Renormalization Group	33
5.1	Beta Functions	33
5.2	Interacting Fixed Points	35
5.3	On the Existence of Interacting Fixed Points	37
6	MSSM Extensions	39
6.1	Fixed Points Within the MSSM	39
6.1.1	MSSM	40

6.1.2	RPV MSSM	41
6.2	Search Strategy For MSSM Extensions	43
6.3	Model Class 1: New Quark Singlets and Leptons	44
6.3.1	Framework	44
6.3.2	Scan	47
6.4	Model Class 2: New Quark Doublets and Leptons	49
6.4.1	Framework	49
6.4.2	Scan	51
6.5	Model Class 3: A Fourth Generation and new Leptons	53
6.5.1	Framework	53
6.5.2	Scan	54
6.6	Analysis of AS Candidates	55
6.6.1	Benchmark	59
6.7	Summary and Remarks on AS MSSM Extensions	61
7	MSSM Extensions with an Additional $SU(N)$	64
7.1	The MSSM+ Framework	64
7.2	Model Scans and Matching onto the SM	68
7.2.1	Benchmark 1 (BM1)	70
7.2.2	Benchmark 2 (BM2)	73
7.2.3	Benchmark 3 (BM3)	75
7.3	Gauge-Mediation in the MSSM+	77
7.3.1	Mass scales and AS in the gauge-mediated scenario	77
7.3.2	Estimate of the mass scales	79
7.3.3	Benchmark demonstration	82
7.4	Phenomenological Aspects of the MSSM+	86
7.4.1	Particle spectrum and dark matter candidates	86
7.4.2	Mass bounds	87
7.4.3	Missing energy at colliders	88
7.5	Summary and Remarks on the MSSM+	88
8	Superconformal Field Theory	90
8.1	Superconformal Algebra and Unitarity Bounds	91
8.2	Maximization of a and the a -Theorem	93
8.2.1	Triangle anomalies	93
8.2.2	Sketch of the proof	94

9	Model Analysis Beyond Perturbation Theory	97
9.1	Perturbative AS MSSM Candidates	98
9.2	Perturbative AS MSSM+ Candidates	102
9.3	MSSM Extensions with an Additional semi-simple Group	102
9.3.1	Exact UV-attractivity and unitarity	104
9.3.2	Large- N two-loop analysis	105
9.3.3	Large- N three-loop analysis	110
9.4	Summary of our Non-Perturbative Investigations	116
10	Conclusions	118
A	On Unnatural Yukawa Beta Functions	122
B	Necessary Condition for Fixed Points	124
C	A Relation Between Fixed Points FP_3 and FP_{23}	127
D	Beta Functions and Fixed Points Formulae	131
D.1	MSSM Extensions	132
D.1.1	Model class 1	132
D.1.2	Model class 2	134
D.1.3	Model class 3	135
D.2	MSSM+	136
	Bibliography	138

Chapter 1

Introduction

In search of a deeper understanding of nature, the Standard Model (SM) of particle physics [1–4] as a quantum field theory and general relativity [5] as a classical field theory emerged as our best descriptions of the universe, so far. On the road towards these two pillars of modern physics, principles played important and success-bringing roles. In this thesis, asymptotic safety (AS) as a principle for fundamental quantum field theories, and supersymmetry (SUSY) as a symmetry principle are put forward, and implications for extensions of the SM are investigated.

Extending the SM is necessary since, despite its many successes, the SM can at best be viewed as a low energy approximation to a more fundamental theory of nature. Some of the reasons for this include the absence of gravity within the SM, the absence of dark matter candidates, and the divergence of the running $U(1)_Y$ hypercharge coupling α_1 , known as the triviality problem [6, 7]. Ideas on how the SM could be extended to tackle some of these challenges are numerous. Asymptotic safety in combination with supersymmetry solves some of these problems and guides the search for SM extensions of this thesis.

Prior to run 1 of the LHC between 2009 and 2013, high energy physicists expected to find superpartners of SM particles in the $\mathcal{O}(1 \text{ TeV})$ -range [8, 9]. Although experimental signals for SUSY are absent in this energy range [10, 11], there is no decisive reason for nature not to be supersymmetric at much larger energy scales and hence SUSY remains one of the theoretically most attractive and promising ways to extend the SM.

In the minimal supersymmetric version of the SM, the MSSM, next to α_1 also the weak $SU(2)_L$ coupling α_2 diverges. Within asymptotically safe extensions, these divergences are cured and theories are well-defined for all energies [12, 13]. Furthermore, hints for the scale of supersymmetry-breaking are provided when the UV-complete AS theory is matched onto the SM. Asymptotic safety refers to the scenario in which the

couplings of a model reach an ultraviolet fixed point at infinitely large energies. In fixed points, theories become conformal [14–16] and general results from conformal field theories (CFTs) [17] can be applied. Away from fixed points, theories can be viewed as spontaneously breaking the conformal symmetry [18]. In combination with supersymmetry, fixed points constitute superconformal field theories (SCFTs) for which additional exact results are known, some of which we explicitly make use of in this thesis [19–23].

This thesis is organized as follows. In chapter 2, we briefly present the SM and go into more detail regarding some remaining challenges. Furthermore, more details on asymptotic safety and supersymmetry, as well as their historical developments are provided. In chapter 3, a model Peter Schuh and I worked on [24] is discussed which offers an explanation for the experimentally observed dark matter energy density. In this model, dark matter candidates are baryon-like bound states of particles purely charged under a new “dark QCD” $SU(3)_D$ gauge sector. The mathematics of SUSY, as well as the MSSM and some of its features are discussed in chapter 4, while supersymmetric renormalization group (RG) equations and some fixed point features within perturbation theory are presented in chapter 5. With these tools at our disposal, we begin our perturbative search for fixed points within the MSSM and extensions thereof in chapter 6. Here, the special features of SUSY allow us to classify MSSM extensions. In chapter 7, AS extensions of the SM with an additional non-abelian $SU(N)$ gauge sector are investigated within perturbation theory. Beginning with chapter 8, we expand our analysis beyond perturbation theory. After providing non-perturbative tools valid for superconformal field theories in this chapter, we utilize these in chapter 9 to perform consistency checks on the AS candidates previously found within perturbation theory. In section 9.3, we present an MSSM extension framework with an additional semi-simple gauge sector $SU(N) \times SU(M)$ motivated by exact relations suggesting that this framework contains models which UV-complete the SM. Comparing two-loop and three-loop results with the corresponding exact results for different model parameters, we are able to identify how well the loop renormalization flows approximate the exact flows. Furthermore, we study the evolution of fixed points going towards model parameters for which the SM becomes UV-complete. We conclude in chapter 10.

Chapter 2

Directions for Physics Beyond the Standard Model

In this chapter, we briefly present the Standard Model and discuss some of its remaining challenges, together with possible directions on how these may be resolved in extensions beyond the SM.

2.1 The Standard Model

Resulting from decades of high energy physics research, the Standard Model of particle physics presently constitutes the overall accepted and experimentally verified particle model of nature. So far, no striking discrepancies between SM predictions and experiments are observed [25]. Some detected anomalies are in agreement with being statistical fluctuations. Future experiments will shed light on these anomalies and possibly discover new physics beyond the SM. Until then, the Standard Model remains our best description of nature.

The SM describes electromagnetism in the framework of quantum electrodynamics (QED) developed by Tomonaga, Schwinger, Feynman and Dyson [26–35], as well as the strong forces by quantum chromodynamics (QCD) [1]. At large energies, electromagnetism and the weak force combine into the electroweak force, described by an $SU(2)_L \otimes U(1)_Y$ gauge theory [2–4]. At low energies, this gauge symmetry is broken by the vacuum expectation value of the Higgs field. This is known as the Higgs mechanism [36–40], which also generates the masses of the elementary particles of the SM. The discovery of the Higgs boson has been confirmed in 2012 [41, 42], completing the Standard Model. By the usual counting, all the elementary particles are given by six

quarks, six leptons, one Higgs boson, one photon, eight gluons and three massive gauge bosons W^\pm and Z^0 . All other observed particles, like the proton, are bound states of these elementary particles.

In more detail, the SM is a gauge Yukawa quantum field theory with gauge group

$$G_{\text{SM}} = \text{SU}(3)_C \otimes \text{SU}(2)_L \otimes \text{U}(1)_Y , \quad (2.1)$$

which is spontaneously broken to $\text{SU}(3)_C \otimes \text{U}(1)_{\text{EM}}$ by the vacuum expectation value of the Higgs field [43]

$$|\langle H \rangle| = \frac{v}{\sqrt{2}} \approx \frac{246 \text{ GeV}}{\sqrt{2}} \approx 174 \text{ GeV} \quad (2.2)$$

of the real and electrically neutral component of the Higgs field H . The (Weyl) fermion fields and the Higgs field of the SM are shown in table 2.1 together with their gauge representations and the chirality of their particles.

Field	Chirality	$\text{SU}(3)_C$	$\text{SU}(2)_L$	$\text{U}(1)_Y$	Multiplicity
Quark doublet Q	Left	3	2	+1/6	3
Up-Quark u	Right	3	1	+2/3	3
Down-Quark d	Right	3	1	-1/3	3
Lepton doublet L	Left	1	2	-1/2	3
Lepton singlet e	Right	1	1	-1	3
Higgs H	Left	1	2	+1/2	1

Table 2.1: All the (Weyl) fermion fields and the Higgs field of the SM with their representations under the SM gauge group (2.1) before spontaneous symmetry breaking. Additionally, we state the chirality of the particles described by the fields.

Additionally to the kinetic and gauge interaction terms, the SM Lagrangian contains Yukawa interactions

$$\mathcal{L}_{\text{Yuk}} = - \sum_{i,j=1}^3 Y_{ij}^d \bar{Q}_i H d_j - \sum_{i,j=1}^3 Y_{ij}^u \bar{Q}_i H^c u_j - \sum_{i,j=1}^3 Y_{ij}^e \bar{L}_i H e_j + \text{h.c} , \quad (2.3)$$

where

$$H^c \equiv i\sigma^2 H^* , \quad (2.4)$$

with σ^2 the second Pauli matrix and “h.c.” denoting hermitian conjugated terms. The Higgs potential

$$\mathcal{L}_{\text{Pot}} = -\mu^2 H^\dagger H + \lambda (H^\dagger H)^2 , \quad (2.5)$$

generates a non-vanishing vacuum expectation value for H which can be chosen to be

$$\langle H \rangle = \frac{1}{\sqrt{2}} \begin{pmatrix} 0 \\ v \end{pmatrix}, \quad \langle H^c \rangle = \frac{1}{\sqrt{2}} \begin{pmatrix} v \\ 0 \end{pmatrix}, \quad (2.6)$$

generating symmetry-breaking mass terms for the W bosons, the Z boson, quarks, and charged leptons. While the gauge boson masses originate from gauge interactions of the Higgs field, fermions acquire their masses via the Yukawa interactions of eq. (2.3):

$$\mathcal{L}_{\text{Yuk}} \supset -\frac{v}{\sqrt{2}} \left(\sum_{i,j=1}^3 Y_{ij}^d \bar{d}_{Li} d_j + \sum_{i,j=1}^3 Y_{ij}^u \bar{u}_{Li} u_j + \sum_{i,j=1}^3 Y_{ij}^e \bar{e}_{Li} e_j + \text{h.c.} \right). \quad (2.7)$$

Diagonalizing the quark Yukawa matrices with unitary matrices yields the mass eigenstates

$$\tilde{u}_L = V_{u,L} u_L, \quad \tilde{d}_L = V_{d,L} d_L, \quad \tilde{u}_R = V_{u,R} u_R, \quad \tilde{d}_R = V_{d,R} d_R. \quad (2.8)$$

This rotation leads to mixing of up and down type quarks in weak gauge interactions, described by the unitary Cabibbo-Kobayashi-Maskawa (CKM) matrix [44, 45]

$$V_{\text{CKM}} = V_{u,L} V_{d,L}^\dagger. \quad (2.9)$$

The absolute values of the CKM matrix entries at the Z -pole mass $M_Z \approx 91.2 \text{ GeV}$ are

$$|V_{\text{CKM}}(M_Z)| = \begin{pmatrix} |V_{ud}| & |V_{us}| & |V_{ub}| \\ |V_{cd}| & |V_{cs}| & |V_{cb}| \\ |V_{td}| & |V_{ts}| & |V_{tb}| \end{pmatrix} \sim \begin{pmatrix} 0.974 & 0.225 & 0.004 \\ 0.225 & 0.973 & 0.041 \\ 0.009 & 0.040 & 0.999 \end{pmatrix}. \quad (2.10)$$

The CKM matrix enters only in gauge interactions involving the W^\pm bosons while all other interactions stay flavor conserving. While the CKM matrix is physical, the Yukawa matrices in eq. (2.3) are not directly measurable.

If we choose charged left lepton mass eigenstates, left up quark mass eigenstates, as well as all right handed quarks to be gauge eigenstates, the (diagonal) mass and Yukawa matrices are related via

$$M^d = \frac{v}{\sqrt{2}} V_{d,L} Y^d, \quad M^u = \frac{v}{\sqrt{2}} Y^u, \quad M^e = \frac{v}{\sqrt{2}} Y^e, \quad (2.11)$$

where we now have $V_{d,L} = V_{\text{CKM}}^\dagger$. Since quarks are not observable as free particles, their pole mass cannot be measured (except for the top quark which decays before it hadronizes). At M_Z , the $\overline{\text{MS}}$ mass parameters for quarks and leptons are [46]

$$\begin{aligned} m_u &\approx 1.27 \text{ MeV}, & m_d &\approx 2.90 \text{ MeV}, & m_s &\approx 55.00 \text{ MeV}, \\ m_c &\approx 0.62 \text{ GeV}, & m_b &\approx 2.89 \text{ GeV}, & m_t &\approx 171.70 \text{ GeV}, \\ m_e &\approx 0.49 \text{ MeV}, & m_\mu &\approx 102.72 \text{ MeV}, & m_\tau &\approx 1746.24 \text{ MeV}. \end{aligned} \quad (2.12)$$

From eqs. (2.11), we find the Yukawa couplings

$$|Y^d(M_Z)| \sim \begin{pmatrix} 1.6 \cdot 10^{-5} & 7.1 \cdot 10^{-5} & 6.6 \cdot 10^{-5} \\ 3.8 \cdot 10^{-6} & 3.1 \cdot 10^{-4} & 6.8 \cdot 10^{-4} \\ 1.5 \cdot 10^{-7} & 1.3 \cdot 10^{-5} & 1.7 \cdot 10^{-2} \end{pmatrix}, \quad (2.13)$$

$$Y^u(M_Z) \sim \begin{pmatrix} 7.3 \cdot 10^{-6} & 0 & 0 \\ 0 & 3.6 \cdot 10^{-3} & 0 \\ 0 & 0 & 0.99 \end{pmatrix}, \quad (2.14)$$

$$Y^e(M_Z) \sim \begin{pmatrix} 2.8 \cdot 10^{-6} & 0 & 0 \\ 0 & 5.9 \cdot 10^{-4} & 0 \\ 0 & 0 & 1 \cdot 10^{-2} \end{pmatrix}. \quad (2.15)$$

In our chosen basis, the entries of Y^u are complex valued, while those of Y^d and Y^e are real.

Since the top Yukawa coupling $y_t = 0.99$ is the largest Yukawa coupling, a convenient approximation is given by setting all the other Yukawa couplings to zero. Within this approximation, the gauge and Yukawa couplings

$$\alpha_1 \equiv \frac{g_1^2}{(4\pi)^2}, \quad \alpha_2 \equiv \frac{g_2^2}{(4\pi)^2}, \quad \alpha_3 \equiv \frac{g_3^2}{(4\pi)^2}, \quad \alpha_t \equiv \frac{y_t^2}{(4\pi)^2} \quad (2.16)$$

run at two loop gauge and one loop Yukawa level as shown in fig. 2.1¹. The gauge couplings g_1, g_2, g_3 belong to the gauge sectors of G_{SM} in (2.1). For some more details on the concept of running couplings, see sec. 2.3. The strong coupling α_3 , the weak coupling α_2 , as well as the top Yukawa coupling α_t vanish in the far UV, making calculations within perturbation theory predictive. This scenario is known as asymptotic freedom [50–52]. At small energies, the strong coupling runs into a confinement pole at $\mu_{\text{conf}} \sim 0.2 \text{ GeV}$. This pole is proposed to be responsible for the observed quark confinement [53]. On the other hand, α_1 grows towards larger energies until it eventually runs into a Landau pole, limiting the SM to a finite energy scale. Long before this pole is reached, gravitational effects become significant at $\mu \sim 10^{19} \text{ GeV}$. Nevertheless, the implied breakdown of the SM due to its Landau pole constitutes the main motivation for the searches of SM extensions within this thesis. More discussions are provided in the subsequent sections.

¹All plots of this thesis are created with Python version 3.7.4 [47] and the Matplotlib package [48]. Occasionally, some editing is done with Inkscape 1.0 [49].

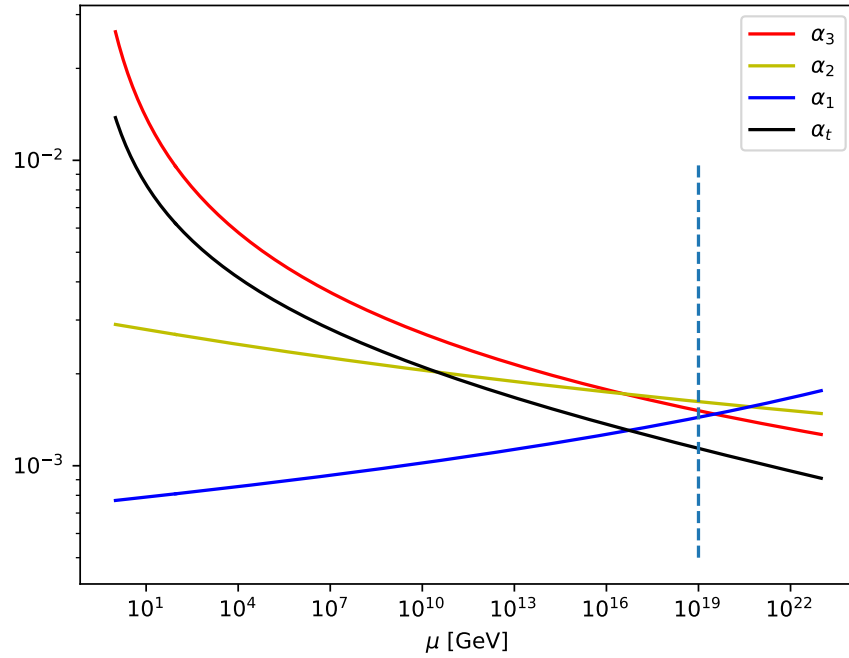


Figure 2.1: Running gauge and top Yukawa couplings of the SM as defined in (2.16) at two-loop gauge and one-loop Yukawa level. While α_3 , α_2 and α_t vanish in the far UV (asymptotic freedom), α_1 eventually runs into a pole (not seen in the plot), signaling the breakdown of the SM. At $\mu_{\text{conf}} \sim 0.2 \text{ GeV}$, the strong coupling evolves a confining pole. The existence of this pole is responsible for chiral symmetry breaking and the confinement of quarks. At $\mu \sim 10^{19} \text{ GeV}$ (blue dashed line), gravitational effects become significant.

2.2 Challenges within the Standard Model

In this section, we briefly discuss three remaining challenges within the SM, namely the absence of gravity, the absence of dark matter and the presence of Landau poles (also known as the triviality problem [7]).

We begin with the most striking evidence for the incompleteness of the SM, given by its inability to describe gravity. There have been many attempts to find consistent theories of quantum gravity, some of these given by string theory (for a beginners overview, see [54]), supergravity [55], and asymptotically safe quantized general relativity [56]. In the asymptotic safety scenario, all running couplings flow into a fixed point in the UV. Such theories are fundamental, even if they are not renormalizable (by power-counting), like gravity [12]. We have more to say on asymptotic safety in sec. 2.3.

The second challenge stems from cosmological observations suggesting that the measured dark matter energy density originates from new particles which are electrically neutral and colorless [57]. There is a plethora of models providing dark matter candidates. A model Peter Schuh and I worked on assumes a dark QCD-like sector described by a new $SU(N)_D$ gauge group with a dark matter candidate given as confined fermions purely charged under this new interaction. This model is briefly summarized in sec. 3.

While the absence of gravity and dark matter within the SM are of phenomenological nature, the last challenge of the SM we mention comes from theoretical considerations and constitutes the central motivation for our studies. It is given by the observation that the electric coupling diverges at the scale μ_{pole} . At two-loop level and with the SM matter content, this scale is given by [58]

$$\mu_{\text{pole}} \sim 10^{34} \text{ GeV} . \quad (2.17)$$

This Landau pole indicates the breakdown of the theory, known as the triviality problem [7], which is present even beyond perturbation theory [59]. Before electroweak symmetry breaking, this Landau pole is present in the $U(1)_Y$ hypercharge coupling. Hence, the SM on its own is not fundamental. One might argue that since this Landau pole lies way beyond the Planck scale ($\mu_{\text{Planck}} \approx 10^{19} \text{ GeV}$), gravitational effects have to be considered. Studies suggest that indeed AS gravity might solve the triviality problem [60]. Nevertheless, additional matter content lowers the scale at which this Landau pole appears and in some well-motivated extensions of the SM this scale appears below the Planck scale [58]. It has been demonstrated that the SM Landau pole can be cured by AS without including gravity [61, 62]. This thesis deals with the task of finding non-gravitational, asymptotically safe and supersymmetric extensions of the SM.

In the minimal supersymmetric version of the SM, there are Landau poles not only in the hypercharge coupling, but also in the weak $SU(2)_L$ coupling.

2.3 Asymptotic Safety

Originally put forward as a possibility for quantized general relativity to be fundamental and predictive despite being perturbatively non-renormalizable [12], asymptotic safety recently has been utilized as a model building tool for non-gravitational theories which are renormalizable in perturbation theory [61–65].

Asymptotic safety refers to the scenario for which running couplings obtain finite interacting fixed point values in the UV, generalizing the notion of asymptotic freedom for which couplings vanish in the UV [50–52, 66]. Running couplings take on different values at different energy scales μ

$$g_a = g_a(\mu) \tag{2.18}$$

and were introduced by Stückelberg and Petermann [67] and independently by Gell-Mann and Low [68] to improve perturbation theory. Perturbation theory is valid as long as these running couplings stay small. The perturbativity condition reads

$$|g_a| \leq 4\pi, \tag{2.19}$$

to also accommodate for loop-factors of $1/(4\pi)$. Taking infinitesimally small steps between energies μ and $\mu + d\mu$, the change of $g_a = g_a(\mu)$ can be described by using so-called beta functions

$$\frac{dg_a}{d \ln(\mu)} = \beta_a(g), \tag{2.20}$$

which depends on all the (massless) couplings g of the theory. Solving beta functions is equivalent to a resummation of log-factors which appear when non-running couplings are used. These log-factors spoil perturbation theory away from the scale at which the non-running coupling is measured, and the resummation extends the validity of perturbation theory. The set of operations which transform the physics from one energy scale to another constitute the so-called renormalization group.

In fig. 2.2, we illustrate evolutions of couplings which either run into a Landau pole, like in QED, become asymptotically free, like in QCD, or become asymptotically safe. In the last two cases, the change of the couplings has to decrease as a function of energy until this change becomes zero in the far UV, meaning that the couplings g^* reached in the far UV fulfill

$$0 = \left. \frac{dg_a}{d \ln(\mu)} \right|_{g=g^*} \stackrel{(2.20)}{=} \beta_a(g^*). \tag{2.21}$$

Points in coupling space fulfilling this condition are generally called fixed points and can be reached along different directions in coupling space either in the far UV ($\ln(\mu) \rightarrow \infty$) or the far IR ($\ln(\mu) \rightarrow -\infty$). Directions along which fixed points are reached in the UV are called “relevant” or “UV-attractive”, while directions reaching fixed points in the IR are called “irrelevant” or “IR-attractive”. The subspace of couplings flowing towards a fixed point in the UV is referred to as the critical surface, whose dimensionality specifies the number of independent model parameters. If the critical surface is finite dimensional, the model becomes predictive since only a finite amount of parameters have to be fixed experimentally. This is the reason why asymptotically safe quantized gravity (with a finite dimensional critical surface) becomes predictive despite having infinitely many Lagrangian terms due to its perturbative non-renormalizability. In fig. 2.3, we illustrate a sample renormalization group flow containing three fixed points G , FP_1 and FP_{12} in a space spanned by two couplings g_1 and g_2 , with arrows pointing towards the IR. For G , the g_1 direction is a relevant direction while g_2 corresponds to an irrelevant direction. Fixed point FP_1 is IR-attractive in the direction of g_1 and UV-attractive in a direction pointing towards FP_2 . The fully-interacting fixed point FP_{12} is completely IR-attractive.

A more modern view on running couplings and the renormalization group was developed by Wilson [13, 69] based on studies performed by Kadanoff [70] in the context of critical phenomena in condensed matter. From this point of view, the physical properties at an energy (or length) scale are obtained by averaging out the physics at larger energy (or smaller length) scales. This perspective is the basis of the functional renormalization group [71, 72], a non-perturbative renormalization group method largely utilized in modern studies of quantum gravity at different energy scales.

The existence of viable UV fixed points within pure quantized general relativity has been established in expansions around the critical spacetime dimension $d = 2 + \varepsilon$, where Newtons coupling has mass dimension $[G_N] = -\varepsilon$ [12, 73–75]. Quantum gravity coupled to N matter fields in the limit of large N also suggests the existence of physical UV fixed points [76–78].

Motivated by these findings in $2 + \varepsilon$ spacetime dimensions and for large numbers of matter fields, research interest in asymptotically safe quantum gravity increased [79–81] and remarkable progress was made over the last decades [82–86]. Applying functional renormalization methods, more evidence for the existence of UV fixed points in quantized gravity has been found. Studies involving the Einstein-Hilbert action [56, 87] as well as additional higher-derivatives implemented through functions $f(R)$ of the Ricci scalar R [88–95] suggest the existence of viable UV fixed points in pure quantized gravity with couplings of lower mass dimensionality being more irrelevant, implying that canonical mass ordering stays a valid ordering principle. The weak gravity conjecture states that

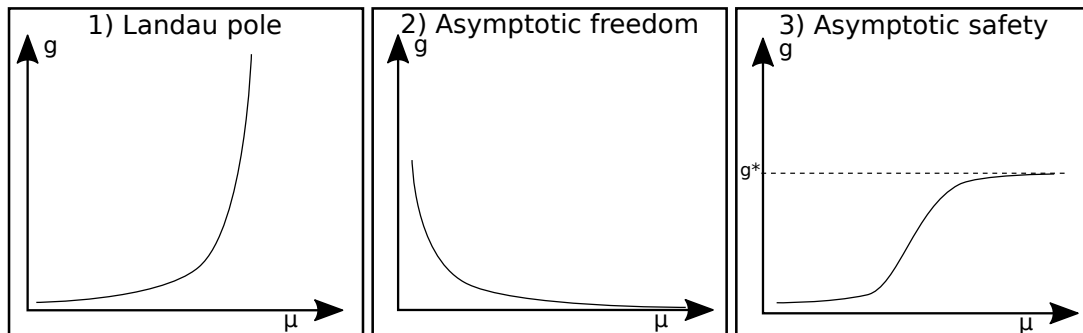


Figure 2.2: Three different cases of coupling evolutions. In the first case, the coupling runs into a Landau pole, indicating the breakdown of the theory. An example for a realistic theory having a Landau pole is quantum electrodynamics (see the blue curve in fig. 2.1). In the second case, known as asymptotic freedom, the coupling vanishes in the far UV, making the theory fundamental and perturbation theory valid at large energies. Quantum chromodynamics is an example for a realistic theory showing this behavior (red curve in fig. 2.1). The last case of asymptotic safety generalizes the concept of asymptotic freedom by letting couplings run into interacting fixed points in the UV. Such theories are, like asymptotically free theories, fundamental and predictive. Within the SM, asymptotic safety is absent. Quantized general relativity as a realistic theory is speculated to be asymptotically safe [12, 79, 80, 85, 86].

gravity stays the weakest force even in the far UV [96, 97]. Under this assumption, asymptotically safe gravity coupled to Yang-Mills theories (also including U(1) groups) without [98] and with matter [99] have been shown to become AF.

In this thesis, we focus on AS in the context of non-gravitational, fundamental SM extensions free from Landau poles. Studies of fermionic Gross-Neveu models in $d = 2 + \varepsilon$ dimensions [100, 101], in exactly $d = 3$ dimensions with a large number of fermions [102], and in up to $d = 4$ dimensions utilizing functional renormalization [103] all unveil physical UV fixed points. Also within pure $SU(N_C)$ Yang-Mills theories in $d = 4 + \varepsilon$ dimensions [104, 105] up to $d = 5$, viable UV fixed points were discovered, in agreement with functional renormalization studies [106]. For self-interacting $O(N)$ symmetric scalar field theories, the existence of an IR fixed point at dimension $d = 3$ has been confirmed beyond perturbation theory [107, 108] while for $d > 4$ UV fixed points seem to be absent [109]. The impact of assumed UV fixed points within the SM has been discussed in 1974 in [110]. About 40 years later, the existence of non-supersymmetric simple [63, 111] and semi-simple [64] gauge theories in exactly four spacetime dimensions has been established and guaranteed to all orders in perturbation theory within a large- N limit known as the Veneziano limit [112]. In this limit, certain degrees of freedom like the number of fields and gauge group dimensionalities go to

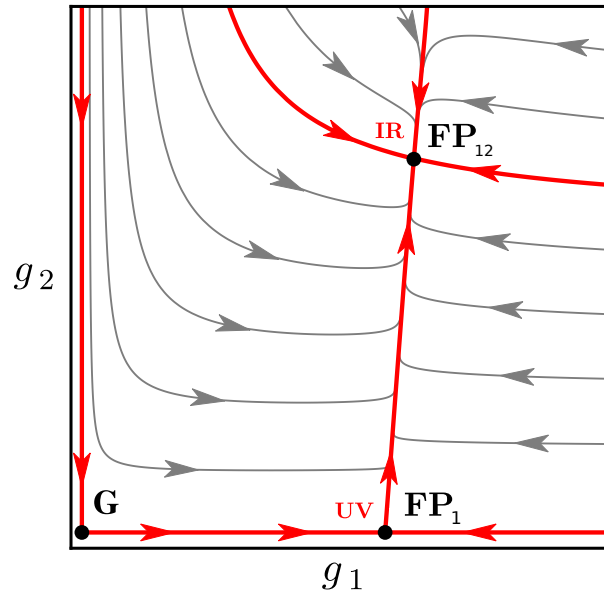


Figure 2.3: Illustration of a sample RG flow for two couplings g_1 and g_2 containing three fixed points G , FP_1 and FP_{12} . Arrows point towards the IR, making FP_{12} an IR fixed point. G is IR-attractive in the g_2 direction and UV-attractive in the direction of g_1 , while FP_1 is IR attractive in the direction of g_1 and UV-attractive in the direction of FP_{12} . This figure is taken from [65] with modifications on coupling and fixed point names.

infinity while specific ratios of these degrees of freedom stay constant, allowing to bring interacting fixed points arbitrarily close to the gaussian fixed point. Theorems for weakly interacting fixed points have been provided which imply that Yukawa interactions [113] and gauge interactions [114] are necessary for general gauge theories to admit UV fixed points. Hence scalars, fermions as well as gauge bosons are required to generate weakly interacting UV fixed points. Asymptotically safe and non-supersymmetric extensions of the SM have been constructed with new physics scales in the TeV-range [61, 62]. Furthermore, asymptotic safety recently has been utilized to naturally explain the anomalous magnetic moments of muons and electrons [115, 116].

In contrast to non-supersymmetric theories, supersymmetry strongly constraints the possibility of UV fixed points [117]. With supersymmetry, simple gauge groups do not allow for interacting UV fixed points [118] and semi-simple gauge groups are a necessity. For supersymmetric models, the existence of semi-simple AS models has been established within the Veneziano limit [65]. In section 5, we will discuss supersymmetric beta functions and limitations for the existence of weakly interacting fixed points.

2.4 Supersymmetry

Supersymmetry has been of greatest interest for the high energy community for some decades now. Even with the LHC lacking any evidence for it [10, 11], there is no decisive reason that nature is not supersymmetric at energies beyond the TeV-range. Due to its theoretical attractiveness, it still remains one of the most promising ways to extend the SM.

Supersymmetry is a symmetry relating fermions and bosons

$$Q|\text{fermion}\rangle = |\text{boson}\rangle, \quad Q|\text{boson}\rangle = |\text{fermion}\rangle, \quad (2.22)$$

with Q denoting its generator. For each fermion, there is a bosonic superpartner with same mass, charges and gauge representations, and vice versa. Since we have not observed any of these superpartners, supersymmetry must be broken in nature at some unknown energy scale. In this thesis, we find hints for this energy scale when imposing asymptotic safety and matching onto the SM.

From (2.22), we see that supersymmetry generators are fermionic and hence extend the Lorentz algebra. As shown by the combined efforts of Coleman and Mandula in 1967, and Haag, Łopuszański and Sohnius in 1975, supersymmetry in fact is the only possibility to extend Lorentz symmetry [119, 120]. Such uniqueness is very much desired for physical theories. The first supersymmetric model has been constructed by Wess and Zumino in 1974 and describes a free, massless Weyl fermion and a free, massless complex scalar [121]. Shortly after, supersymmetric gauge- as well as non-gauge interactions have been introduced [122].

Historically, the cancellation of non-logarithmic UV regulator divergences in the Higgs mass played a huge role in motivating low-scale supersymmetry. With SM superpartner masses in the range of at most some TeV, the enormous difference between the electroweak scale (~ 200 GeV) and the Planck scale ($\sim 10^{19}$ GeV) can be explained naturally. The larger the masses of SM superpartners, the more fine-tuning is necessary to explain this large discrepancy. This is known as the “hierarchy problem” which is more of a philosophical than a physical problem [123, 124]. Nevertheless, it can be argued that minimal supersymmetric SM extensions constrained by current experimental bounds still solve the hierarchy problem [125].

The superfield formalism allows for a suitable description of supersymmetric theories, where fermionic and bosonic degrees of freedom are treated simultaneously as components of superfields [126]. In section 4.1, we present in more detail how to construct supersymmetric Lagrangians in the superfield formalism. Furthermore, some powerful non-perturbative results like the non-renormalization theorem [127, 128] and exact

relations valid in superconformal field theories have been provided. We will address superconformal field theories in more detail in sec. 8. Other theoretically appealing features of supersymmetry are that in string theory, supersymmetry is a necessity, and that treating supersymmetry as a local symmetry yields supergravity. Both, string theory and supergravity, are candidates for consistent theories of quantum gravity.

When supersymmetry is imposed onto the SM, we obtain the MSSM. Each particle of the fields of tab. 2.1, as well as each gauge boson receives a superpartner. Due to the SM Higgs receiving a fermionic superpartner, gauge anomaly cancellation is spoiled unless we introduce a second scalar Higgs field and a second fermionic (Weyl) Higgs field with hypercharges of opposite signs relative to the SM Higgs. This second pair of Higgs fields is also needed to give masses to down-type quarks [129].

In summary, the (gauge-basis) particles of the MSSM are those of tab. 2.2. The bosonic spin-0 superpartners of the quarks and leptons are the squarks and sleptons and the fermionic spin-1/2 superpartners of the Higgs bosons are the higgsinos. Additionally to these particles, the MSSM contains the SM gauge bosons, as well as their fermionic spin-1/2 superpartners. Further details and features of the MSSM, like its non-gauge interactions, its mass spectrum and supersymmetry-breaking are provided in sec. 4.2.

Spin-0	Spin-1/2	Spin-1
squarks	quarks	-
$\tilde{Q} = (\tilde{u}_L, \tilde{d}_L)$	$Q = (u_L, d_L)$	-
\tilde{u}_R^*	u_R^\dagger	-
\tilde{d}_R^*	d_R^\dagger	-
sleptons	leptons	-
$\tilde{L} = (\tilde{\nu}, \tilde{e}_L)$	$L = (\nu_L, e_L)$	-
\tilde{e}_R^*	e_R^\dagger	-
higgses	higgsinos	-
$H_u = (H_u^+, H_u^0)$	$\tilde{H}_u = (\tilde{H}_u^+, \tilde{H}_u^0)$	-
$H_d = (H_d^0, H_d^-)$	$\tilde{H}_d = (\tilde{H}_d^0, \tilde{H}_d^-)$	-
-	photino	photon
-	$\tilde{\gamma}$	γ
-	gluinos	gluons
-	\tilde{g}	g
-	bino	B boson
-	\tilde{B}	B
-	winos	W bosons
-	\tilde{W}	W

Table 2.2: The gauge eigenstate particles of the MSSM. Each squark, quark, slepton and lepton comes in three flavors. The mass eigenstate spectrum is described in sec. 4.2.4.

Chapter 3

Dark QCD With UV Fixed Points

In this chapter, we briefly present a non-supersymmetric SM extension accompanied by an additional (“dark”) QCD-like $SU(3)_D$ sector [24]. For asymptotically safe candidates, particles beyond the SM are integrated out in such a way that bound states formed by QCD-like confining particles carrying only “dark” colors regarding $SU(3)_D$ obtain masses which explain the observed dark matter energy density.

3.1 Dark QCD

In our dark matter model, additionally to the strong $SU(3)_C$ sector, there is an additional dark $SU(3)_D$ sector, so that the gauge group is given by

$$G_{\text{DQCD}} = SU(3)_D \otimes SU(3)_C . \tag{3.1}$$

The SM particles are accommodated by further fermions and complex scalar matrices beyond the SM, presented in tab. 3.1.

Field	SU(3) _C	SU(3) _D	Flavor multiplicity
SM Quark	3	1	6
joint fermion Ψ_J	J_C	J_D	N_J
dark fermion Ψ_D	1	R_D	N_D
joint scalar S_J	1	1	$N_J \times N_J$
dark scalar S_D	1	1	$N_D \times N_D$

Table 3.1: Field content of our dark QCD model. Dirac fermions are highlighted in gray, while complex scalar matrices are not highlighted. The SM SU(3)_C singlets are not listed in this table.

This field content allows for Yukawa interactions

$$\mathcal{L}_{\text{Yuk}} = -y_J \text{Tr}(\bar{\Psi}_J S_J \Psi_J) - y_D \text{Tr}(\bar{\Psi}_D S_D \Psi_D) + \text{h.c.} , \quad (3.2)$$

with Tr implying sums over flavor and gauge indices.

As in previous work from Bai and Schwaller with focus on infrared fixed points, bound states of purely dark fermions are identified as dark matter candidates with an assumed number density comparable to ordinary baryonic matter [130]. Complementary to their study, we investigate dark QCD models with suitable UV fixed points. The confinement pole of the dark coupling $\alpha_D = |y_D|^2 / (4\pi)^2$, indicating masses of dark bound states, is set to appear at ~ 1 GeV to generate the observed dark matter energy density which is approximately five times larger than the visible baryonic energy density [131].

3.2 Benchmark

One asymptotically safe benchmark within the dark QCD framework described in the previous section is given by setting the parameters in tab. 3.1 to

$$N_J = 70 , N_D = 5 , \mathbf{J}_C = \mathbf{6} , \mathbf{J}_D = \mathbf{3} , \mathbf{R}_D = \mathbf{8} . \quad (3.3)$$

At two-loop gauge and one-loop Yukawa level, the fully interacting gauge-Yukawa fixed point

$$\text{GY} = (\alpha_3^*, \alpha_D^*, \alpha_{y_J}^*, \alpha_{y_D}^*) \equiv \left(\frac{g_3^{*2}}{(4\pi)^2}, \frac{g_D^{*2}}{(4\pi)^2}, \frac{|y_J|^{*2}}{(4\pi)^2}, \frac{|y_D|^{*2}}{(4\pi)^2} \right) \approx (0.24, 0.23, 0.07, 0.21) \quad (3.4)$$

is UV attractive in this benchmark. In fig. 3.1, we show a plot of the renormalization group flow in a $\alpha_3 - \alpha_D$ plane. Starting on the UV-safe trajectory (illustrated as a

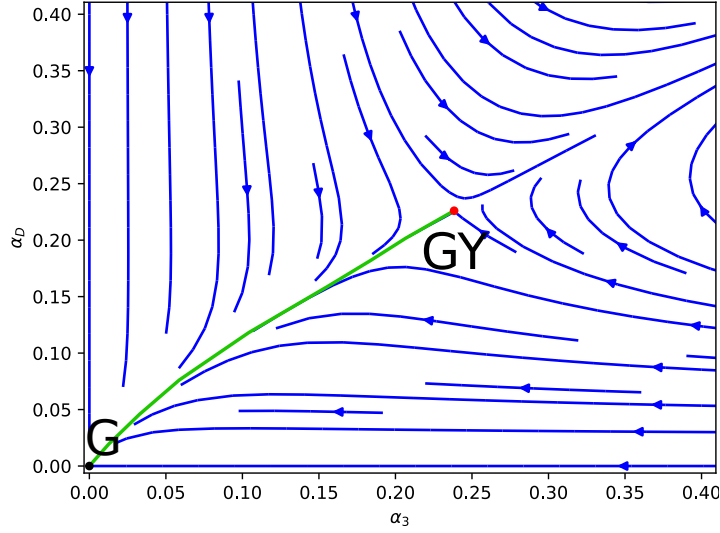


Figure 3.1: RG flow of the dark QCD benchmark given by the parameters in eq. (3.3) (see also tab. 3.1). At each point in this $\alpha_3 - \alpha_D$ plane, the Yukawa couplings α_J, α_D take on their nullcline values, determined by vanishing of their beta functions. Arrows point towards the IR. The green line shows the trajectory connecting GY in the UV with the gaussian fixed point G in the IR.

green curve in fig. 3.1) near GY, and flowing towards smaller energies, we eventually arrive at an energy corresponding to the mass M_J of the jointly charged fermions Ψ_J . At this point, these are integrated out. The evolution of the strong coupling α_3 is now as in the SM, allowing us to infer the value of M_J from α_3 at the point at which we integrate out the jointly charged fermions. At even smaller energies M_D , also the purely dark charged fermions Ψ_D are integrated out. Below this energy, the dark gluons drive the evolution of the dark coupling α_D , which obtains a confinement pole at μ_{conf} . The exact scale at which confinement appears is hard to estimate and setting this scale to μ_{conf} is a practical choice. This confinement pole is set by us to appear at $\mu_{\text{conf}} = 1 \text{ GeV}$ by the condition $\alpha_D(\mu_{\text{conf}}) = 1$, so that for a number density of the dark bound states comparable to that of baryonic bound states, the dark matter energy density is around five times larger than the QCD scale $\mu_{\text{QCD}} \sim 0.2 \text{ GeV}$ (see also fig. 2.1 for the SM running couplings).

In fig. 3.2, we present a sample evolution of the dark coupling α_D with $M_J \sim 36 \times 10^3 \text{ GeV}$ and $M_D \sim 429 \text{ GeV}$. In general, $M_J \neq M_D$ is needed since otherwise M_J appears at energies already well-probed at the LHC, in conflict with the non-observation of the jointly charged fermions Ψ_J .

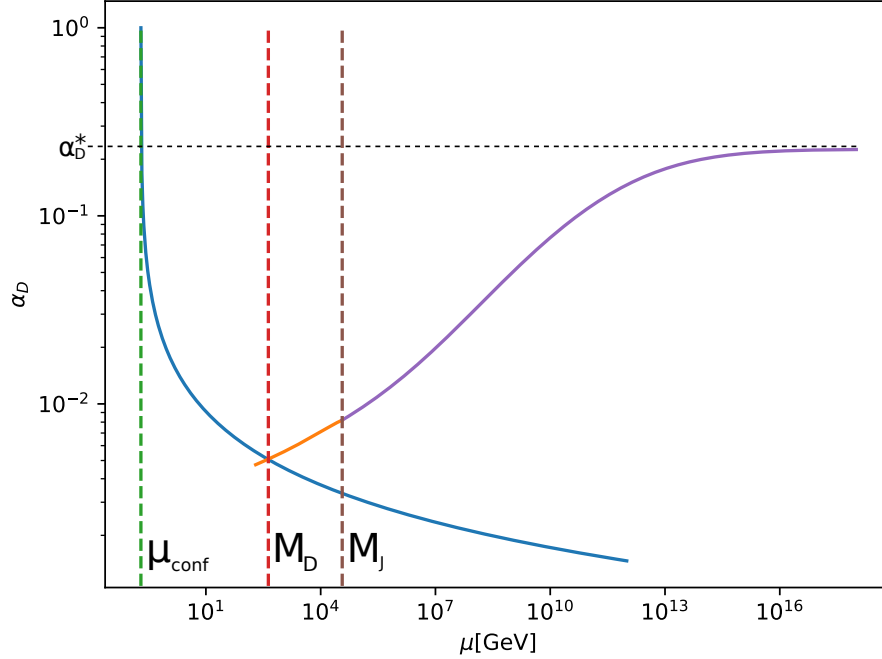


Figure 3.2: Evolution of the dark coupling α_D (blue, orange and purple curves) in the dark QCD benchmark given by the parameters of eq. (3.3) (see also tab. 3.1). Beginning in the far UV near fixed point GY of (3.4), α_D becomes smaller towards smaller energies. At $M_J \sim 36 \times 10^3$ GeV, the jointly charged fermions Ψ_J are integrated out, while the masses of the purely dark charged fermions Ψ_D is given by M_D . At $\mu_{\text{conf}} = 1$ GeV, α_D becomes one, and the confinement pole appears. Near this confinement pole, dark bound states have their masses. The value of μ_{conf} is chosen such that it is five times larger than the QCD confinement scale $\mu_{\text{QCD}} \sim 0.2$ GeV (see fig. 2.1 for the SM coupling evolutions).

3.3 Phenomenology

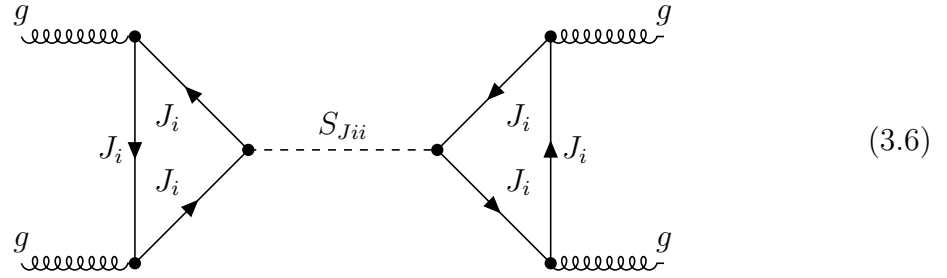
My main contribution to this work is the section on collider signatures, where we set constraints on masses and representations derived from experimental data. To be more specific, we utilize the experimentally measured evolution of the strong coupling, R -hadron signals [132], resonant dijet production and monojets plus missing energy signatures. While the first three of these allow to set a lower bound on the joint fermion mass M_J , monojet plus missing energy signatures turn out to give a handle on allowed field representations.

From the evolution of the strong coupling [133–135], we immediately infer

$$M_J \gtrsim 1.5 \text{ TeV} . \quad (3.5)$$

The mass bounds obtained from non-observation of R -hadrons, long-lived bound states formed by visible and dark partons, depends on the representation of Ψ_J under G_{DQCD} . In tab. 3.2, some of these mass bounds for different representations are stated, inferred by reinterpreting experimental constraints for R -hadrons formed by stable gluinos stated to be heavier than $\sim 1.7 \text{ TeV}$ [136, 137].

Resonant dijet production in our models is assumed to be dominated by the process (3.6), yielding the allowed parameter space shown in fig. 3.3 when compared to experimental data from ATLAS [138].



$M_J^{\text{min}}[\text{TeV}]$	$\mathbf{J}_D = \mathbf{3}$	$\mathbf{J}_D = \mathbf{6}$	$\mathbf{J}_D = \mathbf{8}$	$\mathbf{J}_D = \mathbf{10}$	$\mathbf{J}_D = \mathbf{15}$	$\mathbf{J}_D = \mathbf{15}'$
$\mathbf{J}_C = \mathbf{1}$	1.3	1.7	1.7	2.0	2.0	2.2
$\mathbf{J}_C = \mathbf{3}$	1.5	1.9	1.9	2.2	2.2	2.4

Table 3.2: Lower bounds on the joint fermion mass M_J in the case of $N_J = 1$ (Dirac) joint fermion for different representations $(\mathbf{J}_C, \mathbf{J}_D)$ under $(\text{SU}(3)_C, \text{SU}(3)_D)$. These bounds are inferred from bounds on R -hadron signals with gluinos as their long-lived colored BSM partons, here reinterpreted for long-lived joint fermions Ψ_J . The mass bounds are adopted from [61].

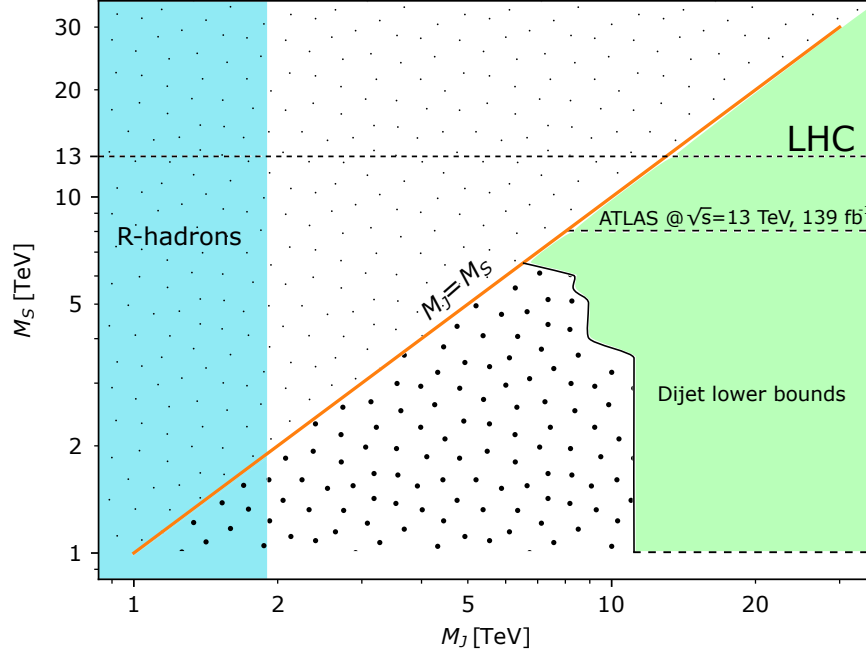
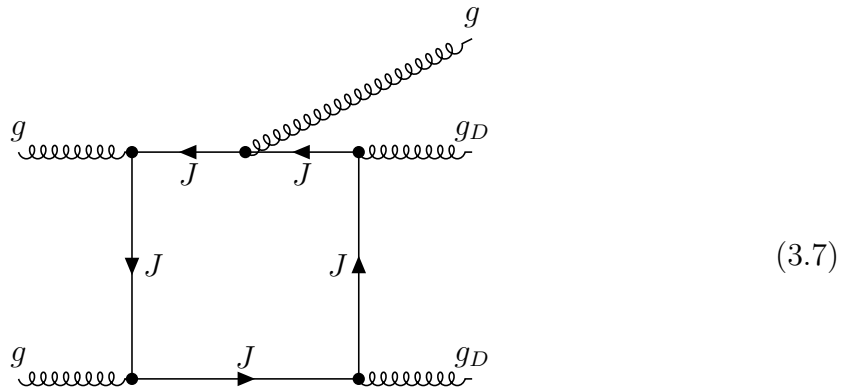


Figure 3.3: Available parameter space (green) according to the 95% C.L. upper limit for BSM contributions to dijet productions stated by ATLAS [138]. Parameter space left to the dijet lower bounds curve, marked by thick black dots, is excluded by ATLAS. The region marked by small black dots is outside of the scope of our models. Up to $M_J \sim 1.9$ TeV (shown in light blue), the parameter space is excluded by R -hadron searches. The green region above 8 TeV is unprobed.

In our dark QCD model, monojet plus missing energy signatures are dominated by the Feynman diagram (3.7).



For the total cross-section at a center of mass energy $\sqrt{s} = 13 \text{ TeV}$, we estimate

$$\sigma_{\text{tot}} \approx 7.4 \times 10^{-9} \text{ GeV}^{-2} \cdot X , \quad (3.8)$$

where

$$X \equiv N_J^2 S_2(J_C)^2 S_2(J_D)^2 \alpha_D(M_J)^2 . \quad (3.9)$$

The cross-section (3.8) turns out to be explicitly independent of the mass M_J , giving a handle on the allowed representations and dark coupling strengths. Only indirectly, through $\alpha_D(M_J)$, the mass of Ψ_J enters in this cross-section. Due to the exponential dependency of M_J on the values of α_D , bounds on M_J obtained in this way are not to be trusted.

Experimental data taken at ATLAS corresponding to a data set with luminosity 36.1 fb^{-1} states an upper limit of 531 fb on the total cross-section (3.8) [139], translating into

$$X \lesssim 0.18 . \quad (3.10)$$

Assuming that statistical uncertainties for the number of events N scale with $1/\sqrt{N}$, we find that at $\sqrt{s} = 13 \text{ TeV}$, the upper bound on X scales with the luminosity L like

$$X \lesssim 0.18 \left(\frac{36.1 \text{ fb}^{-1}}{L} \right)^{\frac{2}{3}} . \quad (3.11)$$

In fig. 3.4, we have plotted these upper limits on X , together with an orange dashed line indicating the current ATLAS luminosity of 36.1 fb^{-1} and the green dashed line at ten times larger L , achievable by the HL-LHC in 2027. At this luminosity of $L = 361 \text{ fb}^{-1}$, X is bounded from above by ~ 0.006 . Hence, ten times larger luminosity translates into an upper bound on X which is 2000 times lower. From the plot 3.4, we also see that beyond the luminosity of the HL-LHC, upper bounds do change much less significantly. Beyond this point, increasing the center of mass energy is preferred over increasing luminosity.

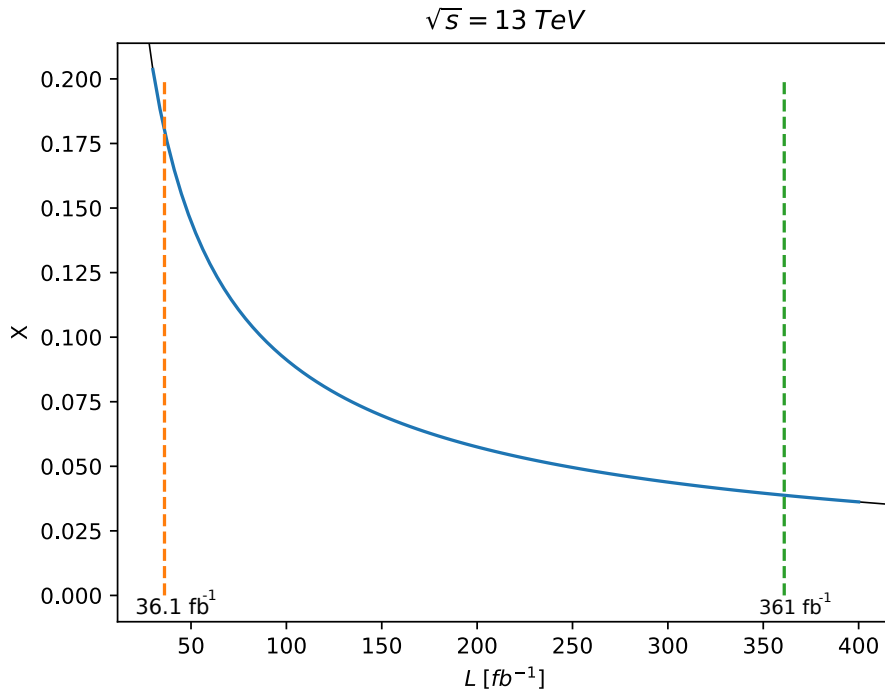


Figure 3.4: Based on the upper limit for $X = N_J^2 S_2(J_C)^2 S_2(J_D)^2 \alpha_D (M_J)^2$ at the LHC luminosity corresponding to a data set of 36.1 fb^{-1} (orange dashed line), we estimate the upper limit on X for other luminosities. In 2027, the HL-LHC is expected to operate at ten times larger luminosities which would yield $X \lesssim 0.006$ (green dashed line).

Chapter 4

Supersymmetry Basics

In this presentation of the very basics of supersymmetry, we at first give general recipes on how to construct supersymmetric models. Next, the minimal Supersymmetric Standard model, the MSSM, and the supersymmetry-breaking scenario known as “gauge-mediated supersymmetry-breaking” are presented. Finally, the mass spectrum of the MSSM gets discussed. Everything shown in this chapter can be found in standard literature on supersymmetry (e.g. [140, 141]).

4.1 Constructing Supersymmetric Theories

As mentioned in sec. 2.4, supersymmetric theories are best described in terms of superfields. Superfields are functions of superspace coordinates

$$\{x^\mu, \theta, \theta^\dagger\}, \quad (4.1)$$

where x^μ are the usual (bosonic) spacetime degrees of freedom and θ, θ^\dagger are newly introduced, two-component (Weyl-spinor) degrees of freedom satisfying the anti-commutator relations

$$\{\theta^\alpha, \theta_{\dot{\alpha}}^\dagger\} = \{\theta^\alpha, \theta^\alpha\} = \{\theta_{\dot{\alpha}}^\dagger, \theta_{\dot{\alpha}}^\dagger\} = 0 \quad (\alpha, \dot{\alpha} = 1, 2). \quad (4.2)$$

These fermionic superspace coordinates are used to mathematically formulate supersymmetric theories and are not physical extra dimensions.

Due to the anti-commutation relations (4.2), Taylor expanding a general superfield

$$S = S(x^\mu, \theta^\alpha, \theta_{\dot{\alpha}}^\dagger) \quad (4.3)$$

with respect to the fermionic superspace coordinates yields only finite terms with spacetime-dependent coefficients. These coefficients have different statistics and constitute usual quantum fields. Imposing further constraints on general superfields (4.3)

yields different types of superfields with which different quantum fields can be described. We are interested in two kinds of superfields, namely chiral- and vector superfields.

Before we present these two kinds of superfields, we have to set up some notation. The index assignment for Spin-1/2 Weyl spinors χ (like the fermionic superspace coordinates) with $\alpha, \dot{\alpha} \in \{1, 2\}$, is

$$\text{left-handed } (1/2, 0) : \chi_\alpha, \quad \text{right-handed } (0, 1/2) : \chi^{\dagger\dot{\alpha}}. \quad (4.4)$$

Anti-left-handed and anti-right-handed Weyl spinors are denoted by switching the height of the indices:

$$\text{anti-left-handed} : \chi^\alpha, \quad \text{anti-right-handed } (0, 1/2) : \chi_{\dot{\alpha}}^\dagger. \quad (4.5)$$

With the epsilon tensors

$$\varepsilon^{12} = -\varepsilon^{21} = \varepsilon_{21} = -\varepsilon_{12} = 1, \quad \varepsilon^{11} = \varepsilon^{22} = \varepsilon_{11} = \varepsilon_{22} = 0. \quad (4.6)$$

Weyl spinors and anti-Weyl spinors are connected via

$$\chi^\alpha = \varepsilon^{\alpha\beta} \chi_\beta, \quad \chi_\alpha = \varepsilon_{\alpha\beta} \chi^\beta, \quad \chi_{\dot{\alpha}}^\dagger = \varepsilon_{\dot{\alpha}\dot{\beta}} \chi^{\dagger\dot{\beta}}, \quad \chi^{\dagger\dot{\alpha}} = \varepsilon^{\dot{\alpha}\dot{\beta}} \chi_{\dot{\beta}}^\dagger. \quad (4.7)$$

We use the Einstein summation convention so that in (4.7) a sum over the β indices is implied. Products with suppressed indices of two Weyl spinors χ and ξ are defined as

$$\chi\xi = \chi^\alpha \xi_\alpha = \chi^\alpha \varepsilon_{\alpha\beta} \xi^\beta = \xi^\beta \chi_\beta = \xi\chi, \quad \chi^\dagger \xi^\dagger = \chi_{\dot{\alpha}}^\dagger \xi^{\dagger\dot{\alpha}} = \chi_{\dot{\alpha}}^\dagger \varepsilon^{\dot{\alpha}\dot{\beta}} \xi_{\dot{\beta}}^\dagger = \xi_{\dot{\beta}}^\dagger \chi^{\dagger\dot{\beta}} = \xi^\dagger \chi^\dagger. \quad (4.8)$$

In the same way we define contractions of electroweak $SU(2)_L$ gauge indices later on in our study of AS MSSM extensions.

Furthermore, we define

$$\sigma^\mu = (1, \vec{\sigma}), \quad \bar{\sigma}^\mu = (1, -\vec{\sigma}), \quad (4.9)$$

with $\vec{\sigma}$ the three-vector composed by the Pauli matrices

$$\sigma^1 = \begin{pmatrix} 0 & 1 \\ 1 & 0 \end{pmatrix}, \quad \sigma^2 = \begin{pmatrix} 0 & -i \\ i & 0 \end{pmatrix}, \quad \sigma^3 = \begin{pmatrix} 1 & 0 \\ 0 & -1 \end{pmatrix}. \quad (4.10)$$

The index assignments to σ^μ and $\bar{\sigma}^\mu$ are

$$(\sigma^\mu)_{\alpha\dot{\alpha}}, \quad (\bar{\sigma}^\mu)^{\dot{\alpha}\alpha}. \quad (4.11)$$

We now have everything together to continue with our presentation of chiral- and vector superfields and the construction of supersymmetric Lagrangians. Chiral superfields Φ are decomposed into

$$\begin{aligned} \Phi(x, \theta, \theta^\dagger) = & \phi(x) + i\theta^\dagger \bar{\sigma}^\mu \theta \partial_\mu \phi(x) + \frac{1}{4} \theta \theta^\dagger \theta^\dagger \partial_\mu \partial^\mu \phi(x) + \sqrt{2} \theta \psi(x) \\ & - \frac{i}{\sqrt{2}} \theta \theta^\dagger \bar{\sigma}^\mu \partial_\mu \psi(x) + \theta \theta F(x) , \end{aligned} \quad (4.12)$$

and their complex conjugates are

$$\begin{aligned} \Phi^*(x, \theta, \theta^\dagger) = & \phi^*(x) - i\theta^\dagger \bar{\sigma}^\mu \theta \partial_\mu \phi^*(x) + \frac{1}{4} \theta \theta^\dagger \theta^\dagger \partial_\mu \partial^\mu \phi^*(x) + \sqrt{2} \theta^\dagger \psi^\dagger(x) \\ & - \frac{i}{\sqrt{2}} \theta^\dagger \theta^\dagger \theta \sigma^\mu \partial_\mu \psi^\dagger(x) + \theta^\dagger \theta^\dagger F^*(x) . \end{aligned} \quad (4.13)$$

Chiral superfields Φ are called left-handed while superfields Φ^* are called right-handed due to their SUSY transformation properties. A closer look into eq. (4.12) and (4.13) shows that besides the complex scalar ϕ and the Weyl fermion ψ , we also have an additional complex scalar F . This auxiliary field allows to use chiral superfields whether they are on-shell or off-shell, since the supersymmetry algebra closes also off-shell as required for path integrals. When constructing Lagrangians below, there will be no kinetic terms for F so that it is allowed to always let F satisfy its classical equation of motions. We also introduce the notation

$$[\Phi]_F = F . \quad (4.14)$$

It is standard to refer to F as the ‘‘F-term’’ of Φ .

Vector superfields V fulfill $V = V^*$ and read

$$V(x, \theta, \theta^\dagger) = \theta^\dagger \bar{\sigma}^\mu \theta A_\mu + \theta^\dagger \theta^\dagger \theta \lambda + \theta \theta^\dagger \lambda^\dagger + \frac{1}{2} \theta \theta^\dagger \theta^\dagger D , \quad (4.15)$$

with A_μ and D complex scalars and λ and λ^\dagger Weyl spinors. The role of D is similar to that of F in (4.12). We define

$$[V]_D = \frac{1}{2} D \quad (4.16)$$

as the ‘‘D-term’’ of V .

We now come to the construction of supersymmetric Lagrangians. The simplest supersymmetric model, first presented by Wess and Zumino as already teased in sec. 2.4, is given by one chiral superfield Φ and the Lagrangian

$$\mathcal{L}_{\text{Wess}} = [\Phi^* \Phi]_D = -\partial^\mu \phi^* \partial_\mu \phi + i\psi^\dagger \bar{\sigma}^\mu \partial_\mu \psi + F^* F + \dots , \quad (4.17)$$

where the dots “...” imply total derivatives, not contributing to the action. This is a theory of a free and massless Weyl-fermion and a free and massless complex scalar.

Supersymmetric models of chiral superfields Φ_i with non-gauge interactions are given by Lagrangians of the form

$$\mathcal{L}_{\text{non-gauge}} = [\Phi_i^* \Phi_i]_D + ([W(\Phi)]_F + \text{c.c.}) , \quad (4.18)$$

where the so-called superpotential $W = W(\Phi)$ is a holomorphic function of only left-handed chiral superfields. For a model of one chiral superfield Φ with the superpotential

$$W = \frac{1}{2}m\Phi\Phi + \frac{1}{6}y\Phi\Phi\Phi , \quad (4.19)$$

we obtain the supersymmetric Lagrangian

$$\begin{aligned} \mathcal{L}_W = \mathcal{L}_{\text{Wess}} - \underbrace{\left(m^2\phi^*\phi + \frac{1}{2}my^*\phi\phi^*\phi^* + \frac{1}{2}m^*y\phi^*\phi\phi + \frac{1}{4}yy^*\phi\phi\phi^*\phi^* \right)}_{=U(\phi)} \\ - \frac{1}{2} \left(m\psi\psi + y\phi\psi\psi + \text{h.c.} \right) , \end{aligned} \quad (4.20)$$

with U being the scalar potential. This Lagrangian demonstrates the remarkable feature of supersymmetric theories that the quartic (and trilinear) scalar couplings are related to Yukawa and bilinear couplings. These relations are responsible for the cancellation of non-logarithmic UV regulator divergences in the Higgs mass, which played a huge role in the history of supersymmetry as a solution to the hierarchy problem as discussed in sec. 2.4. Furthermore, this feature allows to calculate Higgs masses in supersymmetric theories. Within the MSSM, the upper bound on the lightest Higgs mass is in agreement with the measured value of the SM Higgs [142].

In order to describe gauge interactions with vector superfields V^a belonging to a gauge group

$$G = \prod_a G_a \quad (4.21)$$

with generators T^a and gauge couplings g_a , the kinetic D -term in the Lagrangian $\mathcal{L}_{\text{non-gauge}}$ (4.18) is modified to account for interactions between the components of chiral and gauge vector superfields. For this, it is convenient to define the matrix

$$V_i^j = 2g_a T_i^{aj} V^a . \quad (4.22)$$

The modified kinetic D -term is then given by

$$\begin{aligned} \left[\Phi_i^* (\exp(2gt^a V^a))_i^j \Phi_j \right]_D = - \nabla_\mu \phi_i^* \nabla^\mu \phi_i + i\psi_i^\dagger \bar{\sigma}^\mu \nabla_\mu \psi_i - \sqrt{2}g(\phi_i^* t^a \psi_i) \lambda_a \\ - \sqrt{2}g\lambda_a^\dagger (\psi_i^\dagger t^a \phi_i) + F_i^* F_i + g(\phi_i^* t^a \phi_i) D^a . \end{aligned} \quad (4.23)$$

In order to describe self-interactions of vector superfield components, a chiral superfield field strength tensor $\mathcal{W}^{a\alpha}$ is introduced such that we obtain the SUSY invariant F -term

$$\sum_a [\mathcal{W}^{a\alpha} \mathcal{W}_\alpha^a]_F = \sum_a \left[D^a D^a + 2i\lambda^a \sigma^\mu \nabla_\mu \lambda^{\dagger a} - \frac{1}{2} F^{a\mu\nu} F_{\mu\nu}^a + \frac{i}{4} \varepsilon^{\mu\nu\rho\sigma} F_{\mu\nu}^a F_{\rho\sigma}^a \right], \quad (4.24)$$

with $F_{\mu\nu}^a$ the usual field strength tensor known from non-supersymmetric Yang-Mills theories.

Combining the modified D-term (4.23) with gauge self-interactions (4.24), and allowing for further non-gauge interactions via a superpotential W , we obtain the general supersymmetric Lagrangian

$$\mathcal{L} = \left[\Phi_i^* (\exp(2gt^a V^a))_i^j \Phi_j \right]_D + \frac{1}{4} \sum_a ([\mathcal{W}^{a\alpha} \mathcal{W}_\alpha^a]_F + \text{c.c.}) + ([W(\Phi_i)]_F + \text{c.c.}) . \quad (4.25)$$

4.2 The MSSM and its Features

4.2.1 Superfields and superpotential of the MSSM

In the MSSM, each SM field of tab. 2.1 resides within a chiral superfield, together with their superpartners. As discussed in sec. 2.4, an additional chiral Higgs superfield with hypercharge opposite to the SM Higgs is needed to cancel gauge anomalies. Furthermore, each SM gauge boson field becomes a component of a vector superfield, together with their gaugino superpartners. We then have for the MSSM the particles of tab. 2.2, residing in the left-handed chiral superfields of tab. 4.1, and its gauge group is given by the SM gauge group

$$G_{\text{MSSM}} = G_{\text{SM}} = \text{SU}(3)_C \otimes \text{SU}(2)_L \otimes \text{U}(1)_Y . \quad (4.26)$$

To obtain the MSSM, not only supersymmetry together with anomaly-cancellation is imposed onto the SM, but also R -parity [132, 143] given by the global $\text{U}(1)$ operations

$$P_R = (-1)^{3(B-L)+2s} , \quad (4.27)$$

where B , L , and s denote baryon number, lepton number and spin, respectively. If R -parity is conserved, the lightest supersymmetric particle is stable and may serve as a dark matter candidate [144]. The superpotential of the MSSM (defined as being R -parity conserving) reads

$$W_{\text{MSSM}} = Y_u^{ij} \bar{u}_i Q_j H_u + Y_d^{ij} \bar{d}_i Q_j H_d + Y_e^{ij} \bar{e}_i L_j H_d + \mu H_u H_d , \quad (4.28)$$

(Left-handed) Superfield	$SU(3)_C$	$SU(2)_L$	$U(1)_Y$	Flavor multiplicity
quark doublet Q	$\mathbf{3}$	$\mathbf{2}$	$+\frac{1}{6}$	3
up-quark \bar{u}	$\bar{\mathbf{3}}$	$\mathbf{1}$	$-\frac{2}{3}$	3
down-quark \bar{d}	$\bar{\mathbf{3}}$	$\mathbf{1}$	$+\frac{1}{3}$	3
lepton doublet L	$\mathbf{1}$	$\mathbf{2}$	$-\frac{1}{2}$	3
lepton singlet \bar{e}	$\mathbf{1}$	$\mathbf{1}$	$+1$	3
up-Higgs H_u	$\mathbf{1}$	$\mathbf{2}$	$+\frac{1}{2}$	1
down-Higgs H_d	$\mathbf{1}$	$\mathbf{2}$	$-\frac{1}{2}$	1

Table 4.1: Left-handed chiral superfield content of the MSSM and their representation under the MSSM gauge group G_{MSSM} of eq. (4.26).

where gauge indices are suppressed, and sums over $i, j = 1, 2, 3$ relate to the flavor degrees of freedom. In this work, we are mostly interested in the case where the Yukawa matrices \mathbf{Y}_e , \mathbf{Y}_u and \mathbf{Y}_d in (4.28) are approximated by $\mathbf{Y}_e \approx 0$, $\mathbf{Y}_u \approx \text{diag}(0, 0, y_t)$, $\mathbf{Y}_d \approx \text{diag}(0, 0, y_b)$ with y_t and y_b denoting the top and bottom Yukawa couplings, respectively. The μ -term is a mass term and does not play any role in the high energy limit of the theory and can be ignored in our study. We therefore retain only the following terms of the MSSM superpotential

$$W_{\text{MSSM}} \approx y_t \bar{u}_3 Q_3 H_u + y_b \bar{d}_3 Q_3 H_d. \quad (4.29)$$

We include this approximation of the MSSM superpotential in our searches for asymptotically safe MSSM extensions of sec. 6. If R -parity is omitted, we obtain the R -parity violating MSSM (RPV MSSM), with the superpotential

$$\begin{aligned} W_{\text{RPV}} = & W_{\text{MSSM}} \\ & + \lambda^{ijk} \bar{d}_i Q_j L_k + \frac{1}{2} \lambda^{ijk} L_i L_j \bar{e}_k + \mu^i L_i H_u \\ & + \frac{1}{2} \lambda'^{ijk} \bar{u}_i \bar{d}_j \bar{d}_k. \end{aligned} \quad (4.30)$$

The first line of (4.30) is the MSSM superpotential, the terms in the second line change lepton number by $\Delta L = 1$ and the term in the third line changes baryon number by $\Delta B = 1$. The μ' term is a mass term, irrelevant in the high energy limit. We see that violation of R -parity results in lepton and baryon number violating processes like the proton decay. Due to the non-observation of such processes, either the λ , λ' , μ' and λ'' couplings in (4.30) have to be small or superpartner masses are large [143, 145–150].

4.2.2 Soft supersymmetry-breaking

The experimental absence of SM superpartners requires supersymmetry to be broken in nature. There are many ways of breaking supersymmetry and the results depend on the explicit supersymmetry-breaking mechanism.

All of these different supersymmetry-breaking mechanisms can be treated in a model-independent way by introducing effective supersymmetry-breaking terms. To restore supersymmetry at high energies, these terms need to be “soft”, i.e. they have to have mass dimensionalities smaller than four. In the MSSM, the general soft supersymmetry-breaking terms are

$$\begin{aligned}
\mathcal{L}_{\text{soft}}^{\text{MSSM}} = & -\frac{1}{2}(M_3\tilde{g}\tilde{g} + M_2\tilde{W}\tilde{W} + M_1\tilde{B}\tilde{B} + \text{h.c.}) \\
& -(\tilde{u}\mathbf{a}_u\tilde{Q}H_u - \tilde{d}\mathbf{a}_d\tilde{Q}H_d - \tilde{e}\mathbf{a}_e\tilde{L}H_d + \text{h.c.}) \\
& -\tilde{Q}^\dagger\mathbf{m}_Q^2\tilde{Q} - \tilde{L}^\dagger\mathbf{m}_L^2\tilde{L} - \tilde{u}m_{\tilde{u}}^2\tilde{u}^\dagger - \tilde{d}m_{\tilde{d}}^2\tilde{d}^\dagger - \tilde{e}m_{\tilde{e}}^2\tilde{e}^\dagger \\
& -m_{H_u}^2H_u^*H_u - m_{H_d}^2H_d^*H_d - (bH_uH_d + \text{h.c.}) .
\end{aligned} \tag{4.31}$$

Note that in (4.31), there are no superfields present. The parameters M_3 , M_2 and M_1 are gaugino, bino and wino mass parameters, respectively. In the second line of (4.31), we have trilinear scalar interactions involving 3×3 matrices in flavor space. The third line consists of squark and slepton mass terms, while the last line of (4.31) displays contributions to the Higgs potential. The parameter b is necessary in order to achieve electroweak symmetry-breaking.

In the subsequent section, we introduce a supersymmetry breaking mechanism known as “gauge-mediated supersymmetry breaking”.

4.2.3 Gauge-mediated supersymmetry-breaking

The idea of gauge-mediated SUSY-breaking (GMSB) [151, 152] is to introduce a singlet chiral superfield S which couples to some “messenger” superfields via Yukawa interactions. In the most simplest gauge-mediated scenario, the chiral messenger superfields

$$S(\mathbf{1}, \mathbf{1}, \mathbf{1})_0, \quad L_4(\mathbf{1}, \mathbf{1}, \mathbf{2})_{-1/2}, \quad \bar{L}_4(\mathbf{1}, \mathbf{1}, \bar{\mathbf{2}})_{+1/2}, \quad q_4(\mathbf{1}, \mathbf{3}, \mathbf{1})_{-1/3}, \quad \bar{q}_4(\mathbf{1}, \bar{\mathbf{3}}, \mathbf{1})_{+1/3}, \tag{4.32}$$

with gauge charges $(\text{SU}(N), \text{SU}(3)_C, \text{SU}(2)_L)_Y$ are introduced. These fields are used to form new superpotential terms

$$W_{\text{GMSB}} = y_l S L_4 \bar{L}_4 + y_q S q_4 \bar{q}_4. \tag{4.33}$$

The superfield S participates in a superpotential which spontaneously breaks supersymmetry such that the scalar component as well as the F term of S acquire VEVs $\langle S \rangle$ and $\langle F_S \rangle$, respectively.

The VEVs $\langle S \rangle$ and $\langle F_S \rangle$ generate masses of the messenger particles at tree-level

$$m_f^{\text{fermion}} = m_{\bar{f}}^{\text{fermion}} = |y_f \langle S \rangle|, \quad m_{f,\bar{f}}^{\text{scalar}} = \sqrt{|y_f \langle S \rangle|^2 \pm |y_f \langle F_S \rangle|}, \quad (4.34)$$

where $f \in \{L_4, q_4\}$. At one-loop level, we have for the soft supersymmetry-breaking gluino, wino and bino mass parameters

$$M_3 = \alpha_3 \left| \frac{\langle F_S \rangle}{\langle S \rangle} \right|, \quad M_2 = \alpha_2 \left| \frac{\langle F_S \rangle}{\langle S \rangle} \right|, \quad M_1 = \alpha_1 \left| \frac{\langle F_S \rangle}{\langle S \rangle} \right|, \quad (4.35)$$

while the masses of the gauge bosons are protected by gauge symmetry such that they vanish to all orders. A Feynman diagram contributing to gaugino masses is depicted in fig. 4.1. At two-loop level, non-messenger soft scalar mass parameters are given by

$$m_{s_i}^2 = 2 \frac{\langle F_S \rangle^2}{\langle S \rangle^2} \left[C_3(i) \alpha_3^2 + C_2(i) \alpha_2^2 + C_1(i) \alpha_1^2 \right]. \quad (4.36)$$

The Feynman diagram 4.2 illustrates a contribution to these scalar mass parameters.

Eqs. (4.34), (4.35), and (4.36) hold at an energy scale given by the averaged masses of the messenger particles μ_{mess} and are only valid if the fermionic and scalar components of the messenger superfields have approximately the same masses

$$m_f^{\text{fermion}} \approx m_f^{\text{scalar}} \approx m_{\bar{f}}^{\text{scalar}} \equiv m_{\text{mess}}, \quad (4.37)$$

i.e., according to (4.34), for

$$|y_f \langle S \rangle|^2 \gg |y_f \langle F_S \rangle|. \quad (4.38)$$

Note that $\langle F_S \rangle = 0$ also achieves this goal but in this case there is no SUSY-breaking.

We see from eqs. (4.35) and (4.36) that, at least at the RG scale μ_{mess} , the masses of gauginos and sfermions are of the same order μ_{MSSM} . It is expected, that

$$\mu_{\text{mess}} \gg \mu_{\text{MSSM}}. \quad (4.39)$$

4.2.4 Mass spectrum of the MSSM

In this presentation of the non-SM mass spectrum of the MSSM, we begin with a short remark on electroweak symmetry-breaking. The scalar potential of the Higgs doublets

$$H_u = (H_u^+, H_u^0), \quad H_d = (H_d^0, H_d^-) \quad (4.40)$$

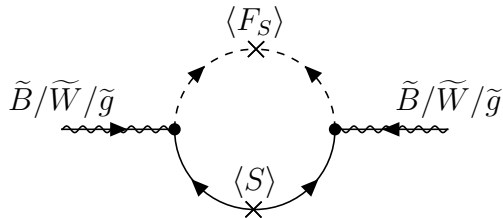


Figure 4.1: One-loop contribution to gaugino masses (4.35) with messenger fermions and scalars running in the loop. Fermionic lines with wavy lines on them represent gauginos. Gaugino-fermion-scalar vertices are provided in the Lagrangian (4.23).

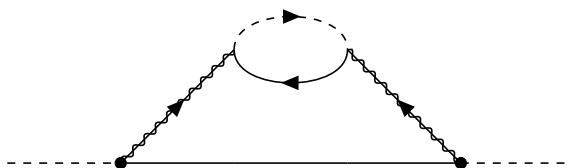


Figure 4.2: Two-loop contribution to scalar mass parameters of non-messenger fields (4.36). Fermionic lines with wavy lines on them again represent gauginos. In the upper loop, messenger fermions and scalars are present, while the lower dashed and solid lines represent non-messenger scalars and their fermionic superpartners, respectively.

is composed by F-terms, D-terms and the soft supersymmetry-breaking terms (4.31). Without the latter, and in particular without b , electroweak symmetry-breaking cannot be achieved. The vacuum expectation values can be set to

$$\langle H_u \rangle_0 = \frac{1}{\sqrt{2}}(0, v_u), \quad \langle H_d \rangle_0 = \frac{1}{\sqrt{2}}(v_d, 0), \quad (4.41)$$

with

$$\frac{v_u^2 + v_d^2}{2} = \frac{2m_Z^2}{g_2^2 + g_1^2} \approx (174 \text{ GeV})^2 \quad (4.42)$$

set to match the Higgs vacuum expectation value (2.2). Conventionally, one writes

$$\tan(\beta) = \frac{v_u}{v_d}. \quad (4.43)$$

From the eight real components of the scalar Higgs doublets, three become longitudinal components of Z^0 and W^\pm , labeled as G^0 and G^\pm , respectively. The other five components combine into two CP-even real scalars h^0 and H^0 , one CP-odd A^0 , one positively charged H^+ and one negatively charged scalar H^- .

The neutral fermionic components of the Higgs superfields, the neutral higgsinos \tilde{H}_u^0 and \tilde{H}_d^0 , combine with the bino \tilde{B} and neutral wino \tilde{W}^0 into four neutralinos $\tilde{N}_{1,2,3,4}$.

The charged higgsinos \widetilde{H}_u^+ and \widetilde{H}_d^- and charged winos \widetilde{W}^\pm yield four charginos $C_{1,2}^\pm$. The fermionic superpartners of the gluons, the gluinos \widetilde{g} , are already mass eigenstates.

Squarks, as well as sleptons, in principle mix into new mass eigenstate squarks and sleptons. Mixing within the first two generations is expected to be negligible, and the mixing in the third generations of stops, sbottoms and staus can then be written as

$$\begin{pmatrix} \widetilde{t}_1 \\ \widetilde{t}_2 \end{pmatrix} = \begin{pmatrix} c_{\widetilde{t}} & -s_{\widetilde{t}}^* \\ s_{\widetilde{t}} & c_{\widetilde{t}}^* \end{pmatrix} \begin{pmatrix} \widetilde{t}_L \\ \widetilde{t}_R \end{pmatrix}, \quad \begin{pmatrix} \widetilde{b}_1 \\ \widetilde{b}_2 \end{pmatrix} = \begin{pmatrix} c_{\widetilde{b}} & -s_{\widetilde{b}}^* \\ s_{\widetilde{b}} & c_{\widetilde{b}}^* \end{pmatrix} \begin{pmatrix} \widetilde{b}_L \\ \widetilde{b}_R \end{pmatrix}, \quad \begin{pmatrix} \widetilde{\tau}_1 \\ \widetilde{\tau}_2 \end{pmatrix} = \begin{pmatrix} c_{\widetilde{\tau}} & -s_{\widetilde{\tau}}^* \\ s_{\widetilde{\tau}} & c_{\widetilde{\tau}}^* \end{pmatrix} \begin{pmatrix} \widetilde{\tau}_L \\ \widetilde{\tau}_R \end{pmatrix}, \quad (4.44)$$

with the matrices being unitary and $\widetilde{t}_1, \widetilde{t}_2, \widetilde{b}_1, \widetilde{b}_2, \widetilde{\tau}_1, \widetilde{\tau}_2$ the mass eigenstates.

Chapter 5

Supersymmetric Renormalization Group Equations

5.1 Beta Functions

In this work, we only consider supersymmetric gauge-Yukawa models which are renormalizable by power counting. Gauge groups G are products of a semi-simple group and further abelian factors. We write G as

$$G = \prod_a G_a , \quad (5.1)$$

where a runs over the simple and abelian group factors after factorizing the semi-simple group. The superpotentials of our models are of the general form

$$W = \frac{1}{6} Y^{ijk} \Phi_i \Phi_j \Phi_k , \quad (5.2)$$

where the indices i, j, k run over different flavor as well as group representation degrees of freedom. The Yukawa coupling matrix Y^{ijk} is totally symmetric and we define its complex conjugate as

$$Y_{ijk} = (Y^{ijk})^* . \quad (5.3)$$

Mass terms are of no relevance for our purposes and are neglected. We also omit canonically irrelevant interactions. Such theories are renormalizable in perturbation theory.

For a running over the group factors G_a , the beta functions of the gauge and Yukawa couplings g_a and Y^{ijk} at two- and one-loop level respectively in the $\overline{\text{DR}}$ scheme are

$$\beta_{g_a} = \frac{d}{dt}g_a = \frac{g_a^3}{(4\pi)^2} \left(-\frac{B_a}{2} + \frac{g_b^2}{(4\pi)^2} \frac{C_{ab}}{2} - \frac{Y^{ijk}Y_{ijk}}{(4\pi)^2} \frac{C_2^{(a)}(k)}{d_a(G)} \right), \quad (5.4)$$

$$\beta_{Y^{ijk}} = \frac{d}{dt}Y^{ijk} = \left(Y^{ijp}\gamma_p^{(1)k} + Y^{pj k}\gamma_p^{(1)i} + Y^{ipk}\gamma_p^{(1)j} \right), \quad (5.5)$$

with $t = \ln(\mu)$ an ‘‘RG time’’ and μ the RG scale [153]¹. Due to the supersymmetric nonrenormalization theorem [127, 128], Yukawa terms do not receive Vertex corrections and Yukawa couplings are only renormalized via the anomalous dimensions of chiral superfields, as can be seen in eq. (5.5). The coefficients and the anomalous dimension matrices in the beta functions are

$$B_a = 6C_2^{(a)}(G) - 2S_a(r), \quad (5.6a)$$

$$C_{aa} = -12[C_2^{(a)}(G)]^2 + 4C_2^{(a)}(G)S_a(r) + 8S_a(r)C_2^{(a)}(r), \quad (5.6b)$$

$$C_{ab} = 8S_a(r)C_2^{(b)}(r), \quad (5.6c)$$

$$\gamma_l^{(1)k} = \frac{Y^{ijk}Y_{ijl}}{2(4\pi)^2} - 2\sum_a \frac{g_a^2}{(4\pi)^2} C_2^{(a)}(k)\delta_l^k. \quad (5.6d)$$

Here, $S_a(r)$ implies summation over the chiral superfield Dynkin indices of irreducible representations r of G_a , while $S_a(r)C_2^{(b)}(r)$ and $S_a(r)C_2^{(a)}(r)$ imply analogous summations over the products of the Dynkin indices and the quadratic Casimir invariants, and $d_a(G)$ is the dimension of the group factor G_a . $C_2^{(a)}(G)$ denotes the Casimir invariant of the adjoint representation of G_a . Dynkin indices $S_a(r)$ and Casimir invariants $C_2^{(a)}(r)$ are related via

$$S_a(r)d_a(G) = C_2^{(a)}(r)d_a(r), \quad (5.7)$$

with $d_a(r)$ the dimension of the representation r . In this work, the generators of the gauge groups are normalized such that the Dynkin index of the fundamental representation of $\text{SU}(N)$ equals 1/2. We refer to working with 2-loop gauge and 1-loop Yukawa beta functions as the 2-1-approximation.

For models where we only have ‘‘natural’’ Yukawa beta functions, i.e. when these beta functions are of the form

$$\beta_i \propto y_i, \quad (5.8)$$

¹At the loop-levels considered in this work there is no difference between the schemes $\overline{\text{DR}}$ and $\overline{\text{MS}}$ [154]

we are able to introduce beta functions for a new set of couplings defined as

$$\alpha_a = \frac{g_a^2}{(4\pi)^2}, \quad \alpha_{ijk} = \frac{|Y^{ijk}|^2}{(4\pi)^2}. \quad (5.9)$$

For these couplings, the beta functions (5.4) and (5.5) become

$$\beta_g = \alpha_g^2 \left[-B_g + \sum_{g,g'} C_{gg'} \alpha_{g'} - \sum_y D_{gy} \alpha_y \right], \quad (5.10)$$

$$\beta_y = \alpha_y \left[\sum_{y,y'} E_{yy'} \alpha_{y'} - \sum_h F_{yh} \alpha_h \right], \quad (5.11)$$

with g, g' now running over gauge indices and y, y' counting through Yukawa couplings. In this study, we restrict our investigations to models yielding natural beta functions. We guarantee this by only allowing superpotentials such that any two superpotential terms have at most one superfield which appears in both of them. For some more details on how unnatural Yukawa beta functions may arise, see appendix A.

Novikov, Shifman, Vainshtein and Zakharov [155] derived a formula for the infinite order supersymmetric beta functions of couplings α_a

$$\begin{aligned} \beta_a^{\text{NSVZ}} &= -2\alpha_a^2 \frac{3C_2^{(a)}(G) - \sum_i S_a(r_i)(1 - 2\gamma_i)}{1 - 2C_2^{(a)}(G)\alpha_a} \\ &\stackrel{(5.6a)}{=} -\alpha_a^2 \frac{B_a + \frac{4}{d_a(G)} \sum_i C_2^{(a)}(r_i) d_a(r_i) \gamma_i}{1 - 2C_2^{(a)}(G)\alpha_a}, \end{aligned} \quad (5.12)$$

where i sums over all irreducible representations r_i of chiral superfields under G_a , and γ_i denotes their anomalous dimension. We have more to say on the NSVZ beta function and anomalous dimensions in chapter 8.

5.2 Interacting Fixed Points

A point α^* in coupling space that fulfills

$$\beta(\alpha^*) = 0 \quad (5.13)$$

for all beta functions is called a fixed point. We label a fixed point α^* “physical” and “perturbative” if its components α_i^* fulfill the conditions

$$0 \leq \alpha_i^* \text{ and } \alpha_i^* < 1, \quad (5.14)$$

respectively. In the case of a simple gauge group G with gauge coupling α and vanishing superpotential, the beta function of this gauge coupling is

$$\beta = \alpha^2[-B + C\alpha] . \quad (5.15)$$

The fixed points of this model are the gaussian fixed point $\alpha^* = 0$ and the interacting fixed point

$$\alpha^* = \frac{B}{C} . \quad (5.16)$$

The gaussian fixed point is always physical, and for $B > 0$ ($B < 0$) it is UV (IR) attractive. The interacting fixed point in this model only becomes physical for $B \cdot C > 0$. For $B < 0$ and $C < 0$, the interacting fixed point would be a UV fixed point. It has been shown that

$$B \leq 0 \quad \Rightarrow \quad C > 0 , \quad (5.17)$$

meaning that in a simple gauge theory with matter and without any further interactions, there are no UV fixed points at two-loop [113]. Inclusion of one Yukawa coupling α_y leads to the beta functions

$$\begin{aligned} \beta &= \alpha^2[-B + C\alpha - D\alpha_y] , \\ \beta_y &= \alpha_y[E\alpha_y - F\alpha] , \end{aligned} \quad (5.18)$$

with $D, E, F > 0$. Solving $\beta_y = 0$ for $\alpha_y \neq 0$ (“nullcline”) and inserting this solution into β , we obtain

$$\beta = \alpha^2[-B + C'\alpha] , \quad C' = C - \frac{DF}{E} , \quad (5.19)$$

which now possibly has the interacting fixed point

$$\alpha^* = \frac{B}{C'} . \quad (5.20)$$

In non-supersymmetric models it is then possible to flip the sign of C' towards negativity for $B < 0$, generating a physical interacting UV fixed point [63].

In supersymmetric models on the other hand, this sign flip is not possible for $B < 0$, as we will argue in sec. 5.3. The impossibility of physical interacting UV fixed points in simple supersymmetric gauge models is well-known to be true even beyond perturbation theory [118]. Nevertheless, using semi-simple gauge groups, supersymmetric AS models have successfully been constructed [65].

The RG flow in the vicinity of fixed points can be approximated by

$$\beta_i(\alpha) \approx \sum_j M_{ij}(\alpha_j - \alpha_j^*) , \quad (5.21)$$

with the stability matrix

$$M_{i,j} \equiv \left. \frac{\partial \beta_i}{\partial \alpha_j} \right|_{\alpha^*}. \quad (5.22)$$

If M has one negative or positive eigenvalue (“critical exponent”), the fixed point α^* respectively has a UV or IR attractive direction given by the corresponding eigenvector. For critical exponents being zero, we obtain no information from the stability matrix on the attractivity of a fixed point in the direction of the corresponding eigenvector. This happens for example for fixed points α^* with some vanishing gauge component α_a . In this case, the corresponding beta function β_a may be written as

$$\beta_a = -B_{a,\text{eff}}^{\alpha^*} \alpha_a^2 + \mathcal{O}(\alpha_a^3), \quad (5.23)$$

with $B_{a,\text{eff}}^{\alpha^*}$ obtained by inserting the non-zero components of α^* into β_a . For $B_{a,\text{eff}}^{\alpha^*} > 0$ (< 0), α^* is UV (IR) attractive in α_a -direction.

5.3 On the Existence of Interacting Fixed Points

We now come to a special feature of supersymmetric models which allows to infer unphysicality of some weakly interacting fixed points just from the signs of the one-loop coefficients B_g specified in eq. (5.6a). With the following feature, we will be able to classify extensions of the MSSM in sec. 6.2.

In order for an $\mathcal{N} = 1$ SUSY gauge-Yukawa model with gauge group $G = \prod_a G_a$ as in (5.1) to allow for a physical interacting fixed point g^ in the 2-1-approximation, it is necessary that at least one gauge sector $G_{a'}$ corresponding to a component $g_{a'}^* \neq 0$ of the fixed point is AF at one-loop level, i.e. the one-loop coefficient $B_{a'}$ as given in (5.4) and (5.6a) is positive.*

Note that this necessary condition is true for all $\mathcal{N} = 1$ supersymmetric theories, not only for MSSM extensions. We proof this condition in appendix. B.

We can now understand why the interacting fixed point (5.20) can never simultaneously be physical and UV attractive for supersymmetric models with simple gauge groups. This is because for this fixed point being UV attractive, we need $B < 0$ which, according to the statement above, immediately renders this fixed point unphysical.

We illustrate some possible fixed points for a gauge group $\text{SU}(3) \otimes \text{SU}(2)$ in fig. 5.1. There we see that for all one-loop B -coefficients being negative, there are no interacting fixed points possible. This can be translated into an upper limit on the number of fields for which interacting fixed points are possible, since more fields lower the value of the B -coefficients (see eq. (5.6a)).

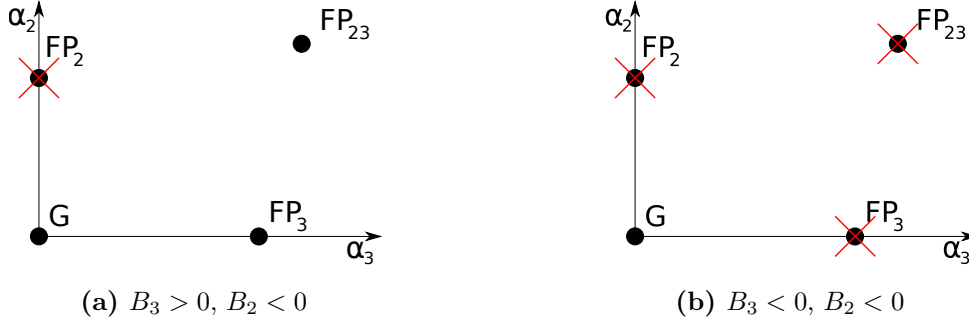


Figure 5.1: Possible fixed points for a gauge group $SU(3) \otimes SU(2)$. On the left side, we have the one-loop coefficients $B_3 > 0$ and $B_2 < 0$, while on the right side these are both negative. Starting on with the sign assignment of the left side and adding colored particles to the model, we eventually end up with the picture on the right side where no interacting fixed points are possible.

Furthermore, we are able to make some statements about the Yukawa structures needed in order to generate physical interacting UV fixed points in supersymmetric theories. The necessary condition above states that we need at least one AF sector to possibly have interacting fixed points. Moreover, Yukawa interactions are a requirement for weakly interacting UV fixed points, as discussed in sec. 5.2. This implies that without Yukawa interactions, fields charged under many gauge sectors simultaneously can never generate UV attractivity of interacting fixed points on their own. On the other hand, if Yukawa interactions only contain fields charged under one gauge sector, UV attractive interacting fixed points can also not be generated in supersymmetric theories (see discussion in sec. 5.2). We conclude that Yukawa interactions containing fields charged under different gauge sectors simultaneously are a necessity for weakly interacting, UV attractive fixed points in the 2-1-approximation.

Chapter 6

MSSM Extensions

6.1 Fixed Points Within the MSSM

In this section, we investigate fixed points of the MSSM, both with and without R -parity conservation. The left-handed chiral superfields of the MSSM are those of tab. 4.1 and its gauge group is G_{MSSM} from eq. (4.26):

$$G_{\text{MSSM}} = G_{\text{SM}} = \text{SU}(3)_C \otimes \text{SU}(2)_L \otimes \text{U}(1)_Y . \quad (6.1)$$

Taking only gauge couplings into account, there are up to seven interacting points. We label these seven interacting fixed points and the single gaussian fixed point as shown in tab. 6.1.

Additionally, the MSSM contains the superpotential (4.28):

$$\begin{aligned} W_{\text{MSSM}} &= Y_u^{ij} \bar{u}_i Q_j H_u + Y_d^{ij} \bar{d}_i Q_j H_d + Y_e^{ij} \bar{e}_i L_j H_d + \mu H_u H_d \\ &\approx y_t \bar{u}_3 Q_3 H_u + y_b \bar{d}_3 Q_3 H_d , \end{aligned} \quad (6.2)$$

which we approximate in this section by only taking the top and bottom Yukawa couplings to be non-zero. If R -parity (4.27) is not conserved, the RPV MSSM superpotential (4.30) containing lepton and baryon number violating terms is obtained:

$$\begin{aligned} W_{\text{RPV}} &= W_{\text{MSSM}} \\ &\quad + \lambda^{ijk} \bar{d}_i Q_j L_k + \frac{1}{2} \lambda^{ijk} L_i L_j \bar{e}_k + \mu^i L_i H_u \\ &\quad + \frac{1}{2} \lambda^{ijk} \bar{u}_i \bar{d}_j \bar{d}_k . \end{aligned} \quad (6.3)$$

Fixed point label	α_1^*	α_2^*	α_3^*	$\vec{\alpha}_y^*$
FP ₀	0	0	0	$\vec{0}$
FP ₁	$\alpha_1^{\text{FP}_1}$	0	0	$\vec{\alpha}_y^{\text{FP}_1}$
FP ₂	0	$\alpha_2^{\text{FP}_2}$	0	$\vec{\alpha}_y^{\text{FP}_2}$
FP ₃	$\alpha_3^{\text{FP}_3}$	0	0	$\vec{\alpha}_y^{\text{FP}_3}$
FP ₁₂	$\alpha_1^{\text{FP}_{12}}$	$\alpha_2^{\text{FP}_{12}}$	0	$\vec{\alpha}_y^{\text{FP}_{12}}$
FP ₁₃	$\alpha_1^{\text{FP}_{13}}$	0	$\alpha_3^{\text{FP}_{13}}$	$\vec{\alpha}_y^{\text{FP}_{13}}$
FP ₂₃	0	$\alpha_2^{\text{FP}_{23}}$	$\alpha_3^{\text{FP}_{23}}$	$\vec{\alpha}_y^{\text{FP}_{23}}$
FP ₁₂₃	$\alpha_1^{\text{FP}_{123}}$	$\alpha_2^{\text{FP}_{123}}$	$\alpha_3^{\text{FP}_{123}}$	$\vec{\alpha}_y^{\text{FP}_{123}}$

Table 6.1: Classification of fixed points regarding their interacting gauge couplings for the MSSM gauge group G_{MSSM} of (4.26). The gauge couplings α_1 , α_2 and α_3 belong to the gauge sectors $U(1)_Y$, $SU(2)_L$ and $SU(3)_C$, respectively. Yukawa couplings are summarized into vectors $\vec{\alpha}_y$.

In the MSSM, the one-loop and two-loop gauge beta coefficients of (5.4) are given by

$$\begin{aligned}
B_1^{\text{MSSM}} &= -22, & C_{11}^{\text{MSSM}} &= \frac{398}{9}, & C_{12}^{\text{MSSM}} &= 18, & C_{13}^{\text{MSSM}} &= \frac{176}{3}, \\
B_2^{\text{MSSM}} &= -2, & C_{21}^{\text{MSSM}} &= 6, & C_{22}^{\text{MSSM}} &= 50, & C_{23}^{\text{MSSM}} &= 48, \\
B_3^{\text{MSSM}} &= 6, & C_{31}^{\text{MSSM}} &= \frac{22}{3}, & C_{32}^{\text{MSSM}} &= 18, & C_{33}^{\text{MSSM}} &= 28.
\end{aligned} \tag{6.4}$$

Negativity of B_2^{MSSM} and B_1^{MSSM} implies that the running couplings α_1 and α_2 both have Landau poles at one-loop level. In this chapter, we study whether we find fixed points in the MSSM which allow to avoid these Landau poles.

6.1.1 MSSM

For the R -parity conserving MSSM superpotential in eq. (6.2), the Yukawa beta functions for the top and bottom couplings $\alpha_{t,b} = |y_{t,b}|^2/(4\pi)^2$ as defined in (5.9) are respectively given by

$$\begin{aligned}
\beta_t &= \alpha_t \left[12\alpha_t + 2\alpha_b - \frac{26}{9}\alpha_1 - 6\alpha_2 - \frac{32}{3}\alpha_3 \right], \\
\beta_b &= \alpha_b \left[12\alpha_b + 2\alpha_t - \frac{14}{9}\alpha_1 - 6\alpha_2 - \frac{32}{3}\alpha_3 \right].
\end{aligned} \tag{6.5}$$

The Yukawa nullclines (for which the beta functions (6.5) vanish) are

$$\alpha_t^* = \frac{71}{315}\alpha_1 + \frac{3}{7}\alpha_2 + \frac{16}{21}\alpha_3, \quad \alpha_b^* = \frac{29}{315}\alpha_1 + \frac{3}{7}\alpha_2 + \frac{16}{21}\alpha_3. \tag{6.6}$$

Inserting these into the gauge beta functions (5.10) with the MSSM coefficients (6.4) and

$$D_{1t} = \frac{52}{3}, D_{1b} = \frac{28}{3}, D_{2t} = 12, D_{2b} = 12, D_{3t} = 8, D_{3b} = 8, \quad (6.7)$$

we are then able to calculate the values of fixed points. For FP_3 , we find

$$\begin{aligned} \text{FP}_3 &= (\alpha_1^{\star\text{FP}_3}, \alpha_2^{\star\text{FP}_3}, \alpha_3^{\star\text{FP}_3}, \alpha_t^{\star\text{FP}_3}, \alpha_b^{\star\text{FP}_3}) = \left(0, 0, \frac{63}{166}, \frac{24}{83}, \frac{24}{83}\right) \\ &\approx (0, 0, 0.38, 0.29, 0.29). \end{aligned} \quad (6.8)$$

Hence, FP_3 is physical and perturbative. The other fixed points with interacting strong couplings turn out to be unphysical due to their following components.

$$\begin{aligned} \text{FP}_{13} : \alpha_1^{\star\text{FP}_{13}} &= -\frac{22755}{17323} \approx -1.31, \\ \text{FP}_{23} : \alpha_2^{\star\text{FP}_{23}} &= -\frac{29}{41} \approx -0.70, \\ \text{FP}_{123} : \alpha_1^{\star\text{FP}_{123}} &= -\frac{507900}{131141} \approx -3.87. \end{aligned} \quad (6.9)$$

For FP_3 , we may calculate the effective coefficients $B_{1,\text{eff}}^{\text{FP}_3}$ and $B_{2,\text{eff}}^{\text{FP}_3}$ as described in (5.23) and obtain for them

$$B_{1,\text{eff}}^{\text{FP}_3} = -\frac{1102}{83} \approx -13.3, B_{2,\text{eff}}^{\text{FP}_3} = -\frac{4242}{83} \approx -51.1. \quad (6.10)$$

These effective coefficients being negative make FP_3 an IR fixed point. Hence, we do not find any interacting UV fixed points in our search within the MSSM¹.

6.1.2 RPV MSSM

In the RPV MSSM, the additional lepton and baryon number violating terms of eq. (6.3) are present in the superpotential. Based on our discussion at the end of sec. 5.3 regarding necessary fields in Yukawa interactions of possibly AS models, our preferred terms of the RPV MSSM superpotential are the λ' terms

$$\lambda'^{ijk} \bar{d}_i Q_j L_k. \quad (6.11)$$

Additionally to the top and bottom Yukawa couplings of the MSSM, we introduce for each $k = 1, 2, 3$ submatrices of $(\lambda'^1)_{ij} = \lambda'^{ij1}$, $(\lambda'^2)_{ij} = \lambda'^{ij2}$ and $(\lambda'^3)_{ij} = \lambda'^{ij3}$. The

¹We explicitly checked that including the Yukawa coupling y_τ and further finite entries in Y_u , Y_d and Y_e of the MSSM superpotential (4.28) yields similar results. Fixed point FP_3 stays physical and IR attractive, while the other interacting fixed points stay unphysical.

investigated fixed points have interacting Yukawa components corresponding to these submatrices. In more detail, these matrices are modeled as

$$\lambda'^1 = \begin{pmatrix} \mathbf{M}_1 & \dots & 0 \\ \vdots & & \vdots \\ 0 & \dots & 0 \end{pmatrix}, \quad \lambda'^2 = \begin{pmatrix} \mathbf{M}_2 & \dots & 0 \\ \vdots & & \vdots \\ 0 & \dots & 0 \end{pmatrix}, \quad \lambda'^3 = \begin{pmatrix} \mathbf{M}_3 & \dots & 0 \\ \vdots & & \vdots \\ 0 & \dots & 0 \end{pmatrix}, \quad (6.12)$$

with the dimensionalities of the submatrices being

$$\mathbf{M}_{1,2,3} : (\text{rows} \times \text{columns}) = (I_d \times I_Q), \quad (6.13)$$

where

$$1 \leq I_Q, I_u, I_d \leq 2. \quad (6.14)$$

The integers (6.14) are chosen such that we avoid unnatural Yukawa beta functions (see appendix A for more details on unnatural Yukawa beta functions).

In our search, we have between 5 and 14 (possibly complex) Yukawa couplings. The evolutions of the corresponding couplings

$$\alpha_t = \frac{|y_t|^2}{(4\pi)^2}, \quad \alpha_b = \frac{|y_b|^2}{(4\pi)^2}, \quad \alpha'_{ijk} = \frac{|\lambda'_{ijk}|^2}{(4\pi)^2} \quad (6.15)$$

are respectively governed by the three beta functions

$$\begin{aligned} \beta_t &= \alpha_t \left[12\alpha_t + 2\alpha_b - \frac{26}{9}\alpha_1 - 6\alpha_2 - \frac{32}{3}\alpha_3 \right], \\ \beta_b &= \alpha_b \left[12\alpha_b + 2\alpha_t - \frac{14}{9}\alpha_1 - 6\alpha_2 - \frac{32}{3}\alpha_3 \right], \\ \beta'_\lambda &= \alpha'_\lambda \left[36I_d I_Q \alpha'_\lambda - \frac{14}{9}\alpha_1 - 6\alpha_2 - \frac{32}{3}\alpha_3 \right], \end{aligned} \quad (6.16)$$

where all couplings $\alpha'_{ijk} \rightarrow \alpha'_\lambda$ evolve according to the same beta function β'_λ . Inserting the nullcline solutions of these Yukawa beta functions into the gauge beta functions (5.10) with the MSSM coefficients (6.4) and

$$\begin{aligned} D_{1t} &= \frac{52}{3}, \quad D_{1b} = \frac{28}{3}, \quad D_{1\lambda} = 28I_d I_Q, \\ D_{2t} &= 12, \quad D_{2b} = 12, \quad D_{2\lambda} = 36I_d I_Q, \\ D_{3t} &= 8, \quad D_{3b} = 8, \quad D_{3\lambda} = 24I_d I_Q, \end{aligned} \quad (6.17)$$

we find again that the only physical interacting fixed point is

$$\begin{aligned} \text{FP}_3 &= (\alpha_1^*, \alpha_2^*, \alpha_3^*, \alpha_t^*, \alpha_b^*, \alpha_\lambda^*) = \left(0, 0, \frac{189}{274}, \frac{72}{137}, \frac{72}{137}, \frac{28}{137 I_d I_Q} \right) \\ &\approx \left(0, 0, 0.69, 0.53, \frac{0.20}{I_d I_Q} \right), \end{aligned} \quad (6.18)$$

which again is IR attractive. Therefore we also do not find any interacting UV fixed points within the RPV MSSM.

6.2 Search Strategy For MSSM Extensions

From the necessary condition for interacting fixed points of sec. 5.3, we are able to set an upper limit on the colored field content beyond the MSSM. More specifically, we may infer that

For interacting fixed points to possibly exist in MSSM extensions within the 2-1-approximation, there are only two possibilities of including colored chiral superfields beyond the MSSM, namely

- 1) *One $SU(3)_C$ fundamental and one $SU(3)_C$ anti-fundamental,*
- 2) *Two $SU(3)_C$ fundamentals and two $SU(3)_C$ anti-fundamentals.*

We stress that the number of $SU(3)_C$ singlets is not limited by this rule. We proceed by proving the statement on the possible colored superfields beyond the MSSM. The one-loop B -coefficients corresponding to $U(1)$ gauge factors are always negative, as can be seen from eq. (5.6a). For MSSM extensions, the coefficient B_2 is negative, while only B_3 may be positive. In the MSSM we have $B_3^{\text{MSSM}} = 6$, and additional superfields lower the B -coefficients according to eq. (5.6a).

Now we examine which additional particle content is allowed to keep B_3 positive. Every additional superfield in the representation R of $SU(3)_C$ lowers B_3 by $2S_3(R)$. For the fundamental or anti-fundamental representations one has $S_3 = 1/2$. In order to avoid gauge anomalies, we always have to include a pair composed by one fundamental and one anti-fundamental superfield to the MSSM which immediately leads to the two possible cases stated above to maintain a positive coefficient B_3 . What about other representations? The sextet and anti-sextet representations have $S_3 = 5/2$, but gauge anomalies again dictate us to include at least two sextet superfields simultaneously which would yield $B_3 = -4$. The representation with the next bigger Dynkin index is the adjoint representation with $S_3 = 3$. Since this is a real representation, it is allowed

to include such fields individually, but even for just one additional $SU(3)_C$ adjoint we already obtain $B_3 = 0$. All other representations have $S_3 > 3$ and hence are also ruled out. With this we have shown the statement from above.

We may now classify all possible MSSM extensions which allow for interacting fixed points in the 2-1-approximation into three model classes with the particle contents beyond the MSSM

- Model class 1: New quark singlets and new leptons ,
- Model class 2: Two new quark doublets and new leptons ,
- Model class 3: A fourth generation and new leptons .

In the subsequent sections, we parameterize different Yukawa interactions of fixed points within these three model classes. Each Yukawa structure is counted as a different model.

In the our investigations, we have the gauge couplings

$$\{\alpha_1, \alpha_2, \alpha_3\} , \quad (6.19)$$

defined as in eq. (5.9). Additionally, the MSSM top- and bottom Yukawa couplings from eq. (4.29) and further BSM Yukawa couplings are present in our models. Due to flavor symmetries in our constructed Yukawa structures, some BSM Yukawa couplings have identical beta functions and we end up with up to 10 different BSM Yukawa beta functions. Only counting corresponding BSM Yukawa couplings, we have altogether the Yukawa couplings

$$\{\alpha_t, \alpha_b, \alpha_4, \dots, \alpha_{13}\} , \quad (6.20)$$

again with the couplings as defined in (5.9).

6.3 Model Class 1: New Quark Singlets and Leptons

6.3.1 Framework

In our first model framework, we include quark singlets as well as lepton doublets to the MSSM. The resulting particle content is that of table 6.2, where all possible field multiplicities are parameterized by the parameters

$$n_u , n_d , n_L , \quad (6.21)$$

counting respectively the number of up-quarks, down-quarks and lepton doublets. To not introduce any gauge anomalies, we furthermore introduce $n_u - 3$ anti-up-quarks, $n_d - 3$ anti-down-quarks and $n_L - 3$ anti-lepton doublets. The case of two additional quark singlets is achieved for $n_u + n_d = 7$ while in the case of four additional quark singlets we have $n_u + n_d = 8$. In our scans we also cover models with more than four new quark singlets to test the limit on colored fields from sec. 6.2. The number of new fields beyond the MSSM is given by

$$N_{\text{BSM}} = \underbrace{2(n_u + n_d - 6)}_{=N_{q,\text{BSM}}} + \underbrace{2(n_L - 3)}_{=N_{L,\text{BSM}}}, \quad (6.22)$$

with $N_{q,\text{BSM}}$ and $N_{L,\text{BSM}}$ the numbers of new quark singlets and new lepton doublets, respectively.

(Left-handed) Superfield	$SU(3)_C$	$SU(2)_L$	$U(1)_Y$	Model 1	MSSM
quark doublet Q	3	2	+1/6	3	3
up-quark \bar{u}	$\bar{\mathbf{3}}$	1	-2/3	n_u	3
down-quark \bar{d}	$\bar{\mathbf{3}}$	1	+1/3	n_d	3
anti-up-quark u	3	1	+2/3	$n_u - 3$	0
anti-down-quark d	3	1	-1/3	$n_d - 3$	0
lepton doublet L	1	2	-1/2	n_L	3
anti-lepton doublet \bar{L}	1	$\bar{\mathbf{2}}$	+1/2	$n_L - 3$	0
lepton singlet \bar{e}	1	1	+1	3	3
up-Higgs H_u	1	2	+1/2	1	1
down-Higgs H_d	1	2	-1/2	1	1

Table 6.2: Left-handed chiral superfields of model class 1 consisting of MSSM fields (see tab. 4.1) and additional quark singlets \bar{u} , \bar{d} , u , d and additional lepton doublets L , \bar{L} beyond the MSSM.

The general gauge invariant superpotential we are studying is given by

$$W_1 = Y^{ijk} \bar{d}_i Q_j L_k + \bar{Y}^{ijk} \bar{u}_i Q_j \bar{L}_k + x_b y_b \bar{d}_3 Q_3 H_d + x_t y_t \bar{u}_3 Q_3 H_u, \quad (6.23)$$

with gauge indices being suppressed, i, j, k running over flavors, and $x_{t,b} \in \{0, 1\}$. With the flavor-counting parameters (6.21), there are up to

$$N_Y^{\text{general}} = 3(n_u n_L + n_d(n_L - 3)) + 2 \quad (6.24)$$

Yukawa couplings present in (6.23).

We focus on a subset of all possible non-zero Yukawa couplings, parameterized by

$$x_b, x_t, I_{12}, I_{13}, I_{1d}, I_{2d}, I_{3d}, I_{1u}, I_{2u}, I_{3u}. \quad (6.25)$$

These integers are used as follows to specify which Yukawa couplings are interacting. The bottom and top Yukawa couplings are switched on and off with $x_t, x_b \in \{1, 0\}$. Only in these two Yukawa terms, the bottom and top quarks \bar{d}_3 and \bar{u}_3 are allowed to appear. The number of times superfields $\bar{d}_i \neq \bar{d}_3$ appear exactly once in the superpotential in terms involving Q_1, Q_2 , or Q_3 is given by I_{1d}, I_{2d} , and I_{3d} , respectively (the analogous cases of fields $\bar{u}_i \neq \bar{u}_3$ appearing exactly once in the superpotential in connection with Q_1, Q_2 , or Q_3 are counted respectively by I_{1u}, I_{2u} , and I_{3u}). We also allow for down-quarks $\bar{d}_i \neq \bar{d}_3$ to be present twice in the superpotential. With I_{12} we count the number of down quark superfields $\bar{d}_i \neq \bar{d}_3$ appearing exactly twice in the superpotential, once in terms involving Q_1 and once in terms involving Q_3 . The cases of down quark superfields $\bar{d}_i \neq \bar{d}_3$ being present exactly twice in the superpotential in connection with terms involving Q_1 and Q_3 are counted by the integer I_{13} . Furthermore, each lepton doublet L and anti-lepton doublet \bar{L} may be present at most once in the superpotential.

In summary, the different cases of Yukawa terms are counted by the integers (6.25) as:

$$\begin{aligned} y_b \bar{d}_3 Q_3 H_d &: x_b, \\ y_t \bar{u}_3 Q_3 H_u &: x_t, \\ y_4 \bar{d}_i Q_1 L_k + y_6 \bar{d}_i Q_2 L_{k'} &: I_{12}, \\ y_5 \bar{d}_i Q_1 L_k &: I_{1d}, \\ y_7 \bar{d}_i Q_2 L_k &: I_{2d}, \\ y_8 \bar{d}_i Q_1 L_k + y_9 \bar{d}_i Q_3 L_{k'} &: I_{13}, \\ y_{10} \bar{d}_i Q_3 L_k &: I_{3d}, \\ y_{11} \bar{u}_i Q_1 \bar{L}_k &: I_{1u}, \\ y_{12} \bar{u}_i Q_2 \bar{L}_k &: I_{2u}, \\ y_{13} \bar{u}_i Q_3 \bar{L}_k &: I_{3u}, \end{aligned} \quad (6.26)$$

where all Yukawa couplings of a type i evolve with the same beta function β_i due to remaining flavor symmetries acting on quark singlets and on lepton doublets appearing in terms of the same Yukawa coupling type. In sec. 6.6.1, we discuss these flavor symmetries for a specific benchmark model. The 12 Yukawa beta functions $\beta_t, \beta_b, \beta_4, \dots, \beta_{13}$ for the couplings $\alpha_t, \alpha_b, \alpha_4, \dots, \alpha_{13}$ are specified in appendix D.1.1.

Some comments on the motivation behind our chosen parameterization for interacting Yukawa couplings are in order. When not allowing for down-quarks $d_i \neq \bar{d}_3$ to appear twice in the superpotential, we find no AS candidates. In further exhaustive investigations, we also never find UV attractive fixed points if we allow for lepton doublets to appear twice in the superpotential while at the same time each quark singlet may appear at most once. On the other hand, with the above described superpotential terms we do find AS candidates in our scan of sec. 6.3.2. Our choice of Yukawa structures corresponds to the simplest case for which we find AS candidates.

Each of our models is then fully specified by the parameters

$$n_u, n_d, n_L, x_b, x_t, I_{12}, I_{13}, I_{1d}, I_{2d}, I_{3d}, I_{1u}, I_{2u}, I_{3u}, \quad (6.27)$$

where the flavor-counting parameters have to be larger than the minimal values stated in (6.30) to accommodate the Yukawa terms specified by the I -parameters.

The number of Yukawa couplings present in our investigations is

$$N_Y = 2(I_{12} + I_{13}) + \sum_{i=1}^3 (I_{id} + I_{iu}) + x_t + x_b. \quad (6.28)$$

In our scan within the next section, N_Y gets up to 10% of the generally possible number of Yukawa couplings N_Y^{general} .

6.3.2 Scan

We scan 3434836 models within the parameter range

$$\begin{aligned} 0 &\leq I_{12}, I_{13}, I_{1d}, I_{2d}, I_{3d}, I_{1u}, I_{2u}, I_{3u} \leq 5, \quad I_{1u} \leq I_{2u}, \\ n_d^{\min} &\leq n_d \leq 7, \quad n_u^{\min} \leq n_u \leq 7, \\ n_L^{\min} &\leq n_L \leq 14, \quad 0 \leq x_t, x_b \leq 1, \end{aligned} \quad (6.29)$$

with

$$\begin{aligned} n_d^{\min} &= \max\{I_{12} + I_{13} + I_{1d} + I_{2d} + I_{3d} + 1, 3\}, \\ n_u^{\min} &= \max\{I_{1u} + I_{2u} + I_{3u} + 1, 3\}, \\ n_L^{\min} &= \max\{2I_{12} + 2I_{13} + I_{1d} + I_{2d} + I_{3d}, I_{1u} + I_{2u} + I_{3u} + 3\}. \end{aligned} \quad (6.30)$$

For this parameter range, we have up to $N_Y = 52$ Yukawa couplings (see eq. (6.28)) out of $N_Y^{\text{general}} = 527$ generally possible ones (see eq. (6.24)). We find 114 AS candidates with FP_3 being UV attractive in α_2 -direction for $N_Y = 8, 9, 10$. In sec. 6.6, these 114 AS candidates are discussed in more detail.

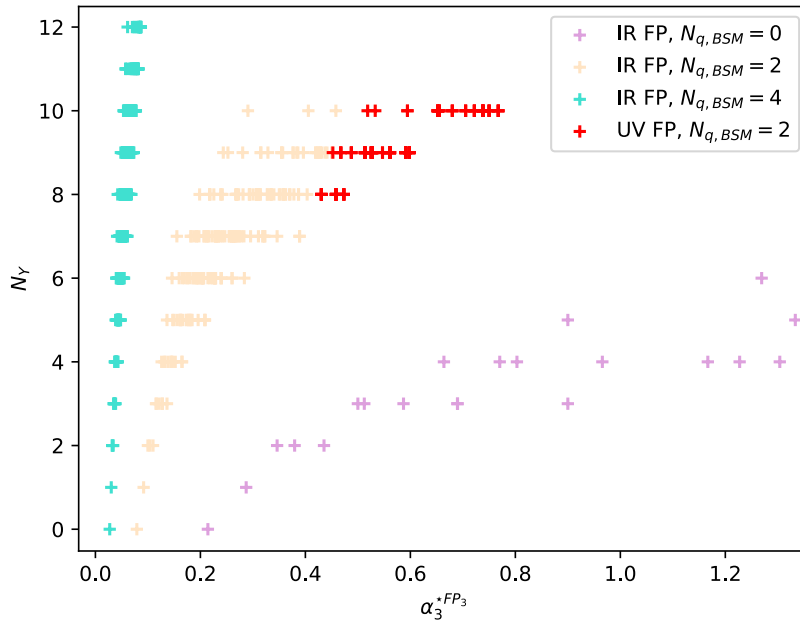


Figure 6.1: For each model within model class 1 (given by the chiral superfields of tab. 6.2 and the superpotential (6.23)) with physical FP_3 (see tab. 6.1), we show its α_3 component on the x-axis and the number of non-zero Yukawa couplings N_Y of eq. (6.28) on the y-axis. We see a pattern of branches which have different numbers of quark singlets $N_{q,BSM}$ (see (6.22)) beyond the MSSM, indicated by the different colors. UV fixed points of all 114 AS candidates are plotted as red plus signs. All other fixed points are IR fixed points. We observe that these UV fixed points match the pattern of branches and that in each branch there is a tendency of α_3^* becoming larger for larger values of N_Y .

In fig. 6.1, we show the strong component of FP_3 for all models where this fixed point is physical. We see that different numbers of $N_{q,BSM}$ lead to different branches, where for each branch there is a tendency of α_3^* becoming larger for larger values of N_Y . The interacting fixed points FP_1 , FP_2 , FP_{13} , FP_{12} and FP_{123} are unphysical in all scanned models.

6.4 Model Class 2: New Quark Doublets and Leptons

6.4.1 Framework

In our second model framework, we introduce a quark doublet $Q_4(\mathbf{3}, \mathbf{2})_{1/6}$ as well as an anti-quark doublet $\bar{Q}_1(\mathbf{3}, \mathbf{2})_{-1/6}$ as the new colored field content beyond the MSSM. Furthermore, we allow for n_L pairs of lepton and anti-lepton doublets $L(\mathbf{1}, \mathbf{2})_{-1/2}$ and $\bar{L}(\mathbf{1}, \bar{\mathbf{2}})_{1/2}$. We also include n_S gauge singlet superfields S . The resulting superfield content is summarized in table 6.3.

(Left-handed) Superfield	$SU(3)_C$	$SU(2)_L$	$U(1)_Y$	Model 2	MSSM
quark doublet Q	$\mathbf{3}$	$\mathbf{2}$	$+1/6$	4	3
anti-quark doublet \bar{Q}	$\bar{\mathbf{3}}$	$\bar{\mathbf{2}}$	$-1/6$	1	0
up-quark \bar{u}	$\bar{\mathbf{3}}$	$\mathbf{1}$	$-2/3$	3	3
down-quark \bar{d}	$\bar{\mathbf{3}}$	$\mathbf{1}$	$+1/3$	3	3
lepton doublet L	$\mathbf{1}$	$\mathbf{2}$	$-1/2$	n_L	3
anti-lepton doublet \bar{L}	$\mathbf{1}$	$\bar{\mathbf{2}}$	$+1/2$	$n_L - 3$	0
lepton singlet \bar{e}	$\mathbf{1}$	$\mathbf{1}$	$+1$	3	3
up-Higgs H_u	$\mathbf{1}$	$\mathbf{2}$	$+1/2$	1	1
down-Higgs H_d	$\mathbf{1}$	$\mathbf{2}$	$-1/2$	1	1
gauge singlets S	$\mathbf{1}$	$\mathbf{1}$	0	n_S	0

Table 6.3: Left-handed chiral superfields of model class 2 given by the MSSM fields (see tab. 4.1) plus two additional quark doublets Q_4 and \bar{Q}_1 , lepton doublets $L_{4,5,\dots,n_L}$, anti-lepton doublets $\bar{L}_{1,2,\dots,n_L-3}$ and gauge singlets S_{1,\dots,n_S} beyond the MSSM.

We study the general superpotential

$$\begin{aligned}
 W_2 = & Y^{ijk} \bar{d}_i Q_j L_k + \bar{Y}^{ijk} \bar{u}_i Q_j \bar{L}_k \\
 & + Y_S^{ik} S_i \bar{Q}_1 Q_k + x_b y_b \bar{d}_3 Q_3 H_d + x_t y_t \bar{u}_3 Q_3 H_u ,
 \end{aligned} \tag{6.31}$$

with i, j, k summing over all flavor indices and $x_t, x_b \in \{0, 1\}$ being again parameters which switch on and off the top and bottom Yukawa couplings of the MSSM. The first line of (6.31) resembles the non-MSSM terms of the superpotential (6.23) of model class 1, with the difference being that here i and j run over different numbers of flavors. We try to accommodate for the smaller amount of quark singlets, present in the Yukawa terms of Y^{ijk} and \bar{Y}^{ijk} , by including terms with Yukawa couplings Y_S^{ik} involving the new anti-quark doublet \bar{Q}_1 .

We again make a choice for the non-zero Yukawa couplings within our scan. For this, we introduce additionally to the lepton- and singlet-counting parameters (see tab. 6.3)

$$n_L, n_S, \quad (6.32)$$

the integers

$$I_d, I_u, I_Q, \quad (6.33)$$

which are used to parameterize interacting Yukawa couplings as follows. Each L and \bar{L} may appear at most once in the superpotential. To describe our investigated Yukawa structures, we introduce matrices \tilde{Y}^{ij} and $\bar{\tilde{Y}}^{ij}$ which encode the information of the non-zero entries of Y^{ijk} and \bar{Y}^{ijk} . For a given matrix \tilde{Y}^{ij} we construct Y^{ijk} by choosing k differently for each pair (i, j) , and analogously for $\bar{\tilde{Y}}^{ij}$ and \bar{Y}^{ijk} . The counting order of these k 's is irrelevant. For a given set of I -parameters (6.33), the new matrices and Y_S^{ik} are given by

$$\tilde{\mathbf{Y}} = \begin{pmatrix} \mathbf{M} & 0 & x_4 \mathbf{C} \\ x_3 \mathbf{R} & 0 & 0 \end{pmatrix}, \quad \bar{\tilde{\mathbf{Y}}} = \begin{pmatrix} \bar{\mathbf{M}} & 0 & \bar{x}_4 \bar{\mathbf{C}} \\ \bar{x}_3 \bar{\mathbf{R}} & 0 & 0 \end{pmatrix}, \quad \mathbf{Y}_S = \begin{pmatrix} 0 & 0 & 0 & x_S \mathbf{S} \\ \vdots & \vdots & \vdots & 0 \\ \vdots & \vdots & \vdots & \vdots \\ 0 & 0 & 0 & 0 \end{pmatrix}, \quad (6.34)$$

with $\mathbf{M}, \mathbf{C}, \mathbf{R}, \bar{\mathbf{M}}, \bar{\mathbf{C}}, \bar{\mathbf{R}}$ and \mathbf{S} being (rows \times columns) matrices of dimensionalities

$$\begin{aligned} \mathbf{M} &: (2 \times 2), \quad \mathbf{C} : (I_d \times 1), \quad \mathbf{R} : (1 \times I_Q), \\ \bar{\mathbf{M}} &: (2 \times 2), \quad \bar{\mathbf{C}} : (I_u \times 1), \quad \bar{\mathbf{R}} : (1 \times I_Q), \quad \mathbf{S} : (n_S \times 1), \end{aligned} \quad (6.35)$$

with $\mathbf{C}, \mathbf{R}, \bar{\mathbf{C}}, \bar{\mathbf{R}}$ and \mathbf{S} only having non-zero entries, and \mathbf{M} and $\bar{\mathbf{M}}$ consisting of submatrices \mathbf{m} and $\bar{\mathbf{m}}$ with non-zero entries

$$\mathbf{M} = \begin{pmatrix} \mathbf{m} & \dots & 0 \\ \vdots & & \vdots \\ 0 & \dots & 0 \end{pmatrix}, \quad \mathbf{m} : (I_d \times I_Q), \quad \bar{\mathbf{M}} = \begin{pmatrix} \bar{\mathbf{m}} & \dots & 0 \\ \vdots & & \vdots \\ 0 & \dots & 0 \end{pmatrix}, \quad \bar{\mathbf{m}} : (I_u \times I_Q). \quad (6.36)$$

The ‘‘switches’’

$$x_3, \bar{x}_3, x_4, \bar{x}_4, x_S, x_t, x_b \in \{0, 1\} \quad (6.37)$$

are used to individually turn on and off some of the Yukawa couplings.

With this choice of Yukawa structures, there are at most nine different Yukawa beta functions $\beta_t, \beta_b, \beta_4, \dots, \beta_{10}$ for the Yukawa couplings $\alpha_i = |y_i|^2 / (4\pi)^2$, specified in appendix D.1.2. We are able to obtain superpotentials similar to superpotentials of

model class 1 of sec. 6.3 for which we find asymptotically safe candidates. For example, for

$$\begin{aligned} I_d = I_u = I_Q = n_S = 1 , \\ x_3 = \bar{x}_3 = x_4 = x_S = x_t = x_b = 1, \bar{x}_4 = 0 , \end{aligned} \quad (6.38)$$

we obtain the superpotential

$$\begin{aligned} Y^{111} \bar{d}_1 Q_1 L_1 + Y^{142} \bar{d}_1 Q_4 L_2 + \bar{Y}^{111} \bar{u}_1 Q_1 \bar{L}_1 + Y^{313} \bar{d}_3 Q_1 L_3 \\ + \bar{Y}^{312} \bar{u}_3 Q_1 \bar{L}_2 + Y_S^{14} S_1 \bar{Q}_1 Q_4 + \underbrace{y_b \bar{d}_3 Q_3 H_d + y_t \bar{u}_3 Q_3 H_u}_{W_{\text{MSSM}}} , \end{aligned} \quad (6.39)$$

for which we need the lepton flavor-counting parameter to fulfill

$$n_L \geq 5 . \quad (6.40)$$

For this example model, the labeling of the beta functions in appendix D.1.2 for the different Yukawa couplings is

$$\begin{aligned} Y^{111} \leftrightarrow \beta_4 , Y^{142} \leftrightarrow \beta_8 , Y^{313} \leftrightarrow \beta_6 , \bar{Y}^{111} \leftrightarrow \beta_5 , \\ \bar{Y}^{312} \leftrightarrow \beta_4 , Y_S^{14} \leftrightarrow \beta_{10} , y_b \leftrightarrow \beta_b , y_t \leftrightarrow \beta_t . \end{aligned} \quad (6.41)$$

The superpotential of (6.39) is to be compared to the superpotential (6.57) of our AS benchmark of model 1. Neglecting hypercharge (so that \bar{d} and \bar{u} have the same gauge representations), we see that these two superpotentials differ in two aspects. The first being that in (6.39), \bar{u}_3 appears once outside of W_{MSSM} , and the second being that the term involving \bar{Q}_1 in (6.39) has its gauge indices contracted in a different manner than in the superpotential of model 1, leading to slightly different coefficients in the beta functions. Otherwise, the superpotential (6.39) is similar to that of eq. (6.57) where AS got established.

6.4.2 Scan

We scan 114480 models, covering the parameter space

$$\begin{aligned} 0 \leq I_d , I_u \leq 2 , \quad 1 \leq I_Q \leq 2 , \quad 1 \leq n_S \leq 5 , \\ 0 \leq x_3 , \bar{x}_3 , x_4 , \bar{x}_4 , x_S , x_t , x_b \leq 1 , \quad n_{L,\text{min}} \leq n_L \leq 11 , \end{aligned} \quad (6.42)$$

with the minimal value of the lepton-counting parameter n_L given by

$$n_{L,\text{min}} = \max\{(1 + x_4)I_d + x_3, (1 + \bar{x}_4)I_u + \bar{x}_3 + 3\} , \quad (6.43)$$

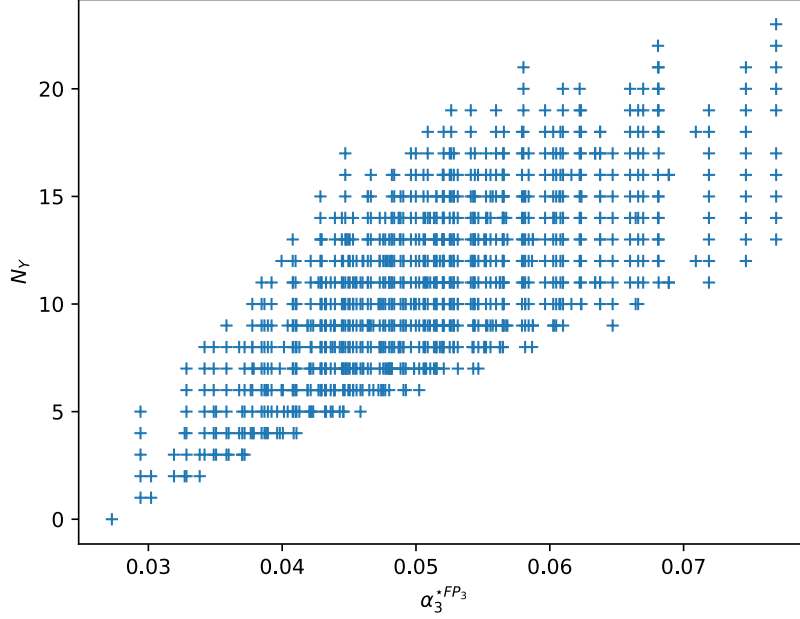


Figure 6.2: The α_3 values of FP_3 (see tab. 6.1) for all scanned models of model class 2 (given by the chiral superfields of tab. 6.3 and the superpotential (6.31)). In our search, FP_3 turns out to always be an IR fixed point. There is a tendency for the strong component of FP_3 becoming larger for larger number of Yukawa couplings N_Y of eq. (6.46).

and find no UV attractive interacting fixed points. For all models, FP_3 is physical, perturbative and IR attractive with

$$0.03 \lesssim \alpha_3^{*\text{FP}_3} \lesssim 0.08, \quad (6.44)$$

while all the other interacting fixed points are unphysical. The number of generally possible non-zero Yukawa couplings in the superpotential (6.31) is

$$N_Y^{\text{general}} = 12n_L + 12(n_L - 3) + 4n_S + 2 \stackrel{\text{Our scan}}{=} 250, \quad (6.45)$$

while the number of Yukawa couplings present in our scans is bounded by

$$N_Y = (I_d + I_u + x_3 + \bar{x}_3)I_Q + x_4I_d + \bar{x}_4I_u + x_S n_S + x_t + x_b \stackrel{\text{Our scan}}{\leq} 22. \quad (6.46)$$

In fig. 6.2, we show the value of α_3 of FP_3 against the number of Yukawa couplings N_Y of all scanned models.

6.5 Model Class 3: A Fourth Generation and new Leptons

6.5.1 Framework

The third and last possibility to include colored fields to the MSSM without B_3 becoming negative is given by a new quark doublet Q_4 and two additional quark singlets \bar{d}_4 and \bar{u}_4 , which constitute a fourth quark generation. To avoid gauge anomalies, also a fourth lepton generation consisting of a lepton doublet L_4 and a lepton singlet \bar{e}_4 is needed. In addition to this fourth particle generation, we allow for $n_L - 4$ new pairs of leptons and anti-leptons (L, \bar{L}) . The arising superfield content of model class 3 is summarized in tab. 6.4.

(Left-handed) Superfield	SU(3) _C	SU(2) _L	U(1) _Y	Model 3	MSSM
quark doublet Q	3	2	+1/6	4	3
up-quark \bar{u}	$\bar{\mathbf{3}}$	1	-2/3	4	3
down-quark \bar{d}	$\bar{\mathbf{3}}$	1	+1/3	4	3
lepton doublet L	1	2	-1/2	$n_L \geq 4$	3
anti-lepton doublet \bar{L}	1	$\bar{\mathbf{2}}$	+1/2	$n_L - 4$	0
lepton singlet \bar{e}	1	1	+1	4	3
up-Higgs H_u	1	2	+1/2	1	1
down-Higgs H_d	1	2	-1/2	1	1

Table 6.4: Left-handed chiral superfields of model class 3 given by the MSSM fields (see tab. 4.1), a fourth generation with superfields Q_4 , \bar{u}_4 , \bar{d}_4 , L_4 , additional lepton doublets L_{5,\dots,n_L} and additional anti-lepton doublets \bar{L}_{1,\dots,n_L-4} beyond the MSSM. The lepton-counting parameter n_L is taken to be larger or equal to four to include the fourth lepton generation which guarantees anomaly cancellation.

The general superpotential of interest for model class 3 reads

$$W_3 = Y^{ijk} \bar{d}_i Q_j L_k + \bar{Y}^{ijk} \bar{u}_i Q_j \bar{L}_k + y_b \bar{d}_3 Q_3 H_d + y_t \bar{u}_3 Q_3 H_u, \quad (6.47)$$

which looks exactly the same as the general superpotential (6.23) of model class 1 with the differences being that the fourth quark doublet Q_4 appears only in (6.51), and that we now always have the top- and bottom Yukawas interacting in fixed points, whereas in (6.23) these can be turned off.

Our parameterized Yukawa structures are also analogous to the ones of model class 1. Each lepton doublet L_i and each anti-lepton doublet \bar{L} may appear at most once in

the superpotential and each $\bar{d}_i \neq \bar{d}_3$ may appear zero times, once or twice. The number of times down-quark singlets appear once in a term with Q_1 or with Q_3 is counted by I_{1d} and I_{3d} , respectively. Appearances of one down-quark in two terms involving Q_1 and Q_2 , or Q_1 and Q_3 , or Q_1 and Q_4 are respectively counted by the parameters I_{12} , I_{13} and I_{14} . On the other hand, we let each up-quark $\bar{u}_i \neq \bar{u}_3$ appear at most once in our investigated superpotentials. Up-quarks appear I_{1u} times in terms with Q_1 , and I_{4u} times in terms with Q_4 . In summary, the parameters of model class 3 are given by the lepton-counting parameter and the I -parameters

$$n_L, I_{12}, I_{13}, I_{14}, I_{1d}, I_{3d}, I_{1u}, I_{4u}. \quad (6.48)$$

Again, flavor symmetries reduce the number of beta functions to be at most 12. These beta functions $\beta_t, \beta_b, \beta_4, \dots, \beta_{13}$ are shown in appendix D.1.3.

6.5.2 Scan

In a scan over the parameters (6.48), the constraints

$$n_L \geq n_{L,\min} = \max\{2I_{13} + 2I_{14} + I_{1d} + I_{3d}, I_{1u} + I_{4u} + 4\}, \quad (6.49)$$

and

$$0 \leq I_{12} + I_{13} + I_{14} + I_{1d} + I_{3d} \leq 3, \quad 0 \leq I_{1u} + I_{4u} \leq 3 \quad (6.50)$$

have to be fulfilled in order to have enough flavors to write down the superpotentials. We see from the last two constraints, that the I -parameters all may at most be three.

Scanning 13948 models within the parameter range

$$0 \leq I_{12}, I_{13}, I_{14}, I_{1d}, I_{3d}, I_{1u}, I_{4u} \leq 3, \quad n_{L,\min} \leq n_L \leq 30, \quad (6.51)$$

we find similar results compared to model class 2. For all scanned models, FP_3 is physical, perturbative and IR attractive with

$$0.03 \lesssim \alpha_3^{\star\text{FP}_3} \lesssim 0.10, \quad (6.52)$$

with the other interacting fixed points all being non-physical. Hence, we do not find any AS candidates within model 3.

In our scans, the largest number of non-zero Yukawa couplings present is

$$N_Y = 2(I_{12} + I_{13} + I_{14}) + I_{1d} + I_{3d} + I_{1u} + I_{4u} + 2 \stackrel{\text{Our scan}}{\leq} 11 \quad (6.53)$$

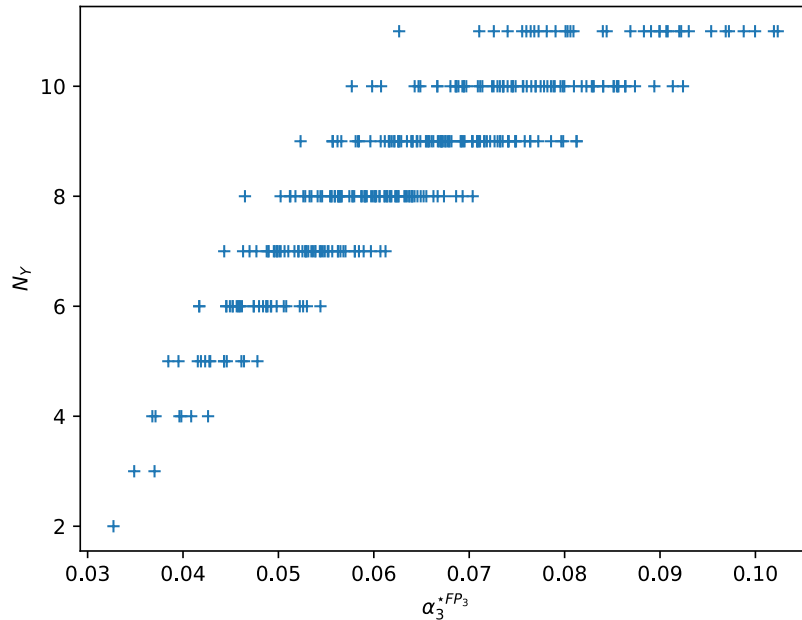


Figure 6.3: The α_3 values of FP_3 (see tab. 6.1) for all scanned models within model class 3 (given by the chiral superfields of tab. 6.4 and the superpotential (6.51)). As in model class 2, all these fixed points turn out to be IR fixed points, and there is a tendency for the strong component of FP_3 becoming larger for larger number of Yukawa couplings N_Y of eq. (6.53).

out of the generally possible amount of non-zero Yukawa couplings

$$N_Y^{\text{general}} = 16n_L + 16(n_L - 4) + 2 \stackrel{\text{Our scan}}{=} 898. \quad (6.54)$$

In fig. 6.3, we present the α_3 values of FP_3 for all scanned models in dependence of the number of present Yukawa couplings N_Y . Again, we see a tendency of α_3 becoming larger for larger numbers of Yukawa couplings.

6.6 Analysis of AS Candidates

In this section, we analyze all 114 AS candidates found perturbatively in the previous sections, all of which appear within model class 1 of sec. 6.3 and have exactly two quark singlets beyond the MSSM. We present one benchmark model and discuss matching onto the SM.

The model-specifying parameters (6.21) and (6.25) of all 114 AS candidates together with the number of superfields N_{BSM} beyond the MSSM, the amount of interacting

Yukawa couplings N_Y , and the strong component α_3^* of FP_3 are given in tab. 6.5. In all these 114 cases, FP_3 is automatically perturbative and FP_{23} is always physical and IR attractive with

$$\alpha_3^{*FP_{23}} > \alpha_3^{*FP_3} \gtrsim 0.43. \quad (6.55)$$

In fig. 6.4, we show the α_3^* values of FP_3 and FP_{23} of the 114 AS candidates. For five candidates, the strong component of FP_{23} is larger than one.

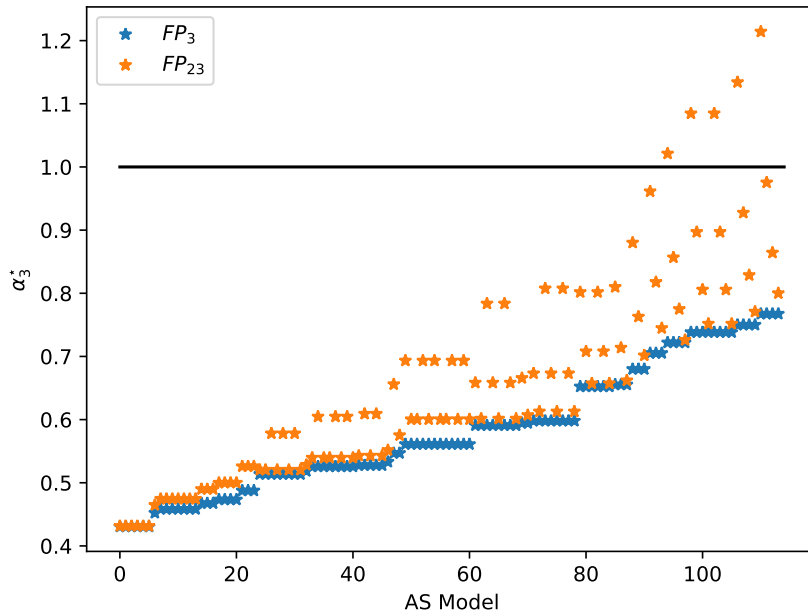


Figure 6.4: The α_3 values of FP_3 and FP_{23} (see tab. 6.1) for all 114 found AS candidates presented in tab. 6.5. All these AS candidates appear within model class 1 of sec. 6.3 and have exactly two quark singlets beyond the MSSM. There is a tendency for the strong component of FP_{23} to increase when the strong component of FP_3 becomes larger. The black line marks $\alpha_3 = 1$, which is exceeded by FP_{23} for five models.

The model specifying parameters (6.21) and (6.25) of all 114 AS candidates are shown in tab. 6.5. For all AS models, we have $I_{12} + I_{13} + I_{1d} + I_{2d} + I_{3d} + I_{1u} + I_{2u} + I_{3u} = 5$, and the sum $I_{12} + I_{13}$ being either 1, 2 or 3. Furthermore, we always find $x_t = x_b = 1$ for all AS candidates, implying that the MSSM top and bottom Yukawa couplings are always interacting in the UV. We summarize some of these results in tab. 6.6.

No.	n_u	n_d	n_L	I_{12}	I_{13}	I_{1d}	I_{2d}	I_{3d}	I_{1u}	I_{2u}	I_{3u}	N_{BSM}	N_Y	α_3^*	No.	n_u	n_d	n_L	I_{12}	I_{13}	I_{1d}	I_{2d}	I_{3d}	I_{1u}	I_{2u}	I_{3u}	N_{BSM}	N_Y	α_3^*
1	3	4	5	0	1	1	1	0	0	1	1	6	8	0.431	58	3	4	6	2	0	0	1	0	1	1	0	8	9	0.561
2	3	4	5	1	0	0	2	0	1	1	0	6	8	0.431	59	3	4	6	2	0	1	0	0	0	2	0	8	9	0.561
3	3	4	5	1	0	1	1	0	0	2	0	6	8	0.431	60	3	4	5	2	0	0	0	1	1	1	0	6	9	0.591
4	3	4	5	0	1	0	1	1	1	1	0	6	8	0.431	61	3	4	5	2	0	1	0	0	0	1	1	6	9	0.591
5	3	4	5	0	1	1	0	1	0	2	0	6	8	0.431	62	4	3	6	2	0	0	0	0	0	1	1	8	9	0.591
6	3	4	5	1	0	2	0	0	1	1	0	6	8	0.431	63	3	4	6	2	0	0	0	1	1	1	0	8	9	0.591
7	3	4	5	0	1	0	2	0	1	1	0	6	8	0.458	64	3	4	6	2	0	1	0	0	0	1	1	8	9	0.591
8	3	4	5	0	1	1	1	0	0	2	0	6	8	0.458	65	4	3	7	2	0	0	0	0	1	1	1	10	9	0.591
9	3	4	5	1	0	0	1	1	1	1	0	6	8	0.458	66	3	4	7	2	0	0	0	1	1	1	0	10	9	0.591
10	3	4	5	1	0	1	0	1	0	2	0	6	8	0.458	67	3	4	7	2	0	1	0	0	0	1	1	10	9	0.591
11	3	4	5	1	0	1	0	1	1	1	0	6	8	0.458	68	3	4	5	1	1	0	1	0	1	1	0	6	9	0.598
12	3	4	5	1	0	1	1	0	0	1	1	6	8	0.458	69	3	4	5	1	1	1	0	0	0	2	0	6	9	0.598
13	3	4	5	1	0	2	0	0	0	1	1	6	8	0.458	70	4	3	6	1	1	0	0	0	1	2	0	8	9	0.598
14	3	4	5	0	1	1	1	0	1	1	0	6	8	0.473	71	3	4	6	1	1	0	1	0	1	1	0	8	9	0.598
15	3	4	5	1	0	1	1	0	1	1	0	6	8	0.473	72	3	4	6	1	1	1	0	0	0	2	0	8	9	0.598
16	3	4	5	1	0	2	0	0	0	2	0	6	8	0.473	73	4	3	7	1	1	0	0	0	1	2	0	10	9	0.598
17	3	4	5	0	1	2	0	0	0	2	0	6	8	0.473	74	3	4	7	1	1	0	1	0	1	1	0	10	9	0.598
18	3	4	5	0	2	1	0	0	0	1	1	6	9	0.452	75	3	4	7	1	1	1	0	0	0	2	0	10	9	0.598
19	3	4	5	2	0	0	1	0	0	2	0	6	9	0.468	76	3	4	6	0	3	0	0	0	1	1	0	8	10	0.519
20	3	4	5	0	2	0	0	1	0	2	0	6	9	0.468	77	3	4	6	2	1	0	0	0	0	0	2	8	10	0.533
21	3	4	5	0	2	0	1	0	0	1	1	6	9	0.468	78	3	4	6	1	2	0	0	0	0	1	1	8	10	0.594
22	3	4	5	2	0	0	1	0	0	0	2	6	9	0.488	79	3	4	7	1	2	0	0	0	0	1	1	10	10	0.594
23	3	4	5	2	0	1	0	0	0	0	2	6	9	0.488	80	3	4	6	0	3	0	0	0	0	2	0	8	10	0.652
24	3	4	5	2	0	0	0	1	0	1	1	6	9	0.488	81	3	4	6	3	0	0	0	0	0	2	0	8	10	0.652
25	3	4	5	1	1	0	0	1	0	2	0	6	9	0.514	82	3	4	7	0	3	0	0	0	0	2	0	10	10	0.652
26	3	4	5	1	1	0	1	0	0	1	1	6	9	0.514	83	3	4	7	3	0	0	0	0	0	2	0	10	10	0.652
27	3	4	5	1	1	0	1	0	0	2	0	6	9	0.514	84	3	4	8	0	3	0	0	0	0	2	0	12	10	0.652
28	4	3	6	1	1	0	0	0	0	2	1	8	9	0.514	85	3	4	8	3	0	0	0	0	0	2	0	12	10	0.652
29	4	3	6	1	1	0	0	0	0	3	0	8	9	0.514	86	3	4	6	3	0	0	0	0	0	0	2	8	10	0.655
30	3	4	6	1	1	0	0	1	0	2	0	8	9	0.514	87	3	4	7	3	0	0	0	0	0	0	2	10	10	0.655
31	3	4	6	1	1	0	1	0	0	1	1	8	9	0.514	88	3	4	8	3	0	0	0	0	0	0	2	12	10	0.655
32	3	4	6	1	1	0	1	0	0	2	0	8	9	0.514	89	3	4	6	1	2	0	0	0	0	1	1	8	10	0.680
33	3	4	5	0	2	0	1	0	0	2	0	6	9	0.526	90	3	4	7	1	2	0	0	0	1	1	0	10	10	0.680
34	3	4	5	2	0	0	0	1	0	2	0	6	9	0.526	91	3	4	8	1	2	0	0	0	1	1	0	12	10	0.680
35	3	4	5	2	0	0	1	0	0	1	1	6	9	0.526	92	3	4	6	2	1	0	0	0	0	1	1	8	10	0.705
36	4	3	6	0	2	0	0	0	0	3	0	8	9	0.526	93	3	4	7	2	1	0	0	0	0	1	1	10	10	0.705
37	3	4	6	0	2	0	1	0	0	2	0	8	9	0.526	94	3	4	8	2	1	0	0	0	0	1	1	12	10	0.705
38	4	3	6	2	0	0	0	0	0	2	1	8	9	0.526	95	3	4	6	3	0	0	0	0	1	1	0	8	10	0.722
39	3	4	6	2	0	0	0	1	0	2	0	8	9	0.526	96	3	4	7	3	0	0	0	0	1	1	0	10	10	0.722
40	3	4	6	2	0	0	1	0	0	1	1	8	9	0.526	97	3	4	8	3	0	0	0	0	0	1	1	12	10	0.722
41	3	4	5	1	1	0	0	1	1	1	0	6	9	0.528	98	3	4	9	3	0	0	0	0	1	1	0	14	10	0.722
42	3	4	5	1	1	1	0	0	0	1	1	6	9	0.528	99	3	4	6	2	1	0	0	0	0	2	0	8	10	0.738
43	4	3	6	1	1	0	0	0	1	1	1	8	9	0.528	100	3	4	7	2	1	0	0	0	0	2	0	10	10	0.738
44	3	4	6	1	1	0	0	1	1	1	0	8	9	0.528	101	3	4	8	2	1	0	0	0	0	2	0	12	10	0.738
45	3	4	6	1	1	1	0	0	0	1	1	8	9	0.528	102	3	4	9	2	1	0	0	0	0	2	0	14	10	0.738
46	3	4	5	1	1	1	0	0	1	1	0	6	9	0.547	103	3	4	6	1	2	0	0	0	0	2	0	8	10	0.738
47	3	4	6	1	1	1	0	0	1	1	0	8	9	0.547	104	3	4	7	1	2	0	0	0	0	2	0	10	10	0.738
48	3	4	5	2	0	1	0	0	1	1	0	6	9	0.561	105	3	4	8	1	2	0	0	0	0	2	0	12	10	0.738
49	3	4	6	2	0	1	0	0	1	1	0	8	9	0.561	106	3	4	9	1	2	0	0	0	0	2	0	14	10	0.738
50	3	4	5	0	2	0	1	0	1	1	0	6	9	0.561	107	3	4	6	3	0	0	0	0	0	1	1	8	10	0.750
51	3	4	5	0	2	1	0	0	0	2	0	6	9	0.561	108	3	4	7	3	0	0	0	0	0	1	1	10	10	0.750
52	3	4	5	2	0	0	1	0	1	1	0	6	9	0.561	109	3	4	8	3	0	0	0	0	0	1	1	12	10	0.750
53	3	4	5	2	0	1	0	0	0	2	0	6	9	0.561	110	3	4	9	3	0	0	0	0	0	1	1	14	10	0.750
54	4	3	6	0	2	0	0	0	1	2	0	8	9	0.561	111	3	4	6	2	1	0	0	0	1	1	0	8	10	0.767
55	3	4	6	0	2	0	1	0	1	1	0	8	9	0.561	112	3	4	7	2	1	0	0	0	1	1	0	10	10	0.767
56	3	4	6	0	2	1	0	0	0	2	0	8	9	0.561	113	3	4	8	2	1	0	0	0	1	1	0	12	10	0.767
57	4	3	6	2	0	0	0	0	1	2	0	8	9	0.561	114	3	4	9	2	1	0	0	0	1	1	0	14	10	0.767

Table 6.5: All 114 MSSM extensions with interacting UV fixed points, appearing exclusively within model class 1 of sec. 6.3 and containing two quark singlets beyond the MSSM. For each model, we show the number of left-handed up-type quark singlets (n_u), down-type singlets (n_d), and lepton (n_L) chiral superfields, the parameters (6.25) characterizing the superpotential, the total number of superfields N_{BSM} beyond the MSSM (6.22), the total number of non-trivial Yukawa couplings N_Y (6.28), and the fixed point values α_3^* of FP_3 (see tab. 6.1). For all AS candidates, the top and bottom Yukawa couplings are interacting in the UV. Models are ordered according to increasing N_Y , α_3^* , and N_{BSM} .

Scanned models	No. AS models		Common features of AS models			
	$\text{FP}_{23} \leq 1$	$\text{FP}_{23} > 1$				
3434836	109	5	$I_{12} + I_{13} + \sum_{i=1}^3 (I_{id} + I_{iu}) = 5$	$x_t = x_b = 1$	FP_{23} IR	$\alpha_3^{\text{FP}_{23}} > \alpha_3^{\text{FP}_3} \gtrsim 0.43$

Table 6.6: Some features of all 114 perturbatively discovered AS candidates presented in tab. 6.5. From the ~ 3.4 million scanned models within model class 1 of sec. 6.3, only these 114 models have interacting UV fixed points FP_3 (see tab. 6.1). Five of these AS candidates have non-perturbative couplings larger than one. The I -integers used as model specifying parameters within model class 1 (see (6.27)) always sum up to five. The parameters x_t, x_b being one for all AS candidates implies that the top and bottom Yukawa couplings are both interacting in the UV. Furthermore, FP_{23} is always IR attractive and its strong coupling is always larger than the strong coupling of FP_3 .

6.6.1 Benchmark

As an AS benchmark within model class 1 of sec. 6.3, we choose model No. 7 from tab. 6.5 given by the parameters

$$\begin{aligned} n_u = 3, \quad n_d = 4, \quad n_L = 5, \quad x_b = x_t = 1, \\ I_{12} = 0, \quad I_{13} = 1, \quad I_{2d} = 2, \quad I_{1d} = I_{3d} = 0, \quad I_{1u} = I_{2u} = 1, \quad I_{3u} = 0, \end{aligned} \quad (6.56)$$

which correspond to the particle content shown in tab. 6.7 and the superpotential

Superfield	SU(3) _C	SU(2) _L	U(1) _Y	Flavor multiplicity
quark doublet Q	3	2	+1/6	3
up-quark \bar{u}	$\bar{\mathbf{3}}$	1	-2/3	3
down-quark \bar{d}	$\bar{\mathbf{3}}$	1	+1/3	3
lepton doublet L	1	2	-1/2	3
lepton singlet \bar{e}	1	1	+1	3
up-Higgs H_u	1	2	+1/2	1
down-Higgs H_d	1	2	-1/2	1
BSM quark \bar{d}_4	$\bar{\mathbf{3}}$	1	+1/3	1
BSM anti-quark d_1	3	1	-1/3	1
BSM lepton doublet $L_{4,5}$	1	2	-1/2	2
BSM anti-lepton doublet $\bar{L}_{1,2}$	1	$\bar{\mathbf{2}}$	+1/2	2

Table 6.7: Left-handed chiral superfield content of our AS MSSM benchmark, model No. 7 of tab. 6.5. The last four rows show additional superfields beyond the MSSM.

$$\begin{aligned} W = & Y^{411} \bar{d}_4 Q_1 L_1 + Y^{432} \bar{d}_4 Q_3 L_2 + Y^{124} \bar{d}_1 Q_2 L_4 + Y^{225} \bar{d}_2 Q_2 L_5 \\ & + \bar{Y}^{211} \bar{u}_2 Q_1 \bar{L}_1 + \bar{Y}^{122} \bar{u}_1 Q_2 \bar{L}_2 + y_t \bar{u}_3 Q_3 H_u + y_b \bar{d}_3 Q_3 H_d. \end{aligned} \quad (6.57)$$

Every term of the superpotential (6.57) contains exactly one superfield beyond the MSSM. Hence even though R -parity violation is a crucial feature of the superpotential (6.23), we can stay within experimental bounds in our benchmark model if the masses of these fields beyond the MSSM are large enough [143, 145–150].

For the eight Yukawa couplings in (6.57), there are only seven different beta functions due to the flavor symmetry

$$(\bar{d}_1, L_4) \leftrightarrow (\bar{d}_2, L_5). \quad (6.58)$$

We have the following correspondence between the Yukawa couplings of (6.57) and the seven out of 12 possible beta functions $\beta_t, \beta_b, \beta_4, \dots, \beta_{13}$ (compare with (6.26)):

$$\begin{aligned} Y^{411} & \rightarrow \beta_8, \quad Y^{432} \rightarrow \beta_9, \quad Y^{124}, Y^{225} \rightarrow \beta_7, \\ \bar{Y}^{211} & \rightarrow \beta_{11}, \quad \bar{Y}^{122} \rightarrow \beta_{12}, \quad y_t \rightarrow \beta_t, \quad y_b \rightarrow \beta_b. \end{aligned} \quad (6.59)$$

The components $(\alpha_3^*, \alpha_2^*, \alpha_1^*, \alpha_{\bar{Y}411}^*, \alpha_{\bar{Y}432}^*, \alpha_{\bar{Y}124}^*, \alpha_{\bar{Y}225}^*, \alpha_{\bar{Y}211}^*, \alpha_{\bar{Y}122}^*, \alpha_{y_t}^*, \alpha_{y_b}^*)$ of the physical fixed points of our benchmark model are given by

$$\begin{aligned} \text{FP}_3 &\approx (0.458, 0, 0, 0.278, 0.208, 0.306, 0.306, 0.361, 0.306, 0.319, 0.319), \\ \text{FP}_{23} &\approx (0.474, 0.025, 0, 0.296, 0.222, 0.326, 0.326, 0.385, 0.326, 0.341, 0.341), \end{aligned} \tag{6.60}$$

with all non-zero components of FP_{23} being slightly larger than the corresponding couplings of FP_3 .

In fig. 6.5, we present the RG flow of our benchmark model in an α_3 - α_2 -plane where the Yukawa values are given by their nullcline values, for which Yukawa beta functions vanish. The RG flows of the other AS candidates consistently look similar. Next to the gaussian fixed point G, we show FP_3 and FP_{23} , as well as the SM trajectory which is approximated at two loop level involving the top Yukawa coupling at one-loop level. In this plot we see that the UV-safe trajectory (orange) intersect with the SM trajectory at a point corresponding to an energy scale in the $\mathcal{O}(100 \text{ MeV})$ range. Due to the large value of $\alpha_3^{\text{FP}_3} \sim 0.43$ shown in eq. (6.55), all AS candidates have such low matching scales. Further investigations show that for all scanned models, we have $B_{1,\text{eff}}^{\text{FP}_3}$ and $B_{1,\text{eff}}^{\text{FP}_{23}}$ positive. From the non-physicality of the fixed points $\text{FP}_1, \text{FP}_{12}, \text{FP}_{13}, \text{FP}_{123}$ for all scanned models we infer that all UV-safe trajectories have vanishing hypercharge coupling. Hence, our AS candidates cannot be matched onto the SM.

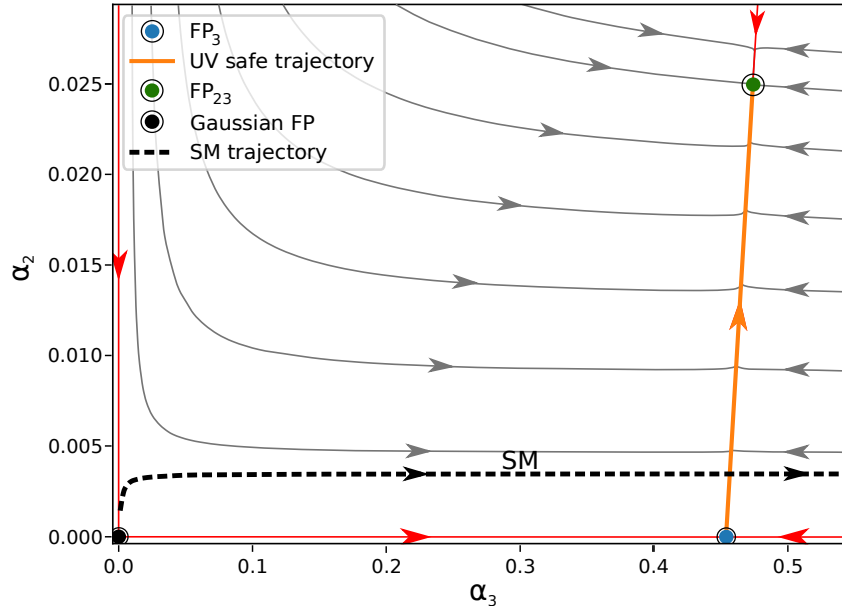


Figure 6.5: The general RG flow of AS MSSM extensions. The plot depicts the RG flow of the benchmark model with the particle content shown in table 6.7 and the superpotential (6.57). The Yukawa values in every point of the plot are given by their nullcline values for which Yukawa beta functions vanish. Additionally the SM trajectory, calculated in the 2-1-approximation including the top Yukawa coupling, is shown as a black dashed line.

6.7 Summary and Remarks on AS MSSM Extensions

As discussed in sec. 6.1, no UV attractive fixed points were found to exist within the MSSM itself, with and without R -parity (4.27) [132, 143].

We performed scans within three classes of MSSM extensions in sections 6.3, 6.4 and 6.5, containing the MSSM superfields and

- Model class 1: New quark singlets and new leptons ,
- Model class 2: Two new quark doublets and new leptons ,
- Model class 3: A fourth generation and new leptons .

Since only for models with at most four quarks beyond the MSSM interacting fixed points can exist within the 2-1-approximation, as discussed in sec. 6.2, we covered all

possible colored field contents allowing for AS in MSSM extensions. Various Yukawa structures were parameterized with the aim of generating interacting UV fixed points.

We indeed found 114 AS MSSM extensions with FP_3 (see tab. 6.1) being UV attractive. All of these AS candidates occur within model class 1 and have exactly two quark singlets and between four and ten leptons beyond the MSSM. The model parameters characterizing these AS candidates are listed in tab. 6.5.

In our scan within model class 1 covering the parameter space (6.29), we went up to 16 quarks beyond the MSSM and 22 leptons beyond the MSSM. In fig. 6.1, we show the strong component of all physical FP_3 found within our scan of model class 1, plotted against the number of interacting Yukawa couplings N_Y of eq. (6.28). Three distinct branches, and a tendency for the strong coupling of FP_3 becoming larger for more interacting Yukawa couplings are observed.

In our AS benchmark model (model No. 7 of tab. 6.5), presented in sec. 6.6.1, we find that the intrinsic R -parity violation of superpotential W_1 from (6.23) can be tuned such that it stays within experimental limits by making BSM masses large [143, 145–150]. The RG flow of this AS benchmark is depicted in fig. 6.5, where we find that supersymmetry-breaking matching scales are in the $\mathcal{O}(100 \text{ MeV})$ range, in conflict with experimental non-observation of SM superpartners at such energy scales [43]. Furthermore, we find that $\alpha_1 = 0$ along the UV-safe trajectory connecting FP_3 and FP_{23} , implying that the hypercharge coupling cannot be matched onto the SM. This RG-flow behavior is qualitatively the same for all AS candidates. From the gauge beta functions (5.10) we find that the value of $\alpha_3^{\star\text{FP}_3}$ is always bounded from below by

$$\alpha_3^{\star\text{FP}_3} = \frac{B_3}{C_{33} - \sum_y D_{3y}\alpha_y} \stackrel{D_{3y} \geq 0}{\geq} \frac{B_3}{C_{33}} \geq \frac{3}{110} \approx 0.027, \quad (6.61)$$

where for the last inequality we inserted the values for B_3 and C_{33} obtained for the MSSM fields plus four quarks beyond the MSSM, using eqs. (5.6a) and (5.6b). This lower bound at best enables matching scales in the range of $\mathcal{O}(1 \text{ GeV})$. Higher loop orders and gravitational corrections might change this picture such that α_1 becomes interacting along UV-safe trajectories, and matching scales are pushed towards larger energies, not in conflict with phenomenology anymore.

In the other two model classes 2 and 3, no AS candidates were found. As seen in figs. 6.2 and 6.3, here the strong component of FP_3 is always much smaller than in the AS cases of model class 1. This is due to the larger amount of colored fields in the model classes 2 and 3, compared to the AS cases of model class 1. Nevertheless, also in these last two cases a tendency of the strong component of FP_3 becoming larger with more interacting Yukawa couplings is observed.

Within our model scans, we observed for FP_3 and FP_{23} that

$$\begin{aligned} \text{FP}_{23} \text{ physical} &\Leftrightarrow \text{FP}_{23} \text{ physical and IR attractive} \\ &\Leftrightarrow \text{FP}_3 \text{ physical and UV attractive} \Leftrightarrow \alpha_3^{\text{FP}_{23}} > \alpha_3^{\text{FP}_3} , \end{aligned} \tag{6.62}$$

which we prove in appendix C to be true for all MSSM extensions in the 2-1-approximation.

Chapter 7

MSSM Extensions with an Additional $SU(N)$ Gauge Sector

Our searches within MSSM extensions of chapter 6 yield AS candidates with supersymmetry-breaking matching scales in conflict with phenomenological observations. Furthermore, we always find in our search that the hypercharge coupling α_1 vanishes on UV-safe trajectories, prohibiting matching onto the SM at all.

With a new non-abelian $SU(N)$ gauge factor, new fixed points are available which allow for small (or even vanishing) MSSM gauge couplings, which is preferred for matching onto the SM at large energies. Fields charged under this new $SU(N)$ ($N \geq 2$) may have hypercharges allowing for UV-safe trajectories to develop interacting α_1 -values along them, so that matching onto the SM becomes possible.

In our following analysis, we present a model framework extending the MSSM by including an additional $SU(N)$ gauge sector and some fields beyond the MSSM, which we call the “MSSM+”. Within this framework, we indeed find candidates exhibiting the desired feature of supersymmetry-breaking matching scales above 1 TeV. For three benchmark models, we demonstrate matching onto the SM. We then proceed to implement supersymmetry-breaking via gauge-mediation and find that we still maintain AS models within the MSSM+ framework.

7.1 The MSSM+ Framework

In the MSSM+ framework, we consider gauge anomaly-free MSSM extensions with gauge groups

$$G_{\text{MSSM}+} = SU(N) \otimes SU(3)_C \otimes SU(2)_L \otimes U(1)_Y , \quad (7.1)$$

which we scan for AS models. In the following investigation, we have additionally to the gauge couplings

$$\{\alpha_+, \alpha_3, \alpha_2, \alpha_1\} , \quad (7.2)$$

up to eight Yukawa couplings

$$\{\alpha_4, \dots, \alpha_{11}\} , \quad (7.3)$$

and focus on fixed points

$$\text{FP}_+ = \left(\alpha_+^*, 0, 0, 0, \alpha_4^*, \dots, \alpha_{11}^* \right) , \quad (7.4)$$

which only have α_+ and some Yukawa couplings interacting.

The left-handed chiral superfields of the MSSM+ are shown in tab. 7.1. The general superpotential we focus on reads

$$W_{\text{MSSM}+} = Y^{ijk} \bar{\Psi}_i \xi_j \chi_k + \bar{Y}^{ijk} \Psi_i \bar{\xi}_j \bar{\chi}_k , \quad (7.5)$$

where we have suppressed gauge indices, and the indices i, j, k summing over all flavors. For some specific values of the hypercharge Y of the χ and $\bar{\xi}$ fields (see tab. 7.1), like $Y = \pm 1/2$, Yukawa couplings involving fields within and beyond the MSSM simultaneously exist. In this study we demand that such Yukawa couplings are absent. For generic values of Y , the absence of such terms is automatically given by gauge invariance, while in all other cases we implement a \mathbb{Z}_2 flavor symmetry to prohibit these terms. This symmetry assigns the following values to the different chiral superfields:

$$\begin{aligned} \chi, \bar{\chi}, \xi, \bar{\xi} &: -1 , \\ \Psi, \bar{\Psi}, \text{MSSM fields} &: +1 . \end{aligned} \quad (7.6)$$

Furthermore, Yukawa terms involving only fields uncharged under the new $\text{SU}(N)$ gauge symmetry, like the MSSM superpotential terms, generally appear in the superpotential. In this study, we focus on fixed points FP_+ (see (7.4)) for which the only interacting gauge component corresponds to the new $\text{SU}(N)$ factor. These fixed points are unaffected by Yukawa terms involving only fields uncharged under the new $\text{SU}(N)$. Hence we do not include such superpotential terms, and in particular do not include the MSSM superpotential.

Superfield	$SU(N)$	$SU(3)_C$	$SU(2)_L$	$U(1)_Y$	Multiplicity	
Q	$\mathbf{1}$	$\mathbf{3}$	$\mathbf{2}$	$+\frac{1}{6}$	3	} MSSM
\bar{u}	$\mathbf{1}$	$\bar{\mathbf{3}}$	$\mathbf{1}$	$-\frac{2}{3}$	3	
\bar{d}	$\mathbf{1}$	$\bar{\mathbf{3}}$	$\mathbf{1}$	$+\frac{1}{3}$	3	
L	$\mathbf{1}$	$\mathbf{1}$	$\mathbf{2}$	$-\frac{1}{2}$	3	
\bar{e}	$\mathbf{1}$	$\mathbf{1}$	$\mathbf{1}$	$+1$	3	
H_u	$\mathbf{1}$	$\mathbf{1}$	$\mathbf{2}$	$+\frac{1}{2}$	1	
H_d	$\mathbf{1}$	$\mathbf{1}$	$\mathbf{2}$	$-\frac{1}{2}$	1	
χ	$\mathbf{1}$	$\mathbf{1}$	$\mathbf{2}$	$+Y$	m	} joint
$\bar{\chi}$	$\mathbf{1}$	$\mathbf{1}$	$\bar{\mathbf{2}}$	$-Y$	m	
ξ	\mathbf{N}	$\mathbf{1}$	$\mathbf{2}$	$-Y$	2	
$\bar{\xi}$	$\bar{\mathbf{N}}$	$\mathbf{1}$	$\bar{\mathbf{2}}$	$+Y$	2	} hidden
Ψ	\mathbf{N}	$\mathbf{1}$	$\mathbf{1}$	0	n	
$\bar{\Psi}$	$\bar{\mathbf{N}}$	$\mathbf{1}$	$\mathbf{1}$	0	n	

Table 7.1: Chiral superfield content of the gauge anomaly-free MSSM+. Additionally to the MSSM fields we include two kinds of $SU(2)_L$ doublets χ and $\bar{\chi}$, as well as jointly charged fields ξ and $\bar{\xi}$, and purely hidden fields Ψ and $\bar{\Psi}$. We set the hypercharge of the superfields $\Psi, \bar{\Psi}$ to zero.

We parameterize the possible interacting Yukawa couplings with the integers

$$I_{12}, I_1, I_2, \bar{I}_{12}, \bar{I}_1, \bar{I}_2, \quad (7.7)$$

which count the following Yukawa terms. Each field $\bar{\Psi}$ and Ψ may appear up to two times in the superpotential. The number of times $\bar{\Psi}$ -fields appear once and in terms involving ξ_1 or ξ_2 is I_1 or I_2 , respectively (analogously, the number of times that the fields Ψ appear once and in terms involving $\bar{\xi}_1$ or $\bar{\xi}_2$ is \bar{I}_1 or \bar{I}_2 , respectively). For the fields $\bar{\Psi}$ being present twice in the superpotential, once in a term involving ξ_1 and once in a term involving ξ_2 , we use I_{12} to count the number of such cases (analogously, for Ψ appearing twice in the superpotential, once in a term involving $\bar{\xi}_1$ and once in a term involving $\bar{\xi}_2$, we use \bar{I}_{12}). Each χ and each $\bar{\chi}$ may appear at most once in the superpotential.

The number of Yukawa terms N_Y in our superpotentials is then

$$N_Y = 2(I_{12} + \bar{I}_{12}) + I_1 + I_2 + \bar{I}_1 + \bar{I}_2. \quad (7.8)$$

In summary, the I -parameters (7.7) count the different possible Yukawa terms as

$$\begin{aligned}
y_4 \bar{\Psi}_i \xi_1 \chi_k + y_5 \bar{\Psi}_i \xi_2 \chi_{k'} &: I_{12} , \\
y_6 \bar{\Psi}_i \xi_1 \chi_k &: I_1 , \\
y_7 \bar{\Psi}_i \xi_2 \chi_k &: I_2 , \\
y_8 \Psi_i \bar{\xi}_1 \bar{\chi}_k + y_9 \Psi_i \bar{\xi}_2 \bar{\chi}_k &: \bar{I}_{12} , \\
y_{10} \Psi_i \bar{\xi}_1 \bar{\chi}_k &: \bar{I}_1 , \\
y_{11} \Psi_i \bar{\xi}_2 \bar{\chi}_k &: \bar{I}_2 ,
\end{aligned} \tag{7.9}$$

with y_4, \dots, y_{11} being eight different types of Yukawa couplings having the same beta function per type due to remaining flavor symmetries acting on the $\Psi, \bar{\Psi}, \chi$ and $\bar{\chi}$ fields appearing in terms of the same Yukawa type. The beta functions of the MSSM+ are presented in appendix (D.2).

When doing scans, the number of $(\chi, \bar{\chi})$ and $(\Psi, \bar{\Psi})$ pairs m and n have to be large enough to accompany for all Yukawa terms, i.e. they have to fulfill

$$\begin{aligned}
m &\geq \max\{2I_{12} + I_1 + I_2, 2\bar{I}_{12} + \bar{I}_1 + \bar{I}_2\} = m^{\min} , \\
n &\geq \max\{I_{12} + I_1 + I_2, \bar{I}_{12} + \bar{I}_1 + \bar{I}_2\} = n^{\min} .
\end{aligned} \tag{7.10}$$

With this, a specific model within the MSSM+ framework is classified completely by the parameters

$$m, n, I_{12}, I_1, I_2, \bar{I}_{12}, \bar{I}_1, \bar{I}_2 . \tag{7.11}$$

We stress that we couple the hidden sector only via the electroweak forces to the visible sector. In an analogous model involving also colored joint fields, we do not find AS MSSM extensions.

In the vicinity of FP_+ , defined in (7.4), the MSSM gauge beta functions are approximated by

$$\beta_3 \Big|_{\text{FP}_+} \approx -B_{3,\text{eff}}^{\text{FP}_+} \alpha_3^2, \quad \beta_2 \Big|_{\text{FP}_+} \approx -B_{2,\text{eff}}^{\text{FP}_+} \alpha_2^2, \quad \beta_1 \Big|_{\text{FP}_+} \approx -B_{1,\text{eff}}^{\text{FP}_+} \alpha_1^2, \tag{7.12}$$

with

$$B_{3,\text{eff}}^{\text{FP}_+} = B_3 - C_{3+} \alpha_+^* + \sum_{i=4}^{11} D_{3i} \alpha_i^*, \tag{7.13}$$

$$B_{2,\text{eff}}^{\text{FP}_+} = B_2 - C_{2+} \alpha_+^* + \sum_{i=4}^{11} D_{2i} \alpha_i^*, \tag{7.14}$$

$$B_{1,\text{eff}}^{\text{FP}_+} = B_1 - C_{1+} \alpha_+^* + \sum_{i=4}^{11} D_{1i} \alpha_i^*. \tag{7.15}$$

Details on the coefficients are given in appendix D.2. For all $B_{i,\text{eff}}^{\text{FP}_+} > 0$ ($i = 3, 2, 1$), FP_+ is UV attractive in the α_3 -, α_2 - and α_1 -directions, suggesting that matching onto the SM is possible. Hence in the following section we scan for (perturbative and physical) fixed points FP_+ , for which these effective B -coefficients are positive. We call such models “asymptotically safe in our sense”.

7.2 Model Scans and Matching onto the SM

We perform model scans for different discrete hypercharges Y of the BSM fields χ and $\bar{\xi}$ (see tab. 7.1) within the range

$$Y \in [0, 2] . \quad (7.16)$$

For each Y , we scan ~ 11.7 million anomaly-free models within the parameter range

$$\begin{aligned} 2 \leq N \leq 10 , \quad 0 \leq I_{12}, I_1, I_2, \bar{I}_{12}, \bar{I}_1, \bar{I}_2 \leq 5 , \quad m^{\min} \leq m \leq 21 , \quad n^{\min} \leq n \leq 16 , \\ \text{with} \quad I_1 \leq I_2 , \quad \bar{I}_1 \leq \bar{I}_2 , \end{aligned} \quad (7.17)$$

and find that for each $N \geq 4$, there exists a minimal hypercharge value Y_{\min} of Y such that AS models in our sense do exist, presented in table 7.2. We also state the number of AS candidates for each listed value of Y as well as the approximate value of Y_{\min} for each N . We observe that Y_{\min} gets smaller for larger N .

From eq. (7.8) we see that we have at most

$$N_Y^{\max} = 40 \quad (7.18)$$

Yukawa couplings present within our scans. For our scanned values of m and n , there are generally up to

$$N_Y^{\text{general}} = 1344 \quad (7.19)$$

Yukawa couplings present in the superpotential (7.5).

We choose three AS benchmark models (see below), with each model possessing different features of interest for us. We also demonstrate that all of these benchmark models can be matched onto the SM at a common mass scale μ_{MSSM} . Since we are interested in new physics above ~ 1 TeV, we verify that matching is indeed possible at 1 TeV, 100 TeV and 10^6 TeV by calculating trajectories starting at SM coupling values and seeing that these all flow towards FP_+ in the UV for our three benchmark scenarios. For the calculation of the UV-safe trajectories, we choose the starting values for the couplings $\alpha_+, \alpha_4, \dots, \alpha_{11} \neq 0$ such that their beta functions vanish (nullcline values) as

	$N=2$	$N=3$	$N=4$	$N=5$	$N=6$	$N=7$	$N=8$	$N=9$	$N=10$	#AS
$Y=0.0$	X	X	X	X	X	X	X	X	X	0
$Y=0.1$	X	X	X	X	X	X	X	X	X	0
$Y=0.15$	X	X	X	X	X	X	X	✓	✓	398
$Y=0.2$	X	X	X	X	X	✓	X	✓	✓	5153
$Y=0.5$	X	X	X	✓	✓	✓	✓	✓	✓	60606
$Y=1.0$	X	X	✓	✓	✓	✓	✓	✓	✓	88627
$Y=1.5$	X	X	✓	✓	✓	✓	✓	✓	✓	95506
$Y=2.0$	X	X	✓	✓	✓	✓	✓	✓	✓	96506
$Y=5.0$	X	X	✓	✓	✓	✓	✓	✓	✓	96506
$Y_{\min} \approx$	-	-	1.0	0.5	0.5	0.2	0.5	0.15	0.15	

Table 7.2: AS candidates in our sense within the parameter range (7.17). These models have physical and perturbative FP_+ of (7.4) with positive coefficients $B_{3,\text{eff}}^{\text{FP}_+}$, $B_{2,\text{eff}}^{\text{FP}_+}$ and $B_{1,\text{eff}}^{\text{FP}_+}$ as defined in eqs. (7.13)-(7.15). A “✓” implies that such candidates are found, while a “X” implies the contrary. In the very right column, we show the number of AS models found for each listed hypercharge Y of the χ and $\bar{\xi}$ fields of tab. 7.1. Additionally, the approximate value of the lower bound Y_{\min} in order to have AS candidates for each N is presented in the very last row.

functions of the couplings $\alpha_3, \alpha_2, \alpha_1$, which in turn are determined by their starting point on the SM trajectory. When calculating UV-safe trajectories, we rely on the approximations (7.12) for β_3, β_2 and β_1 since solving for trajectories flowing towards FP_+ is numerically unstable. For given starting conditions $\alpha_i(\mu_{\text{MSSM}})$, the approximated beta functions have the exact solutions

$$\alpha_i(\mu) = \frac{\alpha_i(\mu_{\text{MSSM}})}{1 + B_{i,\text{eff}}^{\text{FP}_+} \alpha_i(\mu_{\text{MSSM}}) \ln\left(\frac{\mu}{\mu_{\text{MSSM}}}\right)}, \quad i = 3, 2, 1. \quad (7.20)$$

Due to the smallness of the SM gauge couplings (below the Planck scale), the new gauge coupling α_+ as well as the Yukawa couplings $\alpha_4, \dots, \alpha_{11}$ begin at the matching scale in the vicinity of FP_+ , making (7.20) a sufficient approximation¹.

Below μ_{MSSM} , the coupling α_+ runs on its own and may develop a divergence at a scale $\mu_{\text{conf}} < \mu_{\text{MSSM}}$. Taking the scalar and fermionic components of the chiral superfields Ψ and $\bar{\Psi}$ to be massless (or sufficiently light), they all participate in a QCD-like confinement resulting in (dark) baryons with masses m_{DB} near the confinement scale

$$m_{\text{DB}} \sim \mu_{\text{conf}}. \quad (7.21)$$

The vanishing hypercharge of the chiral superfields Ψ and $\bar{\Psi}$ guarantees that the bound states are electrically neutral and hence may serve as dark matter candidates (partially) responsible for the observed dark matter energy density Ω_{DM} .

7.2.1 Benchmark 1 (BM1)

Our first benchmark, BM1, is an AS candidate within the parameter range (7.17). In the gauge-mediated scenario of section 4.2.3, it is no longer an AS candidate. BM1 is given by the parameters

$$N = 4, Y = 1.5, I_{12} = 2, I_1 = 0, I_2 = 3, \bar{I}_{12} = 3, \bar{I}_1 = 1, \bar{I}_2 = 1, m = 8, n = 5, \quad (7.22)$$

which translate into the particle content of table 7.3 and the superpotential

$$\begin{aligned} W_{\text{BM1}} = & \sum_{i=1}^2 Y^{i1i} \bar{\Psi}_i \xi_1 \chi_i + \sum_{i=1}^2 Y^{i2(i+2)} \bar{\Psi}_i \xi_2 \chi_{i+2} + \sum_{i=3}^5 Y^{i2(i+2)} \bar{\Psi}_i \xi_2 \chi_{i+2} \\ & + \sum_{i=1}^3 \bar{Y}^{i1i} \Psi_i \bar{\xi}_1 \bar{\chi}_i + \bar{Y}^{414} \Psi_4 \bar{\xi}_1 \bar{\chi}_4 + \sum_{i=1}^3 \bar{Y}^{i2(i+4)} \Psi_i \bar{\xi}_2 \bar{\chi}_{i+4} + \bar{Y}^{528} \Psi_5 \bar{\xi}_2 \bar{\chi}_8, \end{aligned} \quad (7.23)$$

¹We also checked for our three following benchmark models that within the MSSM+, β_3, β_2 , and β_1 of appendix D.2 are all negative at μ_{MSSM} with the couplings $\alpha_+, \alpha_4, \dots, \alpha_{11}$ given by their nullcline values at this energy. Hence we have guaranteed that we start on the SM trajectory at points which flow towards FP_+ in the UV. We confirm this behavior for all energies above 1 TeV for our benchmark models.

where we have the following Yukawa couplings evolving with the beta functions of appendix D.2

$$\begin{aligned}
Y^{111}, Y^{212} &: \beta_4, \\
Y^{123}, Y^{224} &: \beta_6, \\
Y^{325}, Y^{426}, Y^{527} &: \beta_7, \\
\bar{Y}^{111}, \bar{Y}^{212}, \bar{Y}^{313} &: \beta_8, \\
\bar{Y}^{414} &: \beta_9, \\
\bar{Y}^{125}, \bar{Y}^{226}, \bar{Y}^{327} &: \beta_{10}, \\
\bar{Y}^{528} &: \beta_{11}.
\end{aligned} \tag{7.24}$$

In Benchmark 1, the components of FP_+ are given by

$$\begin{aligned}
\alpha_+^{\text{FP}_+} &\approx 0.88, & \alpha_4^{\text{FP}_+} &\approx 0.73, & \alpha_6^{\text{FP}_+} &\approx 0.40, & \alpha_7^{\text{FP}_+} &\approx 0.65, \\
\alpha_8^{\text{FP}_+} &\approx 0.54, & \alpha_9^{\text{FP}_+} &\approx 0.72, & \alpha_{10}^{\text{FP}_+} &\approx 0.54, & \alpha_{11}^{\text{FP}_+} &\approx 0.72,
\end{aligned} \tag{7.25}$$

which is close to being non-perturbative.

The one-loop B -coefficients and the effective B -coefficients read

$$\begin{aligned}
B_3 &= 6, & B_{3,\text{eff}}^{\text{FP}_+} &= 6, \\
B_2 &= -34, & B_{2,\text{eff}}^{\text{FP}_+} &= 1.72, \\
B_1 &= -310, & B_{1,\text{eff}}^{\text{FP}_+} &= 11.51.
\end{aligned} \tag{7.26}$$

In fig. 7.1, we show the matching onto the SM at 1 TeV, 10^3 TeV, and 10^6 TeV for the gauge couplings α_3 , α_2 and α_1 . The Yukawa couplings $\alpha_4, \dots, \alpha_{11}$ approximately take on their fixed point values along their trajectories.

Superfield	$SU(4)$	$SU(3)_C$	$SU(2)_L$	$U(1)_Y$	Multiplicity	
Q	1	3	2	$+\frac{1}{6}$	3	} MSSM
\bar{u}	1	$\bar{\mathbf{3}}$	1	$-\frac{2}{3}$	3	
\bar{d}	1	$\bar{\mathbf{3}}$	1	$+\frac{1}{3}$	3	
L	1	1	2	$-\frac{1}{2}$	3	
\bar{e}	1	1	1	$+1$	3	
H_u	1	1	2	$+\frac{1}{2}$	1	
H_d	1	1	2	$-\frac{1}{2}$	1	
χ	1	1	2	$+1.5$	8	
$\bar{\chi}$	1	1	$\bar{\mathbf{2}}$	-1.5	8	
ξ	4	1	2	-1.5	2	} joint
$\bar{\xi}$	$\bar{\mathbf{4}}$	1	$\bar{\mathbf{2}}$	$+1.5$	2	
Ψ	4	1	1	0	5	} hidden
$\bar{\Psi}$	$\bar{\mathbf{4}}$	1	1	0	5	

Table 7.3: Chiral superfields of the AS MSSM+ benchmark BM1. The superpotential of BM1 is given in (7.23).

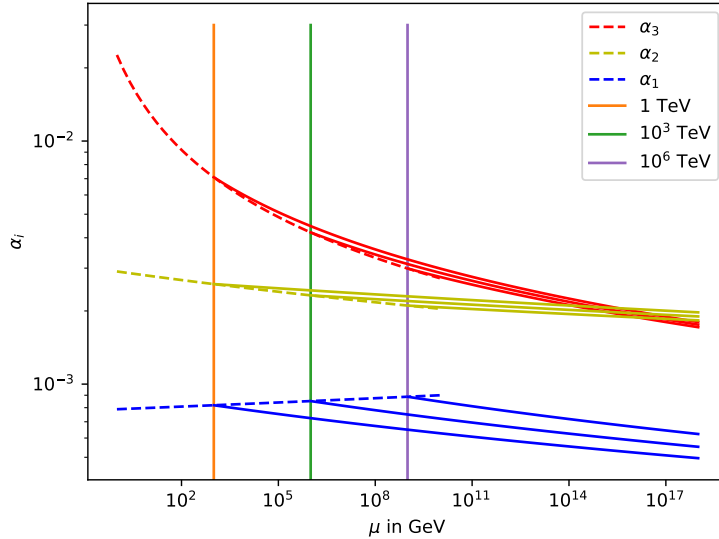


Figure 7.1: Running of the gauge couplings $\alpha_3, \alpha_2, \alpha_1$ matched from BM1 (see tab. 7.3) onto the SM at 1 TeV (orange), 10^3 TeV (green) and 10^6 TeV (purple). Dashed lines show coupling evolutions within the SM at two-loop gauge and one-loop Yukawa order including the top Yukawa, while solid lines are trajectories within BM1.

7.2.2 Benchmark 2 (BM2)

The second AS benchmark, BM2, is even closer than BM1 to being non-perturbative, but it is still an AS candidate in the gauge-mediated scenario of sec. 4.2.3. The parameters of BM2 are

$$N = 4, Y = 1.5, I_{12} = 1, I_1 = 1, I_2 = 3, \bar{I}_{12} = 4, \bar{I}_1 = 0, \bar{I}_2 = 1, m = 9, n = 5, \quad (7.27)$$

which translate into the particle content of table 7.4 and the superpotential

$$\begin{aligned} W_{\text{BM2}} = & Y^{111} \bar{\Psi}_1 \xi_1 \chi_1 + Y^{212} \bar{\Psi}_2 \xi_1 \chi_2 + Y^{123} \bar{\Psi}_1 \xi_2 \chi_3 + \sum_{i=3}^5 Y^{i2(i+1)} \bar{\Psi}_i \xi_2 \chi_{i+1} \\ & + \sum_{i=1}^4 \bar{Y}^{i1i} \Psi_i \bar{\xi}_1 \bar{\chi}_i + \sum_{i=1}^4 \bar{Y}^{i2(i+4)} \Psi_i \bar{\xi}_2 \bar{\chi}_{i+4} + \bar{Y}^{529} \Psi_5 \bar{\xi}_2 \bar{\chi}_9, \end{aligned} \quad (7.28)$$

where we have the following correspondence between Yukawa couplings and beta functions of appendix D.2

$$\begin{aligned} Y^{111} & : \beta_4, \\ Y^{212} & : \beta_5, \\ Y^{123} & : \beta_6, \\ Y^{324}, Y^{425}, Y^{526} & : \beta_7, \\ \bar{Y}^{111}, \bar{Y}^{212}, \bar{Y}^{313}, \bar{Y}^{414} & : \beta_8, \\ \bar{Y}^{125}, \bar{Y}^{226}, \bar{Y}^{327}, \bar{Y}^{428} & : \beta_{10}, \\ \bar{Y}^{529} & : \beta_{11}. \end{aligned} \quad (7.29)$$

In Benchmark 2, the components of FP_+ are given by

$$\begin{aligned} \alpha_+^{\text{FP}_+} \approx 0.96, \quad \alpha_4^{\text{FP}_+} \approx 0.76, \quad \alpha_5^{\text{FP}_+} \approx 0.92, \quad \alpha_6^{\text{FP}_+} \approx 0.49, \\ \alpha_7^{\text{FP}_+} \approx 0.75, \quad \alpha_8^{\text{FP}_+} \approx 0.62, \quad \alpha_{10}^{\text{FP}_+} \approx 0.53, \quad \alpha_{11}^{\text{FP}_+} \approx 0.73, \end{aligned} \quad (7.30)$$

which is even closer to being non-perturbative than BM1.

The one-loop B -coefficients and the effective B -coefficients are given by

$$\begin{aligned} B_3 = 6, \quad B_{3,\text{eff}}^{\text{FP}_+} = 6, \\ B_2 = -36, \quad B_{2,\text{eff}}^{\text{FP}_+} = 3.95, \\ B_1 = -328, \quad B_{1,\text{eff}}^{\text{FP}_+} = 31.53. \end{aligned} \quad (7.31)$$

In fig. 7.2, we show the matching onto the SM at 1 TeV, 10^3 TeV and 10^6 TeV for the gauge couplings α_3 , α_2 and α_1 . The Yukawa couplings again are approximately constant.

Superfield	SU(4)	SU(3) _C	SU(2) _L	U(1) _Y	Multiplicity	
Q	1	3	2	$+\frac{1}{6}$	3	} MSSM
\bar{u}	1	$\bar{\mathbf{3}}$	1	$-\frac{2}{3}$	3	
\bar{d}	1	$\bar{\mathbf{3}}$	1	$+\frac{1}{3}$	3	
L	1	1	2	$-\frac{1}{2}$	3	
\bar{e}	1	1	1	$+1$	3	
H_u	1	1	2	$+\frac{1}{2}$	1	
H_d	1	1	2	$-\frac{1}{2}$	1	
χ	1	1	2	$+1.5$	9	
$\bar{\chi}$	1	1	$\bar{\mathbf{2}}$	-1.5	9	
ξ	4	1	2	-1.5	2	} joint
$\bar{\xi}$	$\bar{\mathbf{4}}$	1	$\bar{\mathbf{2}}$	$+1.5$	2	
Ψ	4	1	1	0	5	} hidden
$\bar{\Psi}$	$\bar{\mathbf{4}}$	1	1	0	5	

Table 7.4: Chiral superfields of the AS MSSM+ benchmark BM2. This second benchmark has the superpotential (7.28)

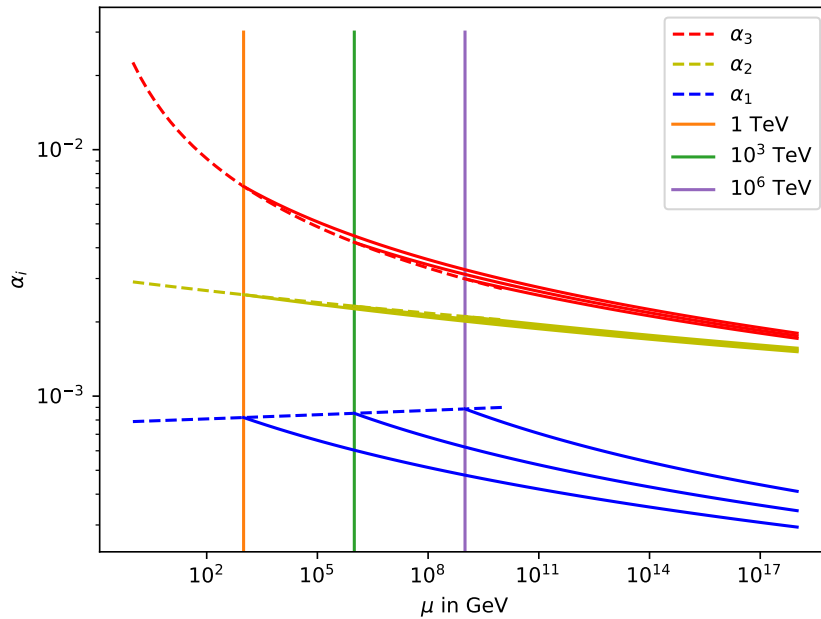


Figure 7.2: An analogous plot to fig. 7.1, here with solid lines showing coupling evolutions within BM2 (see tab. 7.4), and dashed lines again showing coupling evolutions within the SM.

7.2.3 Benchmark 3 (BM3)

Our last benchmark, denoted as BM3, is AS for $Y = 3/2$ as well as for $Y = 1/2$ in both, the MSSM+ and also in the gauge-mediated scenario of sec. 4.2.3. Furthermore, it has the smallest α_+ value for FP_+ found in the parameter regime (7.17), making it perturbatively more viable than BM1 and BM2. BM3 is given by the parameters

$$\begin{aligned} N = 9, \quad I_{12} = 4, \quad I_1 = 5, \quad I_2 = 5, \quad \bar{I}_{12} = 4, \quad \bar{I}_1 = 4, \quad \bar{I}_2 = 4, \quad m = 18, \quad n = 14, \\ Y = 0.5 \text{ or } Y = 1.5, \end{aligned} \quad (7.32)$$

which translate into the field content of table 7.5 and the superpotential

$$\begin{aligned} W_{\text{BM3}} = & \sum_{i=1}^4 Y^{i1i} \bar{\Psi}_i \xi_1 \chi_i + \sum_{i=5}^9 Y^{i1i} \bar{\Psi}_i \xi_1 \chi_i + \sum_{i=1}^4 Y^{i2(i+9)} \bar{\Psi}_i \xi_2 \chi_{i+9} + \sum_{i=10}^{14} Y^{i2(i+4)} \bar{\Psi}_i \xi_2 \chi_{i+4} \\ & + \sum_{i=1}^4 \bar{Y}^{i1i} \Psi_i \bar{\xi}_1 \bar{\chi}_i + \sum_{i=5}^8 \bar{Y}^{i1i} \Psi_i \bar{\xi}_1 \bar{\chi}_i + \sum_{i=1}^4 \bar{Y}^{i2(i+8)} \Psi_i \bar{\xi}_2 \bar{\chi}_{i+8} + \sum_{i=9}^{12} \bar{Y}^{i2(i+4)} \Psi_i \bar{\xi}_2 \bar{\chi}_{i+4}. \end{aligned} \quad (7.33)$$

The Yukawa couplings of BM3 evolve according to the following beta functions of appendix D.2.

$$\begin{aligned} Y^{111}, Y^{212}, Y^{313}, Y^{414} : \beta_4, \\ Y^{515}, Y^{616}, Y^{717}, Y^{818}, Y^{919} : \beta_5, \\ Y^{1^2 2^{10}}, Y^{2^2 2^{11}}, Y^{3^2 2^{12}}, Y^{4^2 2^{13}} : \beta_6, \\ Y^{10^2 2^{14}}, Y^{11^2 2^{15}}, Y^{12^2 2^{16}}, Y^{13^2 2^{17}}, Y^{14^2 2^{18}} : \beta_7, \\ \bar{Y}^{111}, \bar{Y}^{212}, \bar{Y}^{313}, \bar{Y}^{414} : \beta_8, \\ \bar{Y}^{515}, \bar{Y}^{616}, \bar{Y}^{717}, \bar{Y}^{818} : \beta_9, \\ \bar{Y}^{129}, \bar{Y}^{2^2 2^{10}}, \bar{Y}^{3^2 2^{11}}, \bar{Y}^{4^2 2^{12}} : \beta_{10}, \\ \bar{Y}^{9^2 2^{13}}, \bar{Y}^{10^2 2^{14}}, \bar{Y}^{11^2 2^{15}}, \bar{Y}^{12^2 2^{16}} : \beta_{11}. \end{aligned} \quad (7.34)$$

In Benchmark 3, the components of FP_+ are given by

$$\begin{aligned} \alpha_+^{\star\text{FP}_+} \approx 0.23, \quad \alpha_4^{\star\text{FP}_+} \approx 0.18, \quad \alpha_5^{\star\text{FP}_+} \approx 0.21, \quad \alpha_6^{\star\text{FP}_+} \approx 0.18, \quad \alpha_7^{\star\text{FP}_+} \approx 0.21, \\ \alpha_8^{\star\text{FP}_+} \approx 0.19, \quad \alpha_9^{\star\text{FP}_+} \approx 0.22, \quad \alpha_{10}^{\star\text{FP}_+} \approx 0.19, \quad \alpha_{11}^{\star\text{FP}_+} \approx 0.22, \end{aligned} \quad (7.35)$$

independently of the value of the hypercharge Y . We see that BM3 is much closer to being perturbative than BM1 and BM2.

Superfield	SU(9)	SU(3) _C	SU(2) _L	U(1) _Y	Multiplicity	
Q	1	3	2	$+\frac{1}{6}$	3	} MSSM
\bar{u}	1	$\bar{\mathbf{3}}$	1	$-\frac{2}{3}$	3	
\bar{d}	1	$\bar{\mathbf{3}}$	1	$+\frac{1}{3}$	3	
L	1	1	2	$-\frac{1}{2}$	3	
\bar{e}	1	1	1	$+1$	3	
H_u	1	1	2	$+\frac{1}{2}$	1	
H_d	1	1	2	$-\frac{1}{2}$	1	
χ	1	1	2	$+0.5/ +1.5$	18	
$\bar{\chi}$	1	1	$\bar{\mathbf{2}}$	$-0.5/ -1.5$	18	
ξ	9	1	2	$-0.5/ -1.5$	2	} joint
$\bar{\xi}$	$\bar{\mathbf{9}}$	1	$\bar{\mathbf{2}}$	$+0.5/ +1.5$	2	
Ψ	9	1	1	0	14	} hidden
$\bar{\Psi}$	$\bar{\mathbf{9}}$	1	1	0	14	

Table 7.5: Chiral superfields of the AS MSSM+ benchmark BM3, which has the superpotential (7.33).

The one-loop B -coefficients and the effective B -coefficients of BM3 are given by

$$\begin{aligned}
B_3 &= 6, \quad B_{3,\text{eff}}^{\text{FP}+} = 6, \\
B_2 &= -74, \quad B_{2,\text{eff}}^{\text{FP}+} = 23.83, \\
Y = 0.5 : B_1 &= -94, \quad B_{1,\text{eff}}^{\text{FP}+} = 3.83, \\
Y = 1.5 : B_1 &= -670, \quad B_{1,\text{eff}}^{\text{FP}+} = 210.45.
\end{aligned} \tag{7.36}$$

In fig. 7.3a, we show the matching onto the SM at 1 TeV, 10^3 TeV, and 10^6 TeV for the gauge couplings α_3 , α_2 and α_1 with $Y = 0.5$, while fig. 7.3b presents the case for $Y = 1.5$. The Yukawa couplings again are approximately constant and take on their fixed point values along their trajectories.

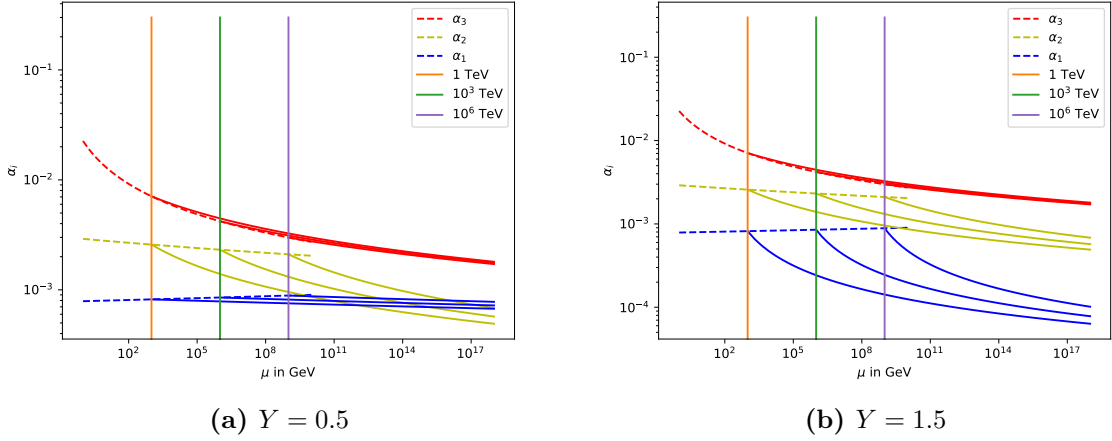


Figure 7.3: Coupling evolutions analogous to figs. 7.1 and 7.2, with solid lines here showing evolutions within BM3 (see tab. 7.5). On the left side we have $Y = 0.5$, while on the right hand side the hypercharge parameter is given by $Y = 1.5$.

We conclude that within our parameter range (7.17) we find many AS models in the MSSM+ framework which can be matched onto the SM for energies $\mu_{\text{MSSM}} \geq 1 \text{ TeV}$.

7.3 Gauge-Mediation in the MSSM+

In this section, we utilize gauge-mediated supersymmetry-breaking, presented in sec. 4.2.3, within the MSSM+ to generate the matching scale μ_{MSSM} . Within the gauge-mediated scenario, there is a second messenger mass scale μ_{mess} . We show that we still find AS candidates in the GMSB scenario. We then use a rough estimate to provide values for the two matching scales μ_{MSSM} and μ_{mess} within our benchmark BM2 of sec. 7.2.2.

7.3.1 Mass scales and AS in the gauge-mediated scenario

When we apply the gauge-mediation mechanism to the MSSM+, the chiral superfields Ψ and $\bar{\Psi}$ as well as the gauge bosons and gauginos of $SU(N)$ stay massless. The fields χ , $\bar{\chi}$, ξ , and $\bar{\xi}$ obtain a mass splitting between their scalar and fermionic components comparable to the mass splitting μ_{MSSM} between SM particles and their superpartners. From the non-observation of the χ and ξ fields we know that their scalar and fermionic components both have to be massive, but within our framework we are not able to state these masses. We expect to find that their masses are of the same order if we set some components to have masses around μ_{MSSM} . Statements on the masses within the

Higgs sector are out of the scope of this work. We also do not model the potential of the SUSY-breaking singlet superfield S and hence cannot state its mass. In practice, we find a difference between the mass parameters of the messengers L_4, \bar{L}_4 and of the messengers q_4 and \bar{q}_4 as seen in the subsequent section, with the latter being larger. In figure 7.4, we visualize the expected mass pattern.

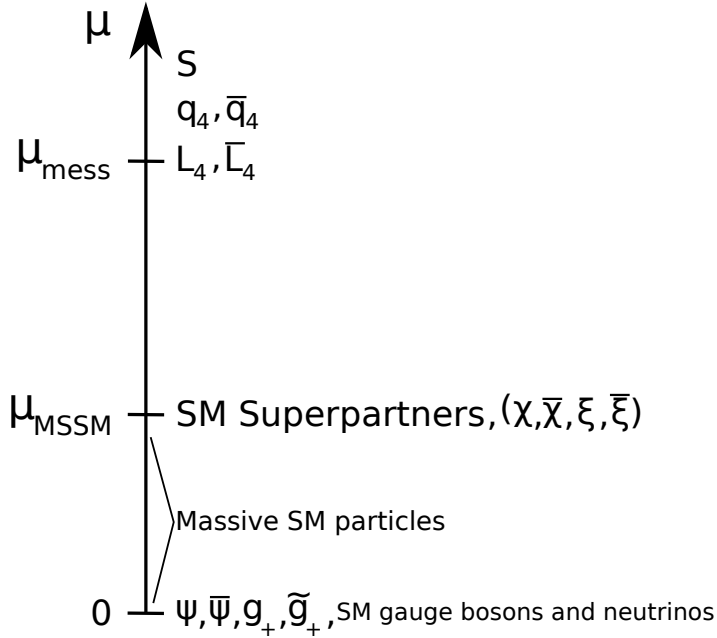


Figure 7.4: Expected mass pattern of gauge-mediated supersymmetry-breaking within the the MSSM+ framework. The chiral superfields $\Psi, \bar{\Psi}, \chi, \bar{\chi}, \xi, \bar{\xi}$ are MSSM+ fields beyond the MSSM shown in tab. 7.1. The chiral superfields q_4, \bar{q}_4, L_4 and \bar{L}_4 are the messenger fields of eq. (4.32), and S is the singlet chiral superfields whose scalar and F term acquire SUSY-breaking VEVs. With g_+, \tilde{g}_+ , respectively the gauge bosons and gauginos of the new $SU(N)$ sector are denoted.

We now have to check whether we still find AS models when the fields (4.32) and the superpotential terms (4.33) are included to the MSSM+. We are interested in models where FP_+ is a UV fixed point, for which y_{χ_i} and y_q vanish. Nevertheless, for the generation of the mass scales, these terms are crucial. The two additional messenger lepton doublets L_4, \bar{L}_4 , and the two additional messenger quark singlets q_4, \bar{q}_4 change some one- and two-loop gauge coefficients of the MSSM+ beta functions of appendix D.2.

The change of these coefficients is

$$\begin{aligned}
\Delta B_3 &= -2, \quad \Delta C_{33} = \frac{68}{3}, \quad \Delta C_{31} = \frac{8}{9}, \\
\Delta B_2 &= -2, \quad \Delta C_{22} = 38, \quad \Delta C_{21} = 2, \\
\Delta B_1 &= -\frac{10}{3}, \quad \Delta C_{11} = \frac{97}{27}, \quad \Delta C_{13} = \frac{64}{9}, \quad \Delta C_{12} = 6.
\end{aligned} \tag{7.37}$$

All the other in the beta functions of the MSSM+ are unchanged. Furthermore, the beta functions of the Yukawas couplings α_l and α_q ($\alpha_{y_{l,q}} = |y_{q,l}|^2/(4\pi)^2$) are given by

$$\begin{aligned}
\beta_l &= \alpha_l(8\alpha_l + 6\alpha_q - 6\alpha_2 - 2\alpha_1), \\
\beta_q &= \alpha_q(10\alpha_q + 4\alpha_l - \frac{32}{3}\alpha_3 - \frac{8}{9}\alpha_1),
\end{aligned} \tag{7.38}$$

which mix into the beta functions β_3 , β_2 and β_1 via the new terms

$$\beta_3^+ = -\alpha_3^2 D_{3q} \alpha_q, \quad \beta_2^+ = -\alpha_2^2 D_{2l} \alpha_l, \quad \beta_1^+ = -\alpha_1^2 (D_{1l} \alpha_l + D_{1q} \alpha_q), \tag{7.39}$$

with

$$D_{2l} = 12, \quad D_{3q} = 8, \quad D_{1l} = 4, \quad D_{1q} = \frac{8}{3}. \tag{7.40}$$

Here, β_i^+ are new terms that appears in the beta function β_i of the MSSM+. As already mentioned, FP_+ remains unaffected by the messenger Yukawa couplings.

Scanning again over the parameters (7.17) with $Y = +3/2$ in our gauge-mediated scenario yields 91899 models which are AS in our sense, all of them having $N \geq 4$. The model within this parameter range possessing the smallest value for $\alpha_+^{\text{FP}_+} \approx 0.23$ is given by benchmark 3 of sec. 7.2.3. For $Y = 1/2$, we still find 56227 AS models (to be compared with the non-GMSB case presented in tab. 7.2).

7.3.2 Estimate of the mass scales

To approximate the mass scales in the GMSB scenario, we assume that between μ_{MSSM} and μ_{mess} , $\langle F_S \rangle$ and $\langle S \rangle$ do not run, and that the eqs. (4.35) and (4.36) are valid anywhere between these two mass scales and not only at μ_{mess} . We then are able to estimate values for the mass scales as described in the following four steps.

1. Choose the matching scale μ_{MSSM} . We calculate the gauge couplings α_3 , α_2 , α_1 at this scale by using the SM running of these couplings. We then obtain

$$\alpha_3^{\text{MSSM}} = \alpha_3(\mu_{\text{MSSM}}), \quad \alpha_2^{\text{MSSM}} = \alpha_2(\mu_{\text{MSSM}}), \quad \alpha_1^{\text{MSSM}} = \alpha_1(\mu_{\text{MSSM}}). \tag{7.41}$$

Demanding that the mass of gluinos M_3 in (4.35) equals the mass scale μ_{MSSM} , allows us to infer the ratio $|\langle F_S \rangle / \langle S \rangle|$:

$$\mu_{\text{MSSM}} \sim M_3 \stackrel{(4.35)}{\Rightarrow} \left| \frac{\langle F_S \rangle}{\langle S \rangle} \right| \text{ fixed.} \quad (7.42)$$

2. We then proceed to calculate the soft SUSY-breaking mass parameters using the formulas (4.35) for the remaining gauginos as well as eq. (4.36) for all mass splittings between SM fermions and sfermions.
3. We choose the mass scale $\mu_{\text{mess}} > \mu_{\text{MSSM}}$ and run the gauge couplings α_3 , α_2 , and α_1 up to this scale using eq. (7.20) with the coefficients $B_{i,\text{eff}}^{\text{FP}+}$ given within the MSSM+. With these couplings

$$\alpha_3^{\text{mess}} = \alpha_3(\mu_{\text{mess}}), \quad \alpha_2^{\text{mess}} = \alpha_2(\mu_{\text{mess}}), \quad \alpha_1^{\text{mess}} = \alpha_1(\mu_{\text{mess}}), \quad (7.43)$$

we set the values of α_l and α_q at μ_{mess} to be given by the nullcline condition

$$\begin{aligned} \alpha_l^{\text{mess}} &= \alpha_l(\mu_{\text{mess}}) = 0.2619 \alpha_1^{\text{mess}} + 1.0714 \alpha_2^{\text{mess}} - 1.1429 \alpha_3^{\text{mess}}, \\ \alpha_q^{\text{mess}} &= \alpha_q(\mu_{\text{mess}}) = -0.01587 \alpha_1^{\text{mess}} - 0.42857 \alpha_2^{\text{mess}} + 1.52381 \alpha_3^{\text{mess}}, \end{aligned} \quad (7.44)$$

which we obtain by setting (7.38) to zero and solving for α_l , $\alpha_q \neq 0$. This choice ensures that α_l and α_q flow into FP_+ in the UV. Setting the mass of the fermionic component of L_4 to be equal to μ_{mess} then allows us to state a value for $|\langle S \rangle|$, using eq. (4.34):

$$\mu_{\text{mess}} \sim m_{L_4}^{\text{fermion}} \stackrel{(4.34)}{\Rightarrow} |\langle S \rangle|. \quad (7.45)$$

There is an obstacle in doing this since eqs. (7.44) in general do not provide positive values for α_l^{mess} and α_q^{mess} . We find in our benchmarks that α_q^{mess} is always positive while α_l^{mess} only becomes positive above a minimal value of μ_{mess} which we denote as $\mu_{\text{mess}}^{\text{min}}$. A sample plot of the values of α_l^{mess} and α_q^{mess} for BM2 with $\mu_{\text{MSSM}} = 10^6 \text{ GeV}$ at different values of μ_{mess} is shown in fig. 7.5. We find that $\mu_{\text{mess}}^{\text{min}}$ becomes smaller for larger μ_{MSSM} . At $\mu_{\text{mess}}^{\text{min}}$, we have exactly $\alpha_l = 0$ and hence $m_{L_4} = 0$. We only show the mass parameters of q_4 at this minimal messenger scale $\mu_{\text{mess}}^{\text{min}}$. Slightly above $\mu_{\text{mess}}^{\text{min}}$, $\alpha_l \neq 0$ and m_{L_4} obtains very quickly values which are somewhat comparable to the mass parameters of q_4 .

We then proceed to determine the other mass parameters of the messenger particles with eqs. (4.34). When the fermionic and scalar masses of the messengers coincide, we are in a regime where the formulas of gauge-mediation is valid. At this point, we

may come across a new obstacle where some messenger mass parameters become imaginary (and their squares negative). In this case, we expect a phase transition due to spontaneous symmetry breaking. We do not consider this case here and exclude such combinations of μ_{MSSM} and $\mu_{\text{mess}}^{\text{min}}$ from our investigations. We indeed find that scalar messenger masses become imaginary as soon as μ_{MSSM} exceeds a specific energy scale which allows us to infer an upper limit on μ_{MSSM} .

4. We run all couplings towards higher energies to demonstrate that they eventually reach FP_+ in the UV. The gauge couplings α_3 , α_2 , and α_1 run according to eq. (7.20) with the coefficients $B_{i,\text{eff}}^{\text{FP}_+}$ given within the MSSM+ above μ_{MSSM} , and within the gauge-mediated scenario above μ_{mess} . The couplings α_+ , α_4 , ... , α_{11} , α_l , and α_q are given by their nullcline conditions in the different energy regimes. Below μ_{mess} , α_l and α_q are constant, while α_4 , ... , α_{11} are constant below μ_{MSSM} , where α_+ runs independently from all the other couplings. There we calculate the trajectory of α_+ numerically.

The fields Ψ , $\bar{\Psi}$ as well as the new gauge bosons and new gauginos stay massless.

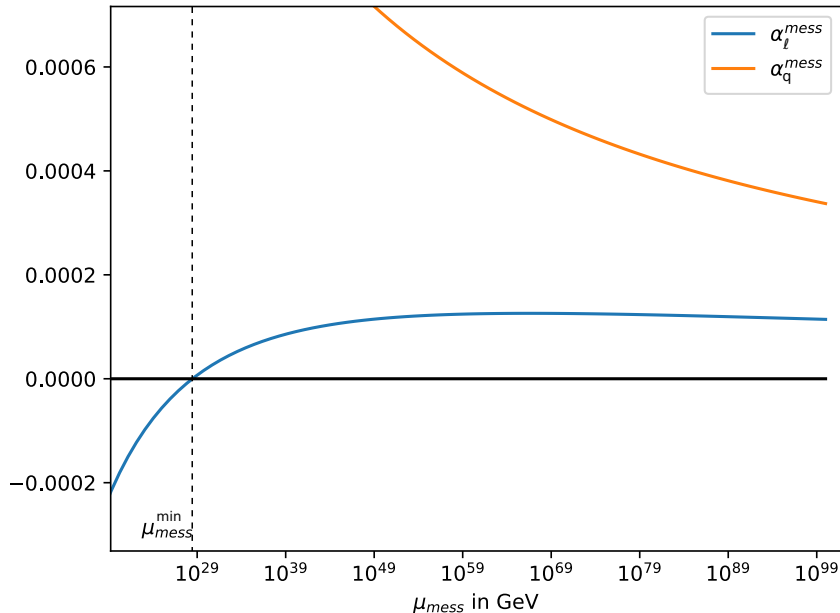


Figure 7.5: Starting values $\alpha_l^{\text{messenger}}$ and $\alpha_q^{\text{messenger}}$ of eq. (7.44) in dependence of the messenger scale $\mu_{\text{messenger}}$ for $\mu_{\text{MSSM}} = 10^6$ GeV. The point at which α_l becomes positive marks $\mu_{\text{messenger}}^{\text{min}}$. Below $\mu_{\text{messenger}}^{\text{min}}$, the α_l Yukawa coupling becomes unphysical, and we discard the theory as being physical. Qualitatively, the shown curves behave similar at different values of μ_{MSSM} .

7.3.3 Benchmark demonstration

We now apply the procedure described in the previous section to our benchmark model BM2 given by the parameters (7.27). In table 7.6, we show the mass parameters for different chosen superpartner scales μ_{MSSM} . The messenger scale $\mu_{\text{messenger}}$ is always given by its required minimal value $\mu_{\text{messenger}}^{\text{min}}$ to produce physical values for $\alpha_l^{\text{messenger}}$ and $\alpha_q^{\text{messenger}}$, as discussed in the previous section.

For $\mu_{\text{MSSM}} = 1$ TeV, the evolution of the gauge and Yukawa couplings is shown in fig. 7.6. We also present the same plots but extended to a much larger UV scale to show that the couplings α_l and α_q indeed run (slowly) towards zero in the UV as required for FP_+ . Figure 7.7 shows analogous plots for $\mu_{\text{MSSM}} = 10^6$ TeV. We observe that $\mu_{\text{messenger}}$ becomes smaller for larger μ_{MSSM} . Above a certain scale for μ_{MSSM} , scalar messenger masses become imaginary and we expect spontaneous symmetry breaking. We do not consider this case here and exclude such combinations of μ_{MSSM} and $\mu_{\text{messenger}}^{\text{min}}$. In fig. 7.8, we present as a green area combinations of μ_{MSSM} and $\mu_{\text{messenger}}$ for which $\alpha_l^{\text{messenger}}$ and $\alpha_q^{\text{messenger}}$

Parameter	Value/GeV \sim		
μ_{MSSM}	1000	1×10^6	1×10^9
M_3	1000	1×10^6	2×10^9
M_2	350	5×10^5	7×10^8
M_1	200	4×10^5	6×10^8
$M_{\tilde{Q}}$	1700	2×10^6	2×10^9
$M_{\tilde{u}}$	1600	2×10^6	2×10^9
$M_{\tilde{d}}$	1600	2×10^6	2×10^9
$M_{\tilde{L}}$	450	7×10^5	9×10^8
$M_{\tilde{e}}$	270	5×10^5	8×10^8
$\mu_{\text{mess}}^{\text{min}}$	7×10^{31}	3×10^{28}	7×10^{24}
$M_{q_4^f}/M_{\bar{q}_4^f}$	2×10^{35}	6×10^{31}	5×10^{27}
$M_{q_4^s}$	2×10^{35}	6×10^{31}	5×10^{27}
$M_{\bar{q}_4^s}$	2×10^{35}	6×10^{31}	5×10^{27}
$ \langle F_S \rangle $	140000	2×10^8	3×10^{11}
$ \langle S \rangle $	4×10^{35}	1×10^{32}	1×10^{28}

Table 7.6: Mass parameters and (minimal) messenger scales for different input values of the superpartner scale μ_{MSSM} in benchmark BM2 (see sec. 7.2.2). We discuss in sec. 7.3.2 how these masses are estimated. The mass parameters are M_3 , M_2 , M_1 of gluinos, winos and binos (eq. (4.35)), $M_{\tilde{Q}}$, $M_{\tilde{u}}$, $M_{\tilde{d}}$, $M_{\tilde{L}}$, $M_{\tilde{e}}$ of left-handed squarks, right-handed up-squarks, right-handed down-quarks, left-handed sleptons, and right-handed charged sleptons (eq. (4.36)), and $M_{q_4^f}$, $M_{\bar{q}_4^f}$, $M_{q_4^s}$ and $M_{\bar{q}_4^s}$ of scalar messengers (eq. (4.34)), respectively. The minimal messenger scales $\mu_{\text{mess}}^{\text{min}}$ are determined by searching for the lowest energy scale at which the messenger Yukawa couplings α_t^{mess} and α_q^{mess} of eq. (7.44) become positive (see fig. 7.44 for their μ_{mess} dependence at $\mu_{\text{MSSM}} = 10^6$ GeV). Our procedure to estimate the VEVs of the scalar component $|\langle S \rangle|$ and the F -term $|\langle F_S \rangle|$ of the singlet chiral superfield S in (4.32) is described in eqs. (7.42) and (7.45) and the main text there.

of eq. (7.44) are physical, while spontaneous symmetry breaking occurs within the red area. We find an upper bound on μ_{MSSM} given by

$$\mu_{\text{MSSM}} \lesssim 10^{13} \text{ GeV} , \quad (7.46)$$

independently of μ_{mess} .

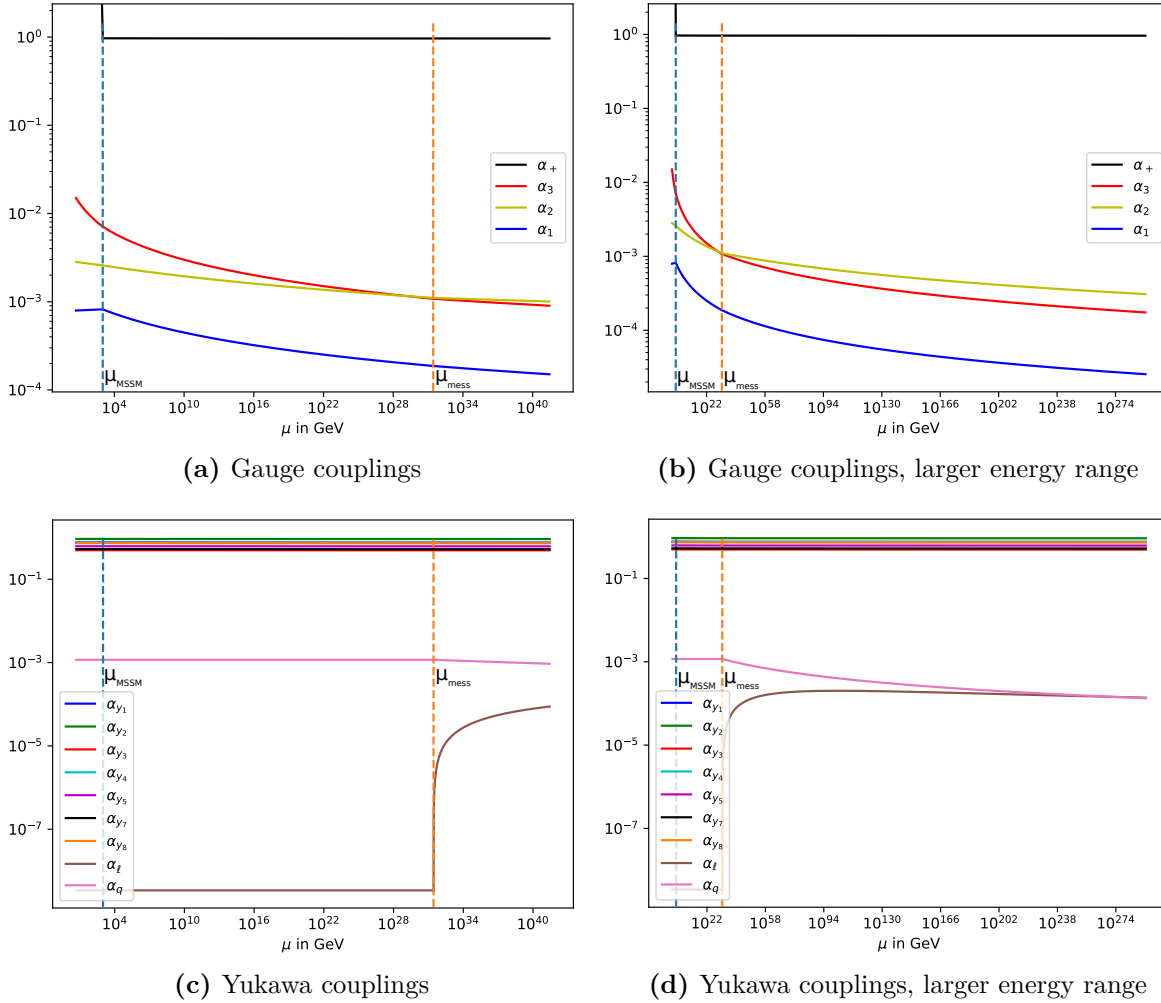


Figure 7.6: The evolution of the gauge and Yukawa couplings for $\mu_{\text{MSSM}} = 10^3 \text{ GeV}$ (blue dotted lines) in BM2 (see sec. 7.2.2). The value of the messenger scale μ_{mess} (orange dotted lines) is here given by its minimal value of $7 \times 10^{31} \text{ GeV}$ as stated in tab. 7.6. On the right hand side, we present the couplings evolutions at larger energy ranges to confirm that α_l and α_q indeed run towards zero in the UV.

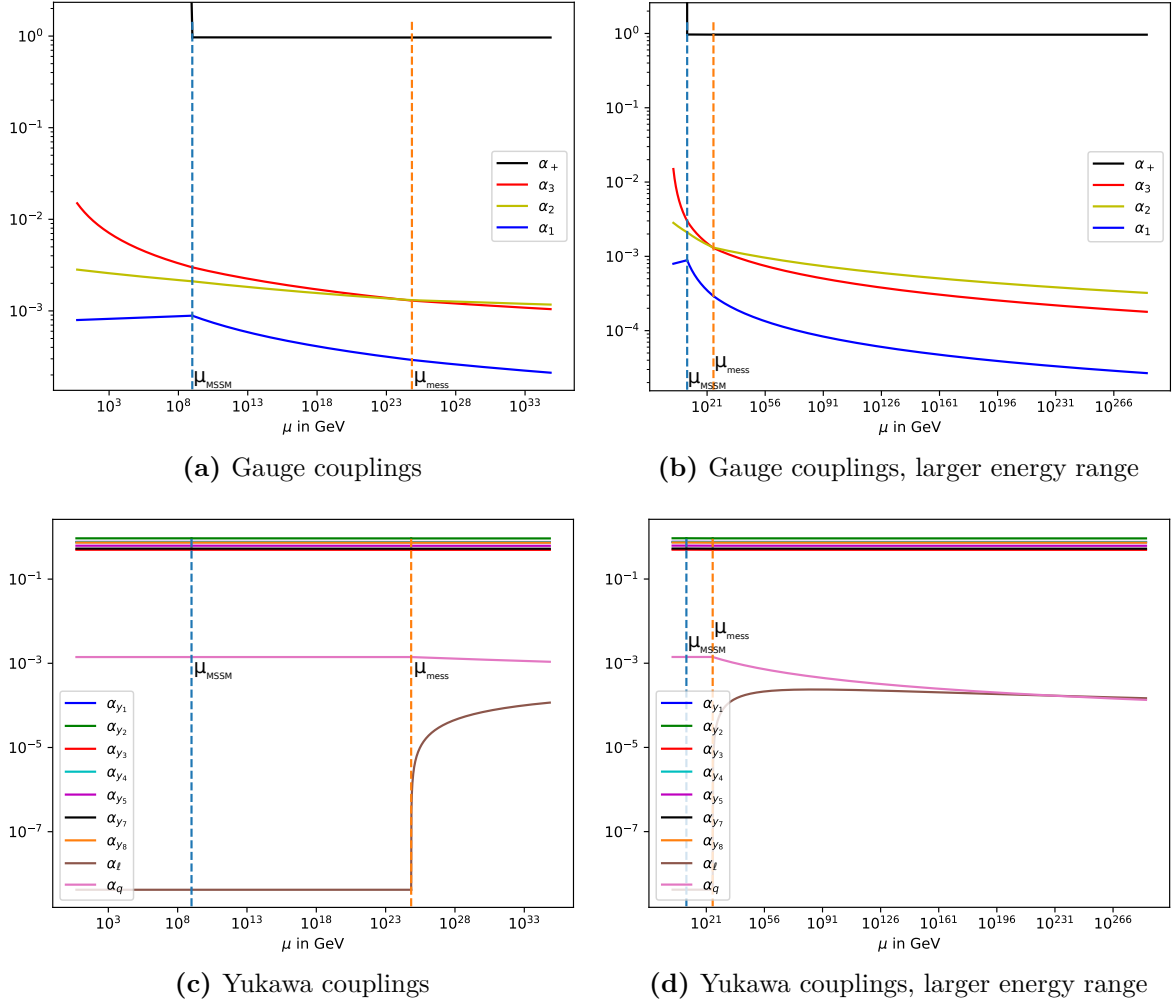


Figure 7.7: Analogously to fig. 7.6 we present the evolution of the gauge and Yukawa couplings in BM2, here for $\mu_{\text{MSSM}} = 10^9$ GeV (blue dotted lines). The messenger scale takes on its minimal value $\mu_{\text{mess}} = 7 \times 10^{24}$ GeV (orange dotted lines) such that the messenger Yukawa couplings α_q and α_l are physical (compare with tab. 7.6). On the right hand side, we again present the couplings evolutions at larger energy ranges to confirm that α_l and α_q indeed run towards zero in the UV.

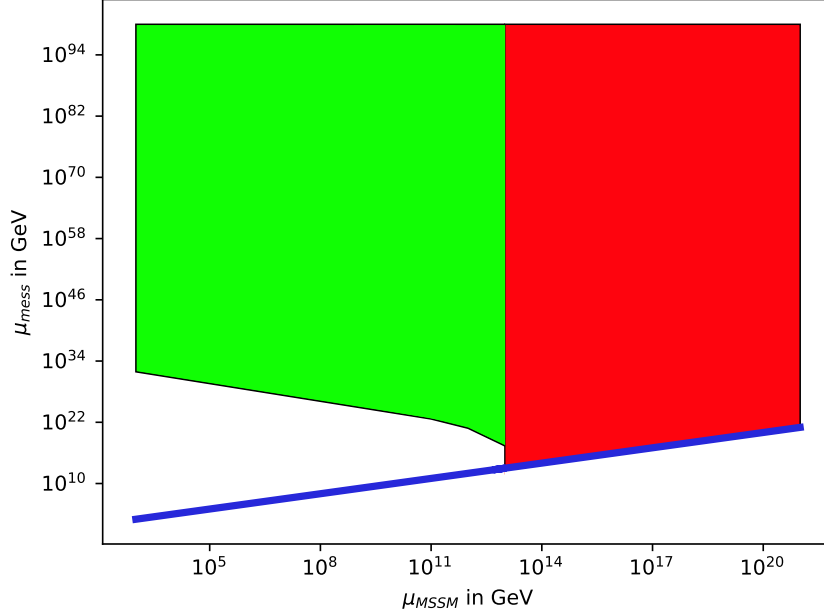


Figure 7.8: Superpartner and messenger scales μ_{MSSM} and μ_{mess} with positive values of α_l^{mess} and α_q^{mess} of eq. (7.44) (green and red area combined). The blue line represents the diagonal $\mu_{\text{MSSM}} = \mu_{\text{mess}}$. We find real messenger masses in the green area while in the red area scalar messenger mass parameters become imaginary. We observe that the latter case occurs above $\mu_{\text{MSSM}} \sim 10^{13}$ GeV, independently of μ_{mess} .

7.4 Phenomenological Aspects of the MSSM+

In this section, we discuss the particle spectrum of the MSSM+ and experimental mass bounds. Furthermore, we present two missing energy scenarios. We assume

$$Y = \pm \frac{1}{2}, \quad (7.47)$$

and implement the \mathbb{Z}_2 flavor symmetry (7.6) to not have Yukawa couplings mixing fields within and beyond the MSSM, as in our previous investigations.

7.4.1 Particle spectrum and dark matter candidates

The chiral superfields of the MSSM+ are those of tab. 7.1. Next to the SM particles, our models contain their superpartners, the squarks sup \tilde{u} , sdown \tilde{d} , scharm \tilde{c} , sstrange \tilde{s} , stop \tilde{t} , sbottom \tilde{b} , the charged sleptons selectron \tilde{e} , smuon $\tilde{\mu}$, stau $\tilde{\tau}$ and their

Particle	Lower bound [GeV]
$\tilde{u}, \tilde{d}, \tilde{c}, \tilde{s}$	1570
\tilde{t}	1450
\tilde{b}	950
\tilde{l}	440
$\tilde{\nu}_\tau$	1900
\tilde{g}	2100
\tilde{C}_1^\pm	1160
\tilde{N}_1^0	1000
\tilde{N}_2^0	1160
\tilde{N}_3^0	635

Table 7.7: Largest lower bounds on the masses of the non-SM MSSM particles, taken from the particle data group [43].

corresponding sneutrinos $\tilde{\nu}_{e,\mu,\tau}$, as well as four Higgs scalars H^0, A^0, H^+, H^- , gluinos \tilde{g} , four neutralinos $\tilde{N}_{1,2,3,4}$ and charginos $\tilde{C}_1^\pm, \tilde{C}_2^\pm$. Additionally, each doublet pair $(\chi, \bar{\chi})$ leads to two neutral scalars $\tilde{\chi}^0, \tilde{\bar{\chi}}^0$, two charged scalars $\tilde{\chi}^\pm$ and two (Dirac) fermions χ, χ^\dagger . The same goes for each $SU(N)$ component of each pair $(\xi, \bar{\xi})$.

The dark matter candidates of the MSSM+ are

- Bound states of the scalars and fermions of the chiral superfields $\bar{\Psi}, \Psi$ (see sec. 7.2),
- The lightest neutralino,
- Electrically neutral scalars and fermions from $\chi, \bar{\chi}, \xi, \bar{\xi}$.

7.4.2 Mass bounds

The MSSM+ of section 7.1 contains in particular the MSSM particle content for which the largest lower mass bounds, stated by the particle data group [43], are shown in tab. 7.7. For the masses M_L of the leptons beyond the MSSM, formed by the $\chi, \bar{\chi}$ and $\xi, \bar{\xi}$ fields, the LEP bound [156]

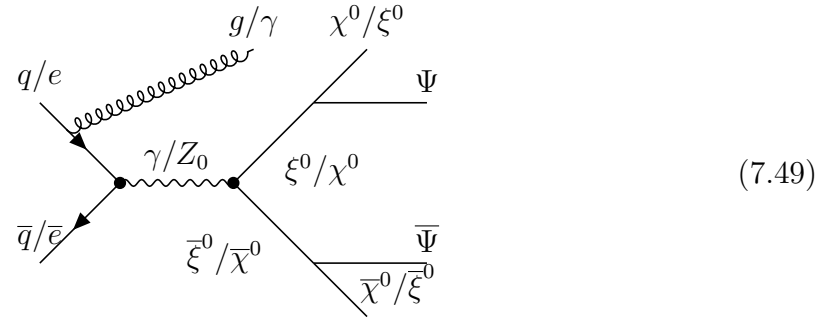
$$M_L > 103 \text{ GeV} \tag{7.48}$$

holds.

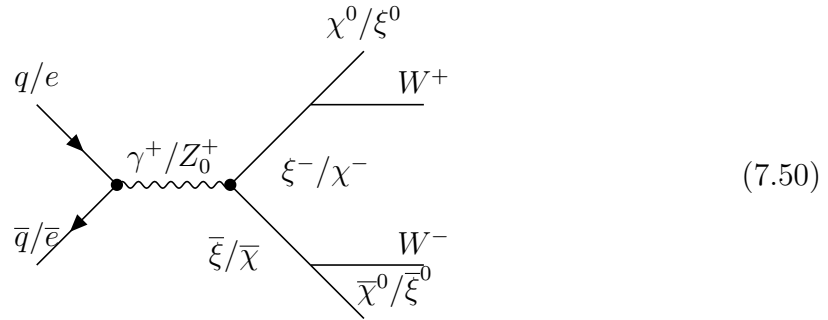
7.4.3 Missing energy at colliders

Due to the new gauge sector, missing energy signatures at colliders are of greatest interest with respect to the MSSM+. In our setup, there are two dominant processes for this.

The first process yields a monojet/monophoton plus missing energy signal. The Feynman diagram (7.49) contributes to this process at tree-level. Due to the scalars and fermions of the chiral superfields $\Psi, \bar{\Psi}$ forming bound states with masses around μ_{MSSM} , we expect this missing energy signal to heavily increase around that energy scale. The neutral particles beyond the MSSM are effectively not detectable.



The second process yields as a signal dileptons plus missing energy, as illustrated by the Feynman diagram (7.50). The end state consists of neutrinos, charged dileptons and neutral particles beyond the MSSM ($W^\pm \rightarrow \ell^\pm \nu$). The missing energy comes from the neutrinos and new neutral particles.



7.5 Summary and Remarks on the MSSM+

In the MSSM+ framework of sec. 7.1, which extends the MSSM by an additional $SU(N)$ gauge sector

$$G_{\text{MSSM}+} = SU(N) \otimes SU(3)_C \otimes SU(2)_L \otimes U(1)_Y ,$$

we found candidates for which FP_+ from (7.4) becomes physical, perturbative and UV attractive in the directions of the MSSM gauge couplings. We refer to such a scenario as being “asymptotically safe in our sense”.

The resulting amount of such candidates found within scans over the parameter space (7.17) are summarized in tab. 7.2 for different fixed values Y of the χ and $\bar{\xi}$ hypercharges (see tab. 7.1). Candidates which are asymptotically safe in our sense occur only for $N \geq 4$. For the three benchmark models BM1, BM2 and BM3, presented respectively in sections 7.2.1, 7.2.2 and 7.2.3, we demonstrated direct matching from the MSSM+ onto the SM for energies above 1 TeV, depicted in figures 7.1, 7.2 and 7.3.

In the MSSM+ framework, we studied the general superpotential (7.5) which only involves fields beyond the MSSM. Imposing the \mathbb{Z}_2 flavor symmetry of eq. (7.6), Yukawa terms composed by fields charged under the MSSM as well as the new $\text{SU}(N)$ are prohibited. Since we focused on FP_+ being the fixed point which gets reached in the UV for which the MSSM gauge couplings become non-interacting, including the MSSM superpotential does not change any of our results. In our framework, we are not able to explain the observed Yukawa structures of the SM, and they rather are generated randomly along UV-safe trajectories.

Incorporating gauge-mediated supersymmetry-breaking (see sec. 4.2.3) into the MSSM+, the additional singlet and messenger chiral superfields

$$S(\mathbf{1}, \mathbf{1}, \mathbf{1})_0, \quad L_4(\mathbf{1}, \mathbf{1}, \mathbf{2})_{-1/2}, \quad \bar{L}_4(\mathbf{1}, \mathbf{1}, \bar{\mathbf{2}})_{+1/2}, \quad q_4(\mathbf{1}, \mathbf{3}, \mathbf{1})_{-1/3}, \quad \bar{q}_4(\mathbf{1}, \bar{\mathbf{3}}, \mathbf{1})_{+1/3}$$

with gauge charges $(\text{SU}(N), \text{SU}(3)_C, \text{SU}(2)_L)_Y$ are present. For $N \geq 4$, we still find AS candidates (see sec. 7.3.1). Within the GMSB scenario, two mass scales μ_{MSSM} and μ_{mess} are present, where the former indicates masses of SM superpartners, and the latter messenger masses. We estimate the mass scales μ_{MSSM} and μ_{mess} in benchmark model BM2, which are shown in tab. 7.6. Furthermore we find that above

$$\mu_{\text{MSSM}} \sim 10^{13} \text{ GeV},$$

messenger mass parameters become imaginary, indicating a quantum phase transition due to spontaneous symmetry breaking (see fig. 7.8).

The particle content and the formation of dark bound states were briefly presented in sec. 7.4.1, and experimental mass bounds were stated in tab. 7.7. As in the dark QCD model, presented in sec. 3, bound states of fields only charged under the new $\text{SU}(N)$ serve as dark matter candidates. For the hypercharge parameters $Y = \pm 1/2$, missing energy with monojets, monophotons or dileptons in the final state are promising signals to occur not only within the MSSM+, but for new physics with hidden sectors in general. Contributions to these processes within the MSSM+ are given by the Feynman diagrams (7.49) and (7.50).

Chapter 8

Superconformal Field Theory

In fixed points, quantum field theories are scale-invariant since the change of couplings with the energy scale vanishes by definition (5.13). In general, scale-invariant field theories are also conformally invariant [14–16]. Hence, fixed points of supersymmetric theories constitute superconformal field theories (SCFTs) for which non-perturbative results are known.

The bosonic part of the four-dimensional $\mathcal{N} = 1$ superconformal algebra includes an abelian symmetry $U(1)_R$, whose generators are referred to as R -charges. The fermionic superspace coordinates θ and θ^\dagger from eq. (4.2) get assigned the R -charges $+1$ and -1 , respectively. For chiral superfields with R -charges R_Φ , we infer from the Taylor expansion (4.12) that their bosonic component has the same R -charge $R_\phi = R_\Phi$, while their fermionic components and F -terms have R -charges $R_\Psi = R_\Phi - 1$ and $R_F = R_\Phi - 2$, respectively. Vector superfields V are real and hence always have R -charge zero (no $U(1)_R$ transformations possible except for the identity operation). From (4.15), we then immediately see that gauge bosons also have $R_{A^\mu} = 0$ and gauginos and the D -term have respectively $R_\lambda = 1$ and $R_D = 0$. In table 8.1, we summarize the different R -charge assignments.

Superfield S	R_S	Bosonic component	Fermionic component	Auxiliary term
Chiral Φ	R_Φ	$R_\phi = R_\Phi$	$R_\Psi = R_\Phi - 1$	$R_F = R_\Phi - 2$
Vector V	$R_V=0$	$R_{A^\mu} = 0$	$R_\lambda = 1$	$R_D = 0$

Table 8.1: Summary of the R -charge assignments for the different components of chiral and vector superfields.

In this chapter, the $\mathcal{N} = 1$ SCFT algebra in four dimensions and a connection between R -charges and scaling dimensions D within superconformal models are discussed, and

the central charges a and c are introduced. Furthermore, we sketch the proof of a theorem which states that superconformal R -charges locally maximize the central charge a [21], and present the a -theorem [157–159] as well as the conformal collider bounds [22, 23].

Finally, we explain how the discussed non-perturbative results are used in chapter 9 to check whether AS candidates found in MSSM extensions of chapter 6 and within the MSSM+ framework of chapter 7 may exist beyond perturbation theory.

8.1 Superconformal Algebra and Unitarity Bounds

Ignoring supersymmetry at first, the generators of the four dimensional conformal group may be represented on a scalar one-particle Hilbert space in positional eigenbasis as

$$\begin{aligned} M_{\mu\nu} &= -i(x_\mu\partial_\nu - x_\nu\partial_\mu) , & P_\mu &= -i\partial_\mu , \\ K_\mu &= -i(x^2\partial_\mu - 2x_\mu x_\nu\partial^\nu) , & \mathcal{D} &= -ix_\nu\partial^\nu , \end{aligned} \tag{8.1}$$

with $M^{\mu\nu}$ and P^μ the generators of Lorentz transformations and spacetime translations and K^μ and \mathcal{D} the generators of conformal transformations and dilations, respectively [160]. The unitary, irreducible representations of the superconformal group generated by the generators (8.1) may be labeled by their $SU(2) \otimes SU(2)$ Lorentz representation indices (j, j') and their scaling dimension D . The scaling dimension D of renormalized operators \mathcal{O} appears in their μ -dependency

$$\mathcal{O}(\mu) \sim \mu^D , \tag{8.2}$$

where $D = D(\mu)$ itself is μ -dependent. Anomalous dimensions $\gamma_{\mathcal{O}}$ are defined via

$$D(\mu) \equiv [\mathcal{O}] + \gamma_{\mathcal{O}}(\mu) , \tag{8.3}$$

with $[\mathcal{O}]$ the mass dimension of \mathcal{O} .

From unitarity, it is possible to set lower bounds on the scaling dimensions D of different gauge invariant (j, j') operators [161]. These lower bounds are for scalar $(0, 0)$, spinor $(1/2, 0)$ or $(0, 1/2)$ and vector $(1/2, 1/2)$ representations respectively given by

$$D_{\text{scalar}} \geq 1 , \quad D_{\text{spinor}} \geq \frac{3}{2} , \quad D_{\text{vector}} \geq 3 . \tag{8.4}$$

The only exception is the scalar identity operator which has $D = 0$.

Now we additionally consider supersymmetry. For chiral superfields, superconformality yields a connection between chiral superfield R -charges $R_\Phi = R_\phi$ of tab. 8.1 and the scaling dimension D of their components, given by [141, 160, 162–164]

$$D = \frac{3}{2}R_\Phi . \quad (8.5)$$

Equating (8.5) and (8.3) and using $[\phi] = 1$ for scalar fields, we obtain

$$R_\Phi = \frac{2}{3}(1 + \gamma_\Phi) . \quad (8.6)$$

We stress an observation regarding the triangle anomaly for $R \otimes G_a \otimes G_a$ with G_a a simple gauge factor of (5.1). Since only fermions contribute to anomalies, and according to tab. 8.1 gluinos have $R_\lambda = 1$ and fermionic components of chiral superfields have $R_\Psi = R_\Phi - 1$, we obtain for the $R \otimes G_a \otimes G_a$ anomaly of a supersymmetric gauge theory containing chiral superfields Φ_i

$$\begin{aligned} \text{Tr}[R \otimes G_a \otimes G_a] &= C_2^{(a)}(G) + \sum_i R_{\Psi_i} S_a(R_i) = C_2^{(a)}(G) + \sum_i (R_{\Phi_i} - 1) S_a(R_i) \\ &\stackrel{(8.6)}{=} \frac{1}{3} [3C_2^{(a)}(G) - \sum_i S_a(R_i)(1 - 2\gamma_i)] . \end{aligned} \quad (8.7)$$

The exact NSVZ beta functions (5.12) are proportional to the square bracket in (8.7). Hence, a superconformal theory as a fixed point α^* always has $R \otimes G_a \otimes G_a$ 't Hooft anomalies vanishing for all a with $\alpha_a^* \neq 0$. A further constraint on superconformal R -charges comes from the R -charge of the superpotential being necessarily two, i.e.

$$R(W) = 2 . \quad (8.8)$$

This is because we use the F -term (4.14) of the superpotential to construct supersymmetric Lagrangians and the fermionic superspace coordinate θ has $R(\theta) = +1$.

The central charge a of conformal field theories appears as a coefficient in front of the curvature term of the trace of the energy-momentum tensor

$$T_\mu{}^\mu \supset -a R_{\mu\nu\rho\lambda} R^{\mu\nu\rho\lambda} , \quad (8.9)$$

with $R_{\mu\nu\rho\lambda}$ the Riemann curvature tensor. Anselmi et. al. [19, 20] showed that for SCFTs, a can be expressed in terms of the $U(1)_R$ 't Hooft anomalies involving superconformal R -charges via

$$a = \frac{3}{32} (3\text{Tr}(R^3) - \text{Tr}(R)) . \quad (8.10)$$

In the next section, we sketch the proof of a powerful theorem shown by Intriligator and Wecht which states that superconformal R -charges locally maximize $a = a(R)$ in (8.10) with R subject to the constraints given by vanishing of the $R \otimes G_a \otimes G_a$ anomalies and the R -charge of the superpotential $R(W) = 2$ [21].

8.2 Maximization of a and the a -Theorem

8.2.1 Triangle anomalies

Before we sketch the proof of a -maximization, we present some basics of triangle anomalies. According to the Noether theorem, a given symmetry S with generators T_S^a of a Lagrangian classically yields conserved currents $J_S^{a\mu}$ with

$$\partial_\mu J_S^{a\mu} = 0 . \quad (8.11)$$

Quantum mechanically these symmetries can be broken, leading to non-conservation of the currents $J_S^{a\mu}$. We refer to such broken symmetries as “triangle anomalies” [165, 166]. In general, triangle anomalies receive contributions from chiral fermions charged under S . Left-handed and right-handed fermions contribute with opposite signs to triangle anomalies so that vectorlike fermions do not yield any anomalous contributions. Also, fermions and their conjugates contribute with opposite signs and real and pseudoreal representations do not exhibit triangle anomalies [167]. Hence we may only consider generators T acting on left-handed fields and hermitian conjugated fields of right-handed fermions. Triangle anomalies of the currents $J_S^{a\mu}$ in an arbitrary gauge background \mathcal{A} are completely determined by one-loop triangle Feynman diagrams as presented in (8.12), with G_i indicating gauge groups and T_{G_i} their generators. Hence the name triangle anomaly. The formula in (8.12) is taken from chapter 22 of [168].

$$\langle \partial_\mu J_S^{a\mu} \rangle_{\mathcal{A}} \supset G_S \text{ (triangle diagram)} = \sum_{b,c} \frac{1}{16\pi^2} \frac{\text{Tr}(\{T_S^a T_{G_1}^b\} T_{G_2}^c)}{2} F_{G_1}^{b\mu\nu} \tilde{F}_{G_2\mu\nu}^c . \quad (8.12)$$

Dual field strength tensors \tilde{F} are defined in terms of field strength tensors F by

$$\tilde{F}_{\mu\nu}^a \equiv \frac{1}{2} \varepsilon_{\mu\nu\rho\lambda} F^{a\rho\lambda} . \quad (8.13)$$

Global symmetries S being anomalous when taken as local symmetries are called ‘t Hooft anomalies. We sometimes also refer to just the factor

$$\frac{\text{Tr}(\{T_S^a T_{G_1}^b\} T_{G_2}^c)}{2} \quad (8.14)$$

as the ‘t Hooft anomaly. In the case of flavor anomalies, for which the flavor generators T_S^a commute with gauge symmetry generators, the ‘t Hooft anomaly is simply given by the trace

$$\text{Tr}(T_S^a T_{G_1}^b T_{G_2}^c) . \quad (8.15)$$

8.2.2 Sketch of the proof

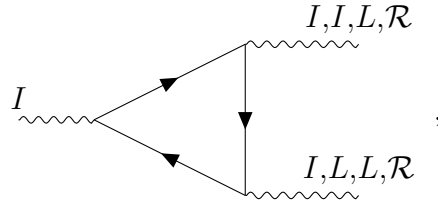
Now we sketch the proof that superconformal R -charges locally maximize a from eq. (8.10), originally presented by Intriligator and Wecht in [21]. For this we consider a general theory with $U(1)_I$ flavor symmetries with generators Q_I and currents J_I^μ . The 't Hooft anomaly for the $U(1)_I$ flavor symmetries in background flavor gauge fields A_I^μ , A_L^μ , as well as a general metric $g_{\mu\nu}$ is given by

$$\begin{aligned} \langle \partial_\mu J_I^\mu \rangle_{A_{I,L}^\mu, g_{\mu\nu}} &= \frac{\text{Tr}(Q_I^3)}{48\pi^2} F_I \tilde{F}_I + \sum_{L \neq I} \left(\frac{\text{Tr}(Q_I Q_I Q_L)}{16\pi^2} F_I \tilde{F}_L + \frac{\text{Tr}(Q_I Q_L Q_L)}{16\pi^2} F_L \tilde{F}_L \right) \\ &+ \frac{\text{Tr}(Q_I)}{384\pi^2} \mathcal{R} \tilde{\mathcal{R}} , \end{aligned} \quad (8.16)$$

where all flavor symmetries are viewed as being gauged. The flavor field strengths F and \tilde{F} are related as in eq. (8.13), while the Riemann curvature tensor $\mathcal{R}_{\mu\nu\lambda\rho}$ and its dual tensor are multiplied in (8.16) as

$$\mathcal{R} \tilde{\mathcal{R}} = \frac{1}{2} \varepsilon^{\mu\nu\lambda\rho} \mathcal{R}_{\mu\nu\sigma\delta} \mathcal{R}_{\lambda\rho}^{\sigma\delta} . \quad (8.17)$$

The first three terms of (8.16) are just the anomalies coming from Feynman diagrams as in (8.12), with the first factor possessing an additional symmetry factor of three. The last term comes from the coupling to the metric via the Riemann curvature tensor which leads to a different factor as for the first three terms. For completeness, we visualize the four terms of (8.16) with the Feynman diagrams



$$, \quad (8.18)$$

where every diagram has the gauge current I attached on the left and the gauge pairs on the right are given for the different diagrams by (I, I) , (I, L) , (L, L) and $(\mathcal{R}, \mathcal{R})$.

In supersymmetric theories, the currents mentioned so far also appear as components of chiral superfields. For example, the super-stress tensor contains as its $\theta = 0$ component the superconformal $U(1)_R$ symmetry, as its components linear in θ and θ^\dagger the SUSY currents and as its other components the energy-momentum tensor. From this connection, Anselmi et al. derived the equation (8.10) expressing the central charge a in terms of the superconformal R -charges. Analogously, flavor currents J_I^μ appear as components of suitable chiral superfields whose other components contain the Riemann curvature tensor

and the other flavor currents. In superconformal theories, R -symmetry also appears as one on these flavor symmetries. Considering only the gauge field of the superconformal R -(flavor) symmetry \mathcal{A}_R^μ and the metric as non-trivial, yields the expression

$$\langle \partial_\mu J_I^\mu \rangle_{\mathcal{A}_R^\mu, g_{\mu\nu}} = \frac{\text{Tr}(Q_I)}{384\pi^2} \left(\mathcal{R}\tilde{\mathcal{R}} + \frac{8}{3} F_R \tilde{F}_R \right), \quad (8.19)$$

with F_R the R -symmetry field strength. Comparing (8.19) with (8.16) for $I = L = R$ then gives the relation

$$\text{Tr}(Q_I) = 9\text{Tr}(Q_I R R), \quad (8.20)$$

where R now denotes the generator of the R -symmetry $U(1)_R$. The relation (8.20) is sufficient to infer that the superconformal R -charges make the central charge a stationary. The reasoning goes as follows. The superconformal R -charge of a theory can be written as a linear combination of an arbitrarily chosen R -charge R_0 and the other non- R flavor charges as

$$R = R_0 + \sum_I c_I Q_I. \quad (8.21)$$

Inserting this into equation (8.10) for the superconformal central charge a and differentiating with respect to c_I yields

$$\frac{\partial a}{\partial c_I} = \frac{32}{3} (9\text{Tr}(R^2 Q_I) - \text{Tr}(Q_I)) \stackrel{(8.20)}{=} 0, \quad (8.22)$$

which shows that superconformal R -charges make a stationary. To see that they even locally maximize a , the relation

$$\text{Tr}(R Q_I Q_L) = -\frac{\tau_{IL}}{3}, \quad (8.23)$$

valid for superconformal theories, is needed [17]. Unitarity requires τ to be positive definite, which means that $\text{Tr}(R Q_I Q_L)$ is a negative definite matrix. Furthermore, this means that the second partial derivative matrix

$$\frac{\partial^2 a}{\partial c_I \partial c_L} \stackrel{(8.10), (8.21)}{=} \frac{27}{16} \text{Tr}(R Q_I Q_L) \quad (8.24)$$

is also negative definite, i.e. has a local maximum at the superconformal R -charges. With this, a -maximization by superconformal R -charges has been proved.

For a theory flowing from the UV with central charge a_{UV} towards the IR with central charge a_{IR} , the a -theorem states that [157–159]

$$a_{UV} > a_{IR}. \quad (8.25)$$

To date, all explicitly investigated models turn out to indeed satisfy (8.25), as for example investigated in [169]. Furthermore, it has been shown that physical theories satisfy the conformal collider bound [22, 23]

$$\frac{1}{2} \leq \frac{a}{c} \leq \frac{3}{2}, \quad (8.26)$$

with c given for superconformal field theories by the R -charges

$$c = \frac{1}{32}(9\text{Tr}R^3 - 5\text{Tr}R). \quad (8.27)$$

Chapter 9

Model Analysis Beyond Perturbation Theory

In this chapter, we check whether the 114 AS candidates of tab. 6.5, found in our search within MSSM extensions of chapter 6, as well as some selected AS candidates of tab. 7.2, found within the MSSM+ framework of chapter 7, are in agreement with non-perturbative results of chapter 8. Furthermore, the infinite-order NSVZ beta functions (5.12) are utilized to check for UV-attractivity of our perturbative UV fixed points.

More specifically, we numerically locally maximize a of eq. (8.10) for each model to obtain the superconformal R -charges of chiral superfields for different fixed points. Hereby, different fixed points yield different constraints to be respected when maximizing a . These constraints are given by vanishing of the 't Hooft anomalies (8.7) for each interacting gauge coupling, and by the R -charge (8.8) of superpotential terms for each interacting Yukawa coupling. From the unitarity bounds (8.4), we infer that our numerically obtained chiral superfield R -charges have to satisfy the bound

$$R \geq \frac{1}{3}. \quad (9.1)$$

Furthermore, we demand that the a -theorem (8.25), as well as the conformal collider bound (8.26) are fulfilled within our models. From the infinite-order NSVZ beta functions (5.12) and the relation (8.6) between R -charges and anomalous dimension we obtain infinite order effective B -coefficients

$$B_{a,\text{eff}}^{\text{NSVZ}} = B_a + \frac{4}{d(G_a)} \sum_i C_2^{(a)}(r_i) d_a(r_i) \gamma_i, \quad (9.2)$$

utilized in fixed points with vanishing α_a -coupling. Analogously to the perturbative effective B -coefficients defined in (5.23), a positive $B_{a,\text{eff}}^{\text{NSVZ}}$ suggest UV-attractivity in

α_a -direction, while a negative $B_{a,\text{eff}}^{\text{NSVZ}}$ implies the contrary. We also check the signs of these infinite order effective B -coefficients within our models.

Finally, we study a new model which demonstrates that discrepancies present between two-loop and infinite-loop order are lifted when going to three-loop order. Furthermore, we are able to investigate the evolution of fixed points when model parameters approach values needed for UV attractivity thereof.

9.1 Perturbative AS MSSM Candidates

We begin with our non-perturbative checks by analyzing the 114 AS candidates of tab. 6.5, found in our searches for AS MSSM extensions of chapter 6.

In tab. 9.1, we show the models for which we succeed in maximizing a for FP_3 such that the unitarity bound (9.1) is fulfilled for all chiral superfields. We also display a , c , a/c , B_2 , $B_{2,\text{eff}}^{\text{FP}_3}$ and $B_{2,\text{eff}}^{\text{FP}_3,\text{NSVZ}}$ for FP_3 . The central charge information obtained for models for which we are able to maximize a in FP_{23} , and for which the unitarity bounds are fulfilled, are presented in tab. 9.2. In tab. 9.3, we show Δa for models for which we succeeded in numerically maximizing a in FP_3 and FP_{23} , simultaneously.

We observe that when we can maximize a for FP_{23} , we can also maximize a for FP_3 , and in these cases the a -theorem and the conformal collider bounds are always fulfilled. Surprisingly, we always find $B_{2,\text{eff}}^{\text{FP}_3,\text{NSVZ}}$ to be negative. To not be in conflict with the a -theorem, there either exists no trajectory connecting FP_3 and FP_{23} , or at least one of the fixed points FP_3 and FP_{23} does not exist in the exact RG flow.

No.	$\alpha_3^{\text{FP}_3}$	a	c	a/c	B_2	$B_{2,\text{eff}}^{\text{FP}_3}$	$B_{2,\text{eff}}^{\text{FP}_3,\text{NSVZ}}$	No.	$\alpha_3^{\text{FP}_3}$	a	c	a/c	B_2	$B_{2,\text{eff}}^{\text{FP}_3}$	$B_{2,\text{eff}}^{\text{FP}_3,\text{NSVZ}}$
1	0.431	3.328	3.905	0.852	-6.000	0.054	-4.262	58	0.561	3.397	3.967	0.856	-8.000	1.709	-5.734
2	0.431	3.328	3.905	0.852	-6.000	0.054	-4.262	59	0.561	3.397	3.967	0.856	-8.000	1.709	-5.734
3	0.431	3.328	3.905	0.852	-6.000	0.054	-4.262	60	0.591	3.311	3.933	0.842	-6.000	4.545	-3.630
4	0.431	3.328	3.905	0.852	-6.000	0.054	-4.262	61	0.591	3.311	3.933	0.842	-6.000	4.545	-3.630
5	0.431	3.328	3.905	0.852	-6.000	0.054	-4.262	62	0.591	3.394	3.960	0.857	-8.000	2.545	-5.630
6	0.431	3.328	3.905	0.852	-6.000	0.054	-4.262	63	0.591	3.394	3.960	0.857	-8.000	2.545	-5.630
7	0.458	3.325	3.897	0.853	-6.000	0.833	-4.143	64	0.591	3.394	3.960	0.857	-8.000	2.545	-5.630
8	0.458	3.325	3.897	0.853	-6.000	0.833	-4.143	65	0.591	3.478	3.988	0.872	-10.000	0.545	-7.630
9	0.458	3.325	3.897	0.853	-6.000	0.833	-4.143	66	0.591	3.478	3.988	0.872	-10.000	0.545	-7.630
10	0.458	3.325	3.897	0.853	-6.000	0.833	-4.143	67	0.591	3.478	3.988	0.872	-10.000	0.545	-7.630
11	0.458	3.325	3.897	0.853	-6.000	0.833	-4.143	68	0.598	3.311	3.932	0.842	-6.000	4.744	-3.624
12	0.458	3.325	3.897	0.853	-6.000	0.833	-4.143	69	0.598	3.311	3.932	0.842	-6.000	4.744	-3.624
13	0.458	3.325	3.897	0.853	-6.000	0.833	-4.143	70	0.598	3.394	3.960	0.857	-8.000	2.744	-5.624
14	0.473	3.324	3.895	0.853	-6.000	1.252	-4.112	71	0.598	3.394	3.960	0.857	-8.000	2.744	-5.624
15	0.473	3.324	3.895	0.853	-6.000	1.252	-4.112	72	0.598	3.394	3.960	0.857	-8.000	2.744	-5.624
16	0.473	3.324	3.895	0.853	-6.000	1.252	-4.112	73	0.598	3.478	3.988	0.872	-10.000	0.744	-7.624
17	0.473	3.324	3.895	0.853	-6.000	1.252	-4.112	74	0.598	3.478	3.988	0.872	-10.000	0.744	-7.624
18	0.452	3.322	3.960	0.839	-6.000	0.664	-4.034	75	0.598	3.478	3.988	0.872	-10.000	0.744	-7.624
19	0.468	3.321	3.958	0.839	-6.000	1.090	-4.015	76	0.519	3.396	4.036	0.841	-8.000	0.521	-5.704
20	0.468	3.321	3.958	0.839	-6.000	1.090	-4.015	77	0.533	3.392	4.027	0.842	-8.000	0.926	-5.581
21	0.468	3.321	3.958	0.839	-6.000	1.090	-4.015	78	0.594	3.390	4.021	0.843	-8.000	2.645	-5.487
22	0.488	3.317	3.948	0.840	-6.000	1.652	-3.859	79	0.594	3.473	4.048	0.858	-10.000	0.645	-7.487
23	0.488	3.317	3.948	0.840	-6.000	1.652	-3.859	80	0.652	3.388	4.015	0.844	-8.000	4.265	-5.405
24	0.488	3.317	3.948	0.840	-6.000	1.652	-3.859	81	0.652	3.388	4.015	0.844	-8.000	4.265	-5.405
25	0.514	3.316	3.945	0.840	-6.000	2.380	-3.814	82	0.652	3.471	4.043	0.859	-10.000	2.265	-7.405
26	0.514	3.316	3.945	0.840	-6.000	2.380	-3.814	83	0.652	3.471	4.043	0.859	-10.000	2.265	-7.405
27	0.514	3.316	3.945	0.840	-6.000	2.380	-3.814	84	0.652	3.554	4.071	0.873	-12.000	0.265	-9.405
28	0.514	3.399	3.973	0.856	-8.000	0.380	-5.814	85	0.652	3.554	4.071	0.873	-12.000	0.265	-9.405
29	0.514	3.399	3.973	0.856	-8.000	0.380	-5.814	86	0.655	3.384	4.006	0.845	-8.000	4.350	-5.273
30	0.514	3.399	3.973	0.856	-8.000	0.380	-5.814	87	0.655	3.467	4.034	0.860	-10.000	2.350	-7.273
31	0.514	3.399	3.973	0.856	-8.000	0.380	-5.814	88	0.655	3.551	4.062	0.874	-12.000	0.350	-9.273
32	0.514	3.399	3.973	0.856	-8.000	0.380	-5.814	89	0.680	3.385	4.009	0.844	-8.000	5.038	-5.315
33	0.526	3.315	3.943	0.841	-6.000	2.718	-3.787	90	0.680	3.469	4.037	0.859	-10.000	3.038	-7.315
34	0.526	3.315	3.943	0.841	-6.000	2.718	-3.787	91	0.680	3.552	4.065	0.874	-12.000	1.038	-9.315
35	0.526	3.315	3.943	0.841	-6.000	2.718	-3.787	92	0.705	3.383	4.003	0.845	-8.000	5.746	-5.227
36	0.526	3.398	3.971	0.856	-8.000	0.718	-5.787	93	0.705	3.466	4.031	0.860	-10.000	3.746	-7.227
37	0.526	3.398	3.971	0.856	-8.000	0.718	-5.787	94	0.705	3.550	4.059	0.875	-12.000	1.746	-9.227
38	0.526	3.398	3.971	0.856	-8.000	0.718	-5.787	95	0.722	3.384	4.006	0.845	-8.000	6.215	-5.269
39	0.526	3.398	3.971	0.856	-8.000	0.718	-5.787	96	0.722	3.468	4.034	0.860	-10.000	4.215	-7.269
40	0.526	3.398	3.971	0.856	-8.000	0.718	-5.787	97	0.722	3.551	4.062	0.874	-12.000	2.215	-9.269
41	0.528	3.315	3.943	0.841	-6.000	2.773	-3.791	98	0.722	3.634	4.090	0.889	-14.000	0.215	-11.269
42	0.528	3.315	3.943	0.841	-6.000	2.773	-3.791	99	0.738	3.382	4.001	0.845	-8.000	6.671	-5.195
43	0.528	3.398	3.971	0.856	-8.000	0.773	-5.791	100	0.738	3.466	4.029	0.860	-10.000	4.671	-7.195
44	0.528	3.398	3.971	0.856	-8.000	0.773	-5.791	101	0.738	3.549	4.057	0.875	-12.000	2.671	-9.195
45	0.528	3.398	3.971	0.856	-8.000	0.773	-5.791	102	0.738	3.632	4.084	0.889	-14.000	0.671	-11.195
46	0.547	3.314	3.941	0.841	-6.000	3.313	-3.756	103	0.738	3.382	4.001	0.845	-8.000	6.671	-5.195
47	0.547	3.398	3.969	0.856	-8.000	1.313	-5.756	104	0.738	3.466	4.029	0.860	-10.000	4.671	-7.195
48	0.561	3.314	3.940	0.841	-6.000	3.709	-3.734	105	0.738	3.549	4.057	0.875	-12.000	2.671	-9.195
49	0.561	3.397	3.967	0.856	-8.000	1.709	-5.734	106	0.738	3.632	4.084	0.889	-14.000	0.671	-11.195
50	0.561	3.314	3.940	0.841	-6.000	3.709	-3.734	107	0.750	3.382	4.000	0.845	-8.000	7.000	-5.175
51	0.561	3.314	3.940	0.841	-6.000	3.709	-3.734	108	0.750	3.465	4.028	0.860	-10.000	5.000	-7.175
52	0.561	3.314	3.940	0.841	-6.000	3.709	-3.734	109	0.750	3.549	4.055	0.875	-12.000	3.000	-9.175
53	0.561	3.314	3.940	0.841	-6.000	3.709	-3.734	110	0.750	3.632	4.083	0.889	-14.000	1.000	-11.175
54	0.561	3.397	3.967	0.856	-8.000	1.709	-5.734	111	0.767	3.382	3.999	0.846	-8.000	7.489	-5.167
55	0.561	3.397	3.967	0.856	-8.000	1.709	-5.734	112	0.767	3.465	4.027	0.860	-10.000	5.489	-7.167
56	0.561	3.397	3.967	0.856	-8.000	1.709	-5.734	113	0.767	3.548	4.055	0.875	-12.000	3.489	-9.167
57	0.561	3.397	3.967	0.856	-8.000	1.709	-5.734	114	0.767	3.632	4.083	0.890	-14.000	1.489	-11.167

Table 9.1: The model numbers (No.) as stated in tab. 6.5 for which we succeeded in numerically maximizing a of eq. (8.10) in the UV fixed point FP_3 (see tab. 6.1). We present its perturbative α_3 value, as well as c of eq. (8.27) and a/c , which needs to satisfy the conformal collider bound (8.26). Furthermore, the one-loop coefficient B_2 of eq. (5.6a), the effective loop-coefficient $B_{2,\text{eff}}^{\text{FP}_3}$ of eq. (5.23), and the exact effective coefficient $B_{2,\text{eff}}^{\text{FP}_3,\text{NSVZ}}$ of eq. (9.24) for each of these models are shown. We see that the conformal collider bound is always fulfilled and that the exact effective coefficients are negative, in contrast to the corresponding loop coefficients, implying that AS is lost at infinite-loop order.

No.	a	c	a/c	No.	a	c	a/c
2	3.124	2.949	1.059	74	3.153	2.912	1.083
3	3.124	2.949	1.059	75	3.153	2.912	1.083
6	3.124	2.949	1.059	77	3.090	2.928	1.055
9	3.121	2.951	1.058	78	3.086	2.927	1.055
10	3.121	2.951	1.058	79	3.153	2.950	1.069
11	3.121	2.951	1.058	81	3.083	2.926	1.054
12	3.121	2.951	1.058	85	3.153	2.914	1.082
13	3.121	2.950	1.058	86	3.072	2.925	1.050
15	3.121	2.951	1.058	87	3.164	2.951	1.072
16	3.121	2.951	1.058	88	3.152	2.915	1.081
28	3.134	2.948	1.063	89	3.078	2.925	1.052
29	3.134	2.948	1.063	90	3.159	2.950	1.071
30	3.133	2.948	1.063	91	3.152	2.915	1.081
31	3.134	2.948	1.063	92	3.071	2.924	1.050
32	3.134	2.948	1.063	93	3.165	2.951	1.073
38	3.134	2.949	1.063	94	3.152	2.916	1.081
39	3.133	2.948	1.063	95	3.075	2.924	1.052
40	3.134	2.949	1.063	96	3.162	2.952	1.071
43	3.134	2.948	1.063	97	3.152	2.915	1.081
44	3.135	2.949	1.063	98	3.144	2.921	1.076
45	3.134	2.948	1.063	99	3.069	2.924	1.050
47	3.134	2.949	1.063	100	3.169	2.953	1.073
49	3.136	2.950	1.063	101	3.152	2.916	1.081
57	3.135	2.950	1.063	102	3.144	2.921	1.076
58	3.135	2.950	1.063	103	3.069	2.924	1.050
59	3.135	2.950	1.063	104	3.166	2.953	1.072
62	3.138	2.952	1.063	105	3.152	2.916	1.081
63	3.139	2.951	1.063	106	3.144	2.921	1.076
64	3.138	2.952	1.063	107	3.068	2.923	1.049
65	3.153	2.911	1.083	108	3.169	2.954	1.073
66	3.153	2.911	1.083	109	3.152	2.916	1.081
67	3.153	2.911	1.083	110	3.144	2.921	1.076
70	3.138	2.953	1.063	111	3.068	2.923	1.050
71	3.138	2.952	1.063	112	3.170	2.953	1.074
72	3.138	2.953	1.063	113	3.152	2.916	1.081
73	3.153	2.912	1.083	114	3.144	2.921	1.076

Table 9.2: The model numbers (No.) as in tab. 6.5, for which we succeeded in maximizing a of eq. (8.10) in FP_{23} (see tab. 6.1). The conformal collider bound (8.26) again is always fulfilled.

No.	Δa	No.	Δa	No.	Δa	No.	Δa
2	0.204	43	0.265	74	0.325	97	0.399
3	0.204	44	0.264	75	0.325	98	0.490
6	0.204	45	0.265	77	0.302	99	0.313
9	0.204	47	0.263	78	0.303	100	0.297
10	0.204	49	0.262	79	0.320	101	0.397
11	0.204	57	0.262	81	0.304	102	0.488
12	0.204	58	0.262	85	0.402	103	0.313
13	0.204	59	0.262	86	0.312	104	0.299
15	0.204	62	0.256	87	0.303	105	0.397
16	0.204	63	0.256	88	0.398	106	0.488
28	0.265	64	0.256	89	0.308	107	0.314
29	0.265	65	0.325	90	0.309	108	0.296
30	0.266	66	0.325	91	0.400	109	0.396
31	0.265	67	0.325	92	0.312	110	0.488
32	0.265	70	0.256	93	0.301	111	0.314
38	0.264	71	0.256	94	0.397	112	0.294
39	0.265	72	0.256	95	0.309	113	0.396
40	0.264	73	0.325	96	0.305	114	0.488

Table 9.3: The model numbers (No.) as in tab. 6.5 for which we succeed in numerically maximizing a in FP_3 and FP_{23} (see tab. 6.1) simultaneously. The positivity of $\Delta a = a_{\text{UV}} - a_{\text{IR}}$ is in agreement with the a -theorem (8.25) for FP_3 being reached in the UV and with FP_{23} being IR attractive.

9.2 Perturbative AS MSSM+ Candidates

Next, we perform our non-perturbative checks for the 398 AS candidates found for $Y = 0.15$, stated in tab. 7.2.

We are able to numerically determine the exact R -charges in FP_+ for all of these 398 AS candidates. The unitarity bound (9.1) is satisfied by all chiral superfields for all AS candidates. Also, all obtained fractions of central charges a/c are in agreement with the conformal collider bound (8.26). Furthermore, we check for the values of the exact effective coefficients

$$\begin{aligned} B_{2,\text{eff}}^{\text{FP}_+,\text{NSVZ}} &= B_2 + \frac{4}{3}\text{Tr}\gamma C_2^{R_2} , \\ B_{3,\text{eff}}^{\text{FP}_+,\text{NSVZ}} &= B_3 + \frac{4}{3}\text{Tr}\gamma C_2^{R_2} , \end{aligned} \tag{9.3}$$

and find that both of these coefficients are negative for all models, contrary to the corresponding loop results.

Explicitly, for our three benchmarks BM1, BM2 and BM3 of sections 7.2.1, 7.2.2 and 7.2.3 we find

$$\begin{aligned} \text{BM1: } \frac{a}{c} &\approx 0.84 , B_{2,\text{eff}}^{\text{FP}_+,\text{exact}} \approx -29.6 , B_{1,\text{eff}}^{\text{FP}_+,\text{exact}} \approx -270.3 , \\ \text{BM2: } \frac{a}{c} &\approx 0.84 , B_{2,\text{eff}}^{\text{FP}_+,\text{exact}} \approx -31.5 , B_{1,\text{eff}}^{\text{FP}_+,\text{exact}} \approx -287.9 , \\ \text{BM3 (} Y = 0.5\text{): } \frac{a}{c} &\approx 0.80 , B_{2,\text{eff}}^{\text{FP}_+,\text{exact}} \approx -56.5 , B_{1,\text{eff}}^{\text{FP}_+,\text{exact}} \approx -76.5 , \\ \text{BM3 (} Y = 1.5\text{): } \frac{a}{c} &\approx 0.80 , B_{2,\text{eff}}^{\text{FP}_+,\text{exact}} \approx -56.5 , B_{1,\text{eff}}^{\text{FP}_+,\text{exact}} \approx -512.9 . \end{aligned} \tag{9.4}$$

Hence the three benchmark models are consistent with non-perturbative results and may exist beyond perturbation theory. As for the perturbative candidates of the MSSM extensions in chapter 6, the NSVZ beta functions (5.12) suggest that asymptotic safety is lost at infinite-loop order for the AS candidates within the MSSM+ framework of chapter 7.

9.3 MSSM Extensions with an Additional semi-simple Gauge Group $\text{SU}(N) \times \text{SU}(M)$ without Superpotentials

So far, all models found to be asymptotically safe within perturbation theory in chapter 6 and chapter 7 turned out to be in agreement with the exact relations from SCFTs

presented in chapter 8, but lose asymptotic safety according to the infinite-order NSVZ beta functions (5.12), as seen in the previous sections 9.1 and 9.2.

In this section, we present a model which extends the MSSM by two additional gauge sectors $SU(N)$ and $SU(M)$ and some chiral superfields. This model contains no superpotential. Exact SCFT relations and the NSVZ beta functions then suggest that we find a fixed point which UV completes the SM. The infinite order NSVZ beta function breaks down for large coupling values due to the pole induced by the denominator, and we have to check whether we are on the physical side of this pole. For this, we compare exact and infinite order expressions with two-loop and three-loop order results.

This new model has the gauge group

$$G = SU(N) \otimes SU(M) \otimes SU(3)_C \otimes SU(2)_L \otimes U(1)_Y , \quad (9.5)$$

with gauge couplings g_N, g_M, g_3, g_2, g_1 . The chiral superfield content of our gauge anomaly-free model is given by the MSSM chiral superfield content plus two chiral superfields $\chi, \bar{\chi}$ and n pairs of superfields $\Psi, \bar{\Psi}$ beyond the MSSM, which have representations as shown in tab. 9.4.

(Left-handed) Superfield	$SU(N)$	$SU(M)$	$SU(3)_C$	$SU(2)_L$	$U(1)_Y$	Multiplicity	R -charge
quark doublet Q	$\mathbf{1}$	$\mathbf{1}$	$\mathbf{3}$	$\mathbf{2}$	$+\frac{1}{6}$	3	R_Q
up-quark \bar{u}	$\mathbf{1}$	$\mathbf{1}$	$\bar{\mathbf{3}}$	$\mathbf{1}$	$-\frac{2}{3}$	3	R_u
down-quark \bar{d}	$\mathbf{1}$	$\mathbf{1}$	$\bar{\mathbf{3}}$	$\mathbf{1}$	$+\frac{1}{3}$	3	R_d
lepton doublet L	$\mathbf{1}$	$\mathbf{1}$	$\mathbf{1}$	$\mathbf{2}$	$-\frac{1}{2}$	3	R_L
lepton singlet \bar{e}	$\mathbf{1}$	$\mathbf{1}$	$\mathbf{1}$	$\mathbf{1}$	$+1$	3	R_e
up-Higgs H_u	$\mathbf{1}$	$\mathbf{1}$	$\mathbf{1}$	$\mathbf{2}$	$+\frac{1}{2}$	1	R_{Hu}
down-Higgs H_d	$\mathbf{1}$	$\mathbf{1}$	$\mathbf{1}$	$\mathbf{2}$	$-\frac{1}{2}$	1	R_{Hd}
χ	\mathbf{N}	$\mathbf{1}$	$\mathbf{1}$	$\mathbf{2}$	$+Y$	n_χ	R_χ
$\bar{\chi}$	$\bar{\mathbf{N}}$	$\mathbf{1}$	$\mathbf{1}$	$\bar{\mathbf{2}}$	$-Y$	n_χ	R_χ
Ψ	\mathbf{N}	\mathbf{M}	$\mathbf{1}$	$\mathbf{1}$	0	n_Ψ	R_Ψ
$\bar{\Psi}$	$\bar{\mathbf{N}}$	$\bar{\mathbf{M}}$	$\mathbf{1}$	$\mathbf{1}$	0	n_Ψ	R_Ψ

Table 9.4: MSSM chiral superfields and chiral superfields beyond the MSSM of our MSSM extension with two additional gauge sectors. Fixed point FM_{NM} (see tab. (9.5)) develops UV-attractivity in the direction of the SM couplings g_2 and g_1 for $M > N$ and large $|Y|$, according to the infinite-loop NSVZ beta functions (5.12) (see eqs. (9.8) and (9.9)). UV-attractivity in the direction of g_3 is automatic.

The parameters of our model are

$$(N, M, n_\chi, n_\Psi, Y) . \quad (9.6)$$

We have no superpotential in our model and only gauge interactions. We work with the new gauge couplings

$$\alpha_N = \frac{g_N^2 N}{(4\pi)^2}, \quad \alpha_M = \frac{g_M^2 M}{(4\pi)^2}, \quad \alpha_i = \frac{g_i^2}{(4\pi)^2}, \quad i = 3, 2, 1. \quad (9.7)$$

Of special interest for this study are the three interacting fixed points FP_M , FP_N and FP_{NM} , described in tab. 9.5 together with the gaussian fixed point G .

9.3.1 Exact UV-attractivity and unitarity

Fixed point	α_N^*	α_M^*	α_3^*	α_2^*	α_1^*	R_χ	R_Ψ	R_{MSSM}
G	0	0	0	0	0	2/3	2/3	2/3
FP_N	X	0	0	0	0	$1 - \frac{N}{2n_\chi + 2M}$	$1 - \frac{N}{2n_\chi + 2M}$	2/3
FP_M	0	X	0	0	0	2/3	$1 - \frac{M}{Nn_\Psi}$	2/3
FP_{NM}	X	X	0	0	0	$1 + \frac{M^2 - N^2}{2Nn_\chi}$	$1 - \frac{M}{Nn_\Psi}$	2/3

Table 9.5: The three fixed points of special interest for this study, and the gaussian fixed point G . An ‘‘X’’ implies that the corresponding coupling is interacting in the fixed point. MSSM fields are free in these fixed points and their R -charges of tab. 9.4 take on the free field value 2/3, i.e. $R_{\text{MSSM}} = R_Q = R_u = R_d = R_L = R_e = R_{Hu} = R_{Hd} = 2/3$.

From the vanishing ‘t Hooft anomalies (8.7), we obtain the R -charges shown in tab. 9.5. In FP_{NM} , we find for the effective NSVZ B -coefficients (9.24):

$$\begin{aligned} B_{3,\text{eff}}^{\text{FP}_{NM},\text{NSVZ}} &= 6, \\ B_{2,\text{eff}}^{\text{FP}_{NM},\text{NSVZ}} &= -2 + 3(M^2 - N^2), \\ B_{1,\text{eff}}^{\text{FP}_{NM},\text{NSVZ}} &= -22 + 12Y^2(M^2 - N^2). \end{aligned} \quad (9.8)$$

We see that for

$$M > N \quad \text{and} \quad |Y| > \sqrt{\frac{11}{6(M^2 - N^2)}}, \quad (9.9)$$

we always achieve positive infinite order effective B -coefficients, implying that FP_{NM} serves as a fixed point reached in the UV when starting on the SM trajectory, assuming that FP_{NM} exists.

In tab. 9.5, we see that for the conditions (9.9), all R -charges except for R_Ψ automatically satisfy the unitarity bound (9.1). In order for R_Ψ to be in agreement with unitarity, we furthermore need

$$n_\Psi \geq \frac{3M}{2N}. \quad (9.10)$$

9.3.2 Large- N two-loop analysis

At 2-loop, the system of beta functions relevant for fixed points FP_N , FP_M and FP_{NM} reads

$$\begin{aligned}\beta_N &= \alpha_N^2[-B_N + C_{NN}\alpha_N + C_{NM}\alpha_M], \\ \beta_M &= \alpha_M^2[-B_M + C_{MM}\alpha_M + C_{MN}\alpha_N].\end{aligned}\tag{9.11}$$

We perform the large- N Veneziano limit

$$N, M, n_\chi \rightarrow \infty,\tag{9.12}$$

with the ratios

$$r \equiv \frac{M}{N} > 0, X \equiv \frac{n_\chi}{N} > 0\tag{9.13}$$

being held constant. In this limit, r and X become real numbers. From (9.9) we see that for $r > 1$, the SM can be UV completed with FP_{NM} being reached in the UV. The beta coefficients in (9.11) read in this limit (9.12)

$$\begin{aligned}B_N &= 6 - 4X - 2n_\Psi r, & B_M &= 6 - 2\frac{n_\Psi}{r}, \\ C_{NN} &= -12 + 4(4X + 2n_\Psi r), & C_{NM} &= 4n_\Psi r, \\ C_{MM} &= -12 + 8\frac{n_\Psi}{r}, & C_{MN} &= 4\frac{n_\Psi}{r}.\end{aligned}\tag{9.14}$$

Due to the general relations [113]

$$B_N \leq 0 \Rightarrow C_{NN} > 0, B_M \leq 0 \Rightarrow C_{MM} > 0,\tag{9.15}$$

and since $C_{NM}, C_{MN} > 0$ (see eq. (5.6c)), we infer from the beta function system (9.11) that in order for FP_{NM} to possibly exist within perturbation theory, we need

$$B_N > 0, B_M > 0,\tag{9.16}$$

which can be translated into the conditions

$$n_\Psi < \frac{3 - 2X}{r}, n_\Psi < 3r.\tag{9.17}$$

The second condition is automatically fulfilled for $r > 1$ when the first condition is satisfied. Together with (9.10), we find

$$\frac{3}{2}r < n_\Psi < \frac{3 - 2X}{r},\tag{9.18}$$

which for $r > 1$ can only be fulfilled for integer values of n_Ψ by

$$n_\Psi = 2,\tag{9.19}$$

and only for

$$X < \frac{1}{2}, \quad r \in \left(1, \frac{3}{2} - X\right). \quad (9.20)$$

Eqs. (9.19) and (9.20) constitute all conditions for which R -charges are unitary, FP_{NM} is UV-attractive in the direction of MSSM couplings, and for which FP_{NM} possibly exists at two-loop order.

The non-vanishing couplings within the interacting fixed points of tab. 9.5 are given at two-loop order by

$$\begin{aligned} \alpha_N^{\star\text{FP}_N} &= \frac{B_N}{C_{NN}}, \\ \alpha_M^{\star\text{FP}_M} &= \frac{B_M}{C_{MM}}, \\ \alpha_N^{\star\text{FP}_{NM}} &= \frac{B_N C_{MM} - B_M C_{NM}}{C_{NN} C_{MM} - C_{NM} C_{MN}}, \quad \alpha_M^{\star\text{FP}_{NM}} = \frac{B_M C_{NN} - B_N C_{MN}}{C_{NN} C_{MM} - C_{NM} C_{MN}}. \end{aligned} \quad (9.21)$$

When the interacting fixed points (9.21) vanish, the corresponding R -charges of tab. 9.5 acquire the free field value $R = 2/3$. To see this, we at first express the R -charges by means of r and X (and with $n_\Psi = 2$ as in (9.19)) as

$$\begin{aligned} R_\chi^{\text{FP}_N} &= R_\Psi^{\text{FP}_N} = 1 - \frac{1}{2(X+r)}, \\ R_\Psi^{\text{FP}_M} &= 1 - \frac{r}{2}, \\ R_\chi^{\text{FP}_{NM}} &= 1 + \frac{r^2 - 1}{2X}, \quad R_\Psi^{\text{FP}_M} = 1 - \frac{r}{2}. \end{aligned} \quad (9.22)$$

In perturbation theory, FP_N vanishes for $2(X+r) = 3$, yielding the free field value $R_\chi^{\text{FP}_N} = R_\Psi^{\text{FP}_N} = 2/3$. Fixed point FP_M becomes gaussian for $r = 2/3$, corresponding to $R_\Psi^{\text{FP}_M} = 2/3$. Vanishing of both, $\alpha_N^{\star\text{FP}_{NM}}$ and $\alpha_M^{\star\text{FP}_{NM}}$, can be shown to be equivalent to $r = 2/3$, $X = 5/6$, for which we again obtain $R_\chi^{\text{FP}_{NM}} = R_\Psi^{\text{FP}_M} = 2/3$. Hence, the formulae for perturbative fixed point values (9.21) and for R -charges (9.22) agree when interacting fixed points approach the gaussian fixed point.

Furthermore, we find parameters X , r within (9.20), for which FP_{NM} indeed exists at two-loop order. In fig. 9.1, we show for $X = 0.01$ the r -dependency of α_N and α_M of FP_{NM} . There we see that for $r \in \{1, 1.076\}$, FP_{NM} is physical in a regime for which non-perturbative and infinite order results suggest that the SM can be UV completed by FP_{NM} .

Nevertheless, we find discrepancies between two-loop and exact RG flows. The effective B -coefficients at two-loop order are

$$\begin{aligned} B_{M,\text{eff}}^{\text{FP}_N,2\text{-loop}} &= B_M - C_{MN}\alpha_N^{\star\text{FP}_N}, \\ B_{N,\text{eff}}^{\text{FP}_M,2\text{-loop}} &= B_N - C_{NM}\alpha_M^{\star\text{FP}_M}, \end{aligned} \quad (9.23)$$

and corresponding infinite-order B -coefficients obtained from the NSVZ beta functions (5.12) are

$$\begin{aligned} B_{M,\text{eff}}^{\text{FP}_N,\text{NSVZ}} &= B_M + \frac{12}{r} \left(R_{\Psi}^{\text{FP}_N} - \frac{2}{3} \right), \\ B_{N,\text{eff}}^{\text{FP}_M,\text{NSVZ}} &= B_N + 12r \left(R_{\Psi}^{\text{FP}_M} - \frac{2}{3} \right). \end{aligned} \quad (9.24)$$

We find within (9.20) that, as soon as FP_{NM} exists perturbatively, also the fixed points FP_N and FP_M exist, with the loop coefficients $B_{M,\text{eff}}^{\text{FP}_N,2\text{-loop}}$ and $B_{M,\text{eff}}^{\text{FP}_N,2\text{-loop}}$ both being negative. On the other hand, the NSVZ coefficients can be shown to have the signs

$$B_{M,\text{eff}}^{\text{FP}_N,\text{NSVZ}} > 0, \quad B_{N,\text{eff}}^{\text{FP}_M,\text{NSVZ}} < 0 \quad (9.25)$$

for $r > 1$. Hence we find a disagreement between two-loop and infinite order perturbation theory. Caveats remain from our 2-loop analysis whether FP_{NM} remains physical at infinite-loop level.

Furthermore, we find for the a -charges (8.10) of the benchmark in fig. 9.1 with $X = 0.01$ and $r > 1$ that

$$a_G > a_N > a_M > a_{NM}. \quad (9.26)$$

The a -theorem (8.25) suggests that RG flows from G to FP_N to FP_{NM} , from G to FP_M to FP_M to FP_{NM} , and from G to FP_{NM} are possible. We see that the 2-loop RG-flow of our benchmark (see fig. 9.2) is in conflict with the a -theorem.

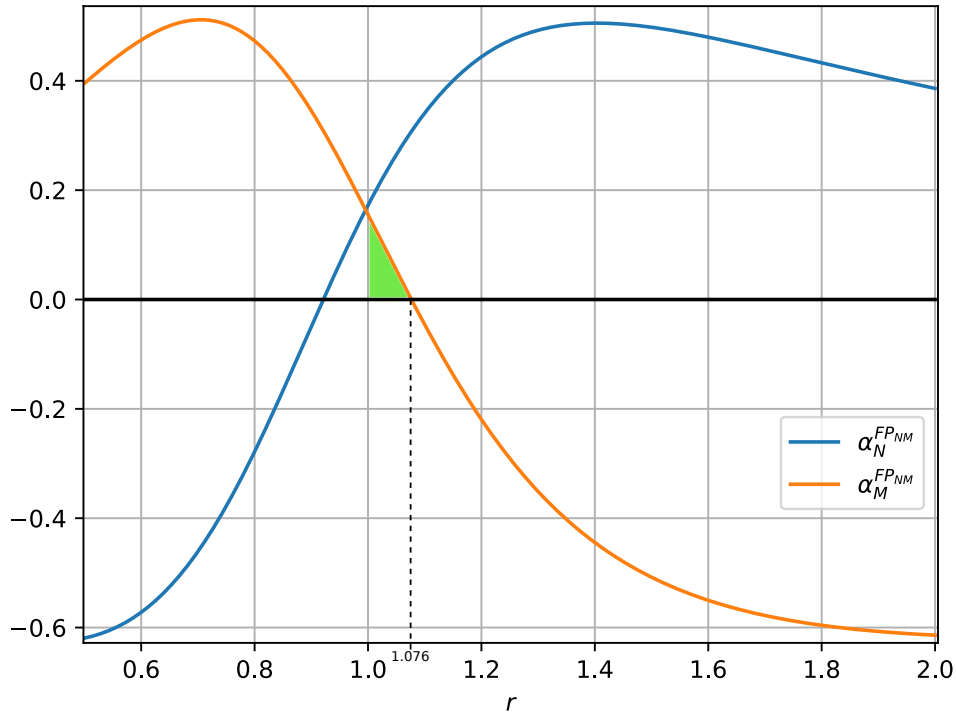


Figure 9.1: The two-loop couplings α_N and α_M of FP_{NM} (see tab. 9.5) in dependency of r for $X = 0.01$. For the definitions of r and X , see (9.13). We see that within (9.20), we find a regime (highlighted in green) for which FP_{NM} becomes physical. In this regime, FP_{NM} becomes UV-attractive in the directions of MSSM couplings, suggesting that it can be reached when starting on the SM trajectory, and hence UV-completing the SM.

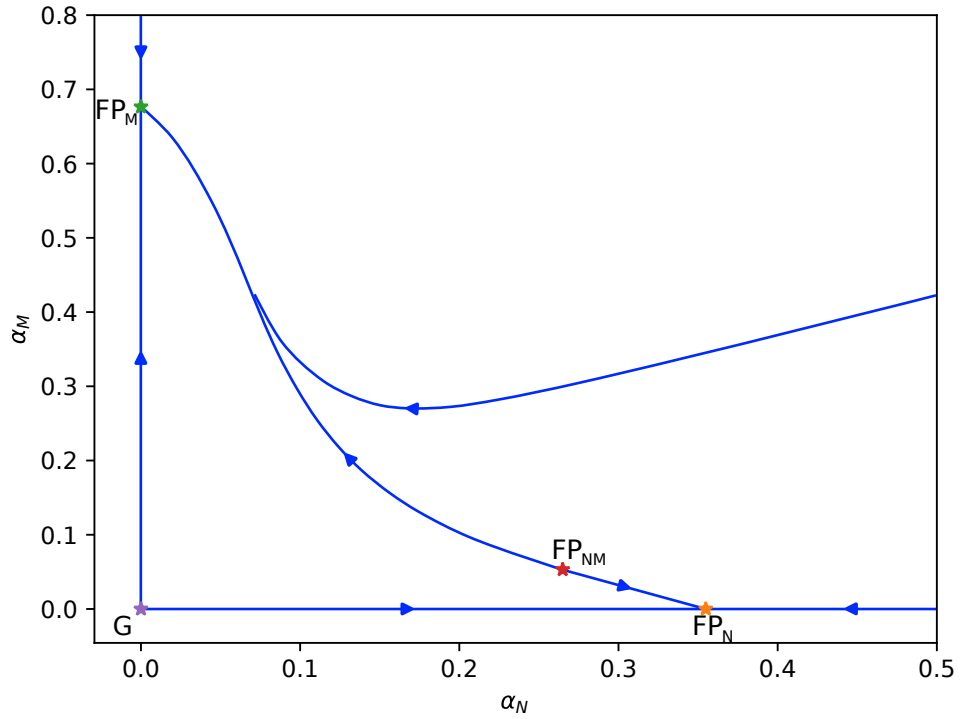


Figure 9.2: Two-loop RG flow for $X = 0.01$ and $r = 1.05$, as defined in eq. (9.13). Here, FP_N (orange), FP_M (green) and FP_{NM} (red) are physical. For more information on these fixed points, see tab. 9.5. Since $r > 1$, FP_{NM} would be UV-attractive in the directions of the MSSM couplings (see eq. (9.8)) if it still exists at infinite-loop order.

9.3.3 Large- N three-loop analysis

At three-loop level, the beta functions for interacting α_N and α_M read

$$\begin{aligned}\beta_N &= \alpha_N^2[-B_N + C_{NN}\alpha_N + C_{NM}\alpha_M + K_{NNN}\alpha_N^2 + K_{NMM}\alpha_M^2 + K_{NNM}\alpha_N\alpha_M], \\ \beta_M &= \alpha_M^2[-B_M + C_{MM}\alpha_M + C_{MN}\alpha_N + K_{MMM}\alpha_M^2 + K_{MNN}\alpha_N^2 + K_{MNM}\alpha_N\alpha_M],\end{aligned}\tag{9.27}$$

with the loop coefficients in the Veneziano limit (9.12) given by (9.14) and

$$\begin{aligned}K_{NNN} &= 24 - 4n_\Psi^2 r^2 + 48X - 16X^2 - 16Xn_\Psi r + 20n_\Psi r, \\ K_{NMM} &= -4n_\Psi(n_\Psi - 2r), \quad K_{NNM} = 4n_\Psi r, \\ K_{MMM} &= -24 + 16\frac{n_\Psi}{r} + 4\frac{n_\Psi}{r^2}(2 - n_\Psi), \\ K_{MNN} &= 4n_\Psi\left(\frac{2}{r} - n_\Psi\right), \quad K_{MMN} = 4\frac{n_\Psi}{r}.\end{aligned}\tag{9.28}$$

For the benchmark

$$X = 0.01, \quad r = 1.05,\tag{9.29}$$

we find the RG flow shown in fig. 9.3 with

$$B_{M,\text{eff}}^{\text{FP}_N,3\text{-loop}} > 0, \quad B_{N,\text{eff}}^{\text{FP}_M,3\text{-loop}} < 0,\tag{9.30}$$

in agreement with the exact NSVZ B -coefficient signs of eq. (9.25). Furthermore, the RG flow at three-loop order of fig. 9.3 is in agreement with the a -theorem (8.25) for a -charges as in eq. (9.26). This suggests that the exact RG flow is sufficiently approximated at three-loop order. We find that FP_{NM} is not physical at this loop order, in contrast to the two-loop result of the previous section (see fig. 9.1).

We now try to understand how FP_{NM} becomes unphysical at three-loop order when starting at parameters for which $r < 1$ so that FP_{NM} is not UV-attractive in the directions of all MSSM couplings and then going to parameters for which $r > 1$. We also check whether the 3-loop approximation is consistent with the infinite-loop order picture.

We introduce the new parameters

$$\varepsilon \equiv B_N \geq 0, \quad \varepsilon P \equiv B_M \geq 0,\tag{9.31}$$

where ε and P have to be positive in order for FP_{NM} to possibly exist. The new parameters and the ratios r and X of (9.13) are related via

$$r = \frac{2n_\Psi}{6 - P\varepsilon}, \quad X = \frac{(6 - \varepsilon)(6 - P\varepsilon) - 4n_\Psi^2}{24 - 4P\varepsilon}.\tag{9.32}$$

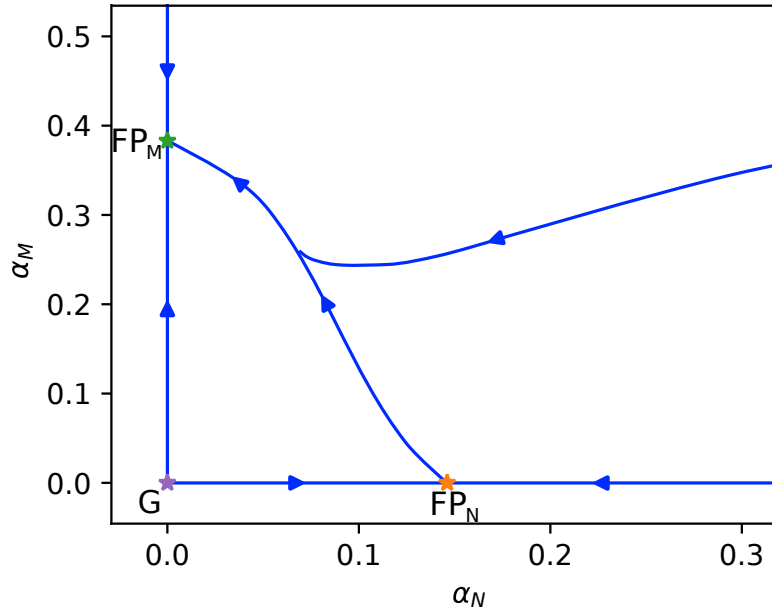


Figure 9.3: Three-loop RG flow for the benchmark with $X = 0.1$, $r = 1.05$ (see (9.13)), analogous to the two-loop picture in fig. 9.1. As in the two-loop case, FP_N and FP_M (see tab. 9.5) are here physical. However, FP_{NM} is unphysical at three-loop order, contrary to the findings at two-loop level. The signs of $B_{M,\text{eff}}^{\text{FP}_N, 3\text{-loop}} > 0$ and $B_{N,\text{eff}}^{\text{FP}_M, 3\text{-loop}} < 0$ are in agreement with the corresponding infinite-order coefficients (9.25). This suggests that the three-loop RG flow sufficiently approximates the infinite-order RG flow and that FP_{NM} is not physical for our benchmark model.

From the positivity of r and X , we find from (9.32) that

$$n_\Psi = 1, 2. \quad (9.33)$$

In tab. 9.6, we set $n_\Psi = 1$ and start at $\varepsilon = 0.5$ and $P = 2$, for which $r = 0.4$ and $X = 1.18$. The hierarchy of a -charges is compatible with the a -theorem and the three-loop RG-flow. The signs of the effective B coefficients agree at three-loop and at infinite-loop order. Hence we conclude that the three-loop RG flow sufficiently approximates the exact RG flow. Since FP_{NM} is physical at three-loop order (see fig. 9.4a), we suspect that it is also physical at infinite-loop order. When increasing ε and P , FP_{NM} wanders towards FP_M (see fig. 9.4b), until it evolves negative α_N values above $P \gtrsim 2.3$ at three-loop order (see fig. 9.4c). The sign-discrepancy of $B_{N,\text{eff}^{\text{FP}_M}}$ at three-loop and at infinite-loop suggests that at infinite-order, FP_{NM} might still be physical. At $P = 2.5$, the sign discrepancy vanishes and three-loop and infinite-loop results agree again. Hence we conclude that for $n_\Psi = 1$ and $\varepsilon = 1.2$, $P \gtrsim 2.5$, for which we have $r \approx 2/3$, FP_{NM} becomes unphysical at infinite-loop order. Note that this is incidentally the same bound (9.10) coming from unitarity. Keeping $P = 2.2$ and increasing ε beyond 1.2 yields that FP_{NM} becomes complex for $\varepsilon = 1.3$ at three-loop order (see fig. 9.4d). The sign discrepancy in $B_{N,\text{eff}^{\text{FP}_M}}$ again suggests that at infinite-loop order, FP_{NM} might still be physical. For $\varepsilon = 1.4$ the sign discrepancy vanishes again, suggesting that now also at infinite-loop order FP_{NM} became complex.

In tab. 9.7, an analogous behavior is found for $n_\Psi = 2$. Here, we are able to achieve $r = 0.81$ for $\varepsilon = 0.7$ and $P = 1.6$, before FP_{NM} becomes unphysical at three-loop and infinite-loop order.

We conclude that the exact RG flow is sufficiently approximated at three-loop order and that FP_{NM} becomes unphysical before it can UV complete the SM.

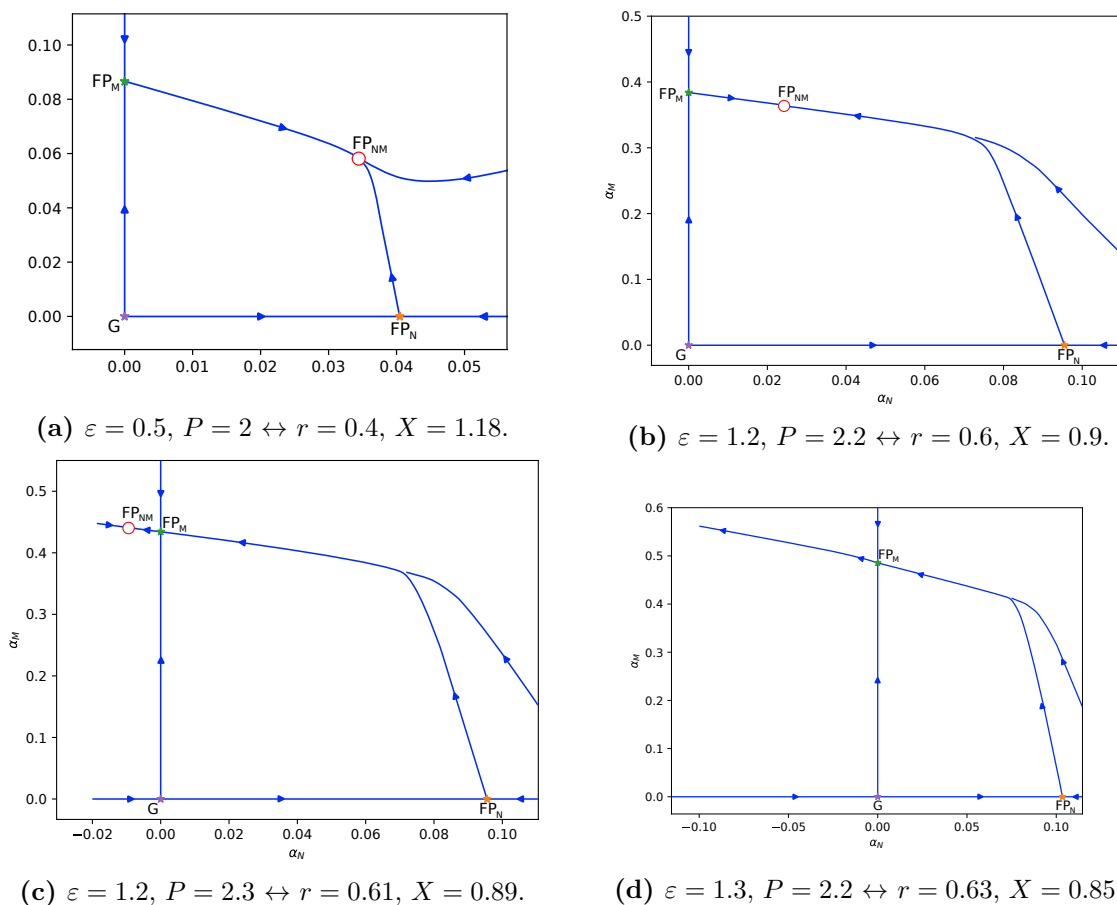


Figure 9.4: Three-loop RG flows for $n_\Psi = 1$ (see tab. 9.4) and for different parameters ε and P , defined in eq. (9.31). The shown plots correspond to the parameters listed in tab. 9.6. The red circles indicate the couplings at which FP_{NM} is identified from the RG flow lines. (a) FP_{NM} is physical. (b) We observe that FP_{NM} approaches FP_M . (c) Here, FP_{NM} crossed FP_M (green) and developed negative α_N components, making it unphysical. For a slightly larger $P = 2.5$ (see fourth row in tab. 9.6, the three-loop RG flow stays almost identical. (d) The fully interacting FP_{NM} does not appear anymore at three-loop, implying that it developed complex couplings. For $\varepsilon = 1.38$ (sixth row of tab. 9.6), the three-loop RG flow is (almost) the same.

ε	P	r	X	a	$B_{M,\text{eff}}^{\text{FP}_N,3\text{-loop}}$	$B_{M,\text{eff}}^{\text{FP}_N,\text{NSVZ}}$	$B_{N,\text{eff}}^{\text{FP}_M,3\text{-loop}}$	$B_{N,\text{eff}}^{\text{FP}_M,\text{NSVZ}}$	RG	$\text{FP}_{NM}^{3\text{-loop}}$	$\text{FP}_{NM}^{\text{NSVZ}}$
0.5	2	0.4	1.18	$a_G > a_N > a_M > a_{NM}$	> 0	> 0	> 0	> 0	9.4a	phys	phys
1.2	2.2	0.6	0.9	$a_G > a_N > a_M > a_{NM}$	> 0	> 0	> 0	> 0	9.4b	phys	phys
1.2	2.3	0.61	0.89	$a_G > a_N > a_M > a_{NM}$	> 0	> 0	< 0	> 0	9.4c	unphys	phys
1.2	2.5	0.66	0.87	$a_G > a_N > a_M > a_{NM}$	> 0	> 0	< 0	< 0	9.4c	unphys	unphys
1.3	2.2	0.63	0.85	$a_G > a_N > a_M > a_{NM}$	> 0	> 0	< 0	> 0	9.4d	unphys	phys
1.38	2.2	0.67	0.82	$a_G > a_N > a_M > a_{NM}$	> 0	> 0	< 0	< 0	9.4d	unphys	unphys

Table 9.6: Benchmarks with $n_\Psi = 1$, specified by the parameters ε and P defined in eq. (9.31). For each benchmark, r and X from (9.32) are stated, as well as the hierarchy of exact a -charges. Furthermore, the signs of the effective 3-loop and infinite-loop (NSVZ) B coefficients in FP_N and FP_M are stated. In the column “RG”, the figure number to the corresponding RG flow is provided. Furthermore, we specify whether we find that FP_{NM} is physical or unphysical at three-loop level and use the signs of the effective B -coefficients to infer information on the physicality of FP_{NM} at infinite-loop order. We see that we reach at most $r \sim 0.66$ before FP_{NM} becomes unphysical. To have FP_{NM} UV attractive in the direction of the MSSM couplings, $r > 1$ is needed.

ε	P	r	X	a	$B_{M,\text{eff}}^{\text{FP}_N,3\text{-loop}}$	$B_{M,\text{eff}}^{\text{FP}_N,\text{NSVZ}}$	$B_{N,\text{eff}}^{\text{FP}_M,3\text{-loop}}$	$B_{N,\text{eff}}^{\text{FP}_M,\text{NSVZ}}$	RG	$\text{FP}_{NM}^{3\text{-loop}}$	$\text{FP}_{NM}^{\text{NSVZ}}$
0.1	1.5	0.68	0.79	$a_G > a_N > a_M > a_{NM}$	> 0	> 0	> 0	> 0	9.5a	phys	phys
0.7	1.5	0.81	0.52	$a_G > a_N > a_M > a_{NM}$	> 0	> 0	> 0	> 0	9.5b	phys	phys
0.7	1.6	0.82	0.51	$a_G > a_N > a_M > a_{NM}$	> 0	> 0	< 0	< 0	9.5c	unphys	unphys
0.8	1.5	0.83	0.47	$a_G > a_N > a_M > a_{NM}$	> 0	> 0	< 0	< 0	9.5d	unphys	unphys

Table 9.7: An analogous table to tab. 9.6 for $n_\Psi = 2$. Qualitatively, we observe the same behavior as for $n_\Psi = 1$, with the difference being that we achieve $r \sim 0.81$ before FP_{NM} becomes unphysical which is still not sufficient to make FP_{NM} UV attractive in the directions of the MSSM couplings for which $r > 1$ is needed.

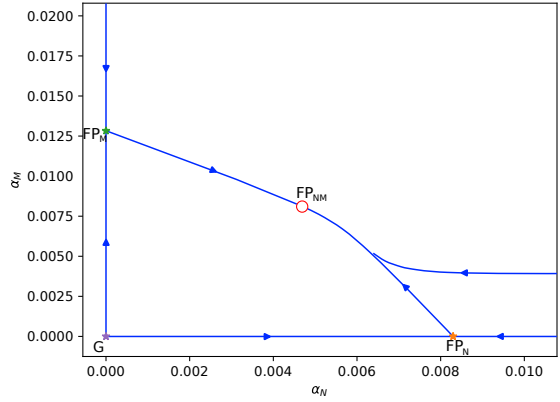
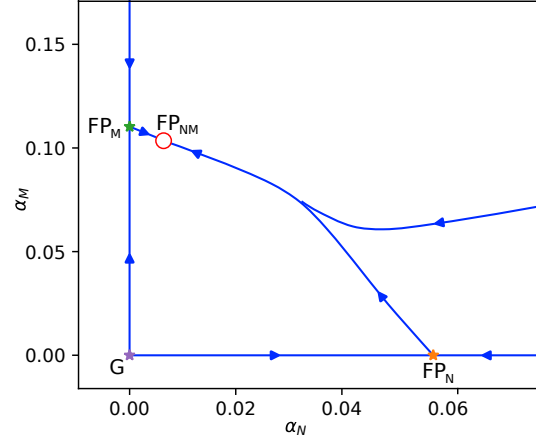
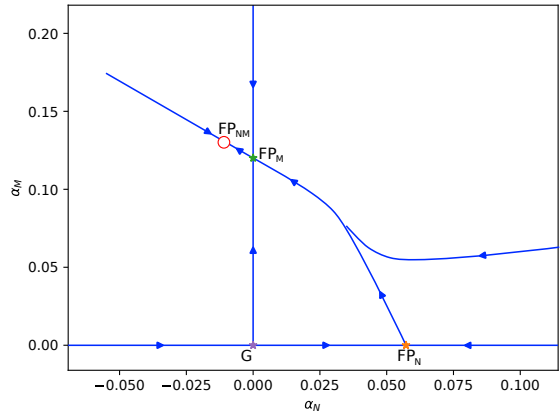
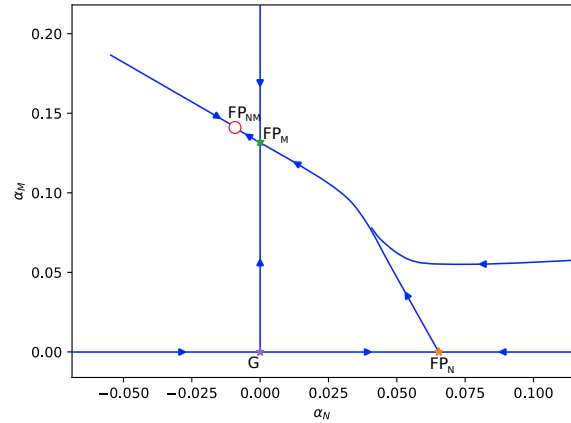

 (a) $\varepsilon = 0.1$, $P = 1.5 \leftrightarrow r = 0.68$, $X = 79$.

 (b) $\varepsilon = 0.7$, $P = 1.5 \leftrightarrow r = 0.81$, $X = 0.52$.

 (c) $\varepsilon = 0.7$, $P = 1.6 \leftrightarrow r = 0.82$, $X = 0.51$.

 (d) $\varepsilon = 0.8$, $P = 1.5 \leftrightarrow r = 0.83$, $X = 0.47$.

Figure 9.5: RG flows at three-loop level for $n_\Psi = 2$ and for different parameters ε and P . The shown plots correspond to the parameters listed in tab. 9.7. The red circles indicate the couplings at which FP_{NM} is identified from the RG flow lines. Three-loop and infinite-order results are in agreement for all four cases. (a) FP_{NM} is physical. (b) We observe that FP_{NM} comes closer to FP_M . (c) Here, FP_{NM} crossed FP_M and evolved negative α_N couplings, making FP_{NM} unphysical. (d) FP_{NM} again evolved negative α_M couplings.

9.4 Summary of our Non-Perturbative Investigations

For our investigations beyond perturbation theory we utilized exact results coming from superconformal field theories, provided in chapter 8, as well as the infinite order NSVZ beta functions (5.12).

With these relations at hand, we checked the perturbative AS candidates of the MSSM extensions in chapter 6 and within the MSSM+ framework of chapter 7. We obtained the exact R -charges of chiral superfields in fixed points by maximizing the central charge a (8.10) which all had to fulfill the unitarity bound $R \geq 1/3$ (9.1) as well as the conformal collider bound $1/2 \leq a/c \leq 3/2$ (8.26). Furthermore, the RG flow between two fixed points had to fulfill the a -theorem $a_{UV} > a_{IR}$ (8.25). We found that the perturbative AS candidates are consistent with these exact SCFT results.

The effective NSVZ coefficients (9.24) turned out to be all negative for the perturbative UV fixed points of the candidate models, implying that AS is lost at infinite-loop order (see secs. 9.1 and 9.2). We conclude that there are major discrepancies between the exact RG flow and its 2-1-approximation.

In sec. 9.3, we presented an MSSM extension with the two additional gauge sectors, so that its gauge group is (9.5):

$$G = \text{SU}(N) \otimes \text{SU}(M) \otimes \text{SU}(3)_C \otimes \text{SU}(2)_L \otimes \text{U}(1)_Y . \quad (9.34)$$

The chiral superfield content of this model is shown in tab. 9.4.

At two-loop level, we found in sec. 9.3.2 that the fixed point FP_{NM} (see tab. 9.5) exists for model parameters for which it becomes UV attractive in the direction of the MSSM couplings $\alpha_1, \alpha_2, \alpha_3$ according to the infinite order NSVZ beta functions. In fig. 9.1, a subset of this parameter window is given by the green area. Nevertheless, the two-loop picture again is in conflict with exact results since the two-loop and infinite-loop effective B -coefficients (9.23) and (9.24) have different signs and the two-loop RG flow shown in fig. 9.2 is in conflict with the a -theorem (8.25) and the superconformal a -charge hierarchy (9.26).

Going to three-loop order in sec. 9.3.3, we find RG flows which are in good agreement with the superconformal relations. We conclude that the three-loop RG flow sufficiently approximates the exact RG flow. Furthermore, we studied the evolution of FP_{NM} along parameters which approach a regime in which FP_{NM} becomes UV attractive in the direction of the MSSM couplings (see tabs. 9.6, (9.7) and the corresponding plots 9.4, 9.5). We find that FP_{NM} becomes unphysical before it UV-completes the SM.

Our non-perturbative investigations suggest that asymptotically safe MSSM extensions could be found within perturbation theory when working at three-loop gauge level. Yukawa beta functions should then be approximated at two-loop level.

Chapter 10

Conclusions

Outside of its original application in quantized general relativity [12, 79–81, 86], asymptotic safety lately developed into a practical model building tool for non-gravitational, realistic theories which complete the standard model in the UV [61, 62]. The SM itself is not fundamental due to the $U(1)_Y$ Landau pole. Another application of asymptotic safety was found in the natural explanation of the measured anomalous magnetic moments of muons and electrons [115, 116].

Recent theoretical advances yield theorems for weakly interacting gauge theories [113]. Sample models for which asymptotic safety could be established to all orders of perturbation theory, with and without supersymmetry, were constructed [63–65]. In the latter case of supersymmetry, asymptotic safety becomes very restrictive [117].

In this thesis, supersymmetric renormalizable extensions of the MSSM were investigated with the goal of finding supersymmetric SM UV completions via asymptotic safety. Within perturbation theory, we found strong limitations on the number of colored chiral superfields beyond the MSSM for which interacting UV fixed points may exist at two-loop gauge and one-loop Yukawa level (see chapter 6). Explicitly, the amount of additional quark singlet chiral superfields beyond the MSSM may at most be four. In exhaustive searches within sections 6.3, 6.4 and 6.5, we were able to find asymptotically safe supersymmetric SM extensions, all of which turned out to contain exactly two quark singlets beyond the MSSM. In the discussions of sec. 6.6 on these AS candidates, R -parity violation and low-scale supersymmetry breaking are found. In our approximations, supersymmetry-breaking occurs at energy scales $\mathcal{O}(1 \text{ GeV})$ in conflict with phenomenology [43], and the hypercharge coupling vanishes on UV-safe trajectories. Higher loop-orders or gravitational corrections might change this picture to enable matching onto SM at phenomenologically viable matching scales.

Extending the MSSM gauge group by a new $SU(N)$ gauge sector offered new UV fixed

points for which matching onto SM at larger energies became possible (chapter 7). Within a model framework which we call “MSSM+” (see sec. 7.1), we explicitly demonstrated this matching onto the SM for energies above 1 TeV for three benchmark scenarios BM1, BM2 and BM3 in sections 7.2.1, 7.2.2 and 7.2.3, respectively. Furthermore, we were able to successfully incorporate gauge-mediated supersymmetry-breaking (see sec. 4.2.3) into the MSSM+ such that UV-completion of the SM stayed intact, as demonstrated in sec. 7.3. We found an upper limit on the mass of superpartners around

$$\mu_{\text{MSSM}} \sim 10^{13} \text{ GeV} .$$

Beyond this bound, messenger mass parameters become imaginary signaling a quantum phase transition due to spontaneous symmetry breaking (see fig. 7.8).

As in our non-supersymmetric dark QCD model, presented in chapter 3, new dark matter candidates within the MSSM+ appear as bound states of particles charged only under the new $SU(N)$ gauge sector. The masses of these bound states are comparable to the confining scale μ_{conf} at which the $SU(N)$ gauge coupling α_+ diverges in the IR. For BM2, we see in figs. 7.6 and 7.7 that this confining scale is close to the mass of the SM superpartners,

$$\mu_{\text{conf}} \sim \mu_{\text{MSSM}} .$$

Mass bounds on the MSSM+ particles and missing energy signals at colliders were presented in sec. 7.4.

In studies going beyond perturbation theory, results from superconformal field theories were presented in chapter 8 and utilized in chapter 9 to check the AS candidates found within perturbation theory for non-perturbative consistency. For these models, superconformal R -charges are in agreement with the unitarity bound $R \geq 1/3$ (9.1), and the a -theorem (8.25) as well as the conformal collider bound (8.26) were satisfied. However, the infinite-order NSVZ beta functions (5.12) suggest that asymptotic safety is lost beyond perturbation theory (secs. 9.1 and 9.2).

For the model of sec. 9.3 which involves two additional gauge sectors $SU(N)$ and $SU(M)$, we were able to study the evolution of fixed points for different model parameters. Approaching parameters for which FP_{NM} (see tab. 9.5) serves as a fixed point which UV-completes the SM, we find at three-loop order in sec. 9.3.3 that this fixed point becomes unphysical before the SM can be UV-completed in this way (see tab. 9.6, 9.7 and the corresponding plots 9.4, 9.5). At this loop order, we find good agreement with the a -theorem (8.25), as well as with the signs of the effective NSVZ B -coefficients (9.24). We conclude that the three-loop RG flow sufficiently approximated the exact RG flow and that our model does not UV-complete the SM since FP_{NM} becomes unphysical

before this UV-completion is possible. In the two-loop studies of sec. 9.3.2, we find discrepancies with the exact relations. This matches our finding that candidate models with UV fixed points in the 2-1-approximation are no longer asymptotically safe beyond perturbation theory.

This thesis lays the foundation for further work on supersymmetric UV-completions of the Standard Model via asymptotic safety. Especially the three-loop investigations motivate further searches at three-loop gauge and two-loop Yukawa level for such UV-completions, analogous to our investigations in the 2-1-approximation. At two-loop gauge and one-loop Yukawa level, this thesis constraints the model space for suitable AS candidates.

Acknowledgements

I am thankful to Gudrun Hiller for enabling me to work on this thesis. With her wide knowledge on high energy physics, she could always direct me towards success bringing paths and suitable literature. I would like to thank Daniel Litim for insightful discussions and his helpful suggestions. For proofreading my thesis in great detail and for his many literature suggestions, I am grateful to Tom Steudtner. I also want to thank Kamila Kowalska for discussions and clarifications of some equations I had issues with. Of course I want to thank all members of our combined departments T3 and T4. I always felt welcome there and my mood got always brightened up by all of you. Especially our Weinberg group meetings were not only educational, but also very entertaining.

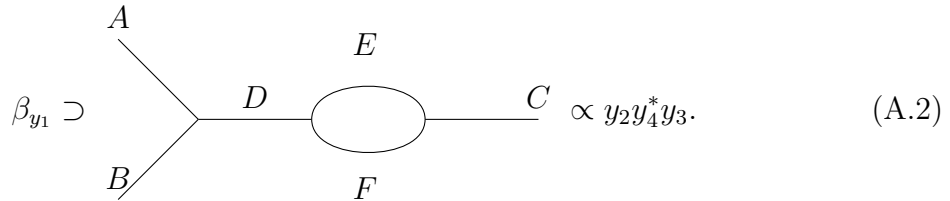
Appendix A

On Unnatural Yukawa Beta Functions

When computing the Yukawa beta functions (5.5), it can happen that the beta function of a Yukawa coupling y_i is not proportional to itself, but instead has some additional terms which do not include y_i at all. Consider for example a model with the superpotential

$$W = y_1 ABC + y_2 ABD + y_3 EFC + y_4 EFD, \quad (\text{A.1})$$

involving chiral superfields A, B, C, D, E and F . Then the Feynman diagram (A.2) yields a contribution $\propto y_2 y_4^* y_3$ to β_{y_1} .



$$\beta_{y_1} \supset \text{Diagram} \propto y_2 y_4^* y_3. \quad (\text{A.2})$$

More explicitly, the system of Yukawa beta functions for the superpotential (A.1) reads

$$\begin{aligned} \beta_{y_1} &= \frac{1}{(4\pi)^2} (y_1 (3|y_1|^2 + 3|y_2|^2 + |y_3|^2) + y_2 y_4^* y_3 - y_1 A_1), \\ \beta_{y_2} &= \frac{1}{(4\pi)^2} (y_2 (3|y_2|^2 + 3|y_1|^2 + |y_4|^2) + y_1 y_3^* y_4 - y_2 A_2), \\ \beta_{y_3} &= \frac{1}{(4\pi)^2} (y_3 (3|y_3|^2 + 3|y_4|^2 + |y_1|^2) + y_4 y_2^* y_1 - y_3 A_3), \\ \beta_{y_4} &= \frac{1}{(4\pi)^2} (y_4 (3|y_4|^2 + 3|y_3|^2 + |y_2|^2) + y_3 y_1^* y_2 - y_4 A_4), \end{aligned} \quad (\text{A.3})$$

with

$$A_i = A_i(g^2) \tag{A.4}$$

linear functions of the gauge coupling squares g^2 [113]. In the absence of the proportionality-breaking terms in (A.3), one obtains a system of linear equations for the new couplings $\alpha_{y_i} \sim |y_i|^2$, $\alpha_{g_i} \sim g_i^2$ from the fixed point condition $\beta(\alpha^*) = 0$ for all beta functions. Otherwise one cannot rewrite the beta functions (A.3) as functions of the newly defined couplings and ends up with a system of non-linear equations of third order.

There is one crucial exception to this argumentation. In the presence of certain flavor symmetries we still obtain linear equations within fixed points even when some beta function β_{y_i} are not proportional to y_i . This is for example the case for (A.1) which we may rewrite as

$$W = y(A, E) \begin{pmatrix} B & B \\ F & F \end{pmatrix} \begin{pmatrix} C \\ D \end{pmatrix}. \tag{A.5}$$

Due to the global $U(2)$ symmetry

$$\begin{pmatrix} A \\ E \end{pmatrix} \rightarrow U \begin{pmatrix} A \\ E \end{pmatrix}, \quad \begin{pmatrix} B \\ F \end{pmatrix} \rightarrow U \begin{pmatrix} B \\ F \end{pmatrix}, \quad \begin{pmatrix} C \\ D \end{pmatrix} \rightarrow U \begin{pmatrix} C \\ D \end{pmatrix}, \quad U \in U(2) \tag{A.6}$$

interacting fixed points have

$$y_1^* = y_2^* = y_3^* = y_4^*, \tag{A.7}$$

which yields a system of linear equations in the newly defined couplings $\alpha_{y_i} \sim |y_i|^2$, $\alpha_{g_i} \sim g_i^2$. A flavor symmetry-breaking term in (A.1) would prohibit this behavior. An example is given by a model with the superpotential

$$W = y_1 ABC + y_2 ABD + y_3 EFC + y_4 EFD + y_5 EDG, \tag{A.8}$$

where only for fixed points with $y_5^* = 0$ the fixed point conditions are reduced to a system of linear equations. Due to computational limitations we restrict ourselves in this work to models with superpotentials possessing flavor structures which yield system of linear equations for their fixed point conditions. For example, in the case of the superpotential (A.8) we would then begin by setting $y_5 = 0$ before doing any calculations.

Appendix B

Necessary Condition for Interacting Fixed Points

We prove the statement of sec. 5.3 stating that

In order for a $\mathcal{N} = 1$ SUSY gauge-Yukawa model with the gauge group $G = \prod_a G_a$ as in (5.1) to have a non-gaussian fixed point g^ in the 2-1-approximation, it is necessary that at least one gauge sector $G_{a'}$ corresponding to a component $g_{a'}^*$ of the fixed point with $g_{a'}^* \neq 0$ is AF at one-loop level, i.e. the one-loop coefficient $B_{a'}$ as given in (5.4) and (5.6a) has to be positive.*

The proof of this condition is basically already provided in [117], with the difference that in there higher order terms are ignored which in fact are non-negligible in interacting fixed points. This is because in an interacting fixed point the one- and two-loop contributions in the gauge beta function cancel each other and are therefore of the same magnitude. We now repeat the proof without neglecting higher orders.

We start with the RG-time derivative of the summed squares of the Yukawa couplings

$$\frac{d}{dt} (Y^{ijk} Y_{ijk}) = 6Y^{ijk} Y_{ijl} \gamma_k^{(1)l}, \quad (\text{B.1})$$

where we used (5.5) to obtain the right-hand side. With the one-loop result for the anomalous dimension matrix (5.6d), we can write this as

$$\frac{d}{dt} (Y^{ijk} Y_{ijk}) = 12(4\pi)^2 \left(\gamma_l^{(1)k} + 2 \sum_a g_a^* C_2^{(a)}(k) \delta_l^k \right) \gamma_k^{(1)l}, \quad (\text{B.2})$$

where a runs over all gauge factors G_a of G . At a fixed point g^* and with $\gamma_l^{(1)k}$ chosen diagonal at this fixed point, eq. (B.2) reads

$$0 = \sum_r d_r |\gamma_r^{(1)}|^2 + 2 \sum_a g_a^{*2} C_2^{(a)}(k) \gamma_k^{(1)k}, \quad (\text{B.3})$$

where r sums over the representations of the whole gauge group of the chiral superfields and d_r denotes their dimensions.¹

Before we continue with (B.3), we first derive a second expression. For this, we multiply the anomalous dimension matrix in eq. (5.6d) with $C_2^{(a)}(k)$, set $l = k$ (implying summation over k) and obtain

$$Y^{ijk}Y_{ijk}C_2^{(a)}(k) = 2(4\pi)^2\gamma_k^{(1)k}C_2^{(a)}(k) + 4\sum_{d,k}g_d^2C_2^{(d)}(k)C_2^{(a)}(k), \quad (\text{B.4})$$

where d is chosen as an index that runs over all the gauge factors G_d to distinguish it from a . Inserting this into the beta function (5.4) of a gauge coupling $g_{a'}$ and evaluating it at an interacting fixed point g^* with $g_{a'}^* \neq 0$ and some other (possibly) non-zero components $g_{b'}^*, g_{d'}^* \neq 0$ leads to the equation

$$0 = -\frac{B_{a'}}{2} + \frac{C_{a'b'}}{2}\frac{g_{b'}^{*2}}{(4\pi)^2} - 2\gamma_k^{(1)k}\frac{C_2^{(a')}(k)}{d_{a'}(G)} - \frac{4}{(4\pi)^2}g_{d'}^{*2}\frac{C_2^{(d')}(k)C_2^{(a')}(k)}{d_{a'}(G)}. \quad (\text{B.5})$$

Rearranging this equation so that we can insert $2\gamma_k^{(1)k}C_2^{(a')}(k)$ into eq. (B.3) yields the condition

$$0 = \sum_r d_r |\gamma_r^{(1)}|^2 + \sum_{a'} g_{a'}^{*2} d_{a'}(G) \left[-\frac{B_{a'}}{2} + \frac{C_{a'b'}}{2}\frac{g_{b'}^{*2}}{(4\pi)^2} - 4\frac{g_{d'}^{*2}}{(4\pi)^2}\frac{C_2^{(d')}(k)C_2^{(a')}(k)}{d_{a'}(G)} \right]. \quad (\text{B.6})$$

Since the first term is positive, the term in the square brackets has to be negative for at least one a' with $g_{a'}^* \neq 0$. Rewriting the last term in these brackets as a sum over representations of the whole gauge group indicated by the index r instead of a sum over all chiral superfield components we end up with the condition

$$-\frac{B_{a'}}{2} + \frac{C_{a'b'}}{2}\frac{g_{b'}^{*2}}{(4\pi)^2} - 4\sum_r \frac{g_{d'}^{*2}}{(4\pi)^2} d_r \frac{C_2^{(d')}(r)C_2^{(a')}(r)}{d_{a'}(G)} < 0 \quad (\text{B.7})$$

for at least one a' with $g_{a'}^* \neq 0$. Inserting the explicit formulas for $C_{a'b'}$ given in (5.6b) and (5.6c), rewritten as a sum over representations r of the whole gauge group as

$$C_{a'a'} = -12C_2^{(a')}(G)^2 + 4C_2^{(a')}(G)\sum_r S_{a'}(r)\frac{d_r}{d_{a'}(r)} + 8\sum_r S_{a'}(r)C_2^{(a')}(r)\frac{d_r}{d_{a'}(r)}, \quad (\text{B.8a})$$

$$C_{a'b'} = 8\sum_r S_{a'}(r)C_2^{(b')}(r)\frac{d_r}{d_{a'}(r)}, \quad (\text{B.8b})$$

¹e.g. for a left-handed quark superfield Q in the MSSM we have $d_Q = 6$.

and using the relation (5.7) between Dynkin indices and Casimir invariants, finally gives the condition

$$-\frac{B_{a'}}{2} + \left[-6C_2^{(a')}(G)^2 + 2C_2^{(a')}(G) \sum_r S_{a'}(r) \frac{d_r}{d_{a'}(r)} \right] \frac{g_{a'}^{*2}}{(4\pi)^2} < 0 \quad (\text{B.9})$$

for at least one a' with $g_{a'}^* \neq 0$. The equation for the coefficient $B_{a'}$ given in (5.6a) rewritten as a sum over r tells us that the term within square brackets is just $-C_2^{(a')}(G)B_{a'}$, and hence the condition is just equivalent to

$$B_{a'} \left[1 + 2C_2^{(a')}(G) \frac{g_{a'}^{*2}}{(4\pi)^2} \right] > 0 \Leftrightarrow B_{a'} > 0 \quad (\text{B.10})$$

for at least one a' with $g_{a'}^* \neq 0$. Thus we have shown the necessary condition stated at the beginning of this appendix.

Appendix C

A Relation Between Fixed Points FP_3 and FP_{23}

In this appendix, we show the relation (6.62) between the fixed points FP_3 and FP_{23} of tab. 6.1, valid in the 2-1-approximation for MSSM extensions. This relation, which we confirm in all our model investigations of sec. 6, states that

$$\begin{aligned} &FP_{23} \text{ physical} \Leftrightarrow FP_{23} \text{ physical and IR attractive} \\ &\Leftrightarrow FP_3 \text{ physical and UV attractive.} \Leftrightarrow \alpha_3^{\star FP_{23}} > \alpha_3^{\star FP_3} , \end{aligned} \quad (C.1)$$

or, phrased in a way more suitable for our proof,

$$\left(FP_{23} \text{ is physical} \Leftrightarrow FP_3 \text{ is physical and } B_{2,\text{eff}}^{FP_3} > 0 \right) \Rightarrow \alpha_3^{\star FP_{23}} > \alpha_3^{\star FP_3} , \quad (C.2)$$

with $B_{2,\text{eff}}^{FP_3}$ defined in (5.23). In general, FP_{23} and FP_3 stand for a class of fixed points which differ by different non-zero Yukawa components. The fixed points in (C.2) are to be understood to have the same Yukawa components non-vanishing. Furthermore we are arguing for models with superpotentials composed by Yukawa terms of the form

$$W = \sum_m y_m (\bar{q}QL)_m , \quad (C.3)$$

involving quark singlets \bar{q} , quark doublets Q , and lepton doublets L . The index m is counting the different Yukawa terms. Such superpotentials are used in our investigations of sec. 6 and have fixed point Yukawa couplings given by

$$\alpha_{y_m}^{\star} = (F_3 \alpha_3 + F_2 \alpha_2) X_m , \quad (C.4)$$

with some α_3, α_2 -independent X_m and

$$F_3 = \frac{32}{3} , \quad F_2 = 6 . \quad (C.5)$$

The gauge beta functions (5.10) read here

$$\beta_3 = \alpha_3^2 \left[-B_3 + C_{33}\alpha_3 + C_{32}\alpha_2 - D_3 \sum_m \alpha_{y_m} \right], \quad (C.6)$$

$$\beta_2 = \alpha_2^2 \left[-B_2 + C_{22}\alpha_2 + C_{23}\alpha_3 - D_2 \sum_m \alpha_{y_m} \right], \quad (C.7)$$

with

$$D_3 = 8, \quad D_2 = 12, \quad (C.8)$$

and

$$\begin{aligned} C_{33} &= -108 + \frac{34}{3} \sum_{i, \text{SU}(3)} d_2(i), & C_{22} &= -48 + 7 \sum_{i, \text{SU}(2)} d_3(i), \\ C_{32} &= 6 \sum_{i, \text{SU}(3) \otimes \text{SU}(2)} 1, & C_{23} &= 16 \sum_{i, \text{SU}(3) \otimes \text{SU}(2)} 1, \end{aligned} \quad (C.9)$$

where $\sum_{i, \text{SU}(3)}$, $\sum_{i, \text{SU}(2)}$ and $\sum_{i, \text{SU}(3) \otimes \text{SU}(2)}$ imply summation over fields charged under $\text{SU}(3)_C$, $\text{SU}(2)_L$ and $\text{SU}(3) \otimes \text{SU}(2)$, respectively. With $d_3(i)$ and $d_2(i)$, the dimensions of the representations of the field i under respectively $\text{SU}(3)_C$ and $\text{SU}(2)_L$ are denoted.

In a fixed point, with eq. (C.4) inserted, we obtain the fixed point conditions

$$0 = \alpha_3^2 [-B_3 + C'_{33}\alpha_3 + C'_{32}\alpha_2], \quad (C.10)$$

$$0 = \alpha_2^2 [-B_2 + C'_{22}\alpha_2 + C'_{23}\alpha_3], \quad (C.11)$$

with the modified coefficients given by

$$\begin{aligned} C'_{33} &= C_{33} - \sum_m D_3 F_3 X_m = C_{33} - \frac{256}{3} \sum_m X_m, \\ C'_{22} &= C_{22} - \sum_m D_2 F_2 X_m = C_{22} - 72 \sum_m X_m, \\ C'_{32} &= C_{32} - \sum_m D_3 F_2 X_m = C_{32} - 48 \sum_m X_m, \\ C'_{23} &= C_{23} - \sum_m D_2 F_3 X_m = C_{23} - 128 \sum_m X_m. \end{aligned} \quad (C.12)$$

The effective coefficient $B_{2, \text{eff}}^{\text{FP}_3}$, as defined in eq. (5.23), is here given by

$$B_{2, \text{eff}}^{\text{FP}_3} = B_2 - C'_{23} \alpha_3^{* \text{FP}_3}. \quad (C.13)$$

Due to the negativity of B_2 in the MSSM and all of its extensions, we infer from the necessary condition of sec. 5.3 the unphysicality of FP_2 , with its α_2 coupling given by

$$\alpha_2^{* \text{FP}_2} = \frac{B_2}{C'_{22}}, \quad (C.14)$$

from which we immediately find that

$$C'_{22} > 0 . \quad (\text{C.15})$$

We now have all the tools together to start our proof of (C.2). We begin with

$$\text{FP}_{23} \text{ is physical} \Rightarrow \text{FP}_3 \text{ is physical} . \quad (\text{C.16})$$

For this we assume that the contrary is true, i.e. that if FP_{23} exists, FP_3 does not. MSSM extensions allowing for interacting fixed points in the 2-1-approximation necessarily have $B_3 > 0$, as discussed in sec. 6.2. The assumption of FP_3 being unphysical is then equivalent to $C'_{33} < 0$. Physicality of FP_{23} yields the conditions $C_{32'} > 0$ and $C_{23'} < 0$, as seen from (C.11). Using the form of the coefficients given in (C.12) we may then infer

$$C_{23} \stackrel{C'_{23} < 0}{<} 128 \sum_m X_m = \frac{8}{3} \cdot 48 \sum_m X_m \stackrel{C'_{32} > 0}{<} \frac{8}{3} C_{32} . \quad (\text{C.17})$$

Inserting C_{23} and C_{32} from eq. (C.9), we can rewrite the above inequality as

$$16 < 16 , \quad (\text{C.18})$$

which is false. Hence our assumption was wrong and we have shown (C.16).

Next we show that

$$\alpha_3^{\star\text{FP}_{23}} > \alpha_3^{\star\text{FP}_3} , \quad (\text{C.19})$$

as soon as FP_{23} exists. For this we note that the rearranged fixed point conditions (C.11) for FP_{23} , together with the positivity of C'_{22} (C.15) and negativity of B_2 for MSSM extensions implies $C'_{23} < 0$ for physical FP_{23} . Using this last inequality together with the modified coefficients (C.12), we obtain

$$C'_{32} = C_{32} - 48 \sum_m X_m = C_{32} - \frac{3}{8} \cdot 128 \sum_m X_m \stackrel{C'_{23} < 0}{<} C_{32} - \frac{3}{8} C_{23} . \quad (\text{C.20})$$

Inserting again the explicit formulas (C.9) for C_{23} and C_{32} , we find

$$C'_{32} < (6 - 6) \cdot \sum_{\text{SU}(3)_C \otimes \text{SU}(2)_L} 1 = 0 , \quad (\text{C.21})$$

for all MSSM extensions for which FP_{23} exists. The sum implies summation over all fields simultaneously charged under $\text{SU}(3)_C$ and $\text{SU}(2)_L$. From (C.11) we can then infer

$$\alpha_3^{\star\text{FP}_{23}} = \frac{B_3}{C_{33}} - C'_{32} \frac{\alpha_2^{\star\text{FP}_{23}}}{C'_{33}} \stackrel{C'_{32} < 0, C'_{33} > 0}{>} \frac{B_3}{C'_{33}} = \alpha_3^{\star\text{FP}_3} , \quad (\text{C.22})$$

which we had set out to prove.

The next claim

$$FP_{23} \text{ is physical} \Rightarrow B_{2,\text{eff}}^{\text{FP}_3} > 0 \quad (\text{C.23})$$

follows straightforwardly from rearranging (C.11) for positive $\alpha_2^{\star\text{FP}_{23}}$

$$0 < \alpha_2^{\star\text{FP}_{23}} = \frac{B_2}{C'_{22}} - C'_{23} \frac{\alpha_3^{\star\text{FP}_{23}}}{C'_{22}} \stackrel{(\text{C.15})}{\Leftrightarrow} C'_{23} < \frac{B_2}{\alpha_3^{\star\text{FP}_{23}}} \quad (\text{C.24})$$

and using this inequality in $B_{2,\text{eff}}^{\text{FP}_3}$ as defined in (C.13)

$$B_{2,\text{eff}}^{\text{FP}_3} = B_2 - C'_{23} \alpha_3^{\star\text{FP}_3} > B_2 \left(1 - \frac{\alpha_3^{\star\text{FP}_3}}{\alpha_3^{\star\text{FP}_{23}}} \right) \stackrel{(\text{C.19})}{>} 0, \quad (\text{C.25})$$

where in the last inequality we used that the strong component of FP_{23} is bigger than the strong component of FP_3 (C.19).

To complete our proof of (C.2) we show that

$$FP_3 \text{ is physical and } B_{2,\text{eff}}^{\text{FP}_3} > 0 \Rightarrow FP_{23} \text{ is physical.} \quad (\text{C.26})$$

From the physicality of FP_3 we get $C'_{33} > 0$ while $B_{2,\text{eff}}^{\text{FP}_3} > 0$ is equivalent to $B_2 > C'_{23} \alpha_3^{\star\text{FP}_3}$, which in particular implies that $C'_{23} < 0$ since $B_2 < 0$ for all MSSM extensions. At first we may then estimate

$$C'_{32} \stackrel{(\text{C.12})}{=} C_{32} - 48 \sum_m X_m = C_{32} - \frac{3}{8} \cdot 128 \sum_m X_m \stackrel{C'_{23} < 0}{<} C_{32} - \frac{3}{8} C_{23} \stackrel{(\text{C.9})}{=} 0. \quad (\text{C.27})$$

C'_{32} being negative implies $\alpha_3^{\star\text{FP}_{23}} > 0$ with $\alpha_3^{\star\text{FP}_{23}} > \alpha_3^{\star\text{FP}_3}$, as can be seen in (C.11). With this we can furthermore infer from $B_{2,\text{eff}}^{\text{FP}_3} > 0$ that

$$B_2 > C'_{23} \alpha_3^{\star\text{FP}_3} \stackrel{C'_{23} < 0}{>} \underset{\alpha_3^{\star\text{FP}_{23}} > \alpha_3^{\star\text{FP}_3}}{C'_{23} \alpha_3^{\star\text{FP}_{23}}} \stackrel{C'_{22} > 0}{\Leftrightarrow} \frac{B_2}{C'_{22}} - C'_{23} \frac{\alpha_3^{\star\text{FP}_{23}}}{C'_{22}} > 0, \quad (\text{C.28})$$

which means that $\alpha_2^{\star\text{FP}_{23}} > 0$, comparing with (C.11). With this we have shown all claims of (C.2).

Appendix D

Beta Functions and Fixed Points Formulae

In this appendix, we present the beta functions of our MSSM extensions from sec. 6 and in the MSSM+ of sec. 7.1. In general, the Yukawa beta functions at one-loop are given by

$$\beta_i = \alpha_i [E_{ij} \alpha_j - F_{ig} \alpha_g] , \quad (\text{D.1})$$

with i, j indices counting Yukawa couplings and g gauge couplings. Appearance of two indices implies summation over them. In gauge-Yukawa fixed points, where all Yukawa couplings are non-vanishing, we can solve (D.1) for the fixed point Yukawa couplings

$$\alpha_i^* = E_{ij}^{-1} F_{jg} \alpha_g^* \quad (\text{D.2})$$

in dependence of the fixed point gauge couplings (assuming that the matrix E is non-singular). The beta functions of the gauge couplings

$$\alpha_g = \alpha_g^2 [-B_g \alpha_g + C_{gg'} \alpha_{g'} - D_{gi} \alpha_i] , \quad (\text{D.3})$$

reduces in fixed points to the equation

$$0 = -B_g \alpha_g^* + C'_{gg'} \alpha_{g'}^* \quad (\text{D.4})$$

for each non-zero gauge coupling. The modified coefficients $C'_{gg'}$ are obtained by plugging in the Yukawa nullcline condition (D.2) and read

$$C'_{gg'} = C_{gg'} - D_{gi} E_{ij}^{-1} F_{jg'} . \quad (\text{D.5})$$

D.1 MSSM Extensions

In our MSSM extensions of sec. 6, the gauge group is given by $SU(3)_C \otimes SU(2)_L \otimes U(1)_Y$ and hence $g = 1, 2, 3$. In the subsequent sections we present the matrices E, F, C, D as well as the coefficients B_g for each of our three model classes.

The gauge components of the possibly physical fixed points FP_3, FP_{23}, FP_{13} and FP_{123} are in terms of the modified coefficients given for FP_3 by

$$\alpha_3^{\star FP_3} = \frac{B_3}{C'_{33}}, \alpha_2^{\star FP_3} = 0, \alpha_1^{\star FP_3} = 0, \quad (D.6)$$

in FP_{13} by

$$\alpha_3^{\star FP_{13}} = \frac{B_3 C'_{11} - B_1 C'_{31}}{C'_{11} C'_{33} - C'_{13} C'_{31}}, \alpha_2^{\star FP_{13}} = 0, \alpha_1^{\star FP_{13}} = \frac{B_1 C'_{33} - B_3 C'_{13}}{C'_{11} C'_{33} - C'_{13} C'_{31}}, \quad (D.7)$$

at FP_{23} by

$$\alpha_3^{\star FP_{23}} = \frac{B_3 C'_{22} - B_2 C'_{32}}{C'_{33} C'_{22} - C'_{32} C'_{23}}, \alpha_2^{\star FP_{23}} = \frac{B_2 C'_{33} - B_3 C'_{23}}{C'_{33} C'_{22} - C'_{32} C'_{23}}, \alpha_1^{\star FP_{23}} = 0, \quad (D.8)$$

and for FP_{123} by

$$\begin{aligned} \alpha_3^{\star FP_{123}} &= \frac{B_3(C'_{12}C'_{21} - C'_{11}C'_{22}) - B_1(C'_{21}C'_{32} - C'_{22}C'_{31}) - B_2(C'_{12}C'_{31} - C'_{11}C'_{32})}{C'_{12}C'_{21}C'_{33} - C'_{12}C'_{23}C'_{31} - C'_{13}C'_{21}C'_{32} + C'_{13}C'_{22}C'_{31} + C'_{11}C'_{23}C'_{32} - C'_{11}C'_{22}C'_{33}}, \\ \alpha_2^{\star FP_{123}} &= \frac{B_1(C'_{21}C'_{33} - C'_{23}C'_{31}) + B_2(C'_{13}C'_{31} - C'_{11}C'_{33}) - B_3(C'_{13}C'_{21} - C'_{11}C'_{23})}{C'_{12}C'_{21}C'_{33} - C'_{12}C'_{23}C'_{31} - C'_{13}C'_{21}C'_{32} + C'_{13}C'_{22}C'_{31} + C'_{11}C'_{23}C'_{32} - C'_{11}C'_{22}C'_{33}}, \\ \alpha_1^{\star FP_{123}} &= \frac{B_1(C'_{23}C'_{32} - C'_{22}C'_{33}) + B_2(C'_{12}C'_{33} - C'_{13}C'_{32}) - B_3(C'_{12}C'_{23} - C'_{13}C'_{22})}{C'_{12}C'_{21}C'_{33} - C'_{12}C'_{23}C'_{31} - C'_{13}C'_{21}C'_{32} + C'_{13}C'_{22}C'_{31} + C'_{11}C'_{23}C'_{32} - C'_{11}C'_{22}C'_{33}}. \end{aligned} \quad (D.9)$$

D.1.1 Model class 1

Due to flavor symmetries in our investigated Yukawa structures we end up with 12 different Yukawa beta functions $\beta_t, \beta_b, \beta_4, \dots, \beta_{13}$. The labeling of Yukawa couplings

possessing the same beta functions is

$$\begin{aligned}
& y_b \bar{d}_3 Q_3 H_d : x_b , \\
& y_t \bar{u}_3 Q_3 H_u : x_t , \\
& y_4 \bar{d}_i Q_1 L_k + y_6 \bar{d}_i Q_2 L_{k'} : I_{12} , \\
& y_5 \bar{d}_i Q_1 L_k : I_{1d} , \\
& y_7 \bar{d}_i Q_2 L_k : I_{2d} , \\
& y_8 \bar{d}_i Q_1 L_k + y_9 \bar{d}_i Q_3 L_{k'} : I_{13} , \\
& y_{10} \bar{d}_i Q_3 L_k : I_{3d} , \\
& y_{11} \bar{u}_i Q_1 \bar{L}_k : I_{1u} , \\
& y_{12} \bar{u}_i Q_2 \bar{L}_k : I_{2u} , \\
& y_{13} \bar{u}_i Q_3 \bar{L}_k : I_{3u} ,
\end{aligned} \tag{D.10}$$

where for a Yukawa coupling of type y_i , the beta function of α_i is β_i . The 12×12 matrix E acting on the coupling space with elements $(\alpha_t, \alpha_b, \alpha_4, \dots, \alpha_{13})$ reads

$$E = \begin{pmatrix}
12 & 2x_b & 0 & 0 & 0 & 0 & 0 & 0 & 2I_{13} & 2I_{3d} & 0 & 0 & 2I_{3u} \\
2x_t & 12 & 0 & 0 & 0 & 0 & 0 & 0 & 2I_{13} & 2I_{3d} & 0 & 0 & 2I_{3u} \\
0 & 0 & 10+2I_{12} & 2I_{1d} & 4 & 0 & 2I_{13} & 0 & 0 & 2I_{1u} & 0 & 0 & 0 \\
0 & 0 & 2I_{12} & 10+2I_{1d} & 0 & 0 & 2I_{13} & 0 & 0 & 2I_{1u} & 0 & 0 & 0 \\
0 & 0 & 4 & 0 & 10+2I_{12} & 2I_{2d} & 0 & 0 & 0 & 0 & 2I_{2u} & 0 & 0 \\
0 & 0 & 0 & 0 & 2I_{12} & 10+2I_{2d} & 0 & 0 & 0 & 0 & 2I_{2u} & 0 & 0 \\
0 & 0 & 2I_{12} & 2I_{1d} & 0 & 0 & 10+2I_{13} & 4 & 0 & 2I_{1u} & 0 & 0 & 0 \\
2x_t & 2x_b & 0 & 0 & 0 & 0 & 4 & 10+2I_{13} & 2I_{3d} & 0 & 0 & 0 & 2I_{3u} \\
2x_t & 2x_b & 0 & 0 & 0 & 0 & 0 & 2I_{13} & 10+2I_{3d} & 0 & 0 & 0 & 2I_{3u} \\
0 & 0 & 2I_{12} & 2I_{1d} & 0 & 0 & 2I_{13} & 0 & 0 & 10+2I_{1u} & 0 & 0 & 0 \\
0 & 0 & 0 & 0 & 2I_{12} & 2I_{2d} & 0 & 0 & 0 & 0 & 10+2I_{2u} & 0 & 0 \\
2x_t & 2x_b & 0 & 0 & 0 & 0 & 0 & 2I_{13} & 2I_{3d} & 0 & 0 & 0 & 10+2I_{3u}
\end{pmatrix} , \tag{D.11}$$

and the 12×3 matrix F mapping from the gauge coupling space $(\alpha_1, \alpha_2, \alpha_3)$ into $(\alpha_t, \alpha_b, \alpha_4, \dots, \alpha_{13})$ is given by

$$F = \begin{pmatrix}
\frac{26}{9} & \frac{14}{9} & \frac{14}{9} & \frac{14}{9} & \frac{14}{9} & \frac{14}{9} & \frac{14}{9} & \frac{14}{9} & \frac{14}{9} & \frac{14}{9} & \frac{26}{9} & \frac{26}{9} & \frac{26}{9} \\
6 & 6 & 6 & 6 & 6 & 6 & 6 & 6 & 6 & 6 & 6 & 6 & 6 \\
\frac{32}{3} & \frac{32}{3} & \frac{32}{3} & \frac{32}{3} & \frac{32}{3} & \frac{32}{3} & \frac{32}{3} & \frac{32}{3} & \frac{32}{3} & \frac{32}{3} & \frac{32}{3} & \frac{32}{3} & \frac{32}{3}
\end{pmatrix}^T . \tag{D.12}$$

The gauge coefficients B_g are

$$B_3 = 18 - 2(n_u + n_d) , \quad B_2 = 4 - 2n_L , \quad B_1 = 4 - \frac{16}{3}n_u - \frac{4}{3}n_d - 2n_L , \tag{D.13}$$

with F mapping from the gauge coupling space $(\alpha_1, \alpha_2, \alpha_3)$. The one-loop gauge coefficients B_g are given by

$$B_3 = 2, \quad B_2 = -8 - 2n_L, \quad B_1 = -\frac{56}{3} - 2n_L, \quad (\text{D.19})$$

and the matrix C acting on the same space reads

$$C = \begin{pmatrix} \frac{1196}{27} + 2n_L & 20 + 6n_L & \frac{368}{9} \\ \frac{20}{3} + 2n_L & 92 + 14n_L & 80 \\ \frac{70}{9} & 30 & \frac{220}{3} \end{pmatrix}. \quad (\text{D.20})$$

For the matrix D going from Yukawa coupling space $(\alpha_t, \alpha_b, \alpha_4, \dots, \alpha_{10})$ to the gauge coupling space $(\alpha_1, \alpha_2, \alpha_3)$ we have in model 2

$$D = \begin{pmatrix} \frac{52}{3}x_t & \frac{28}{3}x_b & \frac{28}{3}I_d I_Q & \frac{52}{3}I_u I_Q & \frac{28}{3}I_Q x_3 & \frac{52}{3}I_Q \bar{x}_3 & \frac{28}{3}I_d x_4 & \frac{52}{3}I_u \bar{x}_4 & \frac{4}{3}n_S x_S \\ 12x_t & 12x_b & 12I_d I_Q & 12I_u I_Q & 12x_3 I_Q & 12\bar{x}_3 I_Q & 12x_4 I_d & 12\bar{x}_4 I_u & 12x_S n_S \\ 8x_t & 8x_b & 8I_d I_Q & 8\bar{x}_1 I_u I_Q & 8x_3 I_Q & 8\bar{x}_3 I_Q & 8x_4 I_d & 8\bar{x}_4 I_u & 8x_S n_S \end{pmatrix},$$

D.1.3 Model class 3

Model 3 is in many ways similar to model 1. The labeling of Yukawa couplings and the case-counting I -parameters are here given by

$$\begin{aligned} & y_b \bar{d}_3 Q_3 H_d, \\ & y_t \bar{u}_3 Q_3 H_u, \\ & y_4 \bar{d}_i Q_1 L_k + y_5 \bar{d}_i Q_2 L_{k'} : I_{12}, \\ & y_6 \bar{d}_i Q_1 L_k + y_7 \bar{d}_i Q_3 L_{k'} : I_{13}, \\ & y_8 \bar{d}_i Q_1 L_k + y_9 \bar{d}_i Q_4 L_{k'} : I_{14}, \\ & y_{10} \bar{d}_i Q_1 L_k : I_{1d}, \\ & y_{11} \bar{d}_i Q_3 L_k : I_{3d}, \\ & y_{12} \bar{u}_i Q_1 \bar{L}_k : I_{1u}, \\ & y_{13} \bar{u}_i Q_4 \bar{L}_k : I_{4u}, \end{aligned} \quad (\text{D.21})$$

with $i \neq 3$ and the top- and bottom Yukawas always present in our investigation. In Yukawa coupling space we have chosen the basis for which the elements read $(\beta_t, \beta_b, \beta_4, \dots, \beta_{13})$, while in gauge coupling space the basis is such that its elements are $(\alpha_1, \alpha_2, \alpha_3)$.

Matrix E , acting on Yukawa coupling space, is given by

$$E = \begin{pmatrix} 12 & 2 & 0 & 0 & 0 & 2I_{13} & 0 & 0 & 0 & 2I_{3d} & 0 & 0 \\ 2 & 12 & 0 & 0 & 0 & 2I_{13} & 0 & 0 & 0 & 2I_{3d} & 0 & 0 \\ 0 & 0 & 10+2I_{12} & 4 & 2I_{13} & 0 & 2I_{14} & 0 & 2I_{1d}I_{1d} & 0 & 2I_{1u} & 0 \\ 0 & 0 & 4 & 10+2I_{12} & 0 & 0 & 0 & 0 & 0 & 0 & 0 & 0 \\ 0 & 0 & 2I_{12} & 0 & 10+2I_{13} & 4 & 2I_{14} & 0 & 2I_{1d} & 0 & 2+I_{1u} & 0 \\ 2 & 2 & 0 & 0 & 4 & 10+2I_{13} & 0 & 0 & 0 & 2I_{3d} & 0 & 0 \\ 0 & 0 & 2I_{12} & 0 & 2I_{13} & 0 & 10+2I_{14} & 4 & 2I_{1d} & 0 & 2I_{1u} & 0 \\ 0 & 0 & 0 & 0 & 0 & 0 & 4 & 10+2I_{14} & 0 & 0 & 0 & 2I_{4u} \\ 0 & 0 & 2I_{12} & 0 & 2I_{13} & 0 & 2I_{14} & 0 & 10+2I_{1d} & 0 & 2I_{1u} & 0 \\ 2 & 2 & 0 & 0 & 0 & 2I_{13} & 0 & 0 & 0 & 10+2I_{3d} & 0 & 0 \\ 0 & 0 & 2I_{12} & 0 & 2I_{13} & 0 & 2I_{14} & 0 & 2I_{1d} & 0 & 10+2I_{1u} & 0 \\ 0 & 0 & 0 & 0 & 0 & 0 & 0 & 2I_{14} & 0 & 0 & 0 & 10+2I_{4u} \end{pmatrix}, \quad (\text{D.22})$$

and matrix F , mapping from gauge coupling space into Yukawa coupling space, reads

$$F = \begin{pmatrix} \frac{26}{9} & \frac{14}{9} & \frac{14}{9} & \frac{14}{9} & \frac{14}{9} & \frac{14}{9} & \frac{14}{9} & \frac{14}{9} & \frac{14}{9} & \frac{14}{9} & \frac{26}{9} & \frac{26}{9} \\ 6 & 6 & 6 & 6 & 6 & 6 & 6 & 6 & 6 & 6 & 6 & 6 \\ \frac{32}{3} & \frac{32}{3} & \frac{32}{3} & \frac{32}{3} & \frac{32}{3} & \frac{32}{3} & \frac{32}{3} & \frac{32}{3} & \frac{32}{3} & \frac{32}{3} & \frac{32}{3} & \frac{32}{3} \end{pmatrix}^T. \quad (\text{D.23})$$

The one-loop gauge coefficients B_g are

$$B_3 = 2, \quad B_2 = 2 - 2n_L, \quad B_1 = -\frac{65}{3} - 2n_L, \quad (\text{D.24})$$

and C , acting on gauge coupling space, is

$$C = \begin{pmatrix} \frac{1358}{27} + 2n_L & -2 + 6n_L & \frac{704}{9} \\ -\frac{2}{3} + 2n_L & 15 + 14n_L & 64 \\ \frac{88}{9} & 24 & \frac{220}{3} \end{pmatrix}. \quad (\text{D.25})$$

Finally, matrix D mapping from Yukawa to coupling space, reads

$$D = \begin{pmatrix} \frac{52}{3} & \frac{28}{3} & \frac{28}{3}I_{12} & \frac{28}{3}I_{12} & \frac{28}{3}I_{13} & \frac{28}{3}I_{13} & \frac{28}{3}I_{14} & \frac{28}{3}I_{14} & \frac{28}{3}I_{1d} & \frac{28}{3}I_{32} & \frac{52}{3}I_{1u} & \frac{52}{3}I_{4u} \\ 12 & 12 & 12I_{12} & 12I_{12} & 12I_{13} & 12I_{13} & 12I_{14} & 12I_{14} & 12I_{1d} & 12I_{32} & 12I_{1u} & 12I_{4u} \\ 8 & 8 & 8I_{12} & 8I_{12} & 8I_{13} & 8I_{13} & 8I_{14} & 8I_{14} & 8I_{1d} & 8I_{32} & 8I_{1u} & 8I_{4u} \end{pmatrix}. \quad (\text{D.26})$$

D.2 MSSM+

In the MSSM+ of sec. 7.1, the gauge group is $SU(N) \otimes SU(3)_C \otimes SU(2)_L \otimes U(1)_Y$ so that $g = +, 1, 2, 3$. For FP_+ , the gauge components read

$$\alpha_+^{*\text{FP}_+} = \frac{B_+}{C'_+}, \quad \alpha_3^{*\text{FP}_+} = \alpha_2^{*\text{FP}_+} = \alpha_1^{*\text{FP}_+} = 0. \quad (\text{D.27})$$

The 8×8 matrix E , acting on Yukawa space $(\alpha_4, \dots, \alpha_{11})$, is

$$E = \begin{pmatrix} 4+2I_{12}+2N & 2I_1 & 4 & 0 & 0 & 0 & 0 & 0 \\ 2I_{12} & 4+2I_1+2N & 0 & 0 & 0 & 0 & 0 & 0 \\ 4 & 2I_2 & 4+2I_{12}+2N & 2I_2 & 0 & 0 & 0 & 0 \\ 0 & 0 & 2I_{12} & 4+2I_2+2N & 0 & 0 & 0 & 0 \\ 0 & 0 & 0 & 0 & 4+2\bar{I}_{12}+2N & 2\bar{I}_1 & 4 & 0 \\ 0 & 0 & 0 & 0 & 2\bar{I}_{12} & 4+2\bar{I}_2+2N & 0 & 0 \\ 0 & 0 & 0 & 0 & 4 & 0 & 4+2\bar{I}_{12}+2N & 2\bar{I}_2 \\ 0 & 0 & 0 & 0 & 0 & 0 & 2\bar{I}_{12} & 4+2\bar{I}_2+2N \end{pmatrix}, \quad (\text{D.28})$$

while F mapping from gauge coupling space $(\alpha_+, \alpha_3, \alpha_2, \alpha_1)$ onto $(\alpha_4, \dots, \alpha_{11})$ is given by

$$F = \begin{pmatrix} 4\frac{N^2-1}{N} & 0 & 6 & 8Y^2 \\ 4\frac{N^2-1}{N} & 0 & 6 & 8Y^2 \\ 4\frac{N^2-1}{N} & 0 & 6 & 8Y^2 \\ 4\frac{N^2-1}{N} & 0 & 6 & 8Y^2 \\ 4\frac{N^2-1}{N} & 0 & 6 & 8Y^2 \\ 4\frac{N^2-1}{N} & 0 & 6 & 8Y^2 \\ 4\frac{N^2-1}{N} & 0 & 6 & 8Y^2 \\ 4\frac{N^2-1}{N} & 0 & 6 & 8Y^2 \end{pmatrix}. \quad (\text{D.29})$$

The one-loop gauge coefficient read

$$\begin{aligned} B_D &= 6N - 8 - 2n, \\ B_3 &= 6, \\ B_2 &= -2 - 2m - 4N, \\ B_1 &= -22 - 2(4m + 8N)Y^2, \end{aligned} \quad (\text{D.30})$$

and the two-loop gauge coefficient matrix acting on $(\alpha_+, \alpha_3, \alpha_2, \alpha_1)$ is

$$C = \begin{pmatrix} -12N^2 + 2\frac{2N^2-1}{N}(8+2n) & 0 & 24 & 4(8+2n)Y^2 \\ 0 & 28 & 18 & \frac{22}{3} \\ 8(N^2-1) & 48 & 50 + 7(2m+4N) & 6 + 4(2m+4N)Y^2 \\ 32(N^2-1)Y^2 & \frac{176}{3} & 18 + 6(4m+8N)Y^2 & \frac{182}{9} + 8(4m+8N)Y^4 \end{pmatrix}. \quad (\text{D.31})$$

Finally, the matrix D reads

$$D = \begin{pmatrix} 8I_{12} & 8I_1 & 8I_{12} & 8I_2 & 8\bar{I}_{12} & 8\bar{I}_1 & 8\bar{I}_{12} & 8\bar{I}_2 \\ 0 & 0 & 0 & 0 & 0 & 0 & 0 & 0 \\ 4NI_{12} & 4NI_1 & 8I_{12} & 4NI_2 & 4N\bar{I}_{12} & 4N\bar{I}_1 & 4N\bar{I}_{12} & 4N\bar{I}_2 \\ 16NI_{12}Y^2 & 16NI_1Y^2 & 16I_{12}Y^2 & 16NI_2Y^2 & 16N\bar{I}_{12}Y^2 & 16N\bar{I}_1Y^2 & 16N\bar{I}_{12}Y^2 & 16N\bar{I}_2Y^2 \end{pmatrix}. \quad (\text{D.32})$$

Bibliography

- [1] H. FRITZSCH, Murray GELL-MANN, and H. LEUTWYLER. “Advantages of the Color Octet Gluon Picture”. In: *Phys. Lett.* 47B (1973), pp. 365–368. DOI: 10.1016/0370-2693(73)90625-4.
- [2] S. L. GLASHOW. “Partial Symmetries of Weak Interactions”. In: *Nucl. Phys.* 22 (1961), pp. 579–588. DOI: 10.1016/0029-5582(61)90469-2.
- [3] Abdus SALAM. “Weak and Electromagnetic Interactions”. In: *Conf. Proc.* C680519 (1968), pp. 367–377.
- [4] Steven WEINBERG. “A Model of Leptons”. In: *Phys. Rev. Lett.* 19 (1967), pp. 1264–1266. DOI: 10.1103/PhysRevLett.19.1264.
- [5] Albert EINSTEIN. “The Foundation of the General Theory of Relativity”. In: *Annalen Phys.* 49.7 (1916). Ed. by Jong-Ping HSU and D. FINE, pp. 769–822. DOI: 10.1002/andp.200590044.
- [6] L. D. LANDAU, A. A. ABRIKOSOV, and I. M. KHALATNIKOV. “An asymptotic expression for the photon Green function in quantum electrodynamics”. In: *Dokl. Akad. Nauk SSSR* 95.6 (1954), pp. 1177–1180. DOI: 10.1016/b978-0-08-010586-4.50085-7.
- [7] David J.E. CALLAWAY. “Triviality Pursuit: Can Elementary Scalar Particles Exist?” In: *Phys. Rept.* 167 (1988), p. 241. DOI: 10.1016/0370-1573(88)90008-7.
- [8] M.J.G. VELTMAN. “The Infrared - Ultraviolet Connection”. In: *Acta Phys. Polon. B* 12 (1981), p. 437.
- [9] Edward WITTEN. “Dynamical Breaking of Supersymmetry”. In: *Nucl. Phys.* B188 (1981), p. 513. DOI: 10.1016/0550-3213(81)90006-7.
- [10] Zara GROUT. “Recent Results on SUSY and Exotica Searches at the LHC”. In: *EPJ Web Conf.* 90 (2015), p. 05003. DOI: 10.1051/epjconf/20159005003.

- [11] Anadi CANEPA. “Searches for Supersymmetry at the Large Hadron Collider”. In: *Rev. Phys.* 4 (2019), p. 100033. DOI: 10.1016/j.revip.2019.100033.
- [12] Steven WEINBERG. *General Relativity: an Einstein Centenary Survey ed. S. W. Hawking and W. Israel*. Cambridge University Press, 1980, pp. 790–831. ISBN: 0521299284, 978-0521299282.
- [13] Kenneth G. WILSON. “Renormalization group and critical phenomena. 1. Renormalization group and the Kadanoff scaling picture”. In: *Phys. Rev. B* 4 (1971), pp. 3174–3183. DOI: 10.1103/PhysRevB.4.3174.
- [14] Curtis G. CALLAN Jr., Sidney R. COLEMAN, and Roman JACKIW. “A New improved energy - momentum tensor”. In: *Annals Phys.* 59 (1970), pp. 42–73. DOI: 10.1016/0003-4916(70)90394-5.
- [15] Joseph POLCHINSKI. “Scale and Conformal Invariance in Quantum Field Theory”. In: *Nucl. Phys. B* 303 (1988), pp. 226–236. DOI: 10.1016/0550-3213(88)90179-4.
- [16] Markus A. LUTY, Joseph POLCHINSKI, and Riccardo RATAZZI. “The a -theorem and the Asymptotics of 4D Quantum Field Theory”. In: *JHEP* 01 (2013), p. 152. DOI: 10.1007/JHEP01(2013)152. arXiv: 1204.5221 [hep-th].
- [17] Joshua D. QUALLS. “Lectures on Conformal Field Theory”. In: (2015). arXiv: 1511.04074 [hep-th].
- [18] Zohar KOMARGODSKI and Adam SCHWIMMER. “On Renormalization Group Flows in Four Dimensions”. In: *JHEP* 12 (2011), p. 099. DOI: 10.1007/JHEP12(2011)099. arXiv: 1107.3987 [hep-th].
- [19] D. ANSELMI, D. Z. FREEDMAN, Marcus T. GRISARU, and A. A. JOHANSEN. “Nonperturbative formulas for central functions of supersymmetric gauge theories”. In: *Nucl. Phys.* B526 (1998), pp. 543–571. DOI: 10.1016/S0550-3213(98)00278-8. arXiv: hep-th/9708042 [hep-th].
- [20] D. ANSELMI, J. ERLICH, D. Z. FREEDMAN, and A. A. JOHANSEN. “Positivity constraints on anomalies in supersymmetric gauge theories”. In: *Phys. Rev.* D57 (1998), pp. 7570–7588. DOI: 10.1103/PhysRevD.57.7570. arXiv: hep-th/9711035 [hep-th].
- [21] Kenneth A. INTRILIGATOR and Brian WECHT. “The Exact superconformal R symmetry maximizes a ”. In: *Nucl. Phys.* B667 (2003), pp. 183–200. DOI: 10.1016/S0550-3213(03)00459-0. arXiv: hep-th/0304128 [hep-th].

- [22] Diego M. HOFMAN and Juan MALDACENA. “Conformal collider physics: Energy and charge correlations”. In: *JHEP* 05 (2008), p. 012. DOI: 10.1088/1126-6708/2008/05/012. arXiv: 0803.1467 [hep-th].
- [23] Diego M. HOFMAN, Daliang LI, David MELTZER, David POLAND, and Fernando REJON-BARRERA. “A Proof of the Conformal Collider Bounds”. In: *JHEP* 06 (2016), p. 111. DOI: 10.1007/JHEP06(2016)111. arXiv: 1603.03771 [hep-th].
- [24] Kevin MOCH and Peter Schuh (in PREPARATION).
- [25] Jens ERLER and Matthias SCHOTT. “Electroweak Precision Tests of the Standard Model after the Discovery of the Higgs Boson”. In: *Prog. Part. Nucl. Phys.* 106 (2019), pp. 68–119. DOI: 10.1016/j.pnpnp.2019.02.007. arXiv: 1902.05142 [hep-ph].
- [26] S. TOMONAGA. “On a relativistically invariant formulation of the quantum theory of wave fields”. In: *Prog. Theor. Phys.* 1 (1946), pp. 27–42. DOI: 10.1143/PTP.1.27.
- [27] Julian S. SCHWINGER. “On Quantum electrodynamics and the magnetic moment of the electron”. In: *Phys. Rev.* 73 (1948), pp. 416–417. DOI: 10.1103/PhysRev.73.416.
- [28] Julian S. SCHWINGER. “Quantum electrodynamics. I A covariant formulation”. In: *Phys. Rev.* 74 (1948). [,36(1948)], p. 1439. DOI: 10.1103/PhysRev.74.1439.
- [29] Julian S. SCHWINGER. “Quantum electrodynamics. 2. Vacuum polarization and selfenergy”. In: *Phys. Rev.* 75 (1948). Ed. by K.A. MILTON, p. 651. DOI: 10.1103/PhysRev.75.651.
- [30] Julian S. SCHWINGER. “Quantum electrodynamics. III: The electromagnetic properties of the electron: Radiative corrections to scattering”. In: *Phys. Rev.* 76 (1949). Ed. by K.A. MILTON, pp. 790–817. DOI: 10.1103/PhysRev.76.790.
- [31] R. P. FEYNMAN. “Space - time approach to quantum electrodynamics”. In: *Phys. Rev.* 76 (1949). [,99(1949)], pp. 769–789. DOI: 10.1103/PhysRev.76.769.
- [32] R. P. FEYNMAN. “The Theory of positrons”. In: *Phys. Rev.* 76 (1949). [,88(1949)], pp. 749–759. DOI: 10.1103/PhysRev.76.749.
- [33] R.P. FEYNMAN. “Mathematical formulation of the quantum theory of electromagnetic interaction”. In: *Phys. Rev.* 80 (1950). Ed. by L.M. BROWN, pp. 440–457. DOI: 10.1103/PhysRev.80.440.
- [34] F.J. DYSON. “The S matrix in quantum electrodynamics”. In: *Phys. Rev.* 75 (1949), pp. 1736–1755. DOI: 10.1103/PhysRev.75.1736.

- [35] F.J. DYSON. “The Radiation theories of Tomonaga, Schwinger, and Feynman”. In: *Phys. Rev.* 75 (1949), pp. 486–502. DOI: 10.1103/PhysRev.75.486.
- [36] Peter W. HIGGS. “Broken symmetries, massless particles and gauge fields”. In: *Phys. Lett.* 12 (1964), pp. 132–133. DOI: 10.1016/0031-9163(64)91136-9.
- [37] Peter W. HIGGS. “Broken Symmetries and the Masses of Gauge Bosons”. In: *Phys. Rev. Lett.* 13 (1964). Ed. by J.C. TAYLOR, pp. 508–509. DOI: 10.1103/PhysRevLett.13.508.
- [38] Peter W. HIGGS. “Spontaneous Symmetry Breakdown without Massless Bosons”. In: *Phys. Rev.* 145 (1966), pp. 1156–1163. DOI: 10.1103/PhysRev.145.1156.
- [39] F. ENGLERT and R. BROUT. “Broken Symmetry and the Mass of Gauge Vector Mesons”. In: *Phys. Rev. Lett.* 13 (1964). Ed. by J.C. TAYLOR, pp. 321–323. DOI: 10.1103/PhysRevLett.13.321.
- [40] G.S. GURALNIK, C.R. HAGEN, and T.W.B. KIBBLE. “Global Conservation Laws and Massless Particles”. In: *Phys. Rev. Lett.* 13 (1964). Ed. by J.C. TAYLOR, pp. 585–587. DOI: 10.1103/PhysRevLett.13.585.
- [41] Georges Aad et al. “Observation of a new particle in the search for the Standard Model Higgs boson with the ATLAS detector at the LHC”. In: *Phys. Lett. B* 716 (2012), pp. 1–29. DOI: 10.1016/j.physletb.2012.08.020. arXiv: 1207.7214 [hep-ex].
- [42] Serguei Chatrchyan et al. “Observation of a New Boson at a Mass of 125 GeV with the CMS Experiment at the LHC”. In: *Phys. Lett. B* 716 (2012), pp. 30–61. DOI: 10.1016/j.physletb.2012.08.021. arXiv: 1207.7235 [hep-ex].
- [43] M. TANABASHI et al. “Review of Particle Physics”. In: *Phys. Rev.* D98.3 (2018), p. 030001. DOI: 10.1103/PhysRevD.98.030001.
- [44] Makoto Kobayashi and Toshihide Maskawa. “CP Violation in the Renormalizable Theory of Weak Interaction”. In: *Prog. Theor. Phys.* 49 (1973), pp. 652–657. DOI: 10.1143/PTP.49.652.
- [45] Nicola Cabibbo. “Unitary Symmetry and Leptonic Decays”. In: *Phys. Rev. Lett.* 10 (1963). [648(1963)], pp. 531–533. DOI: 10.1103/PhysRevLett.10.531.
- [46] Zhi-zhong XING, He ZHANG, and Shun ZHOU. “Updated Values of Running Quark and Lepton Masses”. In: *Phys. Rev. D* 77 (2008), p. 113016. DOI: 10.1103/PhysRevD.77.113016. arXiv: 0712.1419 [hep-ph].
- [47] G. VAN ROSSUM AND F.L. DRAKE (EDS). *Python Reference Manual*. Version 3.7.4. July 8, 2019. URL: <http://www.python.org>.

- [48] J. D. HUNTER. “Matplotlib: A 2D graphics environment”. In: *Computing in Science & Engineering* 9.3 (2007), pp. 90–95. DOI: 10.1109/MCSE.2007.55.
- [49] INKSCAPE PROJECT. *Inkscape*. Version 1.0. May 1, 2020. URL: <https://inkscape.org>.
- [50] H.David POLITZER. “Reliable Perturbative Results for Strong Interactions?” In: *Phys. Rev. Lett.* 30 (1973). Ed. by J.C. TAYLOR, pp. 1346–1349. DOI: 10.1103/PhysRevLett.30.1346.
- [51] David J. GROSS and Frank WILCZEK. “Ultraviolet Behavior of Nonabelian Gauge Theories”. In: *Phys. Rev. Lett.* 30 (1973). [,271(1973)], pp. 1343–1346. DOI: 10.1103/PhysRevLett.30.1343.
- [52] D. J. GROSS and Frank WILCZEK. “Asymptotically free gauge theories. II”. In: *Phys. Rev.* D9 (1974), pp. 980–993. DOI: 10.1103/PhysRevD.9.980.
- [53] Reinhard ALKOFER and J. GREENSITE. “Quark Confinement: The Hard Problem of Hadron Physics”. In: *J. Phys. G* 34 (2007), S3. DOI: 10.1088/0954-3899/34/7/S02. arXiv: hep-ph/0610365.
- [54] David TONG. “String Theory”. In: (2009). arXiv: 0908.0333 [hep-th].
- [55] E. CREMMER, S. FERRARA, L. GIRARDELLO, and Antoine VAN PROEYEN. “Yang-Mills Theories with Local Supersymmetry: Lagrangian, Transformation Laws and SuperHiggs Effect”. In: *Nucl. Phys.* B212 (1983). [,413(1982)], p. 413. DOI: 10.1016/0550-3213(83)90679-X.
- [56] M. REUTER. “Nonperturbative evolution equation for quantum gravity”. In: *Phys. Rev. D* 57 (1998), pp. 971–985. DOI: 10.1103/PhysRevD.57.971. arXiv: hep-th/9605030.
- [57] Gianfranco BERTONE, Dan HOOPER, and Joseph SILK. “Particle dark matter: Evidence, candidates and constraints”. In: *Phys. Rept.* 405 (2005), pp. 279–390. DOI: 10.1016/j.physrep.2004.08.031. arXiv: hep-ph/0404175 [hep-ph].
- [58] M. GOCKELER, R. HORSLEY, V. LINKE, Paul E.L. RAKOW, G. SCHIERHOLZ, and H. STUBEN. “Is there a Landau pole problem in QED?” In: *Phys. Rev. Lett.* 80 (1998), pp. 4119–4122. DOI: 10.1103/PhysRevLett.80.4119. arXiv: hep-th/9712244.
- [59] Holger GIES and Joerg JAECKEL. “Renormalization flow of QED”. In: *Phys. Rev. Lett.* 93 (2004), p. 110405. DOI: 10.1103/PhysRevLett.93.110405. arXiv: hep-ph/0405183 [hep-ph].

- [60] Nicolai CHRISTIANSEN and Astrid EICHHORN. “An asymptotically safe solution to the U(1) triviality problem”. In: *Phys. Lett.* B770 (2017), pp. 154–160. DOI: 10.1016/j.physletb.2017.04.047. arXiv: 1702.07724 [hep-th].
- [61] Andrew D. BOND, Gudrun HILLER, Kamila KOWALSKA, and Daniel F. LITIM. “Directions for model building from asymptotic safety”. In: *JHEP* 08 (2017), p. 004. DOI: 10.1007/JHEP08(2017)004. arXiv: 1702.01727 [hep-ph].
- [62] Kamila KOWALSKA, Andrew BOND, Gudrun HILLER, and Daniel LITIM. “Towards an asymptotically safe completion of the Standard Model”. In: *PoS EPS-HEP2017* (2017), p. 542. DOI: 10.22323/1.314.0542.
- [63] Daniel F. LITIM and Francesco SANNINO. “Asymptotic safety guaranteed”. In: *JHEP* 12 (2014), p. 178. DOI: 10.1007/JHEP12(2014)178. arXiv: 1406.2337 [hep-th].
- [64] Andrew D. BOND and Daniel F. LITIM. “More asymptotic safety guaranteed”. In: *Phys. Rev.* D97.8 (2018), p. 085008. DOI: 10.1103/PhysRevD.97.085008. arXiv: 1707.04217 [hep-th].
- [65] Andrew D. BOND and Daniel F. LITIM. “Asymptotic safety guaranteed in supersymmetry”. In: *Phys. Rev. Lett.* 119.21 (2017), p. 211601. DOI: 10.1103/PhysRevLett.119.211601. arXiv: 1709.06953 [hep-th].
- [66] D. J. GROSS and Frank WILCZEK. “Asymptotically Free Gauge Theories - I”. In: *Phys. Rev.* D8 (1973), pp. 3633–3652. DOI: 10.1103/PhysRevD.8.3633.
- [67] E.C.G. de Breidenbach STUECKELBERG and André PETERMANN. “Normalization of constants in the quanta theory”. PhD thesis. Birkhäuser: Lausanne U., 1953.
- [68] Murray GELL-MANN and F. E. LOW. “Quantum electrodynamics at small distances”. In: *Phys. Rev.* 95 (1954), pp. 1300–1312. DOI: 10.1103/PhysRev.95.1300.
- [69] Kenneth G. WILSON. “Renormalization group and critical phenomena. 2. Phase space cell analysis of critical behavior”. In: *Phys. Rev. B* 4 (1971), pp. 3184–3205. DOI: 10.1103/PhysRevB.4.3184.
- [70] L.P. KADANOFF. “Scaling laws for Ising models near $T(c)$ ”. In: *Physics Physique Fizika* 2 (1966), pp. 263–272. DOI: 10.1103/PhysicsPhysiqueFizika.2.263.
- [71] Christof WETTERICH. “Exact evolution equation for the effective potential”. In: *Phys. Lett. B* 301 (1993), pp. 90–94. DOI: 10.1016/0370-2693(93)90726-X. arXiv: 1710.05815 [hep-th].

- [72] Tim R. MORRIS. “The Exact renormalization group and approximate solutions”. In: *Int. J. Mod. Phys. A* 9 (1994), pp. 2411–2450. DOI: 10.1142/S0217751X94000972. arXiv: hep-ph/9308265.
- [73] R. GASTMANS, R. KALLOSH, and C. TRUFFIN. “Quantum Gravity Near Two-Dimensions”. In: *Nucl. Phys. B* 133 (1978), pp. 417–434. DOI: 10.1016/0550-3213(78)90234-1.
- [74] S.M. CHRISTENSEN and M.J. DUFF. “Quantum Gravity in Two + ϵ Dimensions”. In: *Phys. Lett. B* 79 (1978), pp. 213–216. DOI: 10.1016/0370-2693(78)90225-3.
- [75] Hikaru KAWAI, Yoshihisa KITAZAWA, and Masao NINOMIYA. “Scaling exponents in quantum gravity near two-dimensions”. In: *Nucl. Phys. B* 393 (1993), pp. 280–300. DOI: 10.1016/0550-3213(93)90246-L. arXiv: hep-th/9206081.
- [76] E. TOMBOULIS. “ $1/N$ Expansion and Renormalization in Quantum Gravity”. In: *Phys. Lett. B* 70 (1977), pp. 361–364. DOI: 10.1016/0370-2693(77)90678-5.
- [77] E. TOMBOULIS. “Renormalizability and Asymptotic Freedom in Quantum Gravity”. In: *Phys. Lett. B* 97 (1980), pp. 77–80. DOI: 10.1016/0370-2693(80)90550-X.
- [78] Lee SMOLIN. “A Fixed Point for Quantum Gravity”. In: *Nucl. Phys. B* 208 (1982), pp. 439–466. DOI: 10.1016/0550-3213(82)90230-9.
- [79] Daniel F. LITIM. “Renormalisation group and the Planck scale”. In: *Phil. Trans. Roy. Soc. Lond. A* 369 (2011), pp. 2759–2778. DOI: 10.1098/rsta.2011.0103. arXiv: 1102.4624 [hep-th].
- [80] Daniel F. LITIM. “On fixed points of quantum gravity”. In: *AIP Conf. Proc.* 841.1 (2006). Ed. by Lysiane MORNAS and Joaquin DIAZ ALONSO, pp. 322–329. DOI: 10.1063/1.2218188. arXiv: hep-th/0606044.
- [81] M. NIEDERMAIER. “The Asymptotic safety scenario in quantum gravity: An Introduction”. In: *Class. Quant. Grav.* 24 (2007), R171–230. DOI: 10.1088/0264-9381/24/18/R01. arXiv: gr-qc/0610018.
- [82] Max NIEDERMAIER and Martin REUTER. “The Asymptotic Safety Scenario in Quantum Gravity”. In: *Living Rev. Rel.* 9 (2006), pp. 5–173. DOI: 10.12942/lrr-2006-5.
- [83] Roberto PERCACCI. “Asymptotic Safety”. In: (2007). arXiv: 0709.3851 [hep-th].
- [84] Daniel F. LITIM. “Fixed Points of Quantum Gravity and the Renormalisation Group”. In: *PoS(QG-Ph)024* (2008). arXiv: 0810.3675 [hep-th].

- [85] Astrid EICHHORN. “Status of the asymptotic safety paradigm for quantum gravity and matter”. In: *Found. Phys.* 48.10 (2018), pp. 1407–1429. DOI: 10.1007/s10701-018-0196-6. arXiv: 1709.03696 [gr-qc].
- [86] Astrid EICHHORN. “An asymptotically safe guide to quantum gravity and matter”. In: *Front. Astron. Space Sci.* 5 (2019), p. 47. DOI: 10.3389/fspas.2018.00047. arXiv: 1810.07615 [hep-th].
- [87] Djamel DOU and Roberto PERCACCI. “The running gravitational couplings”. In: *Class. Quant. Grav.* 15 (1998), pp. 3449–3468. DOI: 10.1088/0264-9381/15/11/011. arXiv: hep-th/9707239.
- [88] O. LAUSCHER and M. REUTER. “Flow equation of quantum Einstein gravity in a higher derivative truncation”. In: *Phys. Rev. D* 66 (2002), p. 025026. DOI: 10.1103/PhysRevD.66.025026. arXiv: hep-th/0205062.
- [89] Dario BENEDETTI and Francesco CARAVELLI. “The Local potential approximation in quantum gravity”. In: *JHEP* 06 (2012). [Erratum: *JHEP* 10, 157 (2012)], p. 017. DOI: 10.1007/JHEP06(2012)017. arXiv: 1204.3541 [hep-th].
- [90] Juergen A. DIETZ and Tim R. MORRIS. “Asymptotic safety in the f(R) approximation”. In: *JHEP* 01 (2013), p. 108. DOI: 10.1007/JHEP01(2013)108. arXiv: 1211.0955 [hep-th].
- [91] Kevin FALLS, Daniel F. LITIM, Kostas NIKOLAKOPOULOS, and Christoph RAHMEDE. “A bootstrap strategy for asymptotic safety”. In: *DO-TH 13/02; KA-TP-01-2013* (2013). arXiv: 1301.4191.
- [92] Maximilian DEMMEL, Frank SAUERESSIG, and Omar ZANUSSO. “A proper fixed functional for four-dimensional Quantum Einstein Gravity”. In: *JHEP* 08 (2015), p. 113. DOI: 10.1007/JHEP08(2015)113. arXiv: 1504.07656 [hep-th].
- [93] Nobuyoshi OHTA, Roberto PERCACCI, and Gian Paolo VACCA. “Renormalization Group Equation and scaling solutions for f(R) gravity in exponential parametrization”. In: *Eur. Phys. J. C* 76.2 (2016), p. 46. DOI: 10.1140/epjc/s10052-016-3895-1. arXiv: 1511.09393 [hep-th].
- [94] Kevin G. FALLS, Daniel F. LITIM, and Jan SCHRÖDER. “Aspects of asymptotic safety for quantum gravity”. In: *Phys. Rev. D* 99.12 (2019), p. 126015. DOI: 10.1103/PhysRevD.99.126015. arXiv: 1810.08550 [gr-qc].
- [95] Dario BENEDETTI, Pedro F. MACHADO, and Frank SAUERESSIG. “Asymptotic safety in higher-derivative gravity”. In: *Mod. Phys. Lett. A* 24 (2009), pp. 2233–2241. DOI: 10.1142/S0217732309031521. arXiv: 0901.2984 [hep-th].

- [96] Nima ARKANI-HAMED, Lubos MOTL, Alberto NICOLIS, and Cumrun VAFA. “The String landscape, black holes and gravity as the weakest force”. In: *JHEP* 06 (2007), p. 060. DOI: 10.1088/1126-6708/2007/06/060. arXiv: hep-th/0601001.
- [97] Tom BANKS, Matt JOHNSON, and Assaf SHOMER. “A Note on Gauge Theories Coupled to Gravity”. In: *JHEP* 09 (2006), p. 049. DOI: 10.1088/1126-6708/2006/09/049. arXiv: hep-th/0606277.
- [98] Sarah FOLKERTS, Daniel F. LITIM, and Jan M. PAWLOWSKI. “Asymptotic freedom of Yang-Mills theory with gravity”. In: *Phys. Lett. B* 709 (2012), pp. 234–241. DOI: 10.1016/j.physletb.2012.02.002. arXiv: 1101.5552 [hep-th].
- [99] Nicolai CHRISTIANSEN, Daniel F. LITIM, Jan M. PAWLOWSKI, and Manuel REICHERT. “Asymptotic safety of gravity with matter”. In: *Phys. Rev. D* 97.10 (2018), p. 106012. DOI: 10.1103/PhysRevD.97.106012. arXiv: 1710.04669 [hep-th].
- [100] K. GAWEDZKI and A. KUPIAINEN. “Extract Renormalization for the Gross-Neveu Model of Quantum Fields”. In: *Phys. Rev. Lett.* 54 (1985), pp. 2191–2194. DOI: 10.1103/PhysRevLett.54.2191.
- [101] K. GAWEDZKI and A. KUPIAINEN. “Renormalizing the nonrenormalizable”. In: *Phys. Rev. Lett.* 55 (1985), pp. 363–365. DOI: 10.1103/PhysRevLett.55.363.
- [102] C. de CALAN, P.A. FARIA DA VEIGA, J. MAGNEN, and R. SENEOR. “Constructing the three-dimensional Gross-Neveu model with a large number of flavor components”. In: *Phys. Rev. Lett.* 66 (1991), pp. 3233–3236. DOI: 10.1103/PhysRevLett.66.3233.
- [103] Jens BRAUN, Holger GIES, and Daniel D. SCHERER. “Asymptotic safety: a simple example”. In: *Phys. Rev. D* 83 (2011), p. 085012. DOI: 10.1103/PhysRevD.83.085012. arXiv: 1011.1456 [hep-th].
- [104] Michael E. PESKIN. “CRITICAL POINT BEHAVIOR OF THE WILSON LOOP”. In: *Phys. Lett. B* 94 (1980), pp. 161–165. DOI: 10.1016/0370-2693(80)90848-5.
- [105] Tim R. MORRIS. “Renormalizable extra-dimensional models”. In: *JHEP* 01 (2005), p. 002. DOI: 10.1088/1126-6708/2005/01/002. arXiv: hep-ph/0410142.
- [106] Holger GIES. “Renormalizability of gauge theories in extra dimensions”. In: *Phys. Rev. D* 68 (2003), p. 085015. DOI: 10.1103/PhysRevD.68.085015. arXiv: hep-th/0305208.

- [107] Andrea PELISSETTO and Ettore VICARI. “Critical phenomena and renormalization group theory”. In: *Phys. Rept.* 368 (2002), pp. 549–727. DOI: 10.1016/S0370-1573(02)00219-3. arXiv: cond-mat/0012164.
- [108] Daniel F. LITIM and Dario ZAPPALA. “Ising exponents from the functional renormalisation group”. In: *Phys. Rev. D* 83 (2011), p. 085009. DOI: 10.1103/PhysRevD.83.085009. arXiv: 1009.1948 [hep-th].
- [109] Roberto PERCACCI and Gian Paolo VACCA. “Are there scaling solutions in the $O(N)$ -models for large N in $d > 4$?” In: *Phys. Rev. D* 90 (2014), p. 107702. DOI: 10.1103/PhysRevD.90.107702. arXiv: 1405.6622 [hep-th].
- [110] D. BAILIN and A. LOVE. “Asymptotic Near Freedom”. In: *Nucl. Phys. B* 75 (1974), p. 159. DOI: 10.1016/0550-3213(74)90470-2.
- [111] Andrew D. BOND, Daniel F. LITIM, and Tom STEUDTNER. “Asymptotic safety with Majorana fermions and new large N equivalences”. In: *Phys. Rev. D* 101.4 (2020), p. 045006. DOI: 10.1103/PhysRevD.101.045006. arXiv: 1911.11168 [hep-th].
- [112] G. VENEZIANO. “U(1) Without Instantons”. In: *Nucl. Phys. B* 159 (1979), pp. 213–224. DOI: 10.1016/0550-3213(79)90332-8.
- [113] Andrew D. BOND and Daniel F. LITIM. “Theorems for Asymptotic Safety of Gauge Theories”. In: *Eur. Phys. J. C* 77.6 (2017). [Erratum: *Eur.Phys.J.C* 77, 525 (2017)], p. 429. DOI: 10.1140/epjc/s10052-017-4976-5. arXiv: 1608.00519 [hep-th].
- [114] Andrew D. BOND and Daniel F. LITIM. “Price of Asymptotic Safety”. In: *Phys. Rev. Lett.* 122.21 (2019), p. 211601. DOI: 10.1103/PhysRevLett.122.211601. arXiv: 1801.08527 [hep-th].
- [115] Gudrun HILLER, Clara HORMIGOS-FELIU, Daniel F. LITIM, and Tom STEUDTNER. “Anomalous magnetic moments from asymptotic safety”. In: (2019). arXiv: 1910.14062 [hep-ph].
- [116] Gudrun HILLER, Clara HORMIGOS-FELIU, Daniel F. LITIM, and Tom STEUDTNER. “Model Building from Asymptotic Safety with Higgs and Flavor Portals”. In: (Aug. 2020). arXiv: 2008.08606 [hep-ph].
- [117] Stephen P. MARTIN and James D. WELLS. “Constraints on ultraviolet stable fixed points in supersymmetric gauge theories”. In: *Phys. Rev. D* 64 (2001), p. 036010. DOI: 10.1103/PhysRevD.64.036010. arXiv: hep-ph/0011382 [hep-ph].

- [118] Kenneth INTRILIGATOR and Francesco SANNINO. “Supersymmetric asymptotic safety is not guaranteed”. In: *JHEP* 11 (2015), p. 023. DOI: 10.1007/JHEP11(2015)023. arXiv: 1508.07411 [hep-th].
- [119] Sidney R. COLEMAN and J. MANDULA. “All Possible Symmetries of the S Matrix”. In: *Phys. Rev.* 159 (1967), pp. 1251–1256. DOI: 10.1103/PhysRev.159.1251.
- [120] Rudolf HAAG, Jan T. LOPUSZANSKI, and Martin SOHNIUS. “All Possible Generators of Supersymmetries of the s Matrix”. In: *Nucl. Phys.* B88 (1975). [,257(1974); ,257(1974)], p. 257. DOI: 10.1016/0550-3213(75)90279-5.
- [121] J. WESS and B. ZUMINO. “Supergauge Transformations in Four-Dimensions”. In: *Nucl. Phys.* B70 (1974). [,24(1974)], pp. 39–50. DOI: 10.1016/0550-3213(74)90355-1.
- [122] J. WESS and B. ZUMINO. “Supergauge Invariant Extension of Quantum Electrodynamics”. In: *Nucl. Phys.* B78 (1974), p. 1. DOI: 10.1016/0550-3213(74)90112-6.
- [123] Steven WEINBERG. “Implications of Dynamical Symmetry Breaking”. In: *Phys. Rev. D* 13 (1976). [Addendum: *Phys.Rev.D* 19, 1277–1280 (1979)], pp. 974–996. DOI: 10.1103/PhysRevD.19.1277.
- [124] Eldad GILDENER. “Gauge Symmetry Hierarchies”. In: *Phys. Rev. D* 14 (1976), p. 1667. DOI: 10.1103/PhysRevD.14.1667.
- [125] Xerxes TATA. “Natural Supersymmetry: Status and Prospects”. In: (2020). arXiv: 2002.04429 [hep-ph].
- [126] S. FERRARA, J. WESS, and B. ZUMINO. “Supergauge Multiplets and Superfields”. In: *Phys. Lett.* 51B (1974), p. 239. DOI: 10.1016/0370-2693(74)90283-4.
- [127] Abdus SALAM and J. A. STRATHDEE. “On Superfields and Fermi-Bose Symmetry”. In: *Phys. Rev. D* 11 (1975), pp. 1521–1535. DOI: 10.1103/PhysRevD.11.1521.
- [128] Marcus T. GRISARU, W. SIEGEL, and M. ROCEK. “Improved Methods for Supergraphs”. In: *Nucl. Phys.* B159 (1979), p. 429. DOI: 10.1016/0550-3213(79)90344-4.
- [129] Pierre FAYET. “Supersymmetry and Weak, Electromagnetic and Strong Interactions”. In: *Phys. Lett.* 64B (1976), p. 159. DOI: 10.1016/0370-2693(76)90319-1.
- [130] Yang BAI and Pedro SCHWALLER. “Scale of dark QCD”. In: *Phys. Rev. D* 89 (2014), p. 063522. DOI: 10.1103/PhysRevD.89.063522. arXiv: 1306.4676 [hep-ph].

- [131] N. AGHANIM et al. “Planck 2018 results. VI. Cosmological parameters”. In: (2018). arXiv: 1807.06209 [astro-ph.CO].
- [132] Glennys R. FARRAR and Pierre FAYET. “Phenomenology of the Production, Decay, and Detection of New Hadronic States Associated with Supersymmetry”. In: *Phys. Lett. B* 76 (1978), pp. 575–579. DOI: 10.1016/0370-2693(78)90858-4.
- [133] Vardan KHACHATRYAN et al. “Constraints on parton distribution functions and extraction of the strong coupling constant from the inclusive jet cross section in pp collisions at $\sqrt{s} = 7$ TeV”. In: *Eur. Phys. J. C* 75.6 (2015), p. 288. DOI: 10.1140/epjc/s10052-015-3499-1. arXiv: 1410.6765 [hep-ex].
- [134] Serguei CHATRCHYAN et al. “Measurements of Differential Jet Cross Sections in Proton-Proton Collisions at $\sqrt{s} = 7$ TeV with the CMS Detector”. In: *Phys. Rev. D* 87.11 (2013). [Erratum: Phys.Rev.D 87, 119902 (2013)], p. 112002. DOI: 10.1103/PhysRevD.87.112002. arXiv: 1212.6660 [hep-ex].
- [135] Serguei CHATRCHYAN et al. “Measurement of the Ratio of the Inclusive 3-Jet Cross Section to the Inclusive 2-Jet Cross Section in pp Collisions at $\sqrt{s} = 7$ TeV and First Determination of the Strong Coupling Constant in the TeV Range”. In: *Eur. Phys. J. C* 73.10 (2013), p. 2604. DOI: 10.1140/epjc/s10052-013-2604-6. arXiv: 1304.7498 [hep-ex].
- [136] Vardan KHACHATRYAN et al. “Search for long-lived charged particles in proton-proton collisions at $\sqrt{s} = 13$ TeV”. In: *Phys. Rev. D* 94.11 (2016), p. 112004. DOI: 10.1103/PhysRevD.94.112004. arXiv: 1609.08382 [hep-ex].
- [137] Morad AABOUD et al. “Search for heavy long-lived charged R -hadrons with the ATLAS detector in 3.2 fb^{-1} of proton-proton collision data at $\sqrt{s} = 13$ TeV”. In: *Phys. Lett. B* 760 (2016), pp. 647–665. DOI: 10.1016/j.physletb.2016.07.042. arXiv: 1606.05129 [hep-ex].
- [138] Georges AAD et al. “Search for new resonances in mass distributions of jet pairs using 139 fb^{-1} of pp collisions at $\sqrt{s} = 13$ TeV with the ATLAS detector”. In: (2019). arXiv: 1910.08447 [hep-ex].
- [139] Morad AABOUD et al. “Search for dark matter and other new phenomena in events with an energetic jet and large missing transverse momentum using the ATLAS detector”. In: *JHEP* 01 (2018), p. 126. DOI: 10.1007/JHEP01(2018)126. arXiv: 1711.03301 [hep-ex].
- [140] Stephen P. MARTIN. “A Supersymmetry primer”. In: *Perspectives on supersymmetry. Vol.2*. Ed. by Gordon L. KANE. Vol. 21. 2010, pp. 1–153. DOI: 10.1142/9789812839657_0001. arXiv: hep-ph/9709356.

- [141] J. TERNING. *Modern supersymmetry: Dynamics and duality*. 2006. DOI: 10.1093/acprof:oso/9780198567639.001.0001.
- [142] S. HEINEMEYER, O. STAL, and G. WEIGLEIN. “Interpreting the LHC Higgs Search Results in the MSSM”. In: *Phys. Lett. B* 710 (2012), pp. 201–206. DOI: 10.1016/j.physletb.2012.02.084. arXiv: 1112.3026 [hep-ph].
- [143] Herbert K. DREINER. “An Introduction to explicit R-parity violation”. In: *Perspectives on supersymmetry. Vol.2*. Ed. by Gordon L. KANE. Vol. 21. 2010, pp. 565–583. DOI: 10.1142/9789814307505_0017. arXiv: hep-ph/9707435.
- [144] Gerard JUNGMAN, Marc KAMIONKOWSKI, and Kim GRIEST. “Supersymmetric dark matter”. In: *Phys. Rept.* 267 (1996), pp. 195–373. DOI: 10.1016/0370-1573(95)00058-5. arXiv: hep-ph/9506380.
- [145] Sally DAWSON. “R-Parity Breaking in Supersymmetric Theories”. In: *Nucl. Phys. B* 261 (1985), pp. 297–318. DOI: 10.1016/0550-3213(85)90577-2.
- [146] Riccardo BARBIERI and A. MASIERO. “Supersymmetric Models with Low-Energy Baryon Number Violation”. In: *Nucl. Phys. B* 267 (1986), pp. 679–689. DOI: 10.1016/0550-3213(86)90136-7.
- [147] Vernon D. BARGER, G.F. GIUDICE, and Tao HAN. “Some New Aspects of Supersymmetry R-Parity Violating Interactions”. In: *Phys. Rev. D* 40 (1989), p. 2987. DOI: 10.1103/PhysRevD.40.2987.
- [148] Rohini M. GODBOLE, Probir ROY, and Xerxes TATA. “Tau signals of R-parity breaking at LEP-200”. In: *Nucl. Phys. B* 401 (1993), pp. 67–92. DOI: 10.1016/0550-3213(93)90298-4. arXiv: hep-ph/9209251.
- [149] Gautam BHATTACHARYYA and Debajyoti CHOUDHURY. “D and tau decays: Placing new bounds on R-parity violating supersymmetric coupling”. In: *Mod. Phys. Lett. A* 10 (1995), pp. 1699–1704. DOI: 10.1142/S0217732395001812. arXiv: hep-ph/9503263.
- [150] Florian DOMINGO, Herbert K. DREINER, Jong Soo KIM, Manuel E. KRAUSS, Martín LOZANO, and Zeren Simon WANG. “Updating Bounds on R-Parity Violating Supersymmetry from Meson Oscillation Data”. In: *JHEP* 02 (2019), p. 066. DOI: 10.1007/JHEP02(2019)066. arXiv: 1810.08228 [hep-ph].
- [151] Michael DINE and Willy FISCHLER. “A Phenomenological Model of Particle Physics Based on Supersymmetry”. In: *Phys. Lett.* 110B (1982), pp. 227–231. DOI: 10.1016/0370-2693(82)91241-2.

- [152] Michael DINE, Ann E. NELSON, Yosef NIR, and Yuri SHIRMAN. “New tools for low-energy dynamical supersymmetry breaking”. In: *Phys. Rev. D* 53 (1996), pp. 2658–2669. DOI: 10.1103/PhysRevD.53.2658. arXiv: hep-ph/9507378 [hep-ph].
- [153] Stephen P. MARTIN and Michael T. VAUGHN. “Two loop renormalization group equations for soft supersymmetry breaking couplings”. In: *Phys. Rev. D* 50 (1994). [Erratum: *Phys.Rev.D* 78, 039903 (2008)], p. 2282. DOI: 10.1103/PhysRevD.50.2282. arXiv: hep-ph/9311340.
- [154] Stephen P. MARTIN and Michael T. VAUGHN. “Regularization dependence of running couplings in softly broken supersymmetry”. In: *Phys. Lett.* B318 (1993), pp. 331–337. DOI: 10.1016/0370-2693(93)90136-6. arXiv: hep-ph/9308222 [hep-ph].
- [155] V. A. NOVIKOV, Mikhail A. SHIFMAN, A. I. VAINSHTEIN, and Valentin I. ZAKHAROV. “Exact Gell-Mann-Low Function of Supersymmetric Yang-Mills Theories from Instanton Calculus”. In: *Nucl. Phys.* B229 (1983), pp. 381–393. DOI: 10.1016/0550-3213(83)90338-3.
- [156] P. ACHARD et al. “Search for heavy neutral and charged leptons in e^+e^- annihilation at LEP”. In: *Phys. Lett.* B517 (2001), pp. 75–85. DOI: 10.1016/S0370-2693(01)01005-X. arXiv: hep-ex/0107015 [hep-ex].
- [157] John L. CARDY. “Is There a c Theorem in Four-Dimensions?” In: *Phys. Lett.* B215 (1988), pp. 749–752. DOI: 10.1016/0370-2693(88)90054-8.
- [158] Zohar KOMARGODSKI and Adam SCHWIMMER. “On Renormalization Group Flows in Four Dimensions”. In: *JHEP* 12 (2011), p. 099. DOI: 10.1007/JHEP12(2011)099. arXiv: 1107.3987 [hep-th].
- [159] Zohar KOMARGODSKI. “The Constraints of Conformal Symmetry on RG Flows”. In: *JHEP* 07 (2012), p. 069. DOI: 10.1007/JHEP07(2012)069. arXiv: 1112.4538 [hep-th].
- [160] Shiraz MINWALLA. “Restrictions imposed by superconformal invariance on quantum field theories”. In: *Adv. Theor. Math. Phys.* 2 (1998), pp. 783–851. DOI: 10.4310/ATMP.1998.v2.n4.a4. arXiv: hep-th/9712074 [hep-th].
- [161] G. MACK. “All unitary ray representations of the conformal group SU(2,2) with positive energy”. In: *Commun. Math. Phys.* 55 (1977), p. 1. DOI: 10.1007/BF01613145.

- [162] Moshe FLATO and Christian FRONSDAL. “Representations of Conformal Supersymmetry”. In: *Lett. Math. Phys.* 8 (1984), p. 159. DOI: 10.1007/BF00406399.
- [163] V.K. DOBREV and V.B. PETKOVA. “All Positive Energy Unitary Irreducible Representations of Extended Conformal Supersymmetry”. In: *Phys. Lett. B* 162 (1985), pp. 127–132. DOI: 10.1016/0370-2693(85)91073-1.
- [164] V.K. DOBREV and V.B. PETKOVA. “Group Theoretical Approach to Extended Conformal Supersymmetry: Function Space Realizations and Invariant Differential Operators”. In: *Fortsch. Phys.* 35 (1987), p. 537.
- [165] J.S. BELL and R. JACKIW. “A PCAC puzzle: $\pi^0 \rightarrow \gamma\gamma$ in the σ model”. In: *Nuovo Cim. A* 60 (1969), pp. 47–61. DOI: 10.1007/BF02823296.
- [166] Stephen L. ADLER. “Axial vector vertex in spinor electrodynamics”. In: *Phys. Rev.* 177 (1969), pp. 2426–2438. DOI: 10.1103/PhysRev.177.2426.
- [167] Adel BILAL. “Lectures on Anomalies”. In: (Feb. 2008). arXiv: 0802.0634 [hep-th].
- [168] Steven WEINBERG. *The quantum theory of fields. Vol. 2: Modern applications*. Cambridge University Press, 2013. ISBN: 9781139632478, 9780521670548, 9780521550024.
- [169] Damiano ANSELMI. “Inequalities for trace anomalies, length of the RG flow, distance between the fixed points and irreversibility”. In: *Class. Quant. Grav.* 21.1 (2004), pp. 29–50. DOI: 10.1088/0264-9381/21/1/003. arXiv: hep-th/0210124 [hep-th].

Eidesstattliche Versicherung

Ich versichere hiermit an Eides statt, dass ich die vorliegende Dissertation mit dem Titel “Fixed Points in Supersymmetric Extensions of the Standard Model” selbstständig und ohne unzulässige fremde Hilfe erbracht habe. Ich habe keine anderen als die angegebenen Quellen und Hilfsmittel benutzt, sowie wörtliche und sinngemäße Zitate kenntlich gemacht. Die Arbeit hat in gleicher oder ähnlicher Form noch keiner Prüfungsbehörde vorgelegen.

Ort, Datum

Unterschrift

Belehrung

Wer vorsätzlich gegen eine die Täuschung über Prüfungsleistungen betreffende Regelung einer Hochschulprüfungsordnung verstößt, handelt ordnungswidrig. Die Ordnungswidrigkeit kann mit einer Geldbuße von bis zu 50 000 € geahndet werden. Zuständige Verwaltungsbehörde für die Verfolgung und Ahndung von Ordnungswidrigkeiten ist der Kanzler/die Kanzlerin der Technischen Universität Dortmund. Im Falle eines mehrfachen oder sonstigen schwerwiegenden Täuschungsversuches kann der Prüfling zudem exmatrikuliert werden (§ 63 Abs. 5 Hochschulgesetz –HG–).

Die Abgabe einer falschen Versicherung an Eides statt wird mit Freiheitsstrafe bis zu 3 Jahren oder mit Geldstrafe bestraft.

Die Technische Universität Dortmund wird ggf. elektronische Vergleichswerkzeuge (wie z. B. die Software “turnitin”) zur Überprüfung von Ordnungswidrigkeiten in Prüfungsverfahren nutzen.

Die oben stehende Belehrung habe ich zur Kenntnis genommen.

Ort, Datum

Unterschrift